RECOVERY OF LITHIUM FROM CHINA CLAY WASTE USING A COMBINATION OF FROTH FLOTATION, MAGNETIC SEPARATION, ROASTING AND LEACHING

Edward Siame MSc, BMinSc

Submitted by Edward Siame to the University of Exeter as a thesis for the degree of Doctor of Philosophy in Earth Resources, February 2011.

I certify that all material in this thesis which is not my own work has been identified and that no material has previously been submitted and approved for the award of degree by this or any other University.

E. Siame **(Signature)**

ACKNOWLEDGEMENTS

This PhD was made possible by the sponsorship from the Commonwealth Scholarship Commission of the United Kingdom and I am highly grateful.

I sincerely thank my supervisor Dr Richard D. Pascoe for his guidance throughout the research and the writing of this thesis. He was also instrumental in making sure that the material for research and other requisites were readily available.

Thanks to Goonvean Ltd, UK, for allowing us to sample the china clay waste for this research. I would also like to express my gratitude to Mathews Neighbour and Klaas Peter van der Wielen for their assistance with sample collection.

I am also indebted to the Camborne School of Mines technical staff: Ms Sharon Uren, Ms Fiona Thomas and Mr. Steve Pendray for their support during the laboratory and analytical work. Lastly but not the least my regards go to all Camborne School of Mines staff.

ABSTRACT

This study was aimed at recovering lithium from china clay waste using a combination of froth flotation, magnetic separation, roasting and leaching. The china clay waste produced by Goonvean Ltd contains about 0.84% Li_2O and 0.36% Rb_2O, present in some of the mica minerals. Among the mica minerals, zinnwaldite is the major source of lithium with smaller amounts being contributed by muscovite. The results of the flotation tests showed that the dodecylamine collector dosage had a greater effect on the recovery and grade of mica minerals to concentrate than pH over the range tested. It was found that a mica concentrate containing 1.45% Li_2O, 0.55% Rb_2O and 4.47% Fe_2O_3 could be produced at a recovery of 98.6%, 85.2% and 92.8% respectively. Mineralogical analysis of the flotation products showed that the concentrate consisted mainly of muscovite, zinnwaldite and kaolinite with minor amounts of K-feldspar and quartz. The tailing consisted of mainly quartz, K-feldspar and kaolinite with minor amounts of apatite, topaz, zinnwaldite and muscovite.

Further upgrading of the concentrate was found to be possible using a wet high intensity magnetic separator producing a magnetic fraction containing 2.07% Li_2O, 0.74% Rb_2O and 7.42% Fe_2O_3 with a recovery of 73%, 67% and 77% respectively. A mineralogical analysis of the separation products showed that the magnetic fraction consisted of predominantly zinnwaldite with muscovite as the main contaminant. The non-magnetic fraction consisted of muscovite and kaolinite as the main minerals while zinnwaldite, K-feldspar and quartz were subordinate. Electron-microprobe analysis on individual mica grains have shown that zinnwaldite and muscovite contain on average a calculated Li_2O content of 3.88% and 0.13% respectively.

Lithium extraction from the concentrate is only possible after the lithium has been converted into a water-soluble compound. Thus, in order to convert the lithium in concentrate into a water-soluble compound, the gypsum and limestone lithium extraction methods together with the new method of using sodium sulphate were investigated. The process involved roasting a predetermined amount of lithium-mica concentrate with either gypsum, limestone or sodium sulphate at various temperatures and subsequently leaching the pulverised materials in water at 85^oC. A lithium extraction efficiency of about 84% was obtained using gypsum at 1050^oC while rubidium extraction was very low at 14%. It was found possible to extract about 97% Li and 16% Rb if the concentrate was roasted with sodium sulphate at 850^oC. Processing the concentrate with limestone resulted in very low lithium extraction. Iron co-extraction was low in all cases. The XRD analysis of the gypsum and sodium sulphate roast-products showed that the water soluble lithium species were $KLiSO_4$ and $Li_2KNa(SO_4)_2$ respectively.

Preliminary tests on the leach solution obtained by using sodium sulphate as an additive have shown that a Li_2O_3 product with a purity of > 90% could be produced by precipitation with sodium carbonate although more work is required to reach the industrial target of > 99%. The lithium carbonate obtained with Li_2CO_3 content of about 90% is still suitable for use in the glass and ceramic industries, and as feedstock for the production of high-purity lithium compounds. An economic evaluation of the proposed lithium carbonate production plant has indicated an annual rate of return on the investment before tax of 7.2%.

TABLE OF CONTENTS

APPENDICES

LIST OF FIGURES

LIST OF TABLES

Table of Notations

Abbreviation	Full
XRD	X-Ray Diffraction
XRF	X-Ray Fluorescence
AAS	Atomic Absorption Spectrometry
LOI	Loss on Ignition
WHIMS	Wet High Intensity Magnetic Separation
μm	microns
wt	weight
g	grams
g/t	gram/tonne
cm^3	Cubic centimetres
H_2SO_4	Sulphuric acid
NaOH	Sodium hydroxide
F	Fluorine
Li	Lithium
wt%	weight percent
MIBC	Methyl Isobutyl Carbinol
S/L/G	Solid/Liquid/Gas
UK	United Kingdom
ppm	Parts per million
DDCL	dodecylamine chloride
w/v%	weight volume percent
Fe	Iron
TGA	Thermal Gravimetric Analysis
DTA	Differential Thermal Analysis
Rb	Rubidium
t	tonnes
USGS	United States Geological Survey
PZC	Point-of-Zero-Charge
SQM	Sociedad Quimica y Minera
$\gamma_{s/a}$	Surface energy between solid and air
$\gamma_{s/w}$	Surface energy between solid and water
$\gamma_{w/a}$	Surface energy between water and air
$W_{s/a}$	Work of adhesion between solid-air interface
θ	Contact angle

1. INTRODUCTION

The china clay waste produced by Goonvean Ltd, in St. Austell, United Kingdom, is a potential source of lithium (0.84% Li_2O, 0.36% Rb_2O). Lithium is contained in some of the mica minerals present in this material. The froth flotation technique, using dodecylamine as a collector, and magnetic separation were used to separate the mica minerals from mainly quartz and feldspar contained in the china clay waste. Among the mica minerals, zinnwaldite ($KLiFeAl(AlSi_3)O_{10}(F.OH)_2$) is the major source of lithium with smaller amounts being contributed by muscovite.

Lithium is important for a number of uses, including production of batteries, glass and ceramics, production of aluminium, preparation of greases, rubbers, alloys and pharmaceuticals. Worldwide, rechargeable lithium batteries power about 60% of cellular telephones and about 90% of laptop computers and are a constituent of batteries for electric and hybrid vehicles (Harben, 2002; Garret, 2004; Smith, 2010). The small size of the lithium cation allows it to fit within the molecular structure of other compounds, thus lowering the melting point of glass and ceramics, making them cheaper to produce, giving them greater strength and a lower thermal expansion coefficient (Garret, 2004). Forecasts indicate that the demand for lithium in the next five years is expected to increase by approximately 60% from 102,000t to 162,00t of lithium carbonate or equivalent (LCE), with batteries representing more than 40,000t of the perceived growth (Hykawy, 2010).

The primary sources of lithium are from continental brines which contain about 0.06-0.15% Li followed by pegmatites. The principal lithium minerals from pegmatite with their theoretical maximum lithium content are spodumene $LiAlSi_2O_6$ (8.0% Li_2O), petalite $LiAlSi_4O_{10}$ (4.9% Li_2O), lepidolite $KLiAl_2Si_3O_{10}(F.OH)_3$ (7.7% Li_2O) and zinnwaldite $KLiFeAl(AlSi_3)O_{10}(F.OH)_2$ (2.5-5% Li_2O), which is regarded as a variety of lepidolite with a high iron content (Harben, 2002; Garret, 2004; Wietelman and Bauer, 2008).

Processing of lithium aluminosilicates is based on breaking down the lithium minerals during their heating with chemicals followed by acid or water leaching of the products obtained. This is an energy intensive chemical process. The total cost of the processes is significantly affected by processes such as fine grinding, high temperature roasting and evaporation. The high cost of extracting lithium from silicate minerals has resulted in almost all production of

lithium worldwide to shift to brine deposits. Thus it would be desirable to provide an improved method of extracting lithium from minerals that has lower production costs, so that the china clay waste could be exploited economically. A number of lithium extraction processes have been reported for spodumene, petalite, lepidolite (Wietelmann and Bauer, 2008; Dresler et al., 1998) and zinnwaldite (Alex and Suri, 1996; Jandova et al., 2008, 2009). The gypsum method of lithium extraction, which involves roasting a mixture of lithium concentrate and gypsum has been reported (Jandova et al., 2008, 2009) but there are no reports of the use of sodium sulphate.

It has been estimated that approximately 100,000 tonnes per year of micaceous residues containing about 0.84% Li_2O are available for treatment from Goonvean Ltd. Additional throughput would also be possible by reprocessing material held in nearby tailings dams. The Goonvean china clay waste has several advantages compared to other sources of lithium, apart from brines, in that the material is already fine and therefore there is no need to mine or to grind before flotation, suggesting a substantial cost saving. In addition, the tailing from the flotation process may be further processed to produce quartz and feldspar products.

After the depletion of lithium from brine deposits in the world, the Goonvean china clay wastes may become a reserve source of lithium. And as the lithium demand grows coupled with price increases, there is likely to be increased lithium extraction from pegmatites and possibly from lower grade resources such as the Goonvean china clay waste. Processing these wastes would greatly contribute to the company's income.

The main objectives of this research were:

1. To optimise the reagent dosages (addition rate) and operating conditions (air flowrate, impeller speed and pH) for the separation of mica minerals from china clay waste using froth flotation.

2. To investigate other physical separation techniques for the recovery of lithium-mica from the bulk mica concentrate.

3. To investigate the possibility of extracting lithium from the lithium-mica concentrate by leaching using the gypsum, the limestone and the previously untried sodium sulphate methods, and establish the optimum roasting and leaching conditions.

4. To evaluate the Life Cycle Analysis (LCA) and economics of the proposed lithium extraction process.

The thesis is arranged as follows:

1. Chapter 1 sets the scene as introduction. It gives the background and the objectives of the research undertaken.

2. Chapter 2 covers the extensive use of lithium. This chapter deals with the various application of lithium/lithium bearing minerals in the manufacturing of glass, ceramics, batteries, grease and air conditioning among others.

3. Chapter 3 provides information on the geology of the St Austell area. This region is of great importance primarily as a source of kaolin and secondly as a potential source of lithium. The chapter gives details of the mineralogy of the St Austell granites (including the biotite granite; tourmaline granite; topaz granite and the lithium mica granite).

4. Chapter 4 discusses the processing of china clay from Cornwall and Devon. It further deals in general with the processing of china clay by way of high gradient magnetic and flotation separations.

5. Chapter 5 covers the flotation fundamentals in general. It also deals with the mica separation processes such as flotation with reagents employed and the magnetic separation method.

6. Chapter 6 describes the various commercial lithium minerals. It provides the various lithium extraction methods. The chapter also discusses the global lithium market and production capacity.

7. Chapter 7 covers the experimental work. It gives the source and analyses performed on the material, including the various experimental tests undertaken.

8. Chapter 8 gives the experimental results obtained. The chapter also deals with the estimation of the mineralogy of the separation products.

9. Chapter 9 covers the economic appraisal for the production of lithium carbonate from china clay waste. It provides the proposed process flow diagrams and the cost estimation in setting up and running the processing plant.

10. Chapter 10 talks about the Life Cycle Assessment of the lithium carbonate production plant. It explains the environmental issues related to the processing of china clay waste and the subsequent production of lithium carbonate.

11. Chapter 11 discusses the results obtained.

12. Chapter 12 deals with the conclusions. Major findings of the research are highlighted.

13. Chapter 13 covers the recommendations for future work to supplement and follow on what has been achieved.

The diagram below (Figure 1.1) shows the arrangement of the research and work done.

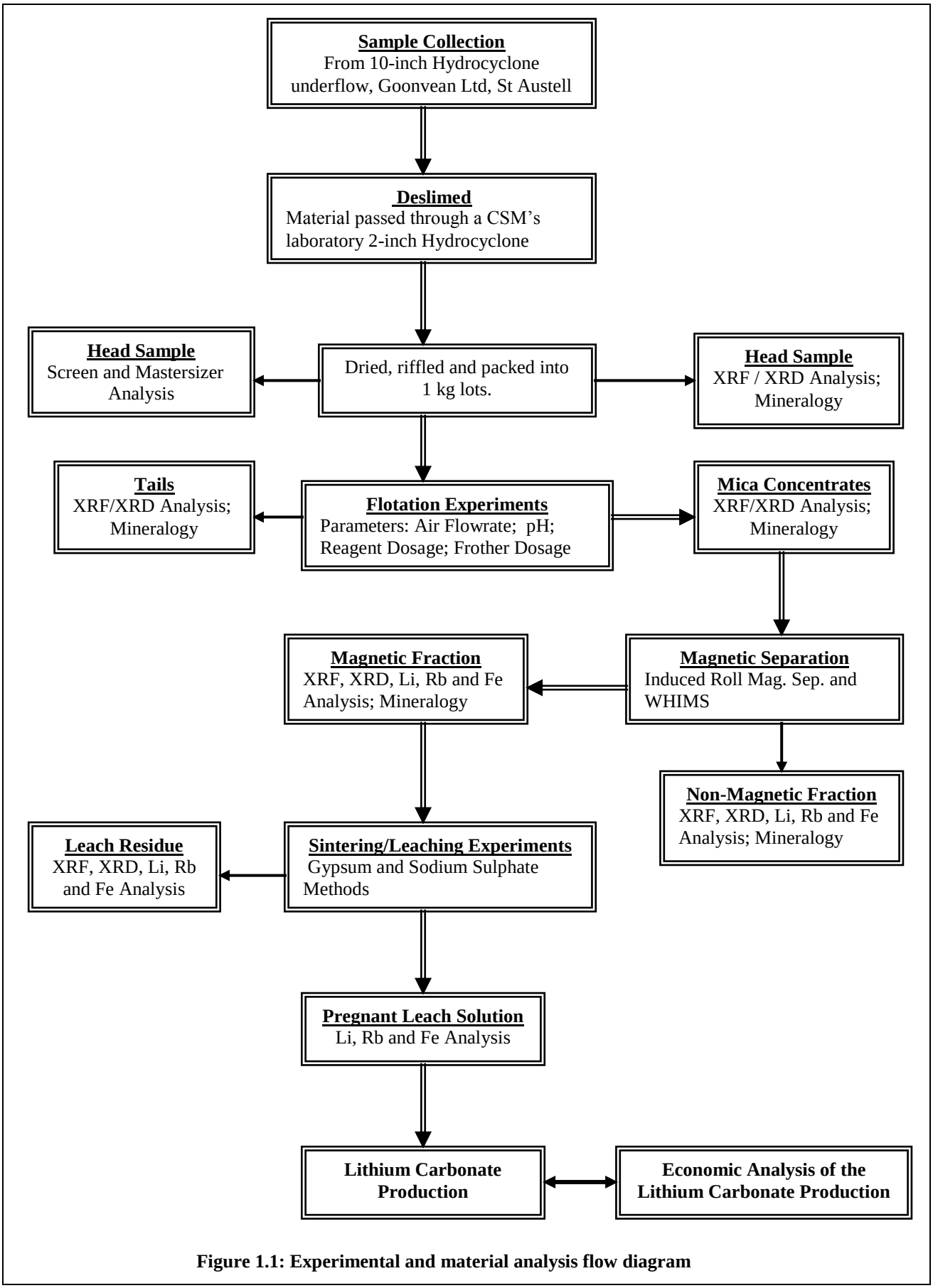

Figure 1.1: Experimental and material analysis flow diagram

2. USES OF LITHIUM

Lithium has a wide variety of uses, which have varied widely over time. In the early days of the industry, battery manufacturers were the largest purchaser of lithium (as metal or chemicals), followed by grease as the dominant customer. Then glass and ceramics followed for 10 - 15 years. From 1990 onwards the market has become much diversified, with glass and ceramics being the largest purchaser of lithium chemicals or ore concentrates (Garrett, 2004, Smith, 2010).

2.1 Glass

In the glass industry lithium helps to make many types of products, such as borosilicate glass, containers and bottles, fibreglass, pharmaceutical glass, television tubes, thermal shock-resistant cookware and sealed-beam headlights. In the preparation of glass lithium is said to have many benefits, such as increasing the melting rate by lowering the viscosity of the glass and reducing the melting temperature (Harben, 1999; Garrett, 2004; Christie and Brathwaite, 2008). Many of the lithium ore concentrates have a low enough iron content to be used directly in some glass formulations, while other glasses require a higher purity lithium source. Garret (2004) also mentioned that some ores can even be used without being transformed into higher-purity concentrates, as long as the lithium content is high enough and the iron sufficiently low. The glass grade spodumene from Australia with a minimum of 4.8% Li_2O and maximum 0.2% Fe_2O_3 is such an example.

2.2 Ceramics

Lithium is used in ceramics to make frits and glazes, sanitaryware, shock-resistant ceramics and porcelain tiles. Lithium has also been reported to lower the melting temperatures with increasing fluxing power when either alone or combined with other compatible materials such as feldspar (Harben, 1999). This has the benefit of improving the product quality, plant efficiency and productivity by lowering the firing temperature (Harben, 1999; Garrett, 2004). Other reported benefits are that it forms products with lower thermal expansion coefficients and more stain resistance. Lithium is also one of the ingredients that has permitted the production of glass-ceramics, in which glass is forced to crystallize into very fine crystals that form a dense, strong and heat-resistant ceramic material. Again both ores and lithium compounds can be used for this application. With ores, petalite is usually preferred over

spodumene, because there is no volume structure or phase change as it is heated (Garret, 2004).

2.3 Batteries

The use of lithium as the battery of choice for most cellular phones today has enabled manufacturers to provide a cellular telephone with a battery life in some cases of up to a week (Smith, 2010). Lithium is the most electropositive of all metals, with a standard electrode potential of 3.045 V compared with 2.71 V for sodium and 0.76 V for zinc. It thus can generate the greatest electrical power per unit weight or volume of any metal, but it is also extremely reactive and thus potentially dangerous (Garret, 2004, Smith, 2010). In 2001 there were four common types of rechargeable batteries: lithium-ion (52% of the market), lithium polymer (4%), nickel metal hydride (27%), and nickel-cadmium (17%), (Garret, 2004). Amongst these, the lithium-ion and lithium polymer batteries could store and deliver the most energy per unit space, with the commercial batteries producing 3.7 V, or about three times more than the nickel cadmium or nickel metal hydride batteries. They were lighter, had a longer shelf life, and did not have the "memory effect" problem (the amount of energy stored was decreased if the battery was charged before having been fully discharged) of the nickel batteries (Garrett, 2004). They were thus preferred for the newer generations of high-performance applications such as in mobile phones, camcorders, laptop computers, hand-held portable electronic devices, home repair or construction tools and medical devices, even though they were more expensive than some other batteries (Garret, 2004). Moores (2010) reported that the lithium-ion (Li-ion) battery is set to see a rise in demand over the next five years and will have positive implications for mineral and chemical producers as the economics of the technology improve.

2.4 Grease

The other use of lithium is in the form of lithium stearate as a thickener for lubricating greases (Christie and Brathwaite, 2008). Considerable lithium hydroxide is also used in making greases, and the demand grew at a steady 2% per year for the period 1980-2000 (Garrett, 2004). Mixtures containing 5-10% of the lithium soap are an excellent lubricant for bearing surfaces, since they are almost totally water insoluble and stable in consistency over a range of shear and temperatures from - 55 to + 200^{o}C (Garrett, 2004).

2.5 Air Conditioning

Lithium is also used in air conditioning where lithium bromide or chloride are used in the dehumidification of air and other gases because of the very low vapour pressure of their solutions, their low viscosity, high stability, non-toxic properties and low corrosivity. Both lithium bromide and chloride are extremely hygroscopic and can dry air or other gases down to very low moisture content. As they remove water from the air, the gas is also cooled, thus providing a refrigeration effect (Harben, 1999; Garrett, 2004; Christie and Brathwaite, 2008).

2.6 Aluminium

In metallurgy lithium metal is used to degas (scavenge or remove gas from) aluminium, copper, bronze, a process which results in these three purified metals having a higher electrical conductivity. Lithium has also been employed in the aluminium industry where it lowers the electric reduction cells' temperature, raises the electrical conductivity of the cell (thus lowering the required overvoltage, which reduces the power requirement), and it reduces the fluorine emissions from the electrolytic cells by 25-50% (Harben, 1999; Garrett, 2004; Christie and Brathwaite, 2008).

2.7 Lithium Metal

The market for lithium metal has been reported to be growing because of its use in making batteries, organic chemicals, alloying and other applications. It is actually made by the electrolysis of a molten lithium chloride-potassium chloride mixture in specially designed cells, with the molten metal collecting in the top while being periodically withdrawn and cooled as ingots. Some lithium is alloyed into lithium-aluminium and lithium-magnesium metals because of their low density, high-temperature performance, improved elasticity, tensile strength and corrosion resistant (Harben, 1999; Garret, 2004). It is also a special ingredient in alloys used in commercial or military aircraft construction.

2.8 Miscellaneous Uses

As a medicine, lithium carbonate or acetate is reported to have been used in the treatment of manic depression. It is used in very small quantities, since too much can be toxic and have serious side-effects, while too little will not be effective and hence it is closely monitored in the blood stream of patients. However, the reason for its effectiveness has remained a mystery

as is the case with some of its modern competitive medicines (Garrett, 2004). Lithium carbonate is also used in large-scale laundries as bleach, and in swimming pools, as it provides excellent sanitation while minimising the growth of algae. Lithium vapour is used to prevent carbon dioxide and oxygen from forming scales in furnaces in heat-treating steel (Christie and Brathwaite, 2008).

3. GEOLOGY OF ST AUSTELL

The St Austell granite is of major importance as a source of high quality kaolin (china clay), supplying up to 3 million tonnes of clay per annum for the paper, ceramics, paints, plastics and rubber industries. Production is supplied from a large number of open pits scattered throughout the western part of the granite outcrop within a complex landscape of spoil heaps and mica lagoons shown in Figure 3.1 (Manning et al., 1996).

In describing the mineralogy of the St Austell granite, Richardson (1923) proposed a threefold classification; biotite-muscovite granite, lithium-mica granite and gilbertite granite. Each phase was considered to be a separate intrusion, but according to Hill and Manning (1987) four different granite types had been identified in southwest England: biotite granite, lithium mica granite, the tourmaline granites and topaz granite. Later Manning et al., (1996) carried out a geological mapping of existing and redundant kaolin workings within the St Austell granite and identified a suite of granitic rocks which showed evidence of complex late-stage magmatic and hydrothermal processes. They said that the coarse biotite granites, like those which predominate in southwest England, occurred much more widely than previously acknowledged, and are intruded by a suite of lithium-mica granites and tourmaline granites. They observed that the tourmaline granites characteristically exhibit very variable textures, with coarse quartz grains set within a fine grained, tourmaline-rich matrix and that a highly evolved fine-grained tourmaline granite represented the most evolved of this suite.

The granites of South West England share several basic characteristic which have been discussed in greater detail in a number of reviews (Alderton, 1990; Floyd et al., 1993; Manning, 1996). Manning et al., (1996) carried out field and petrographic observations which enabled six granite varieties to be distinguished essentially on the basis of texture.

3.1 Biotite Granite

Biotite granite has been reported to be the dominant lithology, forming up to 70% of the outcrop of the St Austell granite, and corresponds to the coarsely porphyritic biotite granites typical of the Lands End and Dartmoor granites (Hawkes et al., 1987; Exley et al., 1983; Manning et., 1996). Two micas are present: biotite varies in composition from siderophyllite to annite, and contains monazite, uraninite, rutile and zircon as accessory phases, while muscovite occurs as rims and overgrowths on biotite. Prismatic tourmaline characteristically

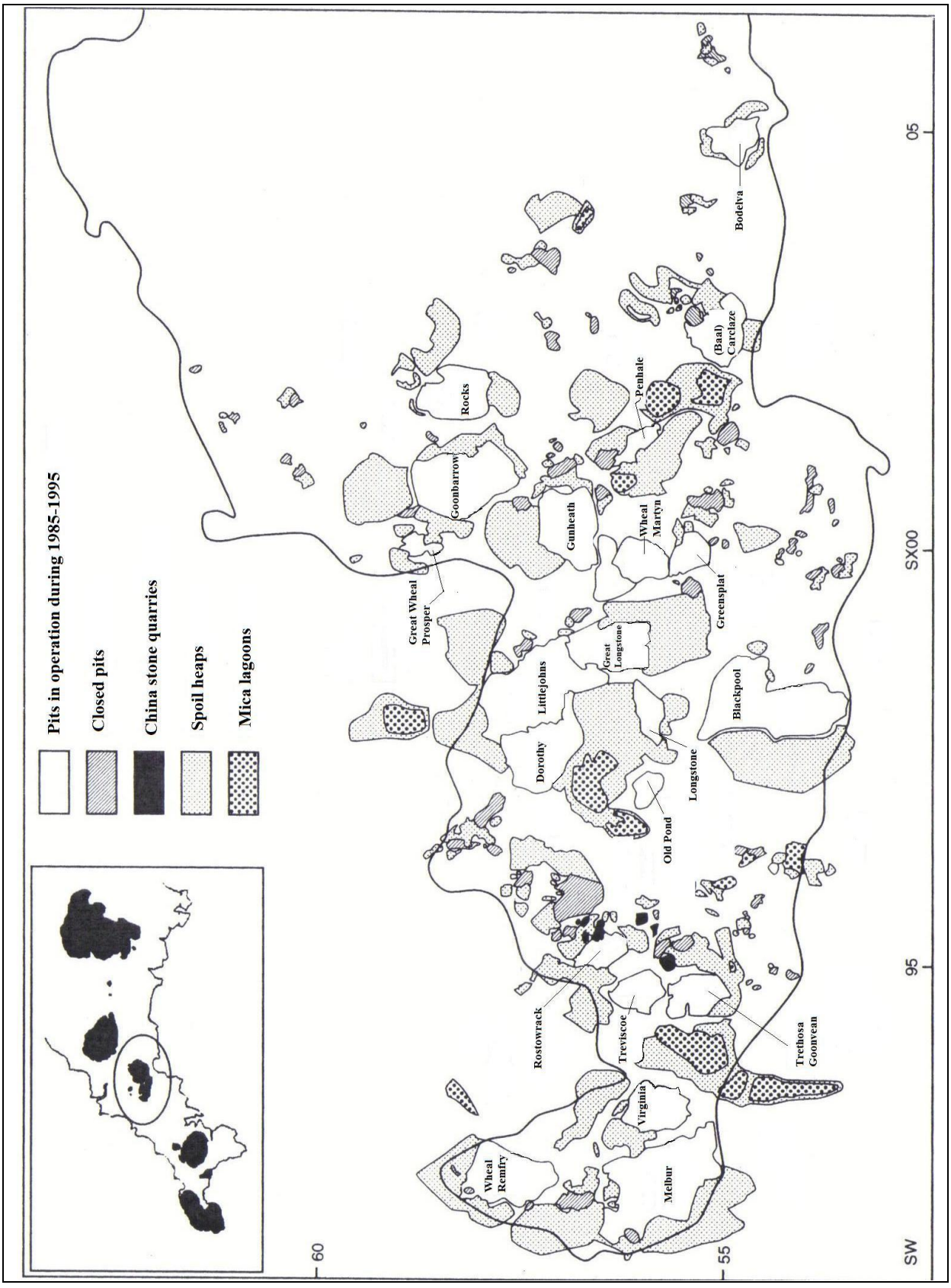

Figure 3.1: Distribution of china clay pits, spoil heaps and mica lagoons in the St Austell area (circled on inset map), Cornwall (from Manning et al., 1996).

displays late-post-magmatic growth, as an interstitial phase associated spatially with biotite, and fingering into K-feldspar (Manning et al., 1996).

3.2 The Lithium-Mica Granite

Extensive work on the lithium potential of the St Austell granite has been carried out by the British Geological Survey (Hawkes et al., 1987). Manning et al., (1996), also described the lithium mica granite as similar in both grain size and texture to the biotite granite. They said it was more leucocratic owing to the presence of lithium mica of zinnwaldite composition. The zinnwaldite appears distinctly, as brown mica in hand specimen, contrasting strongly with black biotite. In additional to quartz and K-feldspar, plagioclase is richer in the albite component, and tourmaline being common as euhedral grains. Accessory phases include apatite, monazite, zircon and rutile, which occur as inclusions within zinnwaldite, while plagioclase contains apatite, fluorite and secondary micas. Additional alteration effects include the development of fine-grained aggregates of topaz, and the replacement of zinnwaldite by tourmaline (Manning et al., 1996).

3.3 The Tourmaline Granites

According to Manning et al., (1996) this tourmaline granite could be subdivided in the field to include facies characterized by large (1-2 cm) rounded quartz grains also known as the globular quartz facies, a medium-coarse-grained equigranular facies and a fine-grained equigranular facies.

They said that unlike other granite varieties, the globular quartz facies characteristically showed considerable textural variation. It contained large quartz grains, up to 2 cm, which in thin section appeared to be polycrystalline aggregates. The lithium mica (zinnwaldite) was said to be corroded while undergoing replacement by quartz and K-feldspar to leave the so called isolated mica ‘islands’ (Manning et al., 1996). The fine grained groundmass formed a mosaic of quartz, K-feldspar, plagioclase, zinnwaldite and tourmaline. A close spatial association between topaz and tourmaline with areas of replacement within lithium mica had been also reported (Manning et al., 1996).

The medium-coarse-grained equigranular facies of the tourmaline granite was of medium grain size (0.5-1 cm), and in the field was characterized by large, euhedral, tourmaline

needles. Manning et al., (1996) reported two micas present, subhedral zinnwaldite which was brown in hand-specimen while colourless-pale brown in thin section and muscovite which appeared as white-yellow in hand-specimen and colourless in thin section. Alteration was indicated by the invasion of K-feldspar by topaz and fluorite, replacement of zinnwaldite by quartz and the presence of topaz aggregates. Accessory phases included apatite, zircon and rutile (Manning et al., 1996).

Manning et al., (1996) reported the fine-grained tourmaline granite as having a grain size of < 0.5 mm and that it was an equigranular rock. They further said the lithium-rich zinnwaldite was again present occurring as aggregates with prismatic zoned tourmaline, quartz and topaz. The tourmaline often formed a central core to extensive secondary skeletal overgrowths which were said to invade and finger into topaz. Accessory phases include apatite, monazite and zircon (Manning et al., 1996).

3.4 Topaz Granite

According to Manning et al., (1996), the topaz granite is fine-medium grained (approx 0.5 mm) and characterised by euhedral-subhedral topaz, anhedral lithium mica of varying in composition from zinnwaldite to lepidolite. It also contained unzoned euhedral albite, anhedral K-feldspar, which included orthoclase and microcline, and subhedral quartz (Manning et al., 1996). They further said this topaz granite contained a smaller proportion of accessory minerals than the other granites, but a wider variety including apatite (Mn bearing), amblygonite, zircon, Nb-Ta oxides and uraninite (Manning et al., 1996). Topaz, tourmaline and the micas also contained zircon, Nb-Ta-Ti oxides and apatite, while apatite itself hosted zircon and uraninite (Manning et al., 1996). London and Manning (1995) have reported tourmaline to be present as ragged grains, which was unusual compared with that in other granite varieties in that it was particularly rich in the albite component. Fluorite has also been reported to be present as an alteration phase along mica cleavages and at the contact between altered topaz and plagioclase (Manning et al., 1996).

Manning et al., (1996) summarised the distribution of the granite types described above in Figure 3.2.

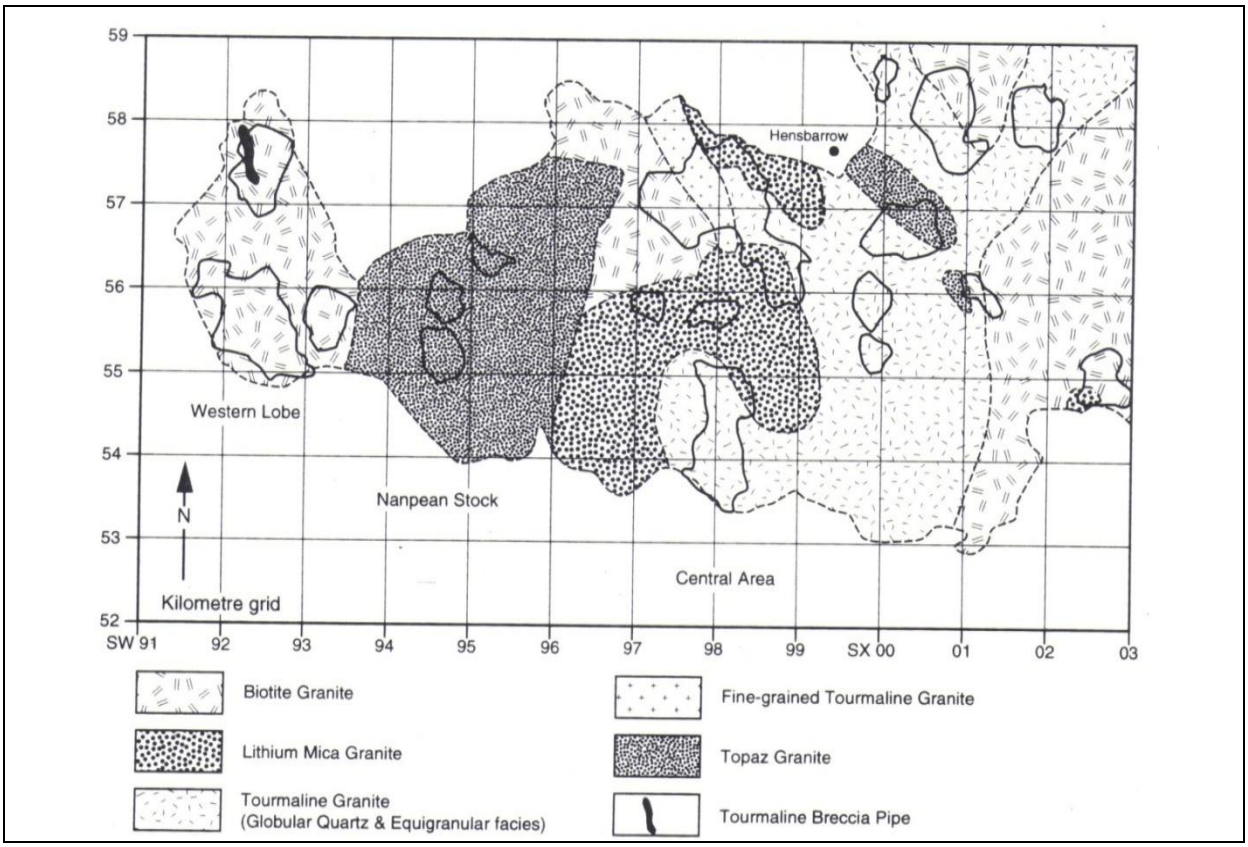

Figure 3.2: Distribution of granite varieties in the western part of the St Austell Granite, identifying the Western Lobe, Nanpean Stock and Central Area which are described in the text (from Manning et al., 2006).

4. CHINA CLAY FROM CORNWALL AND DEVON

Cornwall and Devon produced up to three million metric tons annually of china clay in the 1980s (Highley et al., 2006), although the production now is much lower. China clay is used by the paper, ceramic and many other industries and is a major raw material export for the United Kingdom second only to North Sea oil and gas (Thurlow, 2001).

It has been reported by Thurlow (2001) that the granite moors of Devon and Cornwall, contained three minerals (feldspar, quartz and mica) when first formed about 300 million years ago. In other areas of this granite, it is believed the white feldspar has since been decomposed to a fine sized soft white mineral called kaolinite, which is the main constituent of china clay. The process of kaolinisation has not affected the micas and quartz and thus small amounts of fine particle size quartz and mica tend to be present in the china clay (Thurlow, 2001). According to Thurlow (2001), geologists have debated how feldspar was altered to china clay for almost two centuries and that two theories were proposed. The first was the hydrothermal theory, which stated that kaolinisation took place as a result of hot gases and fluids rising from below ground, through the granite, soon after it was formed. The other proposition was that china clay had been formed as a result of weathering. However, after much scientific research and debate it is now evident that a sequence of events took place which includes both theories (Thurlow, 2001). It is believed now that the hydrothermal action came first and began the alteration process as well as introducing metalliferous deposits such as tin ores and quartz/tourmaline veins. A stage of weathering is said to have taken place afterwards when water from the surface entered cracks in the rocks and that this water was warmed at depth by heat due to the unusually high content of radioactive elements in the granite. Eventually, this resulted in a slow convective circulation of water, which over hundreds of millions of years, altered feldspar to kaolin (Thurlow, 2001).

The processing of china clay has been divided into three main phases and Figure 4.1 shows the processing flow chart redrawn after Thurlow (2001). The process begins with water at high pressure being directed at the decomposed granite to produce raw clay which is pumped to central refining units. The clay is further upgraded for export quality by classification. After undergoing the refining process, it is pumped to a large drying plant where it is dried and stored to await distribution. Currently, china clay is produced after dry mining, milling and classification with Goonvean Ltd producing about 100,000 tonnes per year.

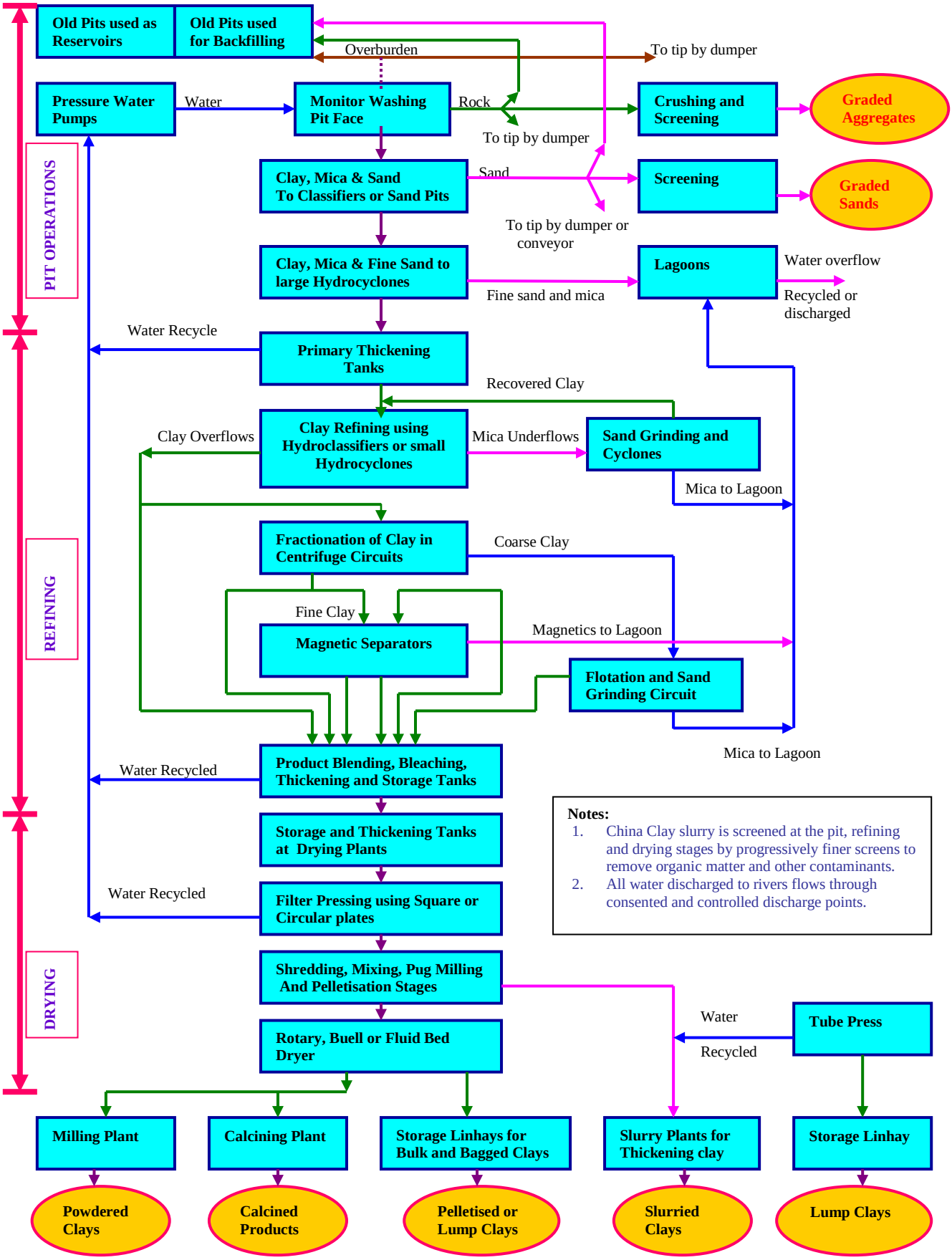

Figure 4.1: Simplified flow diagram of china clay production (from Thurlow, 2001)

4.1 Processing of China Clay

China clay or kaolin is a commercial clay composed principally of the hydrated aluminosilicate clay mineral kaolinite ($Al_2O_3.2SiO_2.2H_2O$). Kaolin is used in many industrial applications due to its unique physical, physiochemical and chemical properties. These include fillers, ceramic, paper, paint, rubber, glass, refractory, agriculture, waste treatment, cosmetic applications and for nanocomposites as coating, pigment and acid/base regulator. The commercial value of kaolin is based on the mineral's whiteness and its fine, but controllable, particle size which may be optimised during processing.

Generally, china clay as mined contains a number of ancillary mineral impurities such as coarse and fine sand (silica), iron oxides, titaniferous minerals, mica, feldspar etc. Depending upon the purity required, the clay is to be processed by suitable techniques to remove or reduce the amount of iron, titaniferous, micaceous and carbonaceous minerals which affect the brightness of kaolin. However, small amounts of 'structural' iron do not affect the brightness (Jepson, 1988).

Around 75% of the world's production of china clay goes to the paper industry alone for coating and filling. The paper coating grade kaolin is specified and controlled in terms of (1) particle size distribution, (2) brightness and sometimes also shade, and (3) rheology as a deflocculated suspension in water (Jepson, 1988). However, the ultimate properties required for the coating grade are the inking ability and final properties of inked paper (Delon et al., 1982).

Recently, research has been conducted on clay samples to determine the surface properties and interfacial interactions of kaolin clay (Hu et al., 2005; Hu, Jiang and Wang, 2003; Hu and Liu, 2003). Because of the size of the kaolin particle and its platelet structure, the beneficiation and dewatering of the material are the main interests of many plants. In order to improve the quality of kaolin clay for industry, the discolouring impurities must be removed from the samples by suitable separation techniques (Raghavan, Chandrasekhar and Damodaran, 1997; Asmatulu, 2002). These separations generally include magnetic separation, froth flotation, selective flocculation, size separation using hydrocyclone or centrifuge and leaching (Basilio, 1997; Yoon and Shi, 1986). Numerous publications are

available for the removal of titaniferous impurities by froth flotation with different reagent combinations (Mullary, 1974; Nott, 1976; Billimoria, 1984; Bacon, 1987).

4.1.1 High-Gradient Magnetic Separation

Kaolin clay sometimes contains several magnetic discolouring impurities, such as anatase, hematite, pyrite, mica and rutile with magnetic susceptibilities of approximately $10^{-6}/cm^{-3}$ (Yoon and Shi, 1986). Conventional and superconducting magnetic separations are typically employed units with 1-2 Tesla and 2-5 Tesla magnetic fields, respectively. The prepared clay sample with a 15 – 25% solid content is fed through a high gradient magnetic field created around the ferromagnetic stainless steel wool fibre. The magnetic separations are generally operated as a batch unit with 10-20 min cycles depending on the size of the units, feed rate, solid content, impurity content, applied field, machine capacity, etc. D'Assumpcao and others (1995) reported the brightness of Brazilian kaolin being increased from 87% to 90% using superconducting high gradient magnetic separation at 5 Tesla magnetic field. The tests were conducted at 25% solid content after the samples were sized in a centrifuge (i.e., 90% is finer than 2 μm). It was also determined that high gradient magnetic separators were effective for the nanosize discolouring elements to produce high brightness clay. Therefore, other processes (i.e. flotation and/or selective flocculation) can be incorporated to increase the brightness of kaolin clay (Basilio, 1997; Khalek et al., 1996). The brightness improvement of china clay by high gradient magnetic separation (HGMS) is due to the combined removal of mica, titaniferous impurities and other iron-containing minerals (Jepson, 1984, 1988).

A more recent high gradient magnetic separator is the high-gradient superconducting type reported by Outotec of Finland (www.outotec.com, 2010). These superconducting magnetic separators, known by the trade name Cryofilter^{R} HGMS, are said to allow separation of the most weakly magnetic particles at high capacity and low cost. They are reported as the world's most powerful industrial-scale superconducting magnetic separators and are important in the magnetic treatment of fine slurries. The equipment can be used in kaolin, $CaCO_3$ and talc applications. They can treat materials of less than 75μm at a magnetic field strength of up to 5 Tesla.

4.1.2 Flotation Separation

The flotation of anatase (titaniferous) in fine kaolin clay is said to be a difficult task in the clay industry. The reason may be that the bubbles generated in conventional flotation cells are too large to capture the ultrafine particles, which are usually less than 2μm (Basilio, 1997). However, froth flotation has been used to remove anatase minerals from kaolin clay due to the better efficiency (high yield and low impurity content) of the method compared to the other separation techniques (Luz et al., 2000; Khalek et al., 1996). In the early flotation process (Yoon and Shi, 1986), the anatase minerals were floated using 3 to 4 kg/t of tall oil or fatty acids as collectors at pH 9-10 after they were activated by divalent cations (i.e. Ca^{2+} and Pb^{2+}). It was determined that approximately 100-150 g/t of calcite carrier (caustic soda) could activate the anatase minerals in the kaolin clay. In the early stage of flotation, the kaolin is dispersed using 3.5 kg/ton of sodium silicate, 3.5 kg/t of ammonium hydroxide for the saponification of the collector and pH regulator and 1.5 kg/t of petroleum sulfonate (Basilio, 1997).

Asmatulu (2002) also reported the reduction in the titanium content from 2.18% to 1.27% TiO_2 with a yield (weight recovery) of 72.6% and improved brightness after the dispersed kaolin clay was subjected to flotation tests at pH 9.5 using 0.75 kg/t of hydroxamates (Aero 6973) as a collector and 120 g/ton of polypropylene glycol (PPG) as a frother.

5. FROTH FLOTATION

Froth flotation has been described as a process used to separate minerals, suspended in liquids, by attaching them to gas bubbles, which rise to the surface of the pulp. It is the cheapest and most extensively used process for the separation of chemically similar minerals.

The process involves imparting a water-repellent (hydrophobic) character to the desired mineral particles with the aid of chemicals that are called collectors or promoters. Under favourable conditions, these chemically coated mineral particles become attached to the air bubbles rising through a pulp and will thus "float" to the surface. If the surface tension of the pulp is then reduced by a second chemical, called a frother, a stabilised froth containing the desired mineral particles will form on the surface of the pulp. All the factors that play a role in this process will be dealt with later in greater detail.

Flotation is a physico-chemical separation process that utilises the difference in surface properties of the valuable minerals and the unwanted gangue minerals (Wills and Napier-Munn, 2006). Nagaraj (2005) observes that this statement actually implies that both physical and chemical factors are equally important in flotation, and that flotation outcome is determined by the complex interactions among all these factors. Thus the flotation system has been represented schematically in various published literature in the form of a triangle shown in Figure 5.1, with the important factors occupying the three corners of this triangle (Nagaraji, 2005). This triangle has been reported to signify an inevitable trade-off. Chemical factors include the interfacial chemistry involving the three phases (viz. solid, liquid and gas) in the flotation system, particularly in the froth phase. Interfacial chemistry is dictated by all the process variables and all the flotation reagents such as collectors, depressants, frothers, activators, pH modifiers, water chemistry and the chemistry of the minerals. Physical factors comprise equipment components (cell design, hydrodynamics, bank configuration, bank control, etc.) and operational components (feed rate, mineralogy, particle size, pulp density, the various pulp flow rates, etc.).

The recovery and selectivity of the flotation process are dependent not only on chemical variables, such as the pulp pH, types and amounts of reagents, but also on the hydrodynamic conditions within the mechanical cell. These conditions facilitate the attachment of hydrophobic particles to air bubbles and allow the levitation of mineralised bubbles to the

froth phase. In other words, the hydrodynamic parameters of flotation machines play a major role in particle / bubble collision, attachment and transport to the froth.

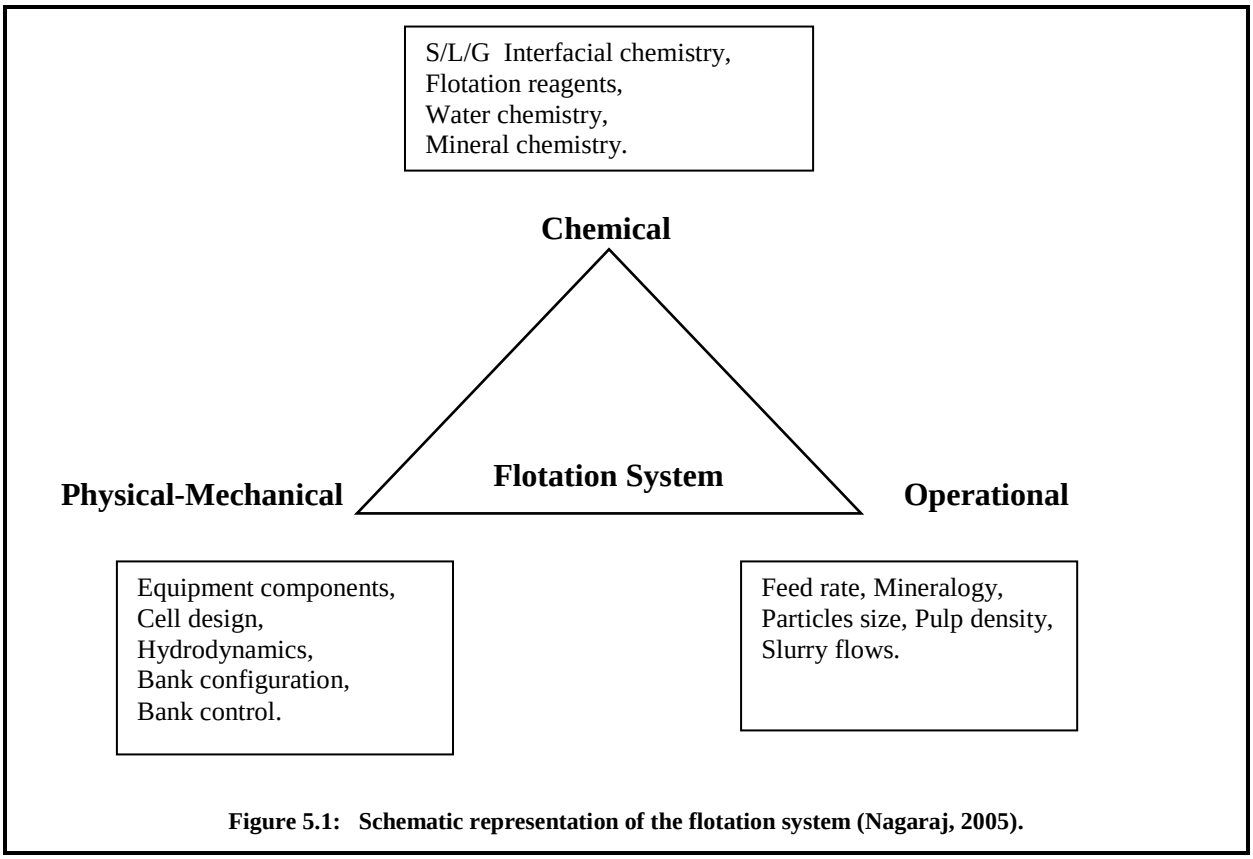

Figure 5.1: Schematic representation of the flotation system (Nagaraj, 2005).

The activity of a mineral surface in relation to flotation reagents in water greatly depends on the forces which operate on that surface (Wills and Napier-Munn, 2006; Fuerstenau et al., 1985). Whether or not bubble attachment and aggregation occur is determined by the degree to which a particle's surface is wetted by water. The surface is said to be hydrophobic when it shows little affinity for water. The stability of this attachment is measured by the contact angle, θ, developed between the three phases: liquid, solid and gas. The forces trying to separate a particle and a bubble are shown in Figure 5.2. These are the forces which lead to the development of an angle between the mineral surface and the bubble surface. The contact angle is zero when the air bubble does not displace the aqueous phase and on the other hand, complete displacement of the water represents a contact angle of 180^{o}C (Fuerstenau et al., 1985). According to Fuerstenau et al., (1985), the values of contact angle between these two extremes give an indication of the degree of surface hydration, or, conversely, the hydrophobic character of the surface. A few naturally hydrophobic minerals such as coal,

molybdenite, sulphur and talc, exhibit contact angles less than 108^{o}C. Fuerstenau et al., (1985) mentioned that there are no known solids that exhibit a contact angle greater than 108^{o}C which is the value obtained with Teflon. Most minerals are hydrophilic and, therefore, must acquire their hydrophobic character by the adsorption of surfactants known as collectors for the air bubble attachment to occur. The three-phase equilibrium between the air bubble, mineral surface and water has been described by the respective interfacial tensions according to Young's equation:

$$\gamma_{s/a} = \gamma_{s/w} + \gamma_{w/a} \cos\theta \tag{5.1}$$

where $\gamma_{s/a}$, $\gamma_{s/w}$ and $\gamma_{w/a}$ are the surface energies (J/m^2) between solid and air, solid and water, and water and air, respectively, and θ is the contact angle between the mineral surface and the bubble (Wills and Napier-Munn, 2006).

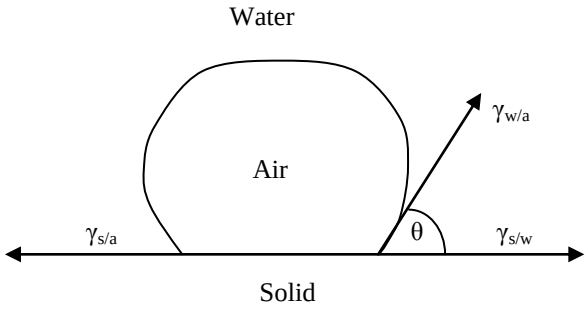

Figure 5.2: Contact angle between bubble and particle in an aqueous medium (Wills and Napier-Munn, 2006).

The force required to break the particle-bubble interface is called the *work of adhesion*, $W_{s/a}$, and is equal to the work required to separate the solid-air interface and produce separate air-water and solid-water interfaces, i.e.

$$W_{s/a} = \gamma_{w/a} + \gamma_{s/w} - \gamma_{s/a} \tag{5.2}$$

Combining with Equation 5.1 gives

$$W_{s/a} = \gamma_{w/a}(1 - \cos\theta) \tag{5.3}$$

Thus it could be seen that the greater the contact angle the greater is the work of adhesion between particle and bubble and, therefore, the more resilient the system is to disruptive

forces (Wills and Napier-Munn, 2006). As the contact angle increases, the hydrophobicity of a mineral also increases and, therefore, minerals with a high contact angle are said to be aerophilic, i.e. they have a higher affinity for air than for water (Wills and Napier-Munn, 2006). Most minerals in their natural state are not water-repellent and, therefore, flotation reagents must be added to the pulp.

It is a well known fact that flotation depends directly on the nature and properties of mineral-water interfaces and according to Fuerstenau (1982), two factors are important: (1) the interaction of water molecules with the mineral surface, both in liquid and gaseous environments, and (2) the electrical double layer at the solid-water interface. Fuerstenau (1982) mentioned that the oriented water layers at mineral surfaces have a paramount effect on the wettability of solids and also on the type of adsorption at an interface. On the other hand, he said that the electrical double layer can affect the flotation process in many different ways and I quote (Fuerstenau, 1982):

1. The sign and magnitude of the surface charge controls the adsorption of physically adsorbing flotation agents.
2. A high surface charge can inhibit the chemisorption of chemically adsorbing collectors.
3. The flocculation and dispersion of mineral suspensions is controlled by the electrical double layer.
4. The double layer on air bubbles has a significant effect on naturally floating mineral systems.
5. Flotation kinetics relate directly to the effect of double layers on the kinetics of film thinning.

Fuerstenau (1982) defined an electrical double layer as a system in which there exists a separation of electrical charge at an interface; meaning that there is a layer of positive charge and a layer of negative charge, with the whole system being electrically neutral. This is important in flotation as it affects the adsorption of surface-active agents. There are many mechanisms by which mineral surfaces become charged such as the isomorphous substitution in the lattice of solids of which a good example is the replacement of S^{4+} by Al^{3+} in the lattice of clays. According to Fuerstenau (1982), the single most important parameter describing the mineral surface is the condition under which the surface charge is zero and the activity of potential-determining ions at which this occurs is called the point-of-zero-charge, the PZC. The PZC is very important in that the sign of the surface charge has a tremendous effect on

the adsorption of all other ions and especially those charged oppositely to the surface because they function as the counter-ions in order to maintain electroneutrality.

Fuerstenau and Fuerstenau (1982) mentioned that the surface properties of silicate minerals are influenced by the crystal chemistry. They said that the formation of an electrical double layer at the interface between a silicate mineral and an aqueous medium has long been considered to be controlled by broken –Si-O and -M-O bonds at the surface of the mineral (M being Al in the case of aluminosilicates). The sheet silicate minerals exhibit a wide range of surface properties. For example, the two-layer silicate, kaolinite, has a hydrophilic surface because its surface consists of broken Si-O and Al-O bonds on the edges, but broken hydrogen bonds on the faces (Fuerstenau and Fuerstenau, 1982). In the case of muscovite, because of the isomorphous substitution of Al^{3+} for Si^{4+} in the silica tetrahedral, the faces of the unit layers carry a fixed negative charge compensated by cations between the unit layers. Therefore, the surface of a mica carries a fixed negative charge, independent of pH and this property is made use of in the flotation of muscovite with cationic collectors at low pH (Fuerstenau and Fuerstenau, 1982). The mineral is readily made hydrophobic by covering these negative sites with a cationic collector.

Selective flotation of silicate ores is possible based on the knowledge of the crystal chemistry of silicate minerals. According to Fuerstenau and Fuerstenau (1982), the knowledge of crystal chemistry of silicate minerals could be applied to separate them from each other by the flotation process, using both physisorbing and chemisorbing collectors. The selective flotation of spodumene, muscovite, feldspar and quartz in pegmatite ores, is such an example. The separation of lithium aluminium silicate from potassium aluminium silicate minerals is said to be related to the availability of Al sites in the spodumene crystal for attachment of the oleate collector. Lowering the pH to almost 1 provides conditions for muscovite flotation with a cationic collector after spodumene has been removed (Fuerstenau and Fuerstenau, 1982). Muscovite retains a negative surface charge on the faces of the crystal sheets because it is a layer silicate with a lattice charge, whereas the charge on feldspar and quartz becomes positive at such low pH. Feldspar and quartz could be separated subsequently, by feldspar activation with fluoride for flotation at low pH (Fuerstenau and Fuerstenau, 1982).

5.1 Flotation Cells

In flotation practice, after the pre-treatment of the pulp has rendered one or more minerals hydrophobic, and thus potentially floatable, the flotation machine provides the hydrodynamic and mechanical conditions which affect the actual separation. The performance of a flotation cell is influenced by physical features such as impeller, stator and tank design, and by operating conditions such as impeller speed and aeration rate. One of the functions of the impeller is to ensure effective suspension and dispersion of ore particles to allow for successful bubble-particle collision and attachment (Harris, 1976, Koh et al., 2000). Flotation cells are conventionally designed using empirical derived relations. The efficiency of the flotation process depends, among other factors, on contact between bubbles and the particles, which facilitates selective adherence of floatable particles to these bubbles. Thus, for an efficient flotation process, the flotation cell should be designed to achieve good mixing of suspending solids and dispersing air (Koh et al., 2000).

The flotation process is dependent on the successful collision and attachment between a particle and a bubble and the overall kinetics may be described by a product of several probabilities:

(i) the probability of collision,
(ii) the probability of attachment between the particle and bubble, and
(iii) the probability of the particle remaining attached to the bubble throughout the flotation process.

The probability of attachment depends mostly on the surface characteristics of the mineral, the degree of collector adsorption on the mineral surface, and the induction time required for attaching the hydrophobic particle to the bubble. The probability of a particle remaining attached to the bubble depends on the turbulence level in the cell as well as size of particle. It is said that the same forces that brought the particle and bubble together are available to separate them. The probability of collision or the particle-bubble collision rate depends on the sizes of the particles and bubbles, and the hydrodynamics of the flotation pulp.

Degner (1986) stated that any flotation machine must provide four functions: (i) provision of good contact between solid particles and air bubbles, (ii) it must maintain a stable froth/pulp interface, (iii) it must adequately suspend the solid particles in the slurry, and (iv) it must

provide sufficient froth removal capacity. In a given machine, the first three of these functions may be understood and even predicted by the hydrodynamic characteristics of that design. Each flotation machine also has a fifth important function: It must provide adequate retention time to allow the desired recovery of the valuable constituent. The retention time is influenced by a machine's hydrodynamic characteristics, but also a function of its volume and rate at which it is fed (Nelson and Lelinski, 2000).

Thus any laboratory flotation cell should be able to promote:

(i) Air dissemination in the pulp;
(ii) Bubble-particle collisions;
(iii) Stability of bubble-particle aggregate.

5.2 Flotation Reagents

The reagents employed in flotation process are generally described as interfacial surface tension modifiers, surface chemistry modifiers, and / or flocculants (Crozier, 1992). They are classified under five headings: collectors, frothers, modifiers, activators and depressants.

5.2.1 Collectors

Collectors are reagents that coat and / or react with mineral surfaces and make them water repellent or attachable to air bubbles. These are heterogeneous compounds that contain a functional inorganic group attached to a hydrocarbon chain. The inorganic group is the portion of the collector molecule that adsorbs onto the mineral surface, while the hydrocarbon chain provides hydrophobicity to the mineral surface during collector adsorption (Wills and Napier-Munn, 2006). Sulphide ore collectors all contain sulphur and are thiols or can hydrolyse to a thiol. Non-sulphide and non-metallic minerals are normally floated using collectors such as fatty acids, amines, sulphonates and petroleum oil (Crozier, 1992). According to Wills and Napier-Munn (2006), collector molecules may be ionising compounds, which dissociate into ions in water, or non-ionising compounds, which are practically insoluble, and render the mineral water-repellent by covering its surface with a thin film. The ionising collectors are classed in accordance with the type of ion, anion or cation that is responsible for the water-repellent effect in water.

5.2.2 Frothers

Frothers are surface active reagents that aid in the formation and stabilisation of air-induced flotation froths. The commonly employed frothing agents are alcohols which are only slightly soluble in water or some recent frothers, which are generally varieties of polyethers or polyglycol ethers that are completely miscible with water (Crozier, 1992). One of the prerequisites for a successful flotation process is the stability of the bubble-particle aggregate. A stable bubble is produced by using a frother, the function of which is to decrease the surface tension of the air-liquid interface (Wills and Napier-Munn, 2006; Subrahmanyam and Forssberg, 1988).

5.2.3 Modifiers, Activators and Depressants

The boundaries between the functions of a specific inorganic flotation aid are not clear. In the case of pH control, lime which is an environmental modifier may be used, but can also act as a depressant for pyrite in copper flotation or for quartz and talc in the flotation of silver ores. Therefore, lime could be classified under both headings. In general, reagents that intensify collector adsorption on the mineral surface are termed as activators and those which inhibit collector adsorption as depressants (Wills and Napier-Munn, 2006). These reagents are necessary in order to float a mineral of interest from a group of similar minerals.

5.3 Mica Separation Process

5.3.1 Flotation Separation

Mica is an aluminosilicate mineral of layered structure. The common mica-type aluminosilicate minerals include biotite, muscovite and lepidolite etc. Mica-type aluminosilicate minerals have been reported to have marked similarities in properties. The bases of the silica tetrahedra are symmetrically opposed so that two opposite hexagonal rings outline a large cavity into which a potassium atom is situated with 12-fold coordination. The potassium ions are used to neutralise the negatively-charged sheets because of the substitution for some of the Si^{4+} within the silica tetrahedra (Fuerstenau et al., 2007).

Mica minerals often occur with quartz and feldspar in granite mineral deposits. Quartz and feldspar belong to the framework silicate class and consist of silica tetrahedral linked by the sharing of oxygen in three dimensions. The quartz crystal is constructed by the sharing of

each oxygen atom between two silicon atoms. The three principal compositional end members of feldspar are K-feldspar ($KAlSi_3O_8$), albite ($NaAlSi_3O8$), and anorthite ($CaAl_2Si_2O_8$), whose abbreviations are Ks, Ab, and An, respectively (Nesse, 2000). According to Nesse (2000) only compositions between albite and anorthite, and between K-feldspar and albite, are found. The former feldspars are known as plagioclase and the latter as alkali feldspars. He further said the plagioclase feldspars represent a continuous solid solution series brought about by a coupled substitution mainly at high temperatures. Albite is at one end of the series and anorthite at the other. It is also reported that Ca^{2+} can substitute for Na^{+} as a result of being the same size and that charge neutrality is maintained by substituting Al^{3+} for Si^{4+}. Continuous solid solution in the alkali feldspars series is also possible because K^{+} and Na^{+} have the same charge but limited to high temperatures because the sizes of these cations are significantly different (Nesse, 2000). There are no compositions intermediate between K-feldspar and anorthite under any geological conditions owing to the fact that Ca^{2+} and K^{+} have substantially different sizes and charges (Nesse, 2000).

Mica is easily floated in both acid and alkaline solutions with an acid system using a cationic collector and a basic system using an anionic collector. Amines are the major cationic collectors used in industry (Fuerstenau et al., 1985). The characteristic property of this group of collectors is that the water-repulsion is produced by the cation where the polar group is based on pentavalent nitrogen (Wills and Napier-Munn, 2006). This reagent is said to ionise in aqueous solution by protonation and in the case of dodecylamine (Fuerstenau et al., 1985),

$$RNH_{2(aq)} + H_2O \leftrightarrows RNH_3^+ + OH^- \qquad (5.1)$$

where *R* is a hydrocarbon radical ($C_{12}H_{25}$). The equation above, in saturated systems becomes,

$$RNH_{2(s)} \leftrightarrows RNH_{(aq)} \qquad (5.2)$$

Depending on the number of hydrocarbon radicals bonded to the nitrogen atom, the amines are classified as primary, secondary, tertiary or quaternary. The amine is termed a primary amine if only one hydrocarbon group is present with two hydrogen atoms and, therefore, correspondingly termed secondary, tertiary and quaternary if the amines contain two, three and four hydrocarbon groups (Fuerstenau et al., 1985). Variations may also be there in the configuration of the hydrocarbon chain of the amine and the amines can be alkyl, aryl and

alkylaryl. The primary, secondary and tertiary amines are said to be weak bases, while the quaternary amines are strong bases. The ionisation of primary, secondary and tertiary amines is pH dependent while the quaternary amines are said to be completely ionised at all values of pH. Their solubility has been reported to be dependent on the length of the hydrocarbon chain and as the length of the hydrocarbon chain is increased, the solubility of the amine is said to reduce (Fuerstenau et al., 1985).

Unlike the xanthates, the amines are considered to adsorb on mineral surfaces primarily due to electrostatic attraction between the polar head of the collector and the charged electrical double layer on the mineral surface (Wills and Napier-Munn, 2006). These cationic collectors are said to be very sensitive to the pH of the medium and being most active in slightly acid solutions and inactive in strongly alkaline and acid media (Wills and Napier-Munn, 2006).

Mica has been readily floated from various ores by an amine collector in a pulp of pH range 2.5-3.5 (Eddy et al., 1972; Manser, 1975; Crozier, 1990; Bayraktar et al., 1997, 1998; Celik et al., 1998; Orhan and Bayraktar, 2006; Bayat et al., 2006). Mica had been floated before under varying flotation conditions and mostly from ores containing feldspar. Although most of the feldspar reserves are saleable, either directly or after simple processing, it appears that the quality of the feldspar could be increased by applying conventional concentration techniques, i.e. flotation and magnetic separation. In general, the gangue minerals associated with feldspar are mica and iron bearing silicates. Mica is conventionally floated first by amine at acidic pH (2.5-3.5), followed by the flotation of iron bearing silicates, using sulphonate type collectors at acidic pH of 3-4. Fine fractions should be removed from the material before flotation because they reduce the efficiency of the flotation process by: (i) consuming a lot of reagents due to their high surface area, and (ii) they cling onto the liberated minerals thereby inhibiting the collector adsorption etc.

Bayat et al., (2006), conducted their experiments in a Denver machine equipped with a 2 dm^3 cell with a sample of about 500 g mixed with 1500 ml tap water at 1400 rpm impeller speed. Also Orhan and Bayraktar (2006) carried out their flotation tests with 500 g samples in a 1.5 dm^3 plexiglass cell at 30% solids using a Denver machine with impeller speed set at 1500 rpm. For the evaluation of the flotation results (Orhan and Bayraktar, 2006), MgO and Na_2O contents were taken into consideration for the representation of mica and feldspar minerals respectively.

Previously, Celik et al., (1998) conducted their flotation experiments in a self aerated Denver machine equipped with a 1.5 dm^3 cell, using an automatic froth skimmer. A sample of about 225 g mixed with 1400 ml was floated at 1000 rpm impeller speed. Bayraktar et al., (1997) performed their flotation tests in a 1-1 self aerated Humboldt Wedag flotation cell with 40% solids and impeller speed of 1500 rpm. No aeration rates are mentioned as the experiments were done under self-aerated condition. In all these experiments, it is very difficult to quantify the recovery of mica since they removed it as waste in order to float the mineral of interest.

In this work the flotation efficiency for mica has been assessed based on the recovery and grade of iron in the concentrates since iron is drawn mainly from mica minerals in these samples. If hematite, magnetite and other iron bearing silicates were present in the feed, they would have reported to the tails and the iron amount in the tails should have been more than the concentrates. In general, after the flotation of mica, iron bearing minerals (metal oxide) are floated by oleate at pH 5-5.5 or by sulphonates at pH of about 3-3.5. Besides the oleate and sulphonates, succinamates, soaps of various vegetable oils (Bayraktar et al., 1997), sarcosine and hydroxamate type collectors (Celik et al., 1998, 2001) can also be used for the flotation of metal-oxide minerals. Thus, it is on this background that the use of iron to assess the flotation performance in this work was justified. The iron that occurs in the concentrates is mainly associated with mica minerals. The source of MgO is mainly from biotite, but due to the lower content of biotite in the ore, it was very difficult to base the flotation efficiency on the recovery and grade of MgO as reported by Orhan and Bayraktar (2006).

Lithium containing micas have also been floated directly from various sources. Although some spodumene pegmatite ore is sold as mined, most operations have reported further upgrading by flotation (Dressler et al., 1998; Peres et al., 1985; Redecker, 1981; Banks et al., 1953). Zinnwaldite has also been reported to be floated using collectors of the Aeromine series directly from the waste emanating from the processing of tin-tungsten ores in the Czech Republic (Samkova, 2009).

In this work, all micas present in the sample were floated together. Silicates are said to differ substantially with respect to flotation capacity. Selective division of individual silicates is a difficult process due to their similar flotation properties, although conditions for selectivity can be created by activation or depression of various minerals in an acidic or basic medium.

Among the mica minerals present in the research material, zinnwaldite, which has a general formula $KLiFeAl(AlSi_3)O_{10}(F.OH)_2$, was the major source of lithium with smaller quantities being contributed by muscovite. Other minerals present in the sample were quartz, kaolinite, K-feldspar, apatite and topaz.

5.3.2 Magnetic Separation

Magnetic separation is a common physical method used for separating minerals with different magnetic properties. Magnetic separation has been used before to separate zinnwaldite from the waste originating from the dressing of tin-tungsten ores mined in the Czech Republic (Botula et al., 2005; Jandova et al., 2008, 2009). Zinnwaldite has significant magnetic properties due to a relatively high content of iron which enables its transformation into a magnetic product. In magnetic separation carried out by Botula et al., (2005) in laboratories of VSB-TU Ostrava in the COOK magnetic analyser (Frantz-Isodynamic), it was discovered that zinnwaldite was transformed into a magnetic product in a relatively broad range of magnetic induction of 3500-7200 x 10^{-4} Tesla and showed relatively strong magnetic properties.

The concept of magnetic separation is based on the ability to magnetise a particular mineral and then physically collect it. The magnetic susceptibility of the mineral is an inherent characteristic directly proportional to the response of a magnetic field and is the single most important variable when addressing the characteristic of magnetic separation (Norrgran and Mankosa, 2002). When subjected to a magnetic field, all particles will respond in a particular manner and can be classified as one of three groups: ferromagnetic, paramagnetic, or diamagnetic (Norrgran and Mankosa, 2002; Wills and Napier-Munn, 2006). Minerals that have a very high magnetic susceptibility and are strongly induced by a magnetic field are ferromagnetic. Minerals that have a low magnetic susceptibility and a weak response to a magnetic field are termed paramagnetic. Diamagnetic are minerals that are repelled when placed in a magnetic field.

The two first order variables that affect separation response in any magnetic separator are the magnetic field intensity and the magnetic field gradient (Norrgran and Mankosa, 2002). High intensity magnetic separators typically operate in regions over 0.5 Tesla while low intensity separators are commonly referenced as those generating a magnetic field strength of less than 0.2 Tesla. The magnetic field gradient refers to the rate of change or the convergence of the

magnetic field strength. The magnetic collection of any specific material could be assessed directly in the laboratory and this assessment will conclusively determine if the material can be treated by magnetic separation. The selected mineral must respond reasonably to a magnetic field so that the magnetic separation can be considered a process option. The magnetic collection of the mineral is usually measured as a function of magnetic field strength.

6. LITHIUM

The lithium-containing minerals, petalite and spodumene, were discovered by Jose de Andrada between 1790 and 1800 in Sweden. Lithium was discovered in 1817 by Johann Arfvedson in Sweden during an analysis of petalite ore. Humphry Davy and Brande independently isolated the metal in 1818 by electrolysis of lithium oxide. The name lithium is from the Greek *lithos* "stone", because it was first discovered in a mineral.

6.1 Commercial Lithium Minerals

6.1.1 Spodumene

The most abundant of the lithium minerals is spodumene ($LiAlSi_2O_6$) a lithium pyroxene containing up to 3.73% Li (8.03% Li_2O), with high-grade deposits usually ranging from 1.35 to 3.56% Li (2.9-7.7% Li_2O) and 0.007 - 0.03% Fe_2O_3, and the lower-grade deposits 0.5 – 1.0% Li (1.0 – 2.2% Li_2O) and 0.6 – 1.5% Fe_2O_3 (Garret, 2004). Some of the larger spodumene deposits are in: Greenbushes, Australia; Ontario and Manitoba, Canada; North Carolina, USA; Bikita, Zimbabwe; Minas Gerais, Brazil; the Chita Region, Russia; and the Altai Mountains, China (Garret, 2004; Harben, 1999).

6.1.2 Petalite

Petalite ($LiAlSi_4O_{10}$) has a theoretical lithium content of 2.27% (4.88% Li_2O), while the more commercial deposits vary from 1.4-2.2% Li (3.0-4.7% Li_2O). The petalite crystal does not accommodate very much iron, so its deposits have very low iron content. Various larger deposits of petalite occur in: Bikita, Zimbabwe; Kenora, Ontario, Canada; Karibib, Namibia; Aracuai, Brazil; Londonerry, Australia; the Transbalkin area of Russia; and at Uto, Sweden (Garrett, 2004; Harben, 1999).

6.1.3 Lepidolite

Lepidolite $[K_2(Li,Al)_{5-6}(Si_{6-7}Al_{1-2}O_{20})(OH,F)_4]$ or $[K_2Li_2Al_4Si_7O_{21}(OH,F)_3]$ or $[KLiAl_2Si_3O_{10}(OH,F)_3]$ is a mica with a complex and variable formula. Its lithium concentration ranges from 1.39% (3.0% Li_2O) to a theoretical maximum of 3.58% Li (7.7% Li_2O). The major commercial deposits of lepidolite are in: Bikita, Zimbabwe; Bernie Lake,

Manitoba, Canada; Karibib, Namibia; Mina Gerais, Brazil; and Sociedad Mineria de Pegmatites, Portugal (Garret, 2004; Harben, 1999).

6.1.4 Amblygonite

The mineral amblygonite ($LiAl[PO_4][F,OH]$), is the fluorine-rich end member of a lithium aluminium phosphate group. Amblygonite's colour is generally white or creamy, although it can vary from colourless to many other pale colours. Its theoretical lithium content is 4.76% (10.2% Li_2O), but most commercial ores contain 3.5-4.4% Li (7.5-9.5% Li_2O). It has been mined in Canada, Brazil, Surinam, Zimbabwe, Rwanda, Mozambique, Namibia, South Africa and the Black Hills and Pala Districts in the United States (Garret, 2004; Harben, 1999; Kesler, 1960).

6.1.5 Eucryptite

Eucryptite ($LiAlSiO_4$) has a theoretical Li content of 5.53% (11.84% Li_2O) and its ore average 2.1-3.0% Li (4.5-6.5% Li_2O). The only large deposit is at Bikita, Zimbabwe with an average grade of 2.34% Li (5.0% Li_2O), and much of the impurity is quartz (Kunasz, 1994). In the early days of the industry eucryptite and amblygonite were the favoured minerals, because the lithium could be leached directly (without roasting) by strong acids. However, their deposits are fairly uncommon, and those that were initially worked were small (Garret, 2004; Harben, 1999).

6.1.6 Zinnwaldite

Zinnwaldite is regarded as a variety of lepidolite with high iron content. Its theoretical lithium content is 1-2.32% (2-5% Li_2O). Zinnwaldite had been recovered from wastes emanating from the processing of tin-tungsten ores mined in the Czech Republic (Jandova and Vu, 2008). The wastes containing 0.20-0.30% Li were subjected to magnetic separation to obtain a zinnwaldite concentrate with 1.36% Li. It must be mentioned that zinnwaldite is no longer an accredited mineral according to the International Mineralogical Association. Micas of this composition are present between the polylithioinite and siderophyllite species, but for the purposes of this thesis, it is more useful to retain the name zinnwaldite.

6.2 Properties of Lithium Minerals

The properties of some lithium minerals are summarised and listed in Table 6.1.

Table 6.1: Properties of some lithium minerals

Name, Formula	Colour	Hardness	Specific Gravity	Lustre	Crystal form	Transparency	Fracture
Amblygonite $LiAlPO_4(F,OH)$	white or grey	5.5-6	3	vitreous-greasy	triclinic	transparent-opaque	conchoidal to uneven, brittle
Eucryptite $LiAlSiO_4$	colourless, white, tan	6.5	2.65	vitreous	trigonal	transparent	conchoidal, brittle
Lepidolite(lithium mica) $K(Li,Al)_3(Si,Al)_4O_{10}(F,OH)_2$	rose red, lilac or white	2.5-3	2.8-3.3	pearly	monoclinic	transparent to translucent	flexible, elastic
Petalite $LiAlSi_4O_{10}$	colourless, white, grey, yellow	6-6.5	2.3-2.5	vitreous to pearly	monoclinic	transparent to translucent	subconchoidal, brittle
Spodumene $LiAlSi_4O_{10}$	colourless, white, grey, yellow,greenish	6.5-7.5	3-3.2	vitreous to dull	monoclinic	transparent to translucent	Uneven hackley to subconchoidal, brittle
Zinnwaldite $KLiFe^{+2}Al(AlSi_3)O_{10}(F,OH)_2$	Grey, brown	2.5-4	2.9-3.3	vitreous	monoclinic	transparent	flexible, elastic

6.3 Country Lithium Reserve and Resource review

Table 6.2 shows the estimates of the lithium reserves of various deposits around the world (Garret, 2004). It is believed the deposits have been formed because of lithium's higher solubility than most cations.

Lithium has sometimes concentrated in flowing and cooling magma and/or its accompanying aqueous fluids, as well as in evaporating brines. Thus its minerals are generally found in the latter stages of alkaline magma flow, intrusion and crystallisation, as occurs in pegmatite formation. The high-lithium brines usually have obtained most of their lithium from geothermal waters, with perhaps some of the lithium coming from surface leaching of volcanic ash, clays or other rocks (Garret, 2004). However, lithium is very difficult to leach from the lattice structure of all rocks and minerals, therefore, very little is dissolved unless the water is very hot (Garret, 2004). Lithium also tends to concentrate in silica-rich rocks and pegmatites containing feldspar, quartz and mica (Harben, 1999).

6.3.1 Europe

There are many small lithium pegmatites in Europe, and in the early days of the industry several of them were commercially extracted. Significant spodumene pegmatites have been found in southern Austria by Minerex, and exploratory underground mining and separation procedures have been conducted (Garret, 2004). The large Koralpe spodumene deposit is

estimated to contain 10 million tonnes of 0.77% Li ore. A large lithium pegmatite has also recently been discovered in Finland, and in 2001 petalite production from it was being considered (USGS, 2002). Previously, only the small Viitaniemi, Eraejaervi, central Finland lithium pegmatite containing mostly lithium phosphate minerals had been discovered (Volborth, 1954). Lithium pegmatites also occur in France, but none appear to be of sufficient size or grade to be commercial deposits (Garret, 2004). One of the minor lithium pegmatites that have also been extensively studied is the Varutrask pegmatite in Sweden. In Portugal there are many lithium pegmatites, with the Barroso-Alvao area of northern Portugal being perhaps the most studied (Garret, 2004).

Table 6.2: Estimated Lithium Reserves of Various Lithium Deposits, 1000 mt Li (Garret, 2004).

Source / Place	Reserves
Brines	
Salar de Uyuni	5000
Salar de Atacama	3000
Salar de Hombre Muerto	800
Clayton valley	30.4
Zabuye Salt Lake, China	1000
Qinghai Lake, China	1000
Smackover oilfield brine	1000
Great Salt Lake	526
Searles Lake	31.6
Salton Sea	1000
Dead Sea	2000
Total	**15,388**
Ore deposits	
Africa (other)	>0.3
Bikita, Zimbabwe	23
Mali	26
Manono-Kitoto, Zaire	309
Namibia	9.8
Argentina	0.2
Australia, (Greenbushes)	150
Austria	10
Brazil	3.3
Canada (total)	240.5
Bernic Lake, Manitoba, Canada	73
Ontario, Quebec, Canada	139
China	500
Portugal	10
Russia	130
United States (other)	44.3
North Carolina, USA	71
Total	**1,739**

6.4 Extraction of Lithium from Lithium-Bearing Materials

The primary source of lithium is from continental brines which contain about 0.06-0.15% Li followed by pegmatites. The principal lithium minerals from pegmatites were discussed in section 6.1. The brine extraction processes are based on the use of solar energy for water evaporation, which makes the production of lithium carbonate from brines the lowest cost process today.

6.4.1 Recovery from Brines

Lithium is recovered from brines located in the Salar de Atacama, Chile which contains about 0.15 % Li and in Salar de Hombre Muerto, Argentina, containing about 0.06% Li. Lithium is also recovered from brines of Searles Lake, California (<100 ppm Li) by concentration and precipitation as dilithium sodium phosphate (Evans, 2008). The mixed phosphate is then converted to lithium carbonate, which is the final lithium containing product. Brines from Clayton Valley, Nevada, contain about 200 ppm Li and low concentrations of alkaline earth, simplifying the recovery. The lithium is recovered after the brine is concentrated by solar evaporation, and alkaline earths are removed by precipitation with sodium carbonate. Lithium carbonate is precipitated by the addition of a solution of sodium carbonate to hot brine (Garret, 2004; Harben, 1999).

6.4.2 Sulphuric Acid Leaching Method for Spodumene

Extraction of lithium from spodumene entails an energy-intensive chemical recovery process. After mining, spodumene is crushed, ground and undergoes a flotation beneficiation process to produce a concentrate. The concentrate is heated to 1075^{o}C to 1100^{o}C, changing the molecular structure of the mineral, making it more reactive to sulphuric acid. A mixture of finely ground converted spodumene and sulphuric acid is heated to 250^{o}C, forming lithium sulphate. Water is added to the mixture to dissolve the lithium sulphate. Insoluble portions are then removed by filtration. The purified lithium sulphate solution is treated with soda ash, forming insoluble lithium carbonate that precipitates from solution. The carbonate is separated and dried for sale or use by the producer as feedstock in the production of other lithium compounds (Dresler et al., 1998).

6.4.3 Gypsum and Limestone Methods for Zinnwaldite

Jandova and Vu (2008) studied the gypsum and limestone methods as a way to process zinnwaldite wastes originating from dressing Sn-W ores mined in the Czech Republic. These methods involve the mixing of the lithium containing concentrate with either gypsum or limestone and then roasting the mixture in a pre-heated furnace at selected temperatures. The resultant roast-product is ground and water leached.

The Jandova and Vu (2008) method involved grinding the zinnwaldite concentrate to grain size < 100 μm, mixing with a determined amount of calcium salts and roasting in a laboratory muffle furnace at selected temperatures for 60 min. If the concentrate was processed by the gypsum method, the weight ratio of concentrate to $CaSO_4.2H_2O$ to $Ca(OH)_2$ was 6:4.0-4.2:2. Roasting temperatures ranged from 900 to 975^oC. When treating the concentrate by limestone method, the weight ratio of concentrate to $CaCO_3$ was 5:1, with roasting temperatures of 800 to 875^oC. Both the composition of the roasted mixtures and roasting conditions were chosen based on the results of their previous studies (Jandova et al., 2007). Laboratory reagents such as $CaSO_4.2H_2O$, $Ca(OH)_2$ and $CaCO_3$ were used in their process.

The zinnwaldite concentrate containing on average 1.36 % Li and 0.94% Rb was prepared from zinnwaldite waste using dry magnetic separation followed by removal of a fraction >100 μm. Typical content of main elements present in the concentrate was 29.14% Si, 13.80%Al, 6.62% K, 6.08% Fe, 0.49% Ca, 0.22% Na and less than 0.1% Cs. Jandova and Vu (2008) also performed XRD analysis which showed that zinnwaldite waste and zinnwaldite concentrate consisted only of three identifiable phases: dominant quartz SiO_2, zinnwaldite $KLiFeAl(AlSi_3)O_{10}(F.OH)_2$ and a small amount of polylithionite $KLi_2AlSi_4O_{10}(F,OH)_2$, a variety of zinnwaldite. The waste fraction involved two dominant phases, anorthite $Ca(Al_2Si_2O_8)$ and orthoclase $K(Al.Fe)Si_2O_8$ as well as an insignificant amount of polylithionite. Rubidium was not identified in any phase.

Their studies showed that it was possible to extract approximately 92-96% of the lithium if zinnwaldite concentrate was processed with gypsum and/or limestone. However, processing the concentrate by the gypsum method resulted in only 25% Rb extraction, in contrast to the treatment of the same concentrate by limestone method which yielded almost 93% Rb. The water-washed lithium carbonate product obtained by the gypsum method contained about 97% Li_2CO_3, whilst that obtained by the limestone method contained only 94% Li_2CO_3.

Jandova and Vu (2008) observed that the main advantage of the gypsum method was to obtain relatively concentrated leach solution even during leaching the sinter at room temperature. However, in comparison with processing the zinnwaldite concentrate by the limestone method, the leach liquors from the gypsum method contained higher calcium concentrations. This must be removed before lithium carbonate precipitation and during precipitation, potassium or sodium concentration increased in the mother liquor. They mentioned that, apart from high rubidium extraction, the main advantage of processing the zinnwaldite concentrate by the limestone method was obtaining practically calcium-free leach liquors, from which a relatively pure Li_2CO_3 was separated by use of potassium carbonate.

6.4.4 Bioleaching of Spodumene

The role of micro-organisms in the weathering of spodumene has been demonstrated (Karavaiko et al., 1980). Bioleaching of aluminosilicate by fungi has been reported (Rossi and Ehrlich, 1990). The role of organic acids and extracellular polymers produced by microorganisms in silicate weathering has been studied (Vandevivere et al., 1994). Taking these facts into account, Rezza et al., (1997) thought it should be possible to use a bioleaching method for extracting lithium from spodumene. From the results they obtained, Rezza et al., (1997) concluded that it was possible to extract lithium from spodumene by leaching with P. purpurogenum and R. rubra micro-organism.

6.4.5 Caustic Leaching Method (Patent – WO/2007/103083)

The lithium bearing mineral is preferably granulated by crushing, grinding to facilitate the extraction of the lithium. The average grain size of the crushed lithium bearing mineral usually affects the reactivity of the extraction process, with smaller grain sizes being more preferred in general.

An example of a pathway is shown below for extracting lithium from spodumene. Adjustments can be made in the temperature, time, fluid/solid ratio and /or pressure of the reaction, and the method of mixing the reactants, to ensure that at least most of the Li is extracted from the lithium bearing mineral. The reaction is usually conducted at a temperature not greater than about 500^oC.

$$6LiAl(SiO_3)_2\,(s) + 8NaOH\,(aq) \rightarrow Na_8Al_6Si_6O_{24}(OH)_2\,(s) + 6LiOH\,(aq) + 6SiO_2\,(s) \qquad (6.1)$$

The use of the basic material to extract lithium is very effective, so that it is not necessary to pre-heat the mineral to change its molecular structure before extraction. If pre-heating is used, it is usually limited to a temperature not greater than the temperature during the reaction. The elimination or reduction of the pre-heating step provides a very large energy savings and lowering the cost of production.

As shown in reaction 6.1 above, when spodumene is reacted with a caustic solution, the product mixture contains lithium in solution. Because the lithium is in solution, it is relatively easy to separate the solution from the remaining solids. The lithium is recovered from the solution by reaction with a carbonate to produce a lithium carbonate. Any suitable carbonate can be used, such as an alkali metal carbonate or bicarbonate, e.g. sodium carbonate (Na_2CO_3) or sodium bicarbonate ($NaHCO_3$) as shown in equation 6.2.

$$2LiOH + Na_2CO_3\,(aq) \rightarrow Li_2CO_3 + 2NaOH \qquad (6.2)$$

Alternatively, the lithium can be recovered by introducing carbon dioxide into the solution. This causes the lithium carbonate to precipitate. The process of precipitation might regenerate a substantial amount of sodium hydroxide that is consumed in the extraction step shown in reaction 6.1.

The lithium carbonate produced from reaction 6.2 is the feedstock used for further lithium processing in most industrial processes. Lithium metal can be produced from lithium carbonate by electrolysis of molten anhydrous lithium chloride after converting the lithium carbonate to lithium chloride.

Unlike the sulphuric acid process described above, this extraction method results in no net production of sulphur or sulphur bearing material, with its potential for associated environmental hazards. Further, this extraction method results in no net production of carbon dioxide or carbon dioxide bearing material. Moreover, this method results in no net production of chlorine or chlorine bearing material, unlike the brine method described above. Thus, the method is considered to be environmentally friendly.

6.5 Production Cost Components

In the case of production from pegmatites and assuming the most common acid leach process is used, costs comprise mining, beneficiation to a moderate or high grade of concentrate, calcination to produce acid/water leachable material, reaction with sulphuric acid and the conversion of lithium sulphate solution with sodium carbonate. The costs of acid, soda ash and energy are very significant percentage of the total costs but they can be partly offset if for example market exists for the sodium sulphate by-product (Evans, 2008).

In the case of continental brines, which are the current major source, costs may vary greatly depending on the location of the brine deposits. Those located in hot regions use solar energy for evaporation and the only cost incurred is for soda ash to convert lithium chloride to lithium carbonate. Brine grades vary greatly ranging currently in the Andes, from approximately 0.3% Li at the SQM operation in Chile to 0.062% and 0.034% at two Argentinian salares of Hombre Muerto and Rincon respectively.

6.6 Global Lithium Carbonate Market and Production Capacity

According to the article Research and Markets: Global and China Lithium Carbonate Industry Report, 2008-2010 (3rd Edition) (http//www.researchandmarkets.com/research) the sectors that consumed the most of lithium carbonate in the world in 2008 were battery, lubricant, ceramics and glass, with proportions of 27%, 12%, 9% and 8%, respectively. The proportions in 2007 were 25%, 12%, 10% and 8%, respectively. The report further stated the lithium carbonate consumption by the battery sector had further increased, while the consumption was somewhat lower for the traditional sectors like ceramics.

The report also mentioned that by the end of 2008, the global lithium carbonate demand was 95,400 tonnes, up 2.9% year on year, and that the global lithium carbonate demand in the past ten years was up over 7%. Chile, China and Argentina were the top three countries in terms of lithium carbonate production capacity, and they together satisfied 94% of global lithium carbonate demand. China's global market share increased to 26% in 2007 from 21% in 2006, but the figure declined to 24% in 2008 as a result of natural disasters.

China's demand for lithium carbonate has also grown rapidly. It is expected that China's lithium carbonate output will reach 45,000 tonnes and its designed production capacity will surpass 60,000 tonnes by 2010. Generally, there has been a steady increase in lithium production capacity in recent years and Figure 6.1 shows the lithium production capacity (tonnes LCE) by country in 1999 (Harben, 1999). The total production capacity of lithium carbonate (LCE) was 117,820 tonnes in 1999. Harben (2002) reports a lithium production with a total of 25,900 tonnes (Li_2O equivalent) derived from spodumene (5%), petalite (4%) and lithium carbonate (40%). Figure 6.2 shows the contribution from various countries (Harben, 2002).

Forecasts indicate that the demand for lithium in the next five years is expected to increase by approximately 60% from 102,000 tonnes to 162,00 tonnes of lithium carbonate or equivalent (LCE), with batteries representing more than 40,000 tonnes of the perceived growth (Hykawy, 2010). Figure 6.3 shows the lithium carbonate demand by end use (Smith, 2010).

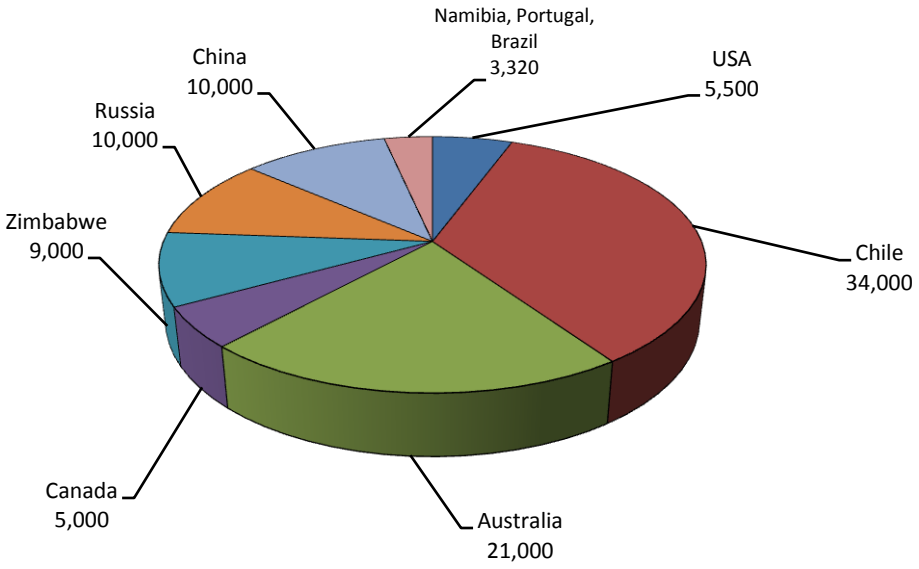

Figure 6.1: Lithium production capacity [tonnes LCE] in 1999 (Harben, 1999).

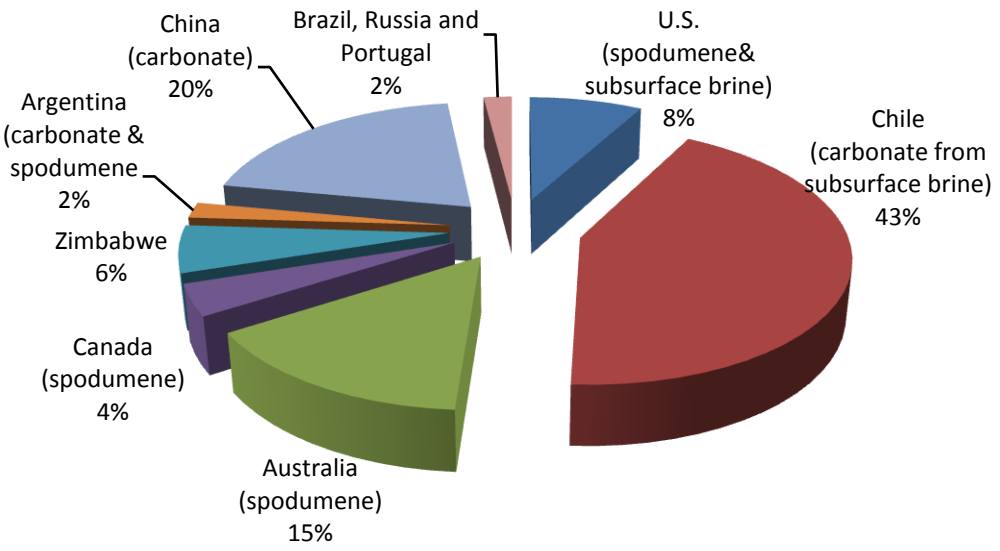

Figure 6.2: Lithium production of 25,900 t [Li_2O equivalent] (Harben, 2002).

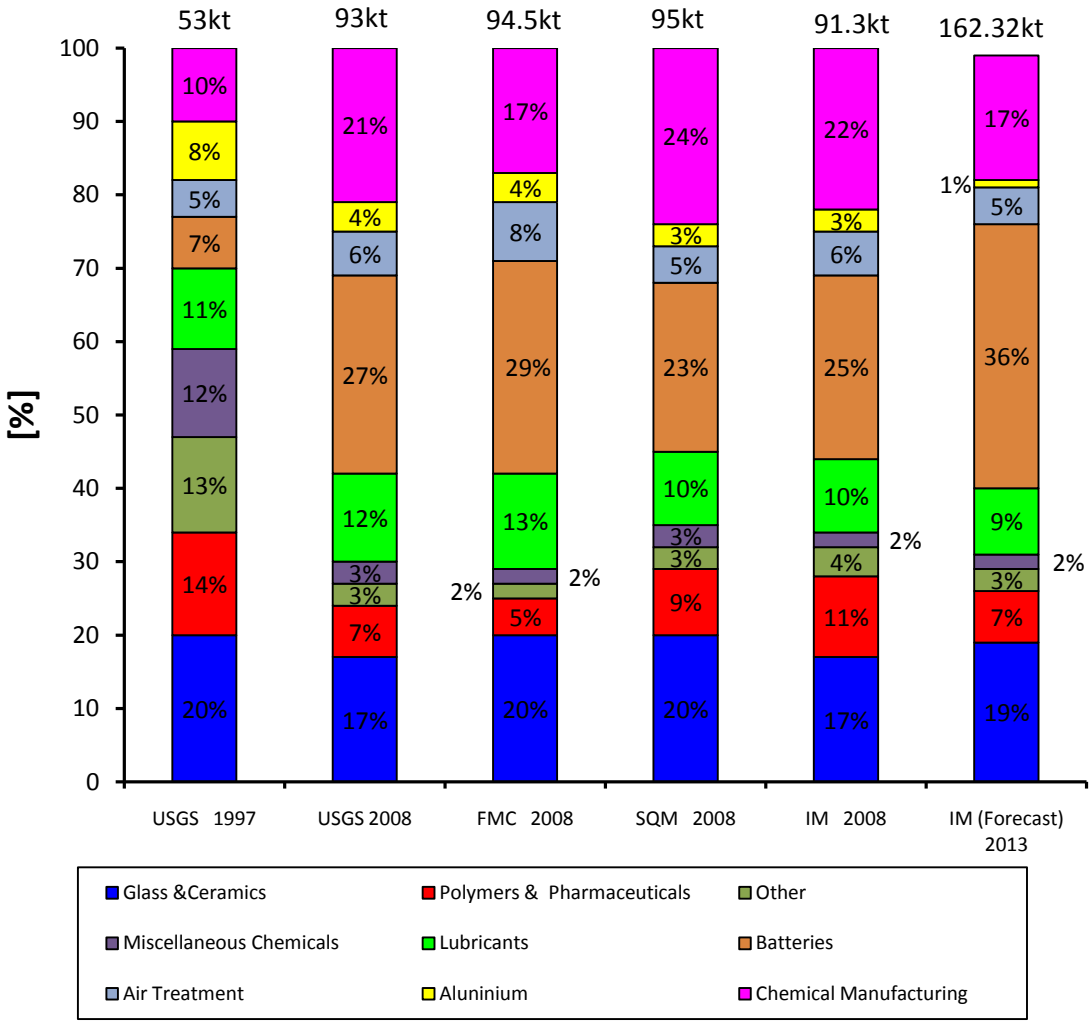

Figure 6.3: Lithium carbonate demand by end use (Smith, 2010).

6.6.1 Specifications of Lithium Sources

The specifications of lithium sources are given based on the lithium content, either as Li_2O content or lithium carbonate equivalent (LCE). Table 6.3 shows the typical specification of some lithium concentrates (Harben, 2002). Lithium carbonate from brines is said to contain a minimum of 99% Li_2CO_3 with low alkalis, and a maximum of 0.02% as insolubles (Harben, 2002). Typical composition of lithium commercial products is given in Table 6.4 (Harben, 2002).

Table 6.3:Typical specification of lithium concentrate (Harben, 2002).

Name	Content (%)		other
	Li_2O	Fe_2O_3	
High grade spodumene conc; Glass-grade	≥7.5 ≥5	<0.1 <0.2	-250µm 0.1% moisture, <810/ >150 µm
Petalite concentrate	≥ 4.40	≤0.05	
Lepidolite concentrate	≥ 4.4	≤0.1	

Table 6.4: Lithium Carbonate Chemical Specifications (Harben, 2002).

Element / compound	From Brines		From Spodumene	
	Powder (max.)	Granular (max.)	Typical	Guaranteed (max.)
Li_2CO_3	99.0%	99.0%	99.2%	99.0%
Cl	0.02%	0.02%	50 ppm	100 ppm
Na	0.12%	0.18%	100 ppm	500 pm
K	3 ppm	3 ppm	20 ppm	100 ppm
Ca	0.04%	0.068%	100 ppm	200 ppm
Mg	0.011%	0.025%	20 ppm	100 ppm
SO_4	0.10%	0.10%	30 ppm	100 ppm
B	10 ppm	10 ppm		
Fe	-	-	20 ppm	35 ppm
Fe_2O_3	0.00%	0.00%		
H_2O	0.20%	0.20%	200 ppm	400 ppm
LOI	0.7%	0.80%	5,500 ppm	6,000 ppm
Insolubles	0.02%	0.02%	300 ppm	800 ppm

6.7 Solubility of Selected Carbonates

Figure 6.4 shows the solubility of selected carbonates (Wikipedia, 2010). This information is vital in the recovery of lithium from brine and leach solutions. As can be seen from Figure 6.4, the solubility of lithium carbonate is very low at all temperatures and this necessitates its recovery from brine and leach solutions by the addition of potassium or sodium carbonate.

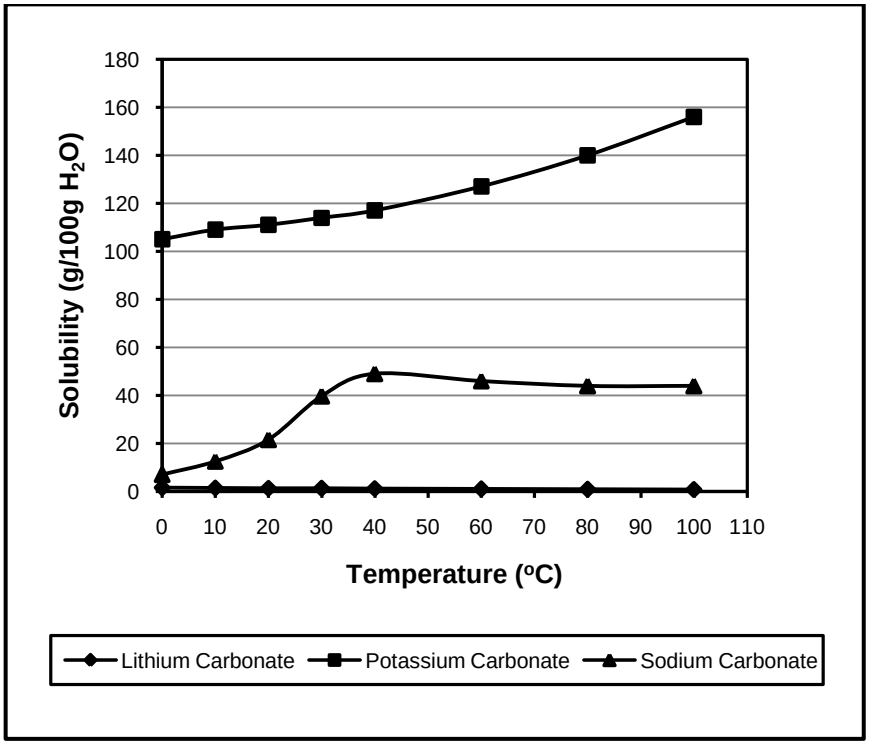

Figure 6.4: Solubility of selected carbonates (from Wikipedia, 2010).

7. EXPERIMENTAL

7.1 Materials

The material used in this test work was obtained from Goonvean Ltd, St. Austell, United Kingdom. The samples were collected from the underflow of a group of ten-inch hydrocyclones, which were processing material for china clay production from the Trelavour Downs and Rostowrack pits. Both of these pits are located within the lithium granite (see Figure 3.2). The overflow is further processed into china clay products ready for sale. The underflow, which consists of fine, mica-rich sand, is discharged to the tailing dam. The hydrocyclone underflow was collected into seven 100 litre barrels and transported to the Camborne School of Mines laboratory. The particles were allowed to settle for two days after which water was decanted off. The hydrocyclone underflow was further classified using a 50 mm laboratory hydrocyclone operated at a pressure of 276 kPa in order to remove the -10µm fraction. The deslimed hydrocyclone underflow was decanted and dried in an oven set at 105^{o}C. The dried hydrocyclone underflow was homogenised before being riffled into 1kg lots. The 1 kg fractions formed the feed for the flotation process.

7.2 Particle Size Analysis

Particle size analysis of the flotation feed sample was performed by a laser sizer (Malvern mastersizer MAF 500). The tests were done in duplicate and the values reported here are the mean of the two. About 20 g of the material was suspended in a beaker with the help of a rotating impeller. The suspended sample was then introduced into the measuring beaker connected to the Malvern mastersizer by using a pipette until the sample concentration was within the acceptable range. Detailed results can be found in Appendix A.

Figure 7.1 shows the graphical representation of particle size distribution. It can be seen from the graph that the d_{50} was 90µm.

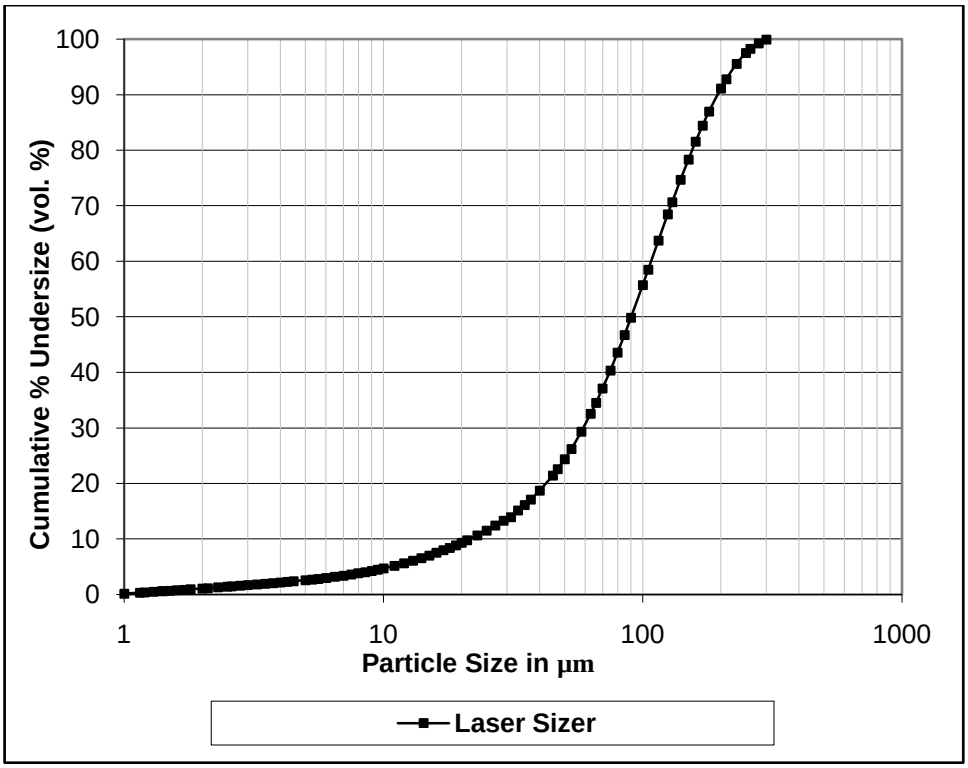

Figure 7.1: Particle size distribution of the china clay waste as obtained by laser-sizer.

7.3 Chemical and Mineralogical Analysis

A small fraction of the homogenised bulk sample was submitted for a number of analyses. X-ray Fluorescence (XRF), Loss on Ignition (LOI) and X-ray Diffraction (XRD) analyses were performed on the samples.

7.3.1 XRF and LOI Analysis of Materials

General Information

X-rays are a short wavelength form of electromagnetic radiation. When a monochromatic beam of X-ray photons falls onto a given specimen, three basic phenomena may result, namely, scatter, absorption or fluorescence.

X-ray fluorescence is used to obtain data upon the elemental composition of a sample. When an atom is subjected to an energy source of short wavelength e.g. X-rays, electrons in the inner orbitals are ejected causing ionisation. Thus the atom becomes unstable and electrons from outer orbitals "jump" down to the inner orbitals to maintain stability. However, because the orbital also represent energy levels for the electrons, with outer orbitals having higher

energy than the inner orbitals, then when an outer electron moves to an inner orbital, energy must be released from the electron and is done via the emission of a photon. A photon has an energy equal to the difference between the energy of the outer orbital and the inner orbital between which the electron moved and is defined by the wavelength of the photon. As the structure of each element is unique then the energy levels with it are also unique and the wavelength of the photon emitted is characteristic of the element from which it was emitted and this bring about a means of elemental identification.

Loss on ignition procedure involved heating a known weight of material in a furnace at 1050^{o}C for 30 min after which the weight difference is determined and calculated as a percentage loss of the original weight of material.

XRF Analysis Procedure

In this work, the boric jacket preparation method was used for XRF analysis (X-ray fluorescence: Bruker S4 Pioneer). A small amount of the flotation feed material was mixed thoroughly with a solution of alvacite (glue) and acetone. After the material had dried, it was then pulverised and put into a hydraulic press sleeve topped with boric acid (powdered) and pressed for about 30 seconds to form the boric jacket. The specimen was labelled accordingly and ready for XRF analysis. This method was also used for flotation concentrates and tails. The XRF analyses are semi-quantitative but the method was chosen as it was easier to obtain the chemical composition of the samples. Quality control standards were applied and this involved the rejection of specimens with broken edges and rough surfaces.

Table 7.1 gives the XRF results of the Goonvean 10-inch hydrocyclone underflow which formed the feed to the flotation test work in this research. The material was analysed for lithium and rubidium by the AAS method (see section 7.3.3 for details). The XRF method could not be used to analyse for lithium due to its lower atomic number but is a much faster multi-element technique than AAS and so was used for all major and minor elements. Rubidium was also analysed by AAS because of better detention limits. It is an important part of the analytical method that Li and Rb are analysed by AAS then combined with XRF for the other major elements.

Table 7.1: Chemical composition of the Goonvean china clay waste

Compound	%
SiO_2	57.31
TiO_2	0.16
Al_2O_3	23.66
Fe_2O_3*	3.23
MnO	0.05
MgO	0.27
CaO	0.20
Li_2O	0.87
Na_2O	0.28
K_2O	7.49
Rb_2O	0.44
P_2O_5	0.19
F	2.27
LOI	3.59
Minus O=F	0.96
Total	99.04

* = Total Fe as Fe_2O_3

7.3.2 XRD Mineralogical Identification

General Information

X-ray diffractometers are used for the study of ore and minerals deposits, plus myriad other applications in pure and applied research.

X-ray photons are produced following the ejection of an inner orbital electron from an irradiated atom, and subsequent transition of atomic orbital electrons from states of high to low energy. When a monochromatic beam of X-ray photons falls onto a given specimen, three basic phenomena may result, namely scatter, absorption or fluorescence. The coherently scattered photons may undergo subsequent interference leading in turn to the generation of diffraction maxima. The angle at which the diffraction maxima occur can be related to the spacing between planes of atoms in the crystal lattice and hence, X-ray generated diffraction patterns can be used to study the structure of solid materials.

The X-ray pattern is characteristic of the material from which it was derived, because each unique compound is made up of a similar unique combination and arrangement of atoms. X-ray diffraction patterns can thus be used to characterise materials. This is the basis of the X-ray powder method.

Of all of the methods available to the analytical chemist for materials characterisation, only X-ray diffraction is capable of providing general purpose qualitative and quantitative information about the presence of phases (e.g. compounds) in an unknown mixture. As described above, a diffraction pattern is characteristic of the atomic arrangement within a given phase and, to this extent, it acts as a *fingerprint* of that particular phase. The powder method derived its name from the fact that the specimen is typically in the form of a microcrystalline powder, although any material which is made up of an ordered array of atoms will give a diffraction pattern.

XRD Analysis Procedure

A small amount of the material to be analysed was placed on the specimen tray, labelled and put in the XRD equipment (Siemens Diffraktometer D5000). The results from the mineralogical analysis of the Goonvean 10-inch hydrocyclone underflow, which is the feed to the flotation process in this work, are given in Table 7.3. The relative abundance was determined from the XRD pattern (Figure 7.2) together with the results of the chemical analysis (Table 7.1). The method involved back-calculating the chemical composition of the feed by using the estimated mineral abundance and the chemical composition of minerals given in Table 7.2 and comparing them with those shown in Table 7.1. Several attempts were made until the calculated chemical composition was almost the same as those determined by the XRF method (see Table 7.1).

Table 7.2: Chemical composition of minerals.

Chemistry	Quartz[#]	Kaolinite[*]	Muscovite[#]	K-feldspar[#]	Zinnwaldite[#]	Apatite[*]	Topaz[*]
Si_2O	97.74	46.55	46.95	63.64	47.57	-	33
TiO_2	n.d.	-	0.09	n.d.	0.19	-	-
Al_2O_3	0.48	39.49	32.44	18.35	20.37	-	56
$Fe_2O_3^+$	0.17	-	2.89	0.07	11.33	-	-
MnO	n.d.	-	0.05	n.d.	0.17	-	-
MgO	n.d.	-	0.41	n.d.	0.26	-	-
CaO	n.d.	-	n.d.	0.12	n.d.	55.58	-
Li_2O	n.d	-	0.23	n.d.	4.10	-	-
Na_2O	n.d.	-	0.19	0.35	0.17	-	-
K_2O	n.d.	-	10.04	15.35	9.67	-	-
Rb_2O	n.d	-	n.a	n.d.	0.72	-	-
P_2O_5	n.d	-	n.d.	n.d.	n.d.	42.22	-
F	n.d.	-	0.97	n.d.	5.28	3.77	11.5
LOI	n.d	13.96	4.48	n.d.	n.d.	-	4.45
Minus O=F	-	-	O.41	-	2.22	1.59	4.84
Total	98.55	100.00	98.33	97.9	97.59	100.01	100.16

Average results of microprobe data; n.d. not detected; * data from webmineral.com (2010); + Total Fe as Fe_2O_3

Table 7.3: Estimated mineralogy of the Goonvean china clay waste

Mineral	Chemical Formula	wt %
Quartz	SiO_2	17
Muscovite	$KAl_2(AlSi_3)O_{10}(F,OH)_2$	27
Zinnwaldite	$KLiFeAl(AlSi_3)O_{10}(F.OH)_2$	20
Kaolinite	$Al_2Si_2O_5(OH)_4$	15
K-Feldspar	$KAlSi_3O_8$	19
Topaz	$Al_2SiO_4(F,OH)_2$	1
Apatite	$Ca_5(PO_4)_3(OH,F,Cl)$	1
Total		100

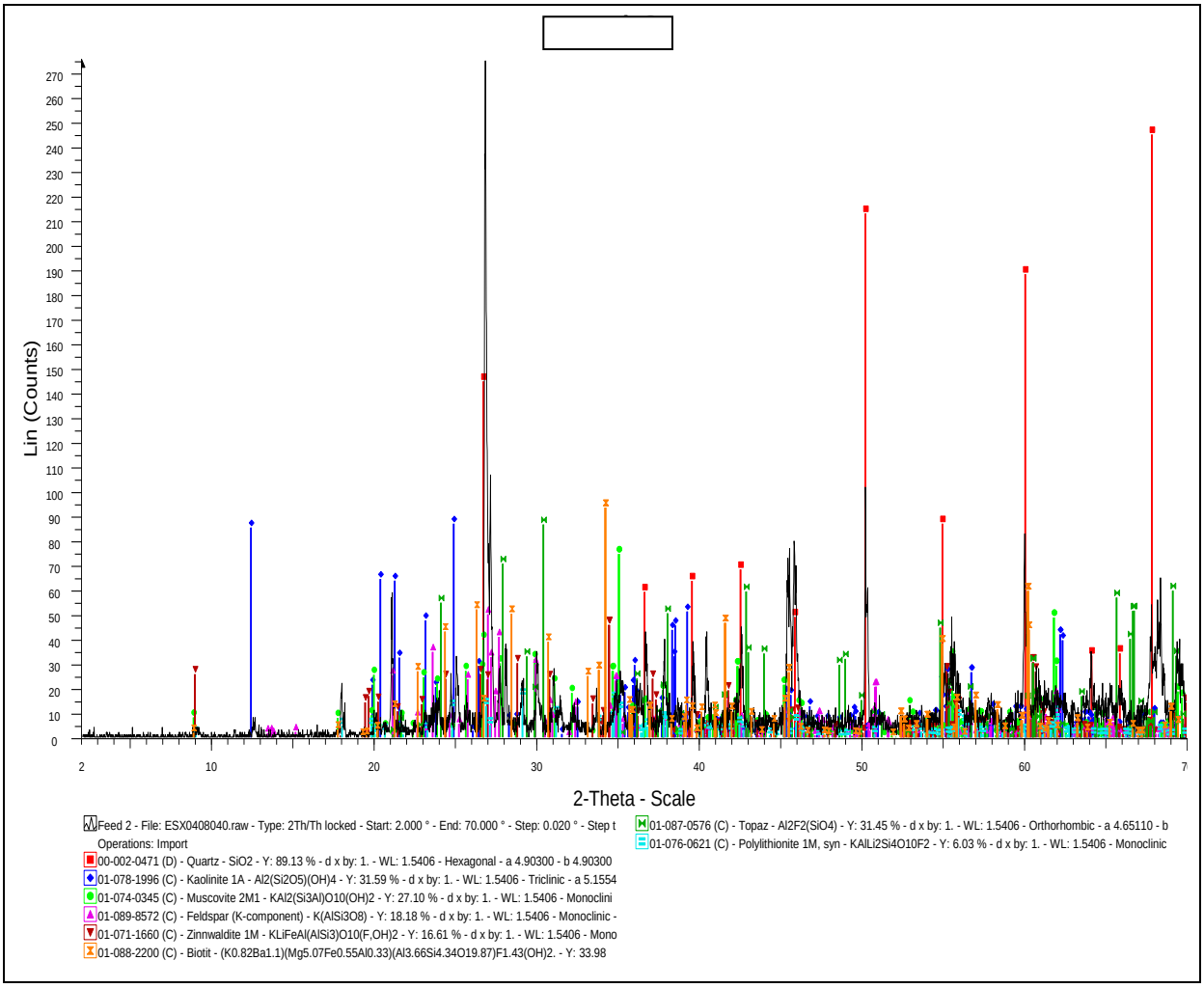

Figure 7.2: XRD pattern of the china clay waste.

7.3.3 Atomic Absorption Spectrophotometry

General Information

Atomic absorption spectrophotometry (AAS) is a spectroanalytical procedure for the qualitative and quantitative determination of chemical elements which uses the absorption of optical radiation by free atoms in the gaseous state. The technique is used in analytical chemistry for determining the concentration of a particular element in a sample. It is reported (Wikipedia, 2010) that AAS can be used to determine over 70 different elements in solution or directly in solid samples. The technique makes use of absorption spectrometry to assess the concentration of an element in a sample. The process requires standard solutions with known elemental content to establish the relation between the measured absorbance and the elemental concentration and depends on the Beer-Lambert Law. The electrons of the atoms in the atomiser can be promoted to higher orbitals for a short period of time by absorbing a defined quantity of energy (radiation of a given wavelength). This amount of energy represented by the wavelength is specific to a particular electron transition in a particular element. Each wavelength, in general, corresponds to only one element, and the width of an absorption line is only of the order of a few picometres and this gives the technique its elemental selectivity. The radiation flux without a sample and with a sample in the atomiser is measured using a detector, and the ratio between the two values (the absorbance) is converted to elemental concentration using the Beer-Lambert Law.

The sample is atomised for its atomic constituents in order to be analysed. The light transmitted has to be atomised so that the content of a given analyte (element) in a sample could be determined. The atomisers most commonly used nowadays are flames and electrothermal atomisers. The atoms are then irradiated by optical radiation, and the radiation source could be an element-specific line radiation source or a continuum radiation source. The radiation is then passed through a monochromator in order to separate the element-specific radiation from any other radiation emitted by the radiation source, and is finally measured by a detector.

The most commonly used and oldest atomisers in AAS are flames of which the most important are the air-acetylene flame with a temperature of about 2300^{o}C and the nitrous oxide (N_2O)-acetylene flame with a temperature of about 2700^{o}C. Liquid or dissolved samples are typically used with flame atomisers. The sample solution is aspirated by a

pneumatic nebuliser, transformed into an aerosol, which is introduced into a spray chamber, where it is mixed with the flame gases and conditioned in way that only the finest aerosol droplets (<10 µm) enter the flame. The radiation beam passes through this flame at its longest axis, and the flame gas flow-rates may be adjusted to produce the highest concentration of free atoms. The burner height may also be adjusted so that the radiation beam passes through the zone of highest atom cloud density in the flame, resulting in the highest sensitivity. In flame AAS a steady-state signal is generated during the time period when the sample is aspirated. This technique is typically used for determinations in the mg/l range and may be extended down to µg/l for some elements.

This method was used to analyse for lithium because it could not be analysed by XRF method due to its lower atomic number. Rubidium is also analysed by this method because of better detection limits.

7.4 Flotation of Mica Minerals

Flotation was conducted in a Denver D-12 laboratory flotation machine equipped with a 3.5 dm^3 Minnovex designed cell described below. A flotation test sample of about 1.2 kg was mixed with 2800 ml tap water to give 30% solids by weight and conditioned at the desired impeller speed. Both conditioning and flotation were performed at the same impeller speed and percent solids by weight. A conditioning period of 5 minutes after collector addition was applied. In general, the method used is similar to those outlined in the literature, i.e. mica flotation by amines at pH 2.5. The pH was adjusted either by addition of dilute H_2SO_4 or NaOH. Dodecylamine (*98% purity, supplied by Sigma-Aldrich Company Ltd, UK*) was used as the cationic collector for mica flotation. A stock solution of dodecylamine was made by dissolving 5 g of dodecylamine in 200 ml of dilute hydrochloric acid to give 2.5 % (w/v) solution. The frother used where necessary was methyl isobutyl carbinol (*99% purity, supplied by Sigma-Aldrich Company Ltd, UK*).

MinnovEX Flotation Test (MFT) Cell

The MinnovEX Flotation Test (MFT) cell has been designed by MinnovEX Technologies Inc. of Canada (Dobby and Savassi, 2005). Figure 7.3 shows the standard MFT cell, which is made of clear plastic to facilitate level control. The cell is also equipped with a froth crowder

to prevent a dead zone from forming behind the impeller. The froth is scraped using a t-shaped paddle standing at 1 cm above the pulp level mark, which has to be maintained by adding extra water. When the froth is scraped the water level goes down since it is a batch process, therefore, it is important to add extra water to maintain the pulp level and a steady froth.

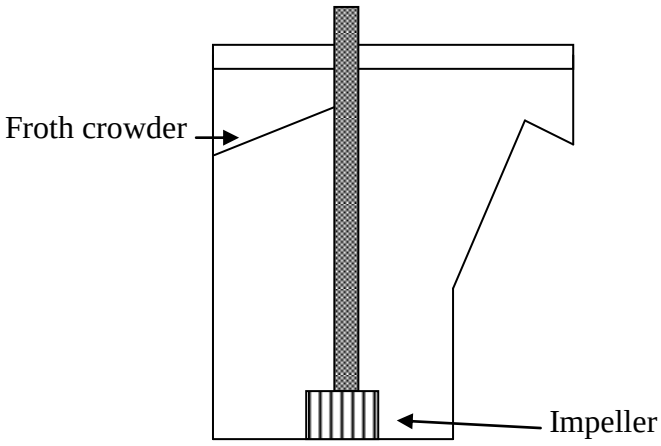

Figure 7.3: MinnovEX Flotation Test cell schematic (MinnovEX, 2004)

According to Dobby and Savassi (2005), the MFT has been designed to minimise the impact of the froth layer upon laboratory results by operating the cell with a shallow froth and rapid scraping rate. The airflow and impeller speed have to be determined through preliminary test work, where the objective is to maximise flotation rate while maintaining a reasonable smooth froth layer. Further details of the MFT standard procedure are available elsewhere (MinnovEX, 2004).

7.4.1 Effect of Impeller Speed, Frother Dosage and Aeration Rate on the Flotation Recovery of Mica Minerals.

These experiments were performed in order to evaluate the effect of impeller speed, frother dosage and aeration rate on the flotation recovery of mica minerals from china clay waste using a factorial experimental design. Table 7.4 shows the three independent variables (factors) chosen at two levels (high and low) while Table 7.5 shows the basic experimental design for a full factorial design of eight flotation tests, designated as 2^3. The response variables (dependent variables) were the recovery and grade of iron (Fe_2O_3) in the

concentrate. Iron is derived from mica minerals in this material. This was a flotation test with two replications and Figure 7.4 shows the flotation flow-sheet. The collector dosage and pH were kept constant at 500g/t and 2.5 respectively.

Table 7.4: Variables and levels

Variable	Name	Low Level (-)	High Level (+)
A	*Impeller Speed*	1200 rpm	1400 rpm
B	*Frother Dosage*	Nil	40 g/t
C	*Aeration Rate*	6 dm^3/min	8 dm^3/min

Table 7.5: Three variable factorial experiments tested at two levels

Test	Variables		
	Impeller Speed (rpm) (*A*)	**Frother Dosage (g/t) (*B*)**	**Aeration Rate (dm^3/min) (*C*)**
(1) and (1)R	1200	0	6
2 and 2R	1400	0	6
3 and 3R	1200	40	6
4 and 4R	1400	40	6
5 and 5R	1200	0	8
6 and 6R	1400	0	8
7 and 7R	1200	40	8
8 and 8R	1400	40	8

R = Duplicated

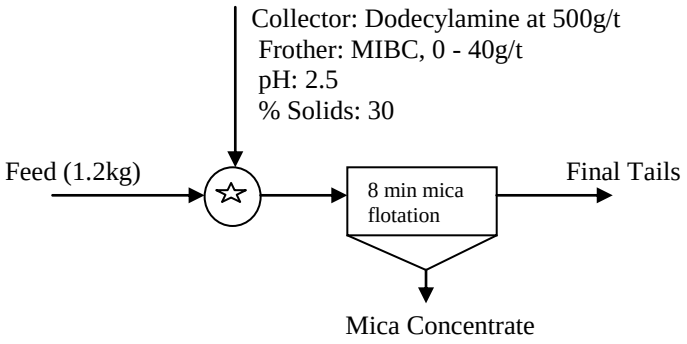

Figure 7.4: Laboratory flotation flow sheet for mica.

7.4.2 Effect of Collector Dosage and pH on the Flotation Recovery of Mica Minerals.

Flotation was again conducted in a Denver D-12 laboratory flotation machine equipped with a 3.5 dm^3 Minnovex designed cell. The impeller speed and air flow rate were set at 1400 rpm and 8dm^3/min respectively. A flotation test sample of about 1.2 kg was mixed with 2800 ml tap water and conditioned at 1400 rpm to give 30% solids by weight. Both pH conditioning and flotation were performed at the same impeller speed and percent solids by weight. A conditioning period of 5 minutes after collector addition was applied. Again the pH was adjusted either by addition of dilute H_2SO_4 or NaOH. Dodecylamine (98% purity) was used as the cationic collector for the mica flotation process.

This was a two-factor factorial experiment using repeated observations in a completely randomised design of n (3) replications of treatment combinations determined by "*a*" levels of factor *A* (collector dosage) and "*b*" levels of factor *B* (pH) as shown in Table C2-1 (Appendix C2). In Table C2-1, a_1, a_2 and a_3 represent the collector dosage of 150 g/t, 250 g/t and 500 g/t respectively while b_1, b_2 and b_3 represent the pH of 2.5, 3.5 and 5 respectively.

This experiment was performed with the aim of determining whether collector dosage and pH affected the flotation recovery of mica minerals and also to determine whether there is an interaction between the two variables. The flotation flow sheet is shown in Figure 7.5.

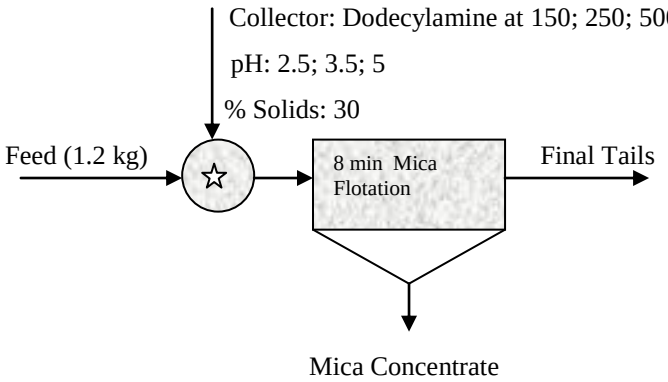

Figure 7.5: Effect of collector dosage and pH on the flotation recovery of mica minerals flow-sheet.

Since the source of iron (Fe_2O_3) in the concentrate is mainly from mica minerals, therefore, the recovery of iron in the concentrates was used to determine the efficiency of mica separation. A 0.05 level of significance was used to test the following hypotheses:

(a) $H_O^{'}$: there is no difference in the mean iron recoveries/grades when different collector dosages are used;

(b) $H_O^{''}$: there is no difference in the mean iron recoveries/grades at the three pH levels used;

(c) $H_O^{'''}$: there is no interaction between the different collector dosages and the different pH levels.

7.4.3 Effect of Stage-Wise Addition of Collector on the Flotation Recovery of Mica Minerals.

During the preliminary mica flotation tests work, 500g/t of collector was used. This produced a lot of froth which possibly could be attributed to over dosage of collector. Hence, there was need to add the collector stage-wise in the cell to investigate the effect. The collector was added in the following order: 40, 30, 40, 50, 60 and 80 g/t for a total of 300g/t as shown in Figure 7.6.

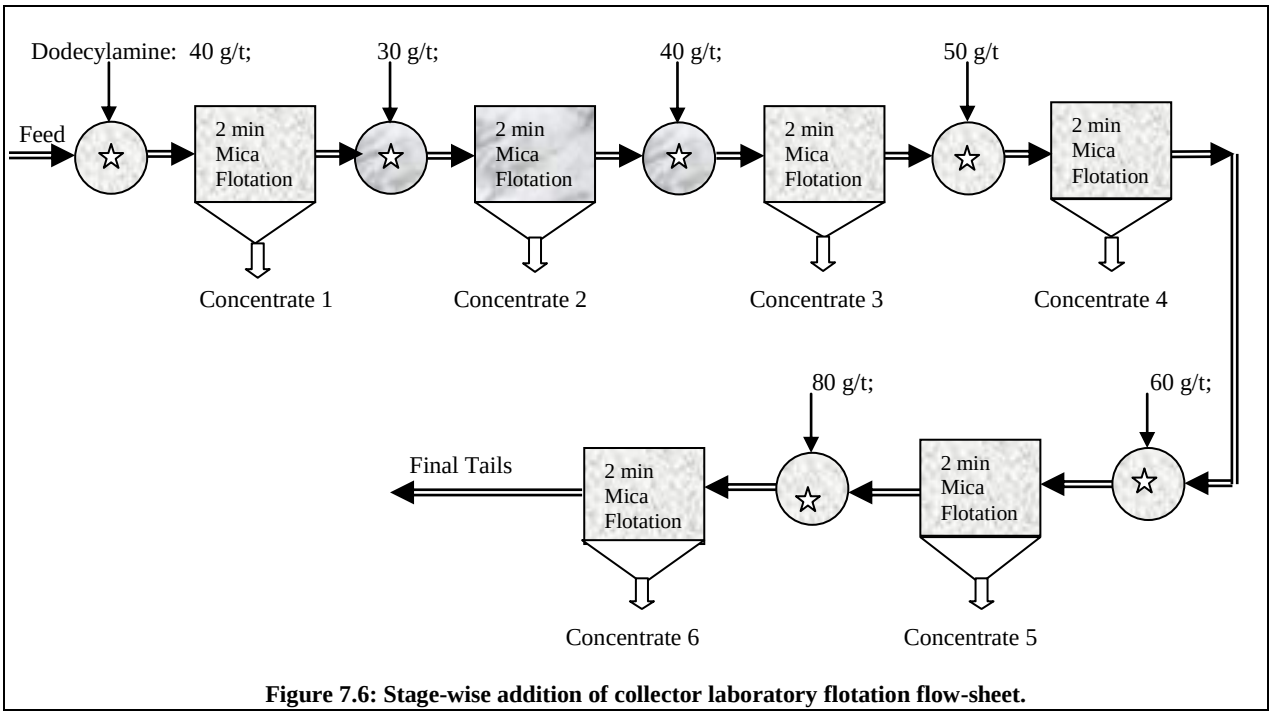

Figure 7.6: Stage-wise addition of collector laboratory flotation flow-sheet.

The experiment was performed with four replications. It was anticipated that the experiment would determine whether starvation quantities were required in order to stabilise the flotation froth and probably reduce the collector dosage with improved flotation recovery and the grade of mica concentrate.

Further experiments were carried out to compare the 300g/t with the 500 g/t collector dosage, each added in two stages of 150g/t and 250g/t respectively. The experiment was conducted in duplicate.

7.5 Recovery of Lithium-Mica from Bulk Mica Concentrate.

Magnetic separation is a common physical method used for separating minerals with different magnetic properties. Among the mica minerals, zinnwaldite is the major source of lithium. Zinnwaldite is weakly magnetic due to its relatively high iron content.

These laboratory magnetic separation experiments were conducted with a view to increasing the lithium content in the mica concentrate for subsequent lithium-leaching experiments. Two laboratory magnetic separators used were the induced roll magnetic separator and the wet high intensity magnetic separator. The other option performed to increase the lithium content in the concentrates was to carry out a cleaner laboratory flotation test on the bulk mica concentrate.

Table 7.6: Chemical composition (XRF Analysis) of the mica flotation concentrate samples.

Component	%
SiO_2	49.21
TiO_2	0.18
Al_2O_3	29.86
Fe_2O_3*	4.56
MnO	0.07
MgO	0.34
CaO	0.08
Na_2O	0.15
K_2O	8.10
P_2O_5	0.06
F	2.17
LOI	5.38
Minus O=F	0.91
Total	99.25

* = Total Fe as Fe_2O_3

The samples used in this study were produced from the mica flotation experiments. The mica concentrate was combined and riffle split into smaller fractions of about 100 g each. The chemical composition (XRF analysis) of the combined concentrate samples is given in Table 7.6. The material was analysed by the AAS method and found to contain 1.45% Li_2O, 0.55% Rb_2O and 4.47% Fe_2O_3.

7.5.1 Induced Roll Magnetic Separation.

Figure 7.7 shows a schematic diagram of the laboratory induced roll magnetic separator used in this test work. The feed to the magnetic separator was the mica concentrate obtained in the flotation experiments. In order to determine the effect of size on the separation efficiency, the concentrates were screened at: 150, 125, 106, 90, 75, 63 and 53 μm. The fraction retained on each sieve was subjected to magnetic separation. Part of the retained fraction was subjected to lithium, rubidium and iron analysis to evaluate their distribution in the respective size fractions.

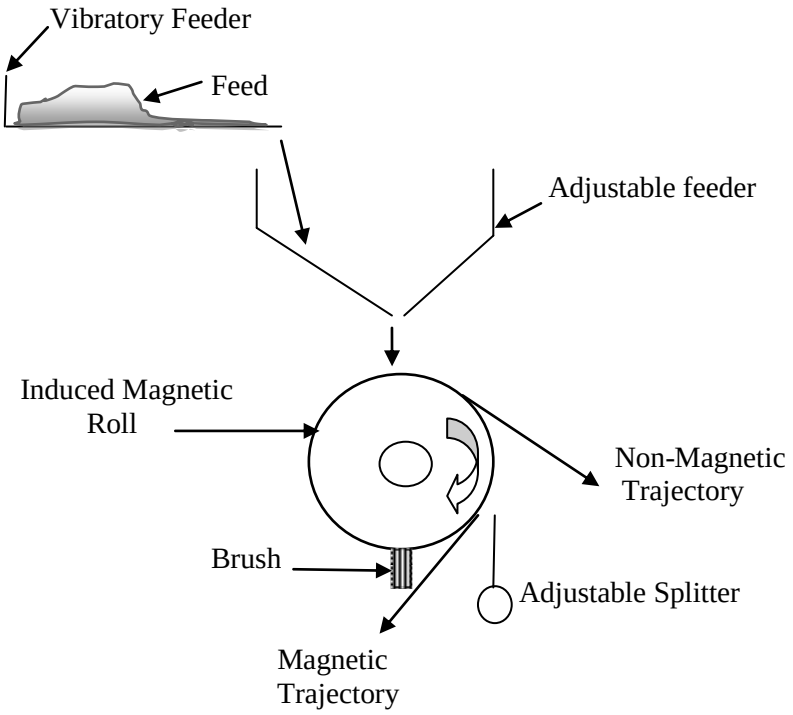

Figure 7.7: Schematic of laboratory induced roll magnetic separator

The mica concentrate was put on the vibrating feed distributor of the magnetic separator and the vibrating mode of the feeder was set. The distance between roll and pole was adjusted to 8 mm. The experiments were performed at currents of 1, 3 and 5 amps with corresponding magnetic field strengths of 0.64, 1.08 and 1.18 Tesla, respectively. The corresponding magnetic field strengths were obtained from the performance curves of magnetic field versus current supplied by the manufacturer of the equipment. Figure 7.8 shows the laboratory magnetic separation process flow sheet used. Each experiment was performed in stages at the respective coil currents as described below.

Stage 1

Magnetic material retained on the revolving cylindrical drum was subsequently brushed off and collected as magnetic 1 (Mag. 1) while the non-magnetic being collected in another pan as non-magnetic 1 (Non-Mag. 1).

Stage 2

The non-magnetic material from Stage 1 was again subjected to magnetic separation, producing the magnetic 2 (Mag. 2) and the non-magnetic 2 (Non-Mag. 2) materials as shown in the flow-sheet.

Stage 3

The Mag. 1 produced from Stage 1 and the Mag. 2 from Stage 2 were mixed and subjected to another magnetic separation. The products obtained here were Mag. 3 and Non-Mag. 3. The Mag. 3 was the final product.

Stage 4

Magnetic separation was performed on the non-magnetic material produced from Stage 3 (Non-Mag.3). The products of this separation process were the magnetic 4 (Mag. 4) and the non-magnetic 4 (Non-Mag. 4) materials. The Mag. 4 was mixed with Mag. 3 as a final magnetic product while the Non-Mag. 4 was mixed with Non-Mag. 2 representing the final non-magnetic material.

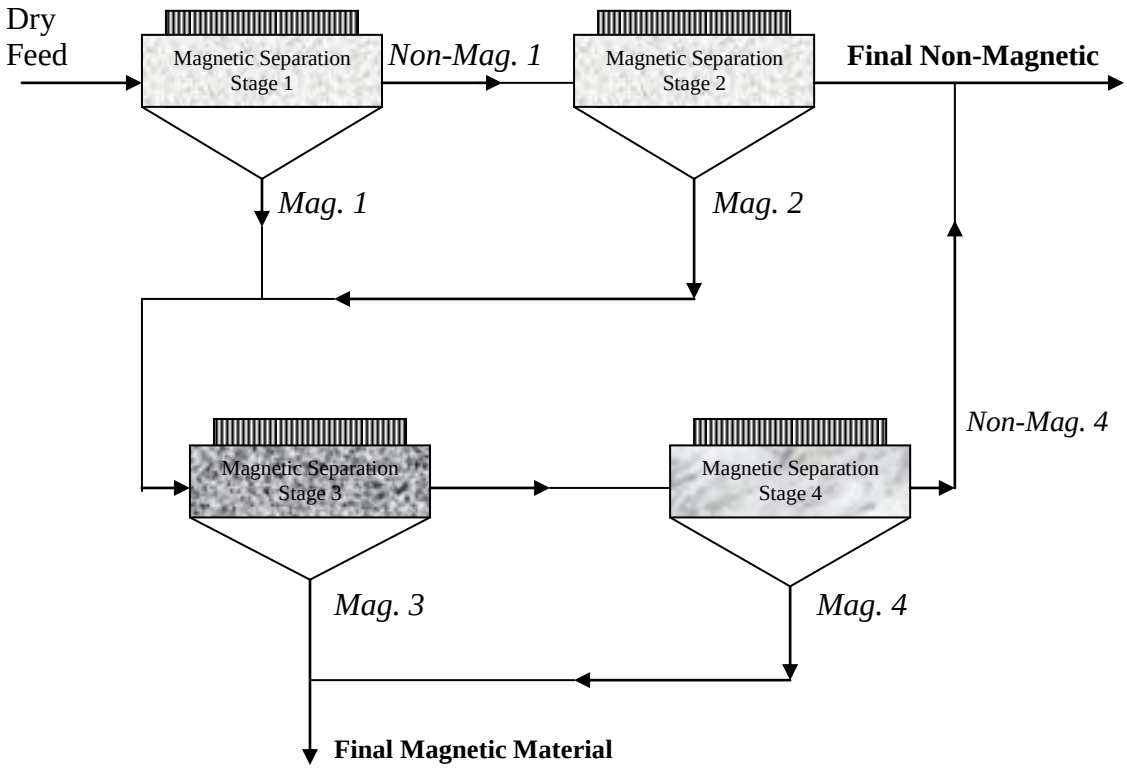

Figure 7.8: Laboratory dry induced roll magnetic separation flow-sheet.

The final magnetic and non-magnetic materials obtained at each magnetic field strength tested were analysed for lithium, rubidium and iron in order to determine the efficiency of the separation process.

7.5.2 Wet High-Intensity Magnetic Separation.

The laboratory batch type wet high intensity magnetic separator (WHIMS) manufactured by Rapid Magnetic Limited, UK, was used to separate weakly magnetic from non-magnetic minerals. It is noteworthy to mention that the manufacturer recommends the equipment to be used for experiments for less than 30 minutes to prevent the coils from overheating. Therefore, for safety reasons, the equipment is designed to trip the current when the coil is heated to a certain temperature. Figure 7.9 shows a schematic diagram of the WHIMS used in this experiment. A 1-mm matrix was used throughout the experiment.

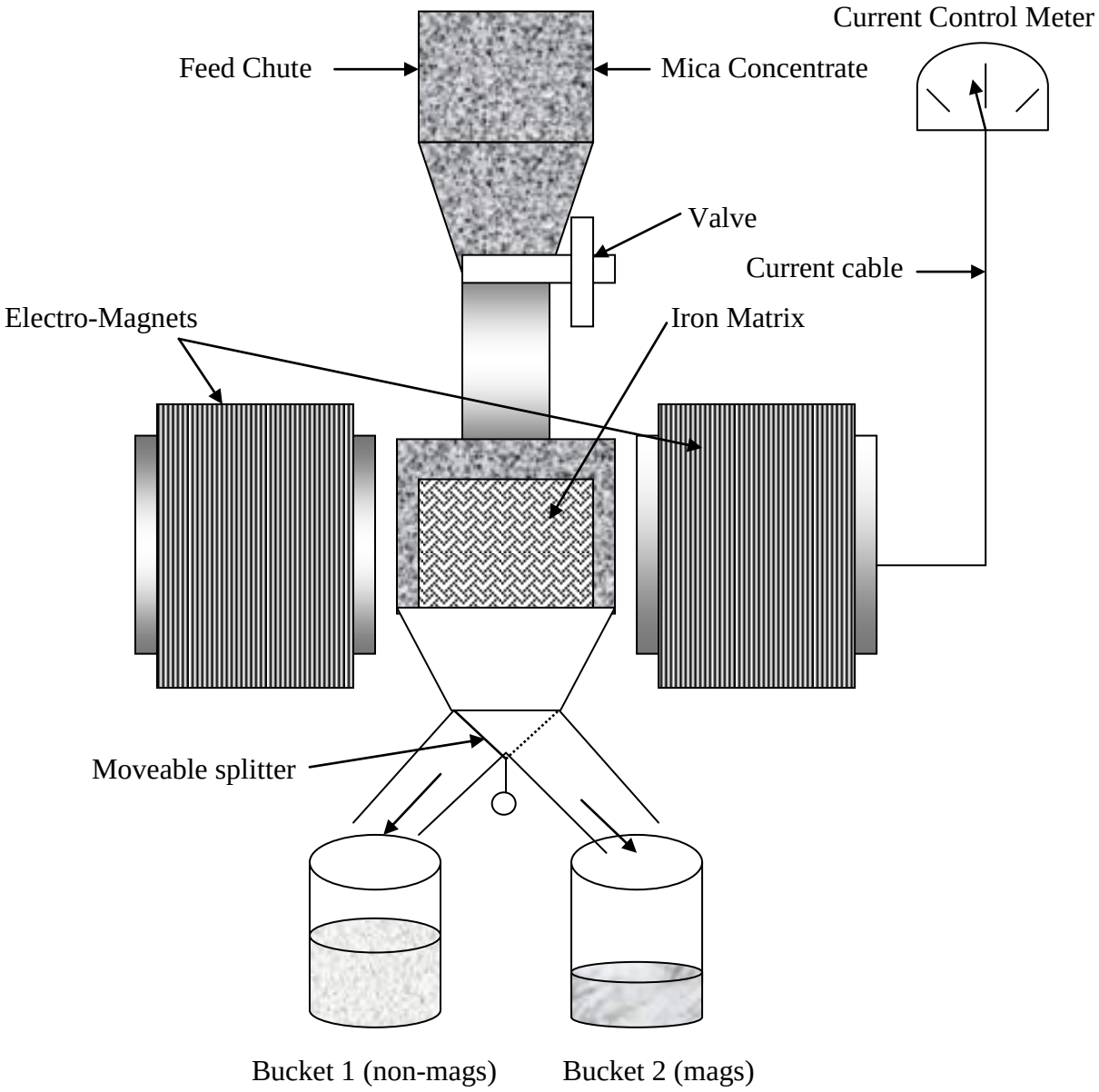

Figure 7.9: Schematic diagram of the laboratory WHIMS.

About 70 g of mica concentrate was mixed with water to give a density of about 30% solids by weight and fed into the separating chamber with the matrix in place and coil current at desired settings. Magnetic material was retained in the matrix in the chamber after flushing with water while the non-magnetic material was collected in product bucket number 1. After turning off the magnetic field, the magnetic fraction was washed from the matrix into the separate bucket number 2.

Each test was performed in three separation stages at the respective coil current. The non-magnetic material from each preceding stage became the feed to the next stage. A three stage magnetic separation at the same current is illustrated in Figure 7.10. In the first test, the coil current was set at 5 amps while in the second, third, fourth and fifth tests, the coil currents were set at 10, 15, 20 and 25 amps respectively, corresponding to magnetic fields of 0.94, 1.40, 1.77, 1.95 and 2.06 Tesla. The corresponding magnetic fields in Tesla were obtained from the performance graph of current versus magnetic field supplied by the manufacturer.

The aim of this study was to investigate the possibility of using the wet high intensity magnetic separator to recover the lithium-mica from the bulk mica concentrate produced by the flotation of china clay waste. Lithium extraction experiments were conducted on the subsequently upgraded lithium-rich mica magnetic material produced at the optimised field strength.

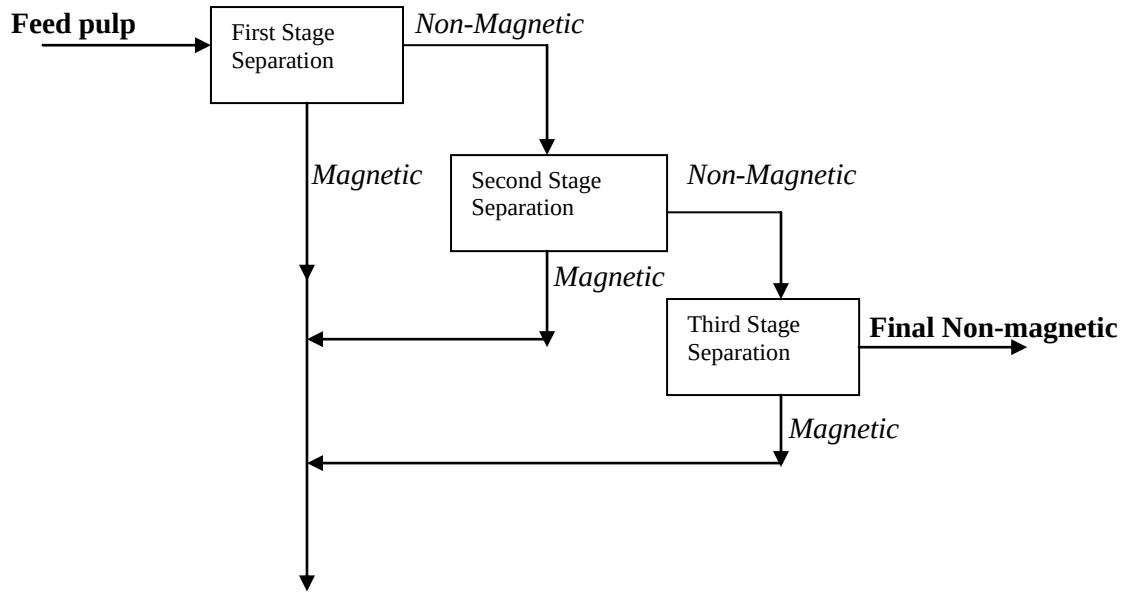

Figure 7.10: Schematic of three-stage separation on WHIMS.

7.5.3 Cleaner Flotation Separation

Three cleaner flotation tests were conducted on the bulk mica concentrate. The cleaner flotation tests were also conducted in a Denver machine equipped with a 3.5 dm^3 Minnovex designed cell. The impeller speed and air flow rate were set at 1400 rpm and 8dm^3/min respectively. A flotation test sample of about 1.2 kg was mixed with 2800 ml tap water and conditioned at 1400 rpm impeller speed. Both pH (2.5) conditioning and flotation were performed at the same impeller speed and percent solids by weight. A conditioning period of 5 minutes after collector addition was applied. The pH was adjusted by using either dilute H_2SO_4 or NaOH. Dodecylamine (98%) was again used as the cationic collector for mica flotation. A stock solution of dodecylamine was made by dissolving 5 g of dodecylamine in 200 ml of dilute hydrochloric acid to give 2.5 % (w/v) solution. The collector and frother dosages used were 500g/t and 40g/t respectively.

7.6 Lithium Extraction by Roasting and Leaching.

The paramagnetic mica concentrate used in these experiments was upgraded using a laboratory wet high intensity magnetic separator (WHIMS) operated at 20 amps (1.95 Tesla) based on the experiments conducted above. About 3 kg of paramagnetic mica concentrate was produced by a series of runs through the WHIMS. The material was analysed using the AAS method and found to contain 2.07% Li_2O, 0.74% Rb_2O and 7.41% Fe_2O_3. The content of main elements present in the concentrate as analysed by the XRF method is given in Table 7.7.

Table 7.7: Chemical analysis (XRF) of the separation products at magnetic field of 1.95 Tesla

Fraction	wt%	Content (%)														
		SiO_2	Al_2O_3	Fe_2O_3*	TiO_2	MgO	CaO	K_2O	Na_2O	P_2O_5	F	Li_2O	Rb_2O	LOI	Minus O=F	Total
Magnetic	50.31	40.1	27.76	7.42	0.27	0.11	0.07	9.56	0.15	0.06	3.36	2.07	0.74	3.39	1.41	93.65
Non-mag	49.69	50.64	32.00	2.28	0.11	0.33	0.1	6.84	0.14	0.08	1.27	0.76	0.37	6.37	0.53	100.76
Head	100.00	45.34	29.87	4.87	0.19	0.22	0.08	8.21	0.15	0.07	2.32	1.42	0.56	4.87	0.97	97.20
Fraction	**wt%**	**Recovery (%)**														
		SiO_2	Al_2O_3	Fe_2O_3	TiO_2	MgO	CaO	K_2O	Na_2O	P_2O_5	F	Li_2O	Rb_2O			
Magnetic	50.31	44.50	46.76	76.72	71.31	25.23	41.48	58.59	52.03	43.16	72.82	73.39	66.94			
Non-mag	49.69	55.50	53.24	23.28	28.69	74.77	58.52	41.41	47.97	56.84	27.18	26.61	33.06			
Head	100	100	100	100	100	100	100	100	100	100	100	100	100			

* = Total Fe as Fe_2O_3

Three methods of lithium extraction were tested on the concentrate i.e. gypsum ($CaSO_4.2H_2O$), limestone ($CaCO_3$) and sodium sulphate (Na_2SO_4) methods. The methods involved mixing the paramagnetic mica concentrate with gypsum, limestone or sodium sulphate respectively and roasting the mixture in the pre-heated furnace at a selected temperature for 60 minutes.

7.6.1 Roasting Process

In preparation for the roasting process, the paramagnetic mica concentrate was pulverised in a Tema mill with a tungsten carbide pot for 3 minutes before being mixed with the gypsum, calcium carbonate or sodium sulphate. Figure 7.11 shows the particle size distribution of raw and pulverised paramagnetic mica concentrate. A predetermined weight of pulverised paramagnetic mica concentrate (90% <100 μm) and the respective calcium and sodium salts were mixed and put in ceramic crucibles before being roasted in a pre-heated Carbolite furnace (CWF 1200) at selected temperatures for 60 minutes.

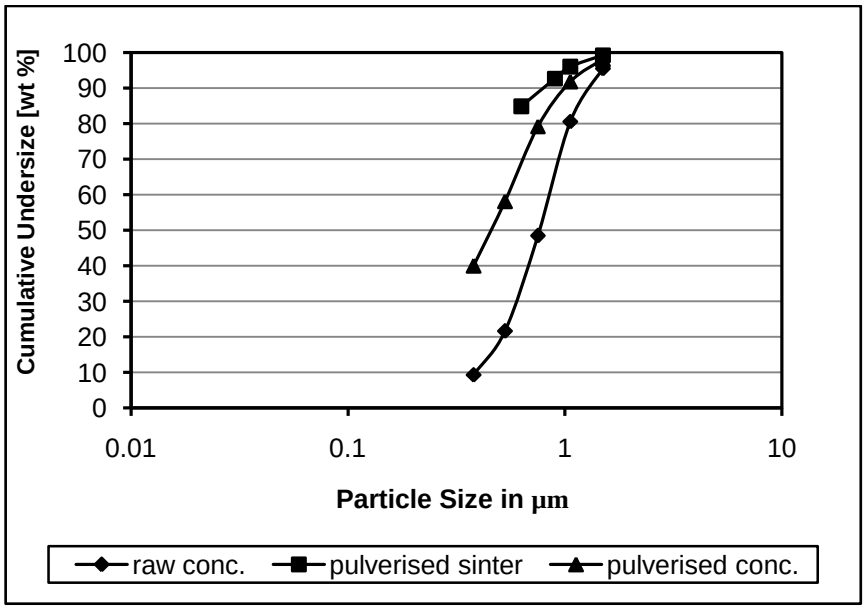

Figure 7.11: Particle size distributions of raw and ground mica concentrate.

The weight ratio of mica concentrate to $CaSO_4.2H_2O$ or Na_2SO_4 was 2:1 for the roasting temperature optimisation. The roasting temperatures ranged from 250 to 1100^oC. The mica concentrate to calcium or sodium salt ratio optimisation was carried out at the optimised roasting temperature. The concentrate to gypsum ratio in material ranged from 2:1 to 10:1

while that of concentrate to sodium sulphate ranged from 2:1 to 7:1. Analytical reagent grade calcium sulphate dihydrate (>98% purity) was supplied by Fisher Scientific Ltd, while sodium sulphate anhydrous powder (>99.5% purity) was supplied by Hopkins and Company, UK. Tables showing the reagent specifications are presented in Appendix H4.

When treating the concentrate by the limestone method, three weight ratios of concentrate to $CaCO_3$ of 5:1, 5:2 and 3:1 were studied with roasting temperatures of 250-1050^oC. The calcium carbonate (>99% purity) was supplied by BDH Laboratory Supplies, UK, and the Table showing the limits of impurities in the reagent is also presented in Appendix H4.

7.6.2 Leaching Process

During the roasting process the mica concentrate reacted with the respective calcium and sodium salts to form a solid product which required pulverising before leaching. The typical size distribution of the pulverised sinter is given in Figure 7.11. The pulverised roasted products were water leached in a stirred-glass reaction vessel placed in a water bath maintained at a temperature of within $\mp 2^oC$ of the set temperature in the range of 20 to 85^oC. About 10 g of roast-product was leached with deionised water at a leaching time ranging from 2 to 60 minutes and a liquid-solid ratio of 10:1. Leaching was conducted at the "natural" pH of the pulp. After leaching for the specified time, samples were filtered, the leach solution (filtrate) collected and the residues dried.

7.6.3 Analysis and Equipment

Samples of mica concentrate, roast-product and leach residues were subjected to X-Ray Fluorescence (XRF) analysis (Bruker S4 Pioneer) and X-Ray Diffraction (XRD) analysis (Siemens Diffraktometer D5000). To analyse for Li, Rb and Fe in roasted material and leach residue, about 1g of material was mixed with 5 ml of perchloric acid ($HClO_4$) and 10 ml of hydrofluoric acid (HF) in a PTFE beaker and put on the hot plate for decomposition by evaporation in a fume chamber until a solid residue remained. Then about 10 ml each of hydrochloric acid (HCl) and boric acid (H_3BO_3) was added together with about 30 ml of deionised water and gently heated for 15 minutes to dissolve the solid residue. After cooling, the solution was put in a 250 ml volumetric flask and topped up to the mark with deionised water before being taken for elemental composition determination by the Atomic Absorption Spectrophotometry (AAS) method (Unicam SP 9) explained in section 7.3.3.

7.7 Thermal Analysis of the Leaching Materials

General Information

Thermal analysis (TA) comprises a group of techniques in which a physical property of a substance is measured as a function of temperature, while the substance is subjected to a controlled temperature programme. Thermogravimetry (TG) monitors changes in the mass of the specimen on heating. Differential thermal analysis (DTA) involves heating or cooling a test sample and an inert reference under identical conditions, while recording any temperature difference between the sample and reference. This differential temperature is then plotted against temperature or against time. Changes in the sample which lead to the absorption or evolution of heat can be detected relative to the inert reference. DTA can therefore be used to study thermal properties and phase changes which do not lead to a change in enthalpy. Thus, DTA may formally be defined as a technique for recording the difference in temperature between a substance and a reference material against either time or temperature as the two specimens are subjected to identical temperature regimes in an environment heated or cooled at a controlled rate (Bhadeshia, 2002; Mackenzie, 1973).

Equipment

The equipment used in these experiments was a Stanton Redcroft STA 780 Simultaneous Thermal Analyser Series, designed to give simultaneous thermogravimetric (TG) records and differential thermal analysis (DTA) curves.

Thermocouple system: The hang-down arrangement housed the Pt v 13% Rh-Pt flat plate thermocouple system for ΔT and T.

Sample containers: The sample and reference materials were housed in shallow Pt-Rh dishes of approximate volume 135 mm^3 and 6 mm diameter.

The materials used for the leaching experiments were subjected to thermal analysis in the equipment described above, that measures differential temperature (ΔT), change in mass and the environment temperature (T) of the specimen. The idea was to understand how the materials responded to heat treatment, the nature of chemical reactions taking place in the samples and the mineral phases being formed.

The key features of a differential thermal analysis apparatus were as follows:

1. Sample holder comprising thermocouples, sample containers and a ceramic or metallic block.
2. Furnace.
3. Temperature programmer.
4. Recording system.

The essential requirements of the furnace are that it should provide a stable and sufficient large hot-zone and must be able to respond rapidly to commands from the temperature programmer. A temperature programmer is essential in order to obtain constant heating rates. The recording system must have a low inertia to faithfully reproduce variations in the experimental set-up.

The sample holder assembly consisted of a thermocouple each for the sample and reference, surrounded by a block to ensure an even heat distribution. The sample was contained in a small Pt-Rh crucible. Not more than 10 mg of the sample should be used for each test. The materials tested were gypsum, limestone, sodium sulphate, calcium hydroxide, paramagnetic mica and paramagnetic-mica mixed with gypsum, limestone and sodium sulphate respectively.

8. RESULTS

8.1 Effect of Impeller Speed, Frother Dosage and Aeration Rate on the Flotation Recovery of Mica Minerals.

8.1.1 Flotation Results

The experimental procedure of the factorial design is given in section 7.4.1. Detailed results of the XRF and LOI analyses on concentrates and tailings are presented in Appendix B1.

Figure 8.1 shows graphically all the possible combinations and the results (average of the two duplicates) obtained as a function of (a) Fe_2O_3 recovery and (b) Fe_2O_3 grade in the concentrate.

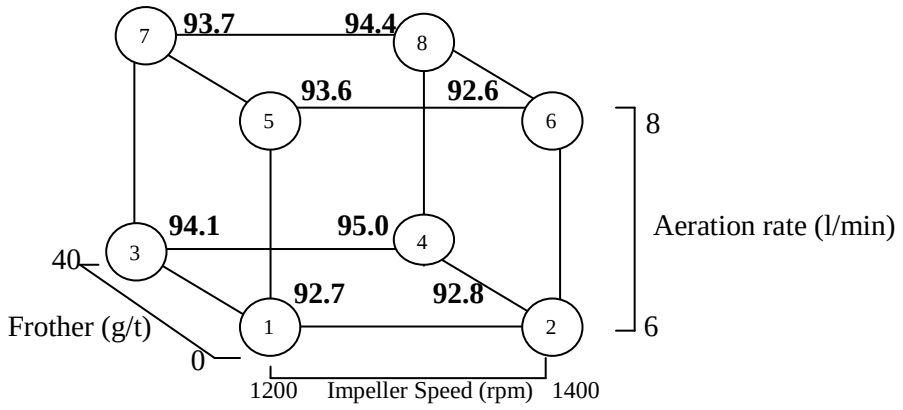

(a)

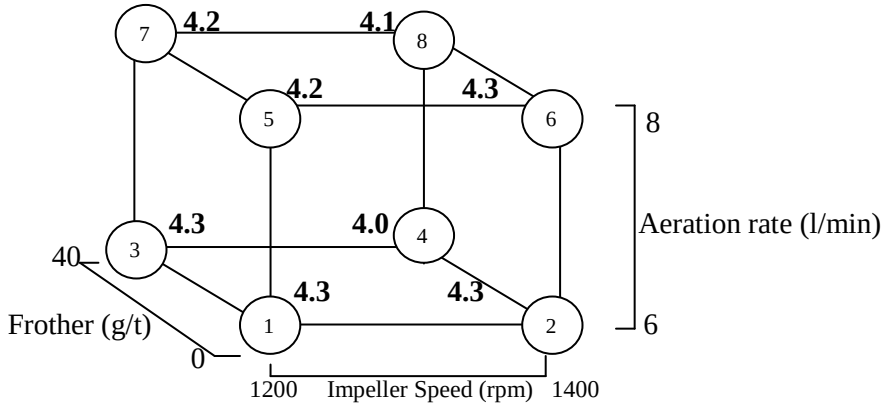

(b)

Figure 8.1: Graphical presentation of the obtained results (average of the two replicates) as a function of: (a) Fe_2O_3 recovery % and (b) Fe_2O_3 grade % in concentrate.

8.1.2 Statistical Analysis of the Flotation Results

Detailed analysis of variance (ANOVA) of the obtained results as a function of Fe_2O_3 recovery and grade in the concentrate is given in Appendix B2.

The ANOVA of the results as a function of recovery of Fe_2O_3 in concentrate shows that all the variables, impeller speed (*A*), frother dosage (*B*) and aeration rate (*C*) with their respective combinations do not significantly affect the Fe_2O_3 recovery or grade in the concentrate at the 95% confidence level.

The ANOVA of the obtained results shows that all the variables studied, as well as their combinations, did not significantly affect the grade and recovery of mica minerals in the concentrate. This could be attributed to effective bubble-particle collision and attachment under the same pulp chemical environment and also that the variable range tested was too close to give significantly different results. The collector dodecylamine probably possesses some frothing characteristics since no froth developed in the absence of the collector when the air was turned on. In the absence of frothers, air bubbles produced by a rotating impeller may coalesce as the air streams impinge on the stator blades (Levich, 1962; Cho and Laskowski, 2002; Grau and Heiskanen, 2005).

The combined mica concentrates and tails from these experiments were analysed for lithium and rubidium. The concentrates contained about 1.43% Li_2O and 0.52% Rb_2O while the tailings assayed about 0.03% Li_2O and 0.14% Rb_2O, giving a recovery on average of 98.87% and 87.21% respectively.

8.2 Effect of Collector Dosage and pH on the Flotation Recovery of Mica Minerals.

8.2.1 Flotation Results

Section 7.4.2 shows the experimental procedure. Detailed metallurgical balance sheets for these flotation tests are given in Appendix C1. Figure 8.2 shows the iron (Fe_2O_3) recovery (average) in concentrate as a function of collector dosage at various pH levels while Figure 8.3 shows the Fe_2O_3 grade profiles. It can be seen from Figure 8.2 that the highest recovery of iron in the concentrate was about 93% and 92% at pH 2.5 and 3.5 both at 500g/t of

collector dosage respectively. It is also evident from Figure 8.3 that the pH range tested had no significant effect on the concentrate grades.

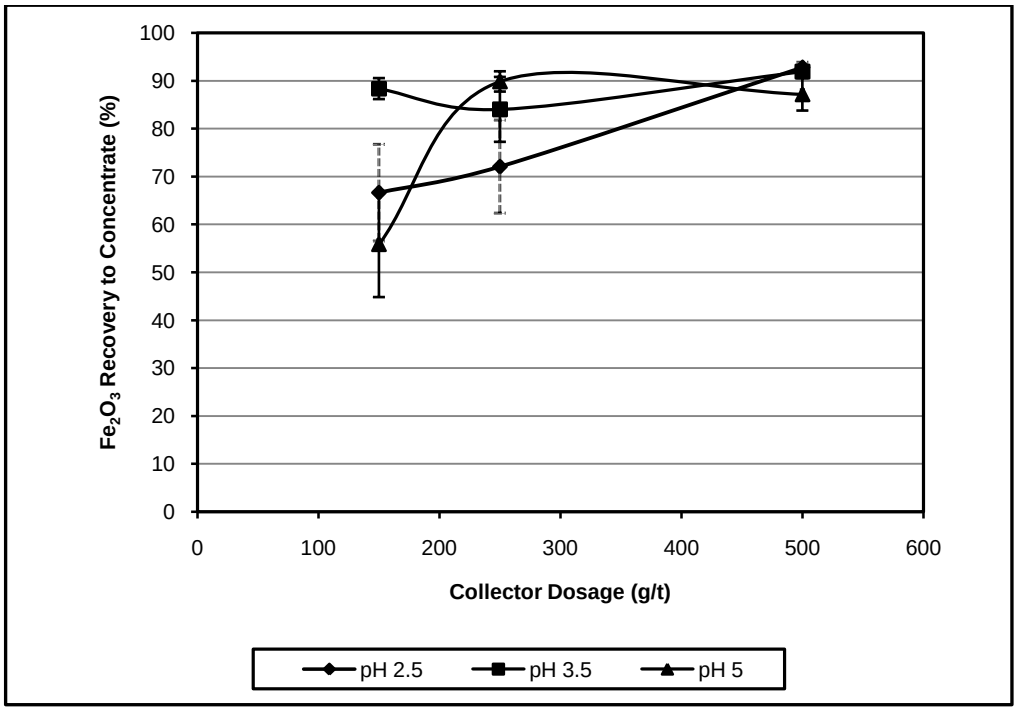

Figure 8.2: Recovery profiles of Fe_2O_3 as a function of collector dosage and pH.

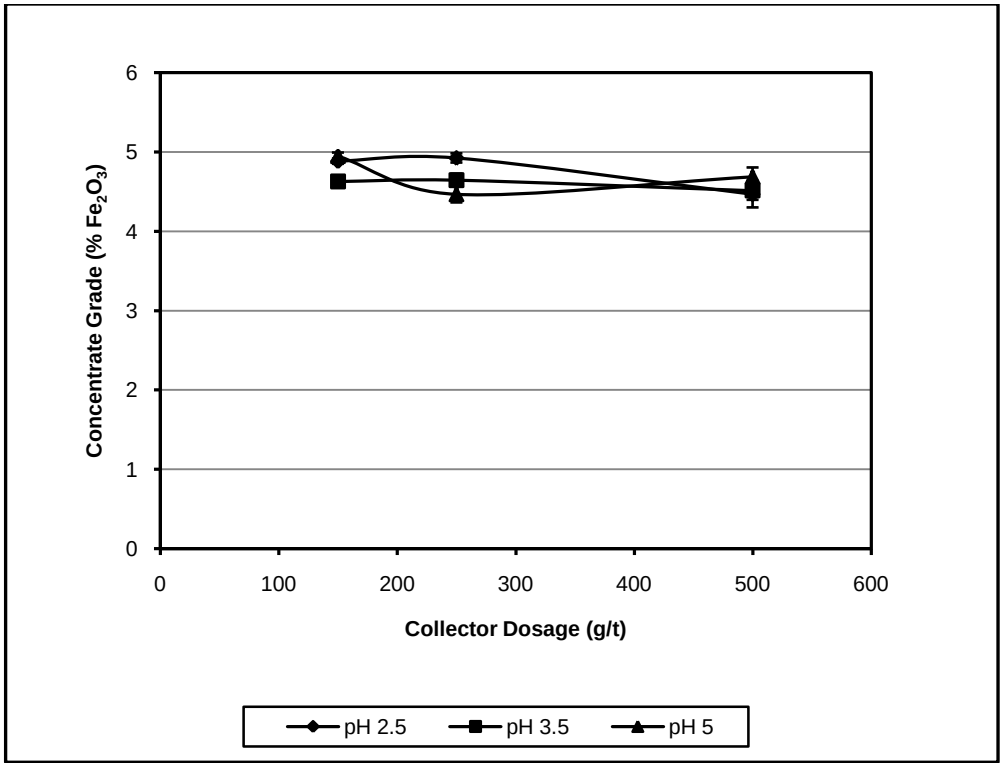

Figure 8.3: Grade profiles of Fe_2O_3 as a function of collector dosage and pH.

8.2.2 Statistical Analysis of the Flotation Results

Table 8.1 shows the analysis of variance (ANOVA) of the results expressed in recovery of iron in concentrate. As seen from Table 8.1, different collector dosages result in different Fe_2O_3 recoveries as the computed *f* is significant at 99% confidence level [$f_{0.01}$ (2,18) = 6.01]. Furthermore, pH has no significant effect on the recovery [[$f_{0.05}$ (2, 18) = 3.55] of iron in the concentrate. Additionally, pH and collector interaction have no significant effect on recovery [$f_{0.05}$ (4,18) = 2.93].

Table 8.1: Analysis of variance of the results expressed in recovery of Fe_2O_3 in the concentrate

Source of variation	Sum of squares	Degrees of freedom	Mean square	Computed *f*	Theoretical *f*	
					α = 0.01	α = 0.05
Collector dosage	1876.61	2	938.31	7.27	6.01	3.55
pH	689.66	2	344.83	2.67	6.01	3.55
Interaction	1501.63	4	575.41	2.91	4.58	2.93
Error	2322.81	18	129.05			
Total		26				

Table 8.2 shows the analysis of variance of the results expressed in grade of Fe_2O_3 in concentrates. As seen from the results, different collector dosages result in different grades of iron in concentrate since the computed *f* is significant only at 95% confidence level [$f_{0.05}$ (2,18) = 3.55]. The pH has no significant effect on the grades of iron in concentrate even at 95% confidence level [$f_{0.05}$ (2,18) = 3.55] while its interaction with the collector dosage significantly affects the grades only at 95% confidence level [$f_{0.05}$ (4,18) = 2.93].

Table 8.2: Analysis of variance of the results expressed in grade of Fe_2O_3 in the concentrate.

Source of variation	Sum of squares	Degrees of freedom	Mean square	Computed *f*	Theoretical *f*	
					α = 0.01	α = 0.05
Collector dosage	0.312585	2	0.156293	5.764891	6.01	3.55
pH	0.123474	2	0.061737	2.277186	6.01	3.55
Interaction	0.447593	4	0.111898	4.127391	4.58	2.93
Error	0.488000	18	0.027111			
Total	1.371652	26				

8.3 Effect of Stage-Wise Addition of Collector on the Flotation Recovery of Mica Minerals.

8.3.1 Flotation Results

Four flotation tests were performed to investigate the effect of stage-wise addition of collector on the flotation recovery of mica minerals (see section 7.4.3). Detailed metallurgical results of the flotation tests are given in Appendix D. Table 8.3 shows the average results expressed as cumulative recovery and grade of iron in the concentrates. The recovery of Fe_2O_3 in the concentrates was again used as a measure of mica flotation efficiency. It can be seen from Table 8.3 that stage wise addition of collector resulted in a lower amount of collector being used but gave similar recovery and grade of Fe_2O_3 in concentrate as obtained in the previous test work at 500 g/t collector dosage. The collector was added in six stages totalling 300g/t. The total flotation time was 12 minutes.

Table 8.3: Summarised results of the six-stage collector addition.

Test Number	Total Collector Dosage, g/t	Cumulative wt %	Cumulative Grade % Fe_2O_3*	Cumulative Recovery % Fe_2O_3
Run 1	300	53.97	4.83	92.60
Run 2	300	58.40	4.53	95.59
Run 3	300	56.47	4.62	93.88
Run 4	300	57.29	4.57	93.96
Mean	***300***	***56.53***	***4.64***	***94.01***
Standard Deviation		***1.88***	***0.13***	***1.23***

* Total Fe as Fe_2O_3

Further experiments were carried out to compare the 300g/t with the 500g/t collector dosage, each added in two stages of 150g/t and 250g/t respectively. The experiment was conducted in duplicate and Table 8.4 shows the summary of the results. Each flotation test was conducted for 8 minutes.

Using the *t-test* for two *means*, the 500 g/t collector dosage was found to give significantly higher recovery than 300g/t with 95% confidence (single-tailed test), while the grade of the 300g/t was found to be significantly higher than that of the 500 g/t with 99% confidence (single-tailed test).

Comparing the results of the six-stage collector addition at 300g/t with those of the two-stage collector addition at 500g/t, it was found that both the recovery and grade were not significantly different at +99% confidence level.

Table 8.4: Summarised results of the two-stage collector addition

Test Number	wt %	300 g/t collector dosage	
		Cumulative Grade % Fe_2O_3*	Cumulative Recovery % Fe_2O_3
Run 1	45.64	4.90	79.92
Run 2	49.72	4.87	86.71
Mean	***47.68***	***4.89***	***83.32***
Standard deviation	***2.89***	***0.02***	***4.80***
		500 g/t collector dosage	
Test Number	**wt %**	**Cumulative Grade % Fe_2O_3**	**Cumulative Recovery % Fe_2O_3**
Run 1	57.14	4.62	93.52
Run 2	56.82	4.55	93.54
mean	***56.98***	***4.59***	***93.53***
Standard deviation	***0.226***	***0.05***	***0.01***

* Total Fe as Fe_2O_3

8.4 Recovery of Lithium-Mica from the Bulk Mica Concentrate.

8.4.1 Induced Roll Magnetic Separation.

The experimental procedure is given in section 7.5.1. The mica concentrate was screened at the following sieve sizes: 150, 125, 106, 90, 75, 63 and 53µm. A series of magnetic separation tests was conducted on each size fraction. Detailed magnetic separation results are given in the Appendix E. Figure 8.4 shows the size by assay of lithium, rubidium and iron oxides distribution in the mica concentrate. As can be seen from the figure the grade of lithium, rubidium and iron increased from finer to coarser size fractions.

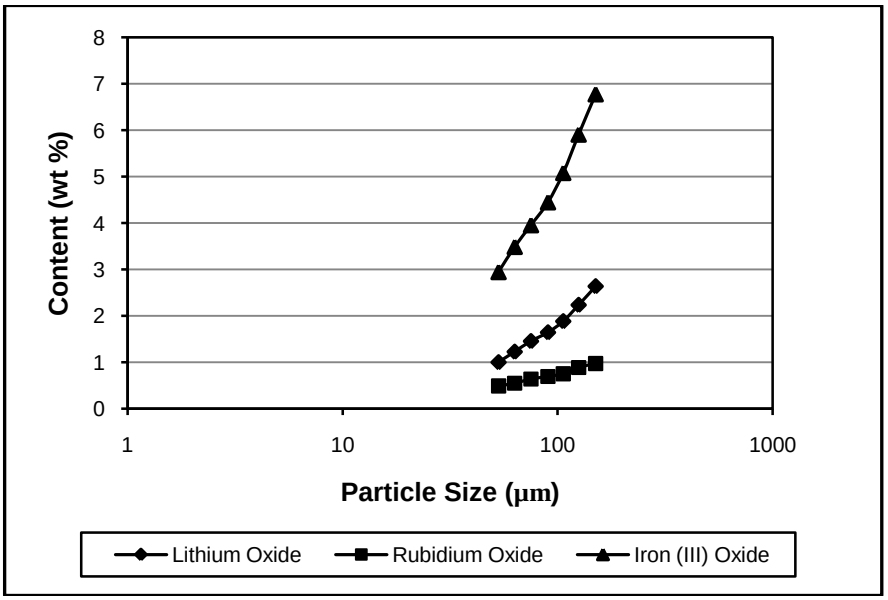

Figure 8.4: Size by assay lithium, rubidium and iron oxides content in flotation concentrate.

Figure 8.5 shows the magnetic product weight recovery as a function of magnetic field strength. It can be seen from the figure that the weight recovery in the finer sizes increased as the field strength was increased while that of the coarser size gradually decreased. The increase in the finer sizes could be attributed to physical entrapment rather than magnetic separation. The induced roll magnetic separator results were very poor and all the results are not shown here but can be seen in Appendix E.

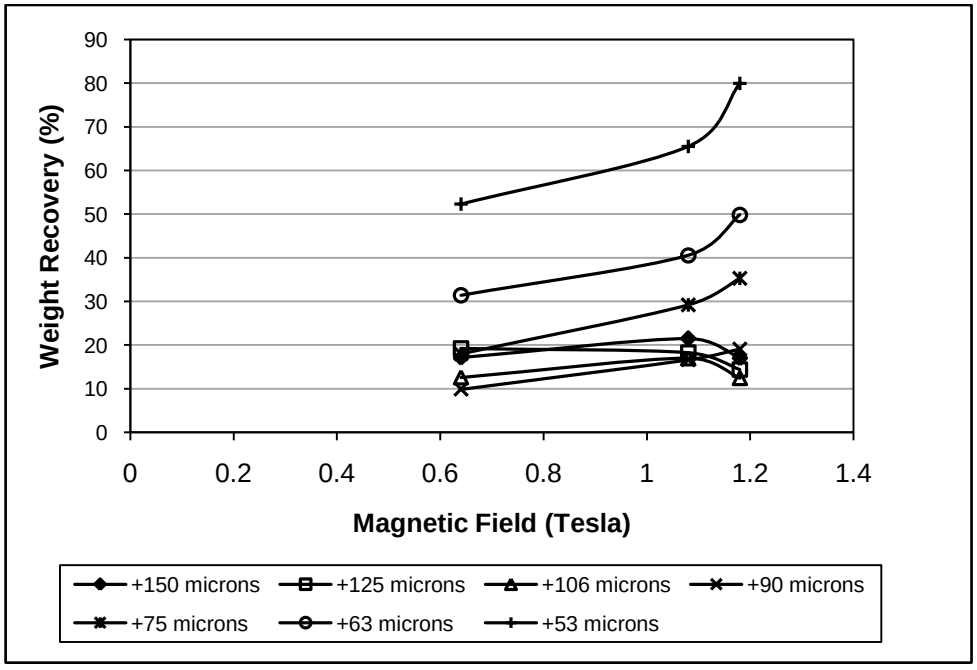

Figure 8.5: Magnetic product weight recovery as a function of magnetic field strength and particle size.

8.4.2 Wet High-Intensity Magnetic Separation.

Section 7.5.2 gives the experimental procedure. Detailed results of the wet high intensity magnetic separation of high-iron/high-lithium mica minerals from bulk mica concentrate are given in Appendix F1.

A series of tests were conducted to determine the effect of magnetic field strength on separation efficiency. These results are shown in Figures 8.6 and 8.7 as recovery and grade profiles of lithium oxide (Li_2O), rubidium oxide (Rb_2O) and iron (III) oxide (Fe_2O_3) as a function of magnetic field respectively. As seen from Figure 8.6, the recovery of both, lithium, rubidium and iron increased as the magnetic field was increased from 0.94 Tesla to 2.06 Tesla. Between 1.95 Tesla and 2.06 Tesla the recovery reached a plateau showing that

any further increase in magnetic field did not result in significant increase in recovery. It can also be observed from Figure 8.7 that the grade of lithium, rubidium and iron decreased gradually as the magnetic field was increased from 0.94 Tesla to 2.06 Tesla.

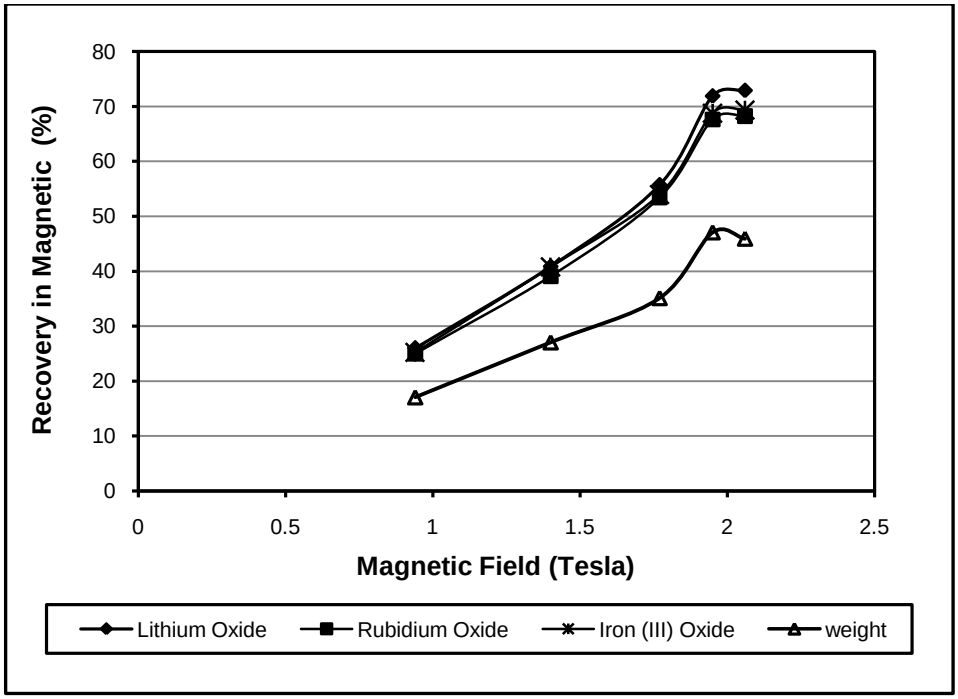

Figure 8.6: Magnetic product recovery profiles as a function of magnetic field.

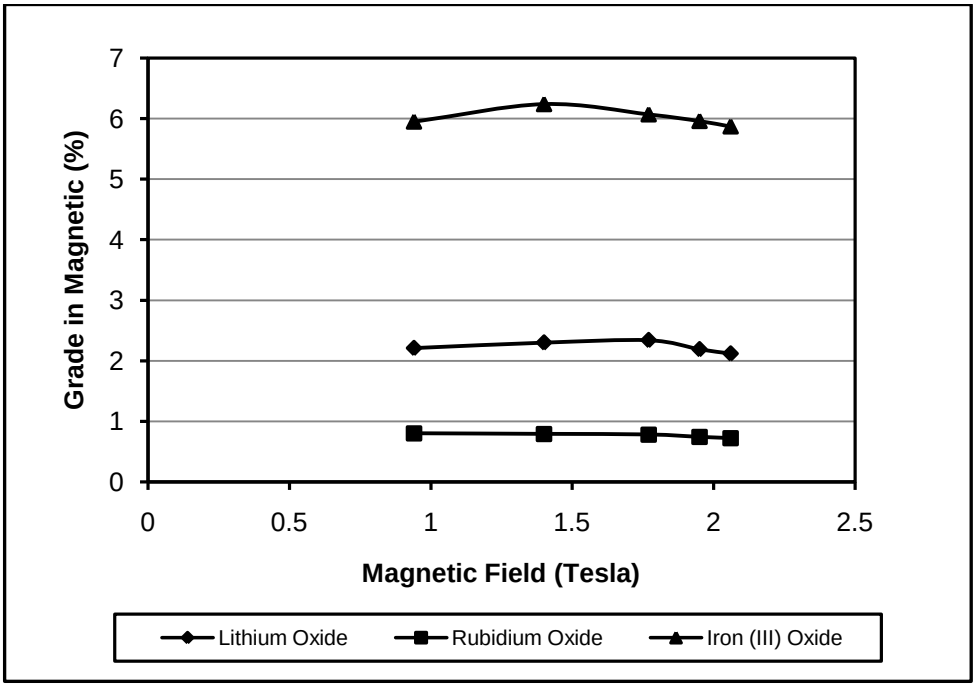

Figure 8.7: Magnetic product grade profiles as a function of magnetic field.

In order to determine the effect of particle size on the separation efficiency, each of the magnetic and non-magnetic products obtained at 1.40, 1.77, 1.95 and 2.06 Tesla were screened. The screens used were 150, 106, 75, 53 and 38 µm. The size by size weight recovery in the magnetic product as a function of magnetic field is shown in Figure 8.8. As can be seen from the Figure, there was a general increase in the weight recovery of all size fractions as the magnetic field was increased. The maximum weight recovery of about 64% occurred in the +150µm and +106µm size fractions at a magnetic field of 1.95 Tesla. The effect of magnetic field strength as well as particle size on recovery is evident.

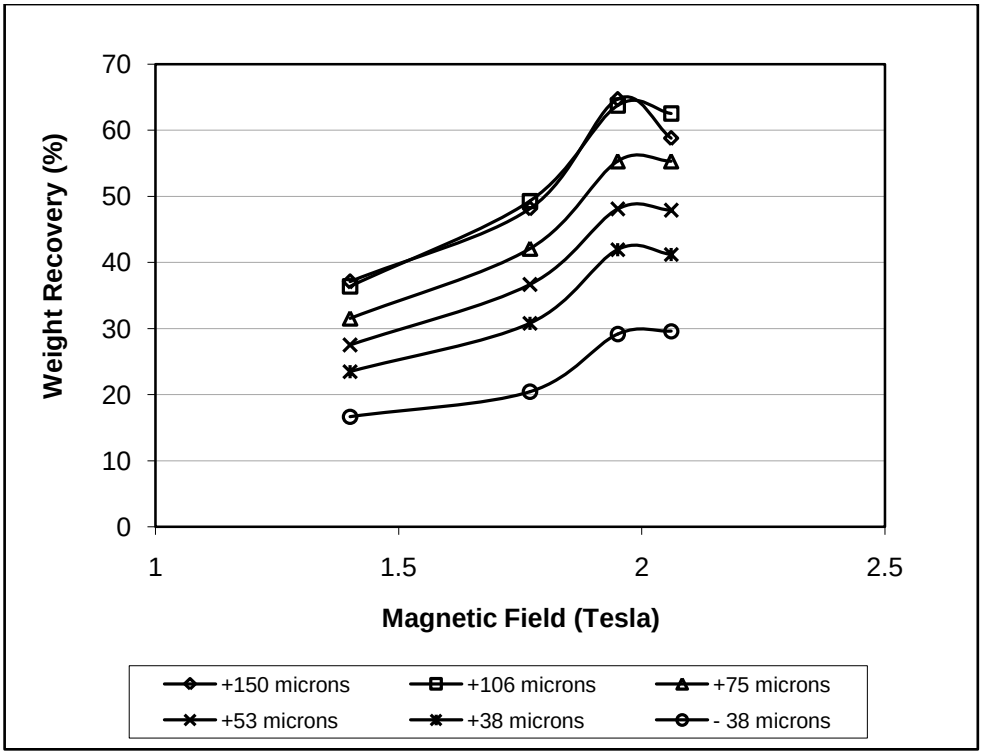

Figure 8.8: Size by size weight recovery in the magnetic as a function of magnetic field.

The graphs of the size by size recovery in the magnetic product of Li_2O, Rb_2O and Fe_2O_3 are shown in Figures 8.9 – 8.11 respectively. Figure 8.9 shows the size by size recovery of Li_2O in the magnetic product as a function of magnetic field. As can be seen from the Figure, the Li_2O recovery in the magnetic product increased in all size fractions reaching a maximum at a magnetic field of 1.95 Tesla. Further increasing the magnetic field beyond 1.95 Tesla decreased the recovery in all size fractions. The highest recovery of Li_2O in the magnetic product occurred in the + 150µm at a magnetic field of 1.95 Tesla.

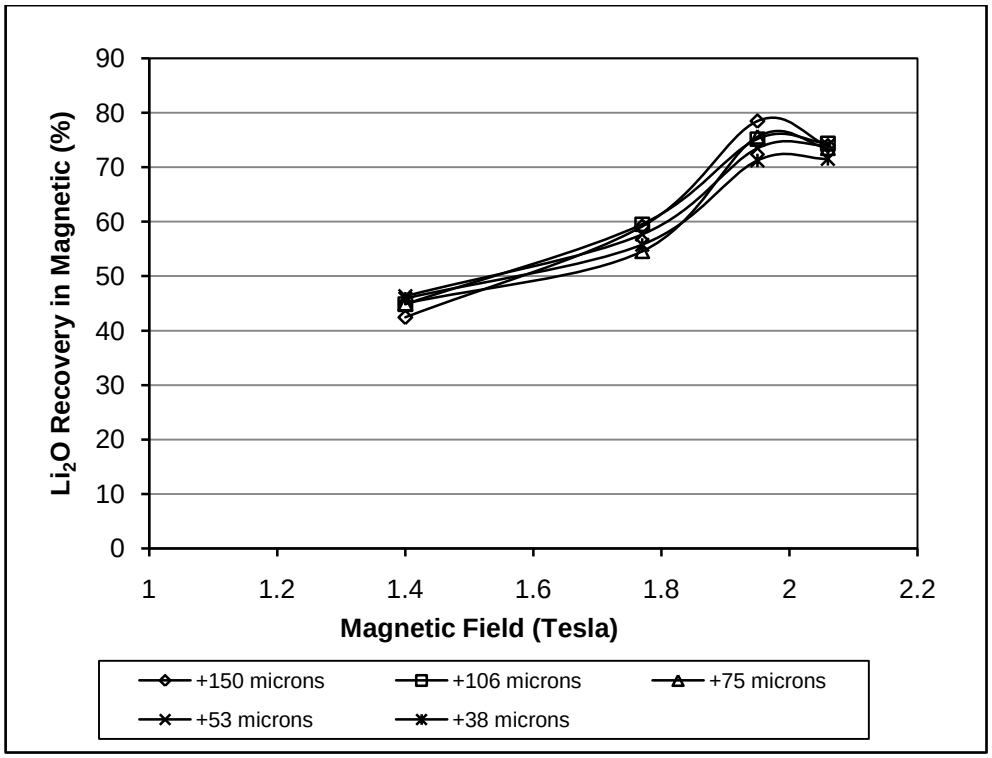

Figure 8.9: Size-by-size Li_2O recovery in the magnetic product as a function of magnetic field.

Figure 8.10 gives the size by size recovery of Rb_2O in the magnetic product as a function of magnetic field strength. The same trend as observed with the recovery of Li_2O in the magnetic is exhibited here. The Figure shows that the recovery of Rb_2O in the magnetic product increased in all sizes with the maximum of about 76% observed again at a magnetic field of 1.95 Tesla in the +150 size fraction.

The size by size recovery of Fe_2O_3 in the magnetic product is shown in Figure 8.11. Again the same trend as observed in the recovery of Li_2O and Rb_2O in the magnetic products is repeated where the recovery of Fe_2O_3 in the magnetic product increased in all sizes as the magnetic field was increased, reaching a maximum at 1.95 Tesla. The highest recovery of about 81% Fe_2O_3 occurred in the +150 µm size fraction at a magnetic field of 1.95 Tesla.

It can be seen from the figures above that increasing the magnetic field beyond 1.95 Tesla resulted in slightly lower recovery of Li_2O, Rb_2O and Fe_2O_3 in the magnetic product. This could be attributed to the magnetic field strength being saturated beyond 1.95 Tesla.

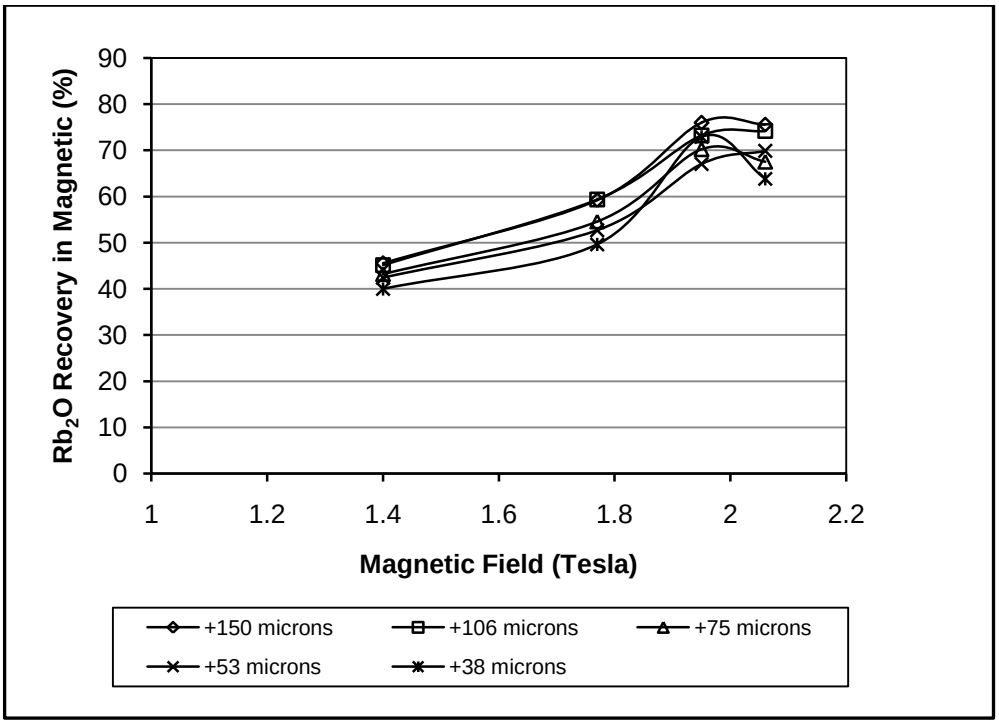

Figure 8.10: Size-by-size Rb_2O recovery in the magnetic product as a function of magnetic field.

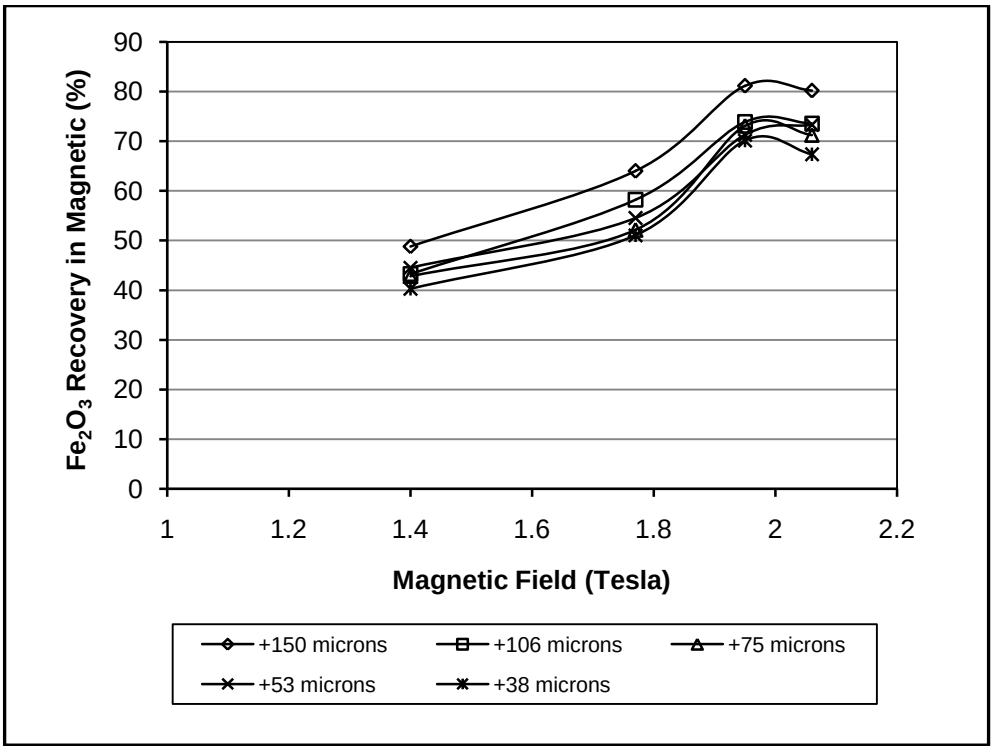

Figure 8.11: Size-by-size Fe_2O_3 recovery in the magnetic product as a function of magnetic field.

Thus, a series of experiments were conducted with the current set at 20 amps (1.95 Tesla) to produce about 3 kg of concentrate for the subsequent leaching experiments.

XRD Analysis of the Magnetic Separation Products

The magnetic and non-magnetic products were subjected to XRD analysis. Figure 8.12 shows the XRD profiles of the magnetic mica while Figure 8.13 shows the XRD profiles of the non-magnetic mica. It can be observed that the two profiles are almost similar and only differ in the proportions of minerals present. It is evident from the two profiles that there was more polylithionite than zinnwaldite in the non-magnetic fraction. This showed that polylithionite was difficult to recover by magnetic separation and was responsible for most of the lithium present in the non-magnetic fraction.

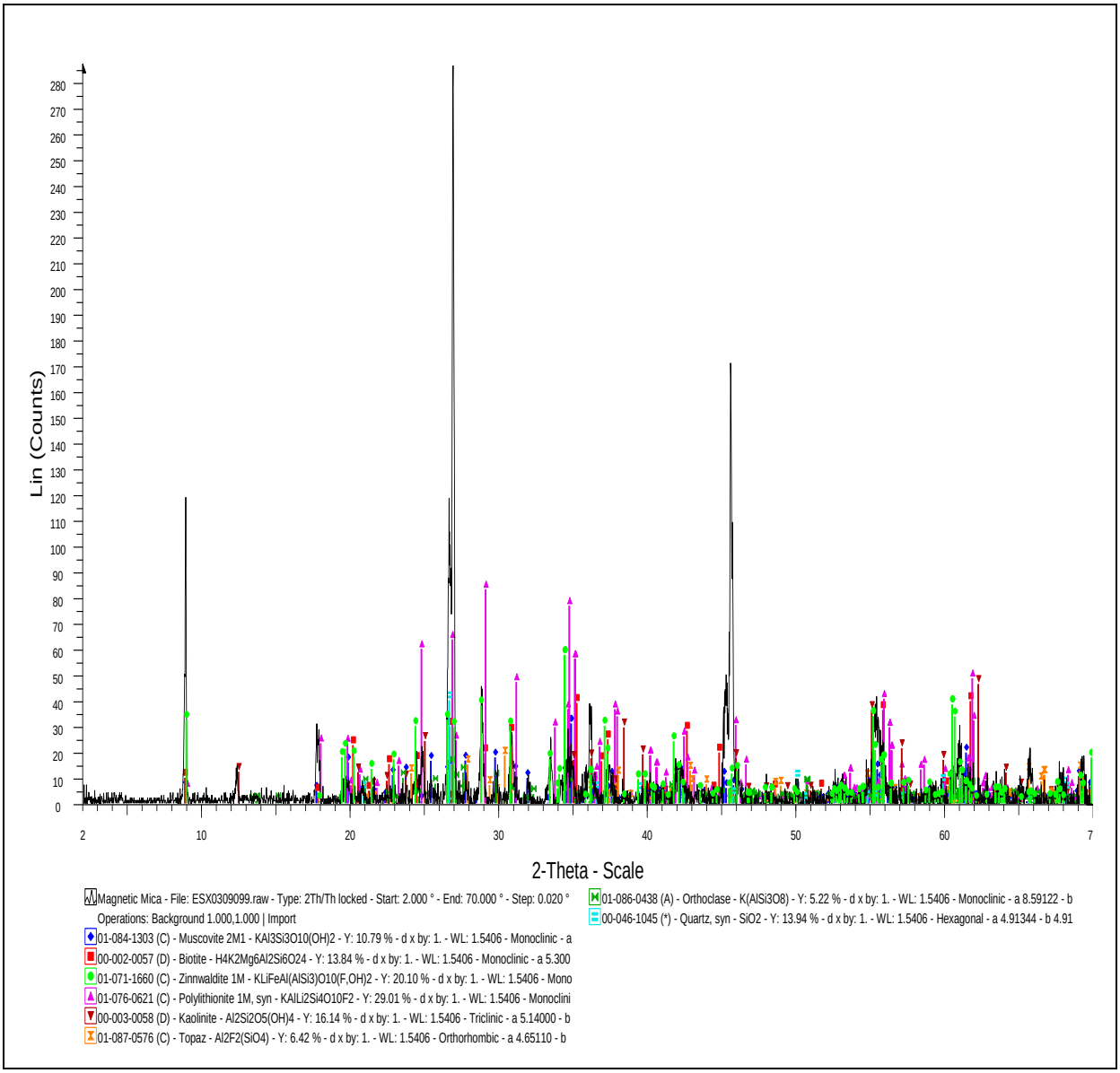

Figure 8.12: XRD profile of magnetic mica

It can also be seen that the dominant phase in the non-magnetic fraction was quartz. Kaolinite was present in both fractions, almost in the same proportion due its fine nature.

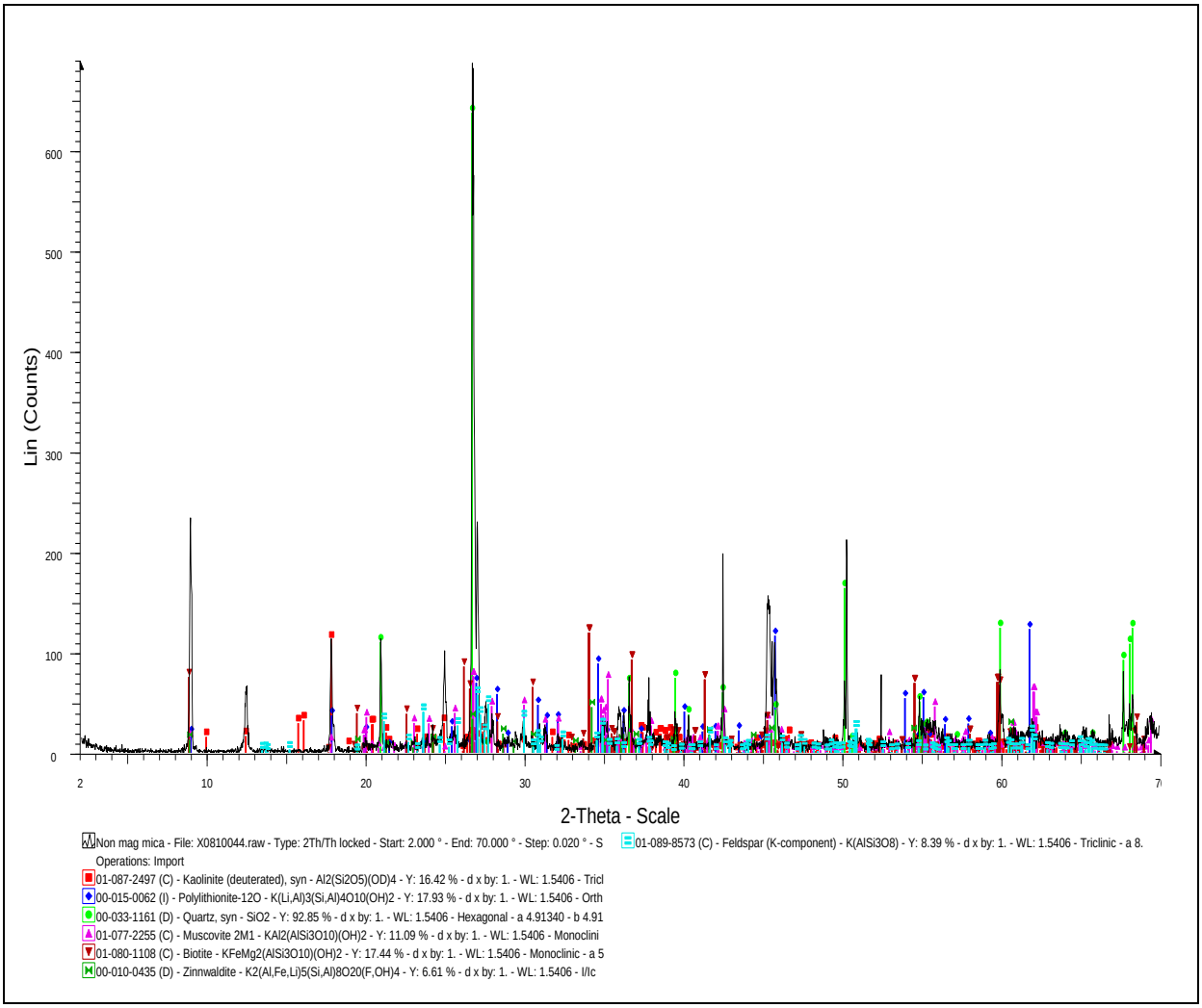

Figure 8.13: XRD profile of non-magnetic mica

8.4.3 Cleaner Flotation Separation

The experimental procedure is given in section 7.5.3. This experiment was conducted in order to determine the best method to recover the lithium mica from the bulk mica concentrate between magnetic separation and a cleaner flotation separation. Detailed metallurgical balance sheets for these flotation tests are given in Appendix G. Tables 8.5 and 8.6 show the results of three flotation tests expressed in terms of grade and recovery of Li_2O and Fe_2O_3 in concentrates and tails respectively. As seen from Table 8.5 the grade of lithium was lower than that obtained by wet high intensity magnetic separation.

Table 8.5: Cleaner flotation concentrates.

Test	Wt %	Grade (%)		Recovery (%)	
		Li_2O	Fe_2O_3*	Li_2O	Fe_2O_3
Run 1	93.91	1.66	5.04	99.15	99.46
Run 2	93.10	1.61	4.83	98.80	99.33
Run 3	94.59	1.62	4.27	99.17	99.55
Mean	***93.87***	***1.63***	***4.71***	***99.04***	***99.45***
Standard Deviation	***0.75***	***0.03***	***0.40***	***0.21***	***0.11***

Table 8.6: Cleaner flotation tails

Test	Wt %	Grade (%)		Recovery (%)	
		Li_2O	Fe_2O_3	Li_2O	Fe_2O_3
Run 1	6.09	0.22	0.42	0.85	0.54
Run 2	6.90	0.27	0.44	1.20	0.67
Run 3	5.41	0.24	0.34	0.83	0.45
Mean	***6.13***	***0.24***	***0.40***	***0.96***	***0.55***
Standard Deviation	***0.75***	***0.03***	***0.05***	***0.21***	***0.11***

* Total Fe as Fe_2O_3

8.5 Estimated Mineralogy of the Mica Flotation and Magnetic Separation Products.

The magnetic separation products were subjected to electron-microprobe analysis [JEOL JXA-8200, Wavelength-Dispersive (WD) / Energy-Dispersive (ED) combined Micro-analyzer] to determine the nature of the lithium-rich micas. First the magnetic and non-magnetic micas were prepared into standard, 30µm thick polished and carbon coated sections before being subjected to the electron-microprobe analysis. After obtaining the microprobe data of the micas, the Li_2O and H_2O content in the micas was calculated using a Microsoft Excel spreadsheet programme based on Tindle and Webb (1990) and Monier and Robert (1986a). The Li_2O calculation in muscovite was after Monier and Robert (1986) while the H_2O was after Tindle and Webb (1990). In the zinnwaldite, the Li_2O and H_2O calculations were after Tindle and Webb (1990). Detailed results of the electron-microprobe analysis are given in Appendix F2. Micas with identification numbers starting from *1* to *44* are from the non-magnetic fraction while those from *45* to *96* are from the magnetic fraction. The data for minerals which appear to be muscovite or zinnwaldite are arranged together respectively.

The mineralogy of the mica flotation and magnetic separation products were estimated using the XRF data and the chemical composition of the minerals derived from the microprobe data. The estimated mineral abundance together with the recoveries was used to back-calculate the chemical composition of the separation products and match them with the determined

chemical composition (XRF data). Tables 8.7 and 8.8 show the chemical composition of the minerals used in the prediction of the estimated mineral abundance of the separation products.

Table 8.7: Average analyses for magnetic fraction (microprobe data).

Chemistry	Quartz	Muscovite	K-feldspar	Zinnwaldite
Si_2O	96.87 (4.35)$^+$	47.35 (1.01)	63.12 (1.94)	46.81 (2.12)
TiO_2	n.d	0.07 (0.05)	n.d	n.d
Al_2O_3	0.90 (2.16)	30.99 (1.51)	18.05 (0.42)	20.6 (1.05)
Fe_2O_3*	0.31 (0.27)	3.98 (1.11)	0.1 (0.09)	13.09 (2.25)
MnO	n.d.	0.06 (0.04)	0.02 (0.03)	0.15 (0.07)
MgO	n.d.	0.36 (0.46)	0.00 (0.01)	0.26 (0.12)
CaO	n.d.	n.d.	0.23 (0.5)	n.d.
Li_2O	n.d.	0.33 (0.16)	n.d.	3.88 (0.61)
Na_2O	n.d.	0.14 (0.05)	0.26 (0.07)	0.19 (0.07)
K_2O	n.d.	10.18 (0.44)	15.35 (0.46)	9.62 (0.47)
P_2O_5	n.d.	n.d.	n.d.	n.d.
F	0.13 (0.20)	1.30 (0.51)	n.d.	4.78 (0.99)
LOI	n.d.	4.48	n.d.	n.d
Minus O=F	0.05	0.55	-	2.01
Total	98.33	97.03	97.38	96.22

+ Standard deviation in parentheses; n.d. not detected; * Total Fe as Fe_2O_3

Table 8.8: Average analyses for non-magnetic fraction (microprobe data).

Chemistry	Quartz#	Kaolinite#	Muscovite#	K-feldspar#	Zinnwaldite#	Apatite*	Topaz*
Si_2O	98.61 (0.81)$^+$	45.85	46.55 (0.84)	64.15 (0.31)	48.32 (1.32)	-	33
TiO_2	n.d.	n.d.	0.11 (0.10)	n.d.	0.24 (0.11)	-	-
Al_2O_3	0.05 (0.04)	36.69	33.89 (1.83)	18.65 (0.27)	20.14 (0.66)	-	56
Fe_2O_3*	n.d.	0.51 (0.44)	1.80 (1.42)	0.03 (0.03)	10.87 (1.48)	-	-
MnO	n.d.	n.d.	0.04 (0.05)	0.02 (0.03)	0.18 (0.06)	-	-
MgO	n.d.	0.03 (0.02)	0.45 (0.51)	n.d.	0.25 (0.08)	-	-
CaO	n.d.	n.d.	n.d.	n.d.	n.d.	55.58	-
Li_2O	n.d.	n.d.	0.13 (0.15)	n.d	4.32 (0.39)	-	-
Na_2O	n.d.	0.05 (0.06)	0.23 (0.08)	0.43 (0.10)	0.15 (0.04)	-	-
K_2O	n.d.	2.02 (2.69)	9.90 (1.15)	15.34 (0.40)	9.72 (0.20)	-	-
P_2O_5	n.d.	n.d.	n.d.	n.d.	n.d.	42.22	-
F	n.d.	0.17	0.63 (0.53)	n.d.	5.78	3.77	11.5
LOI	n.d.	13.96	4.48	n.d	n.d	-	4.45
Minus O=F	-	0.07	0.55	-	2.43	1.59	4.84
Total	98.80	99.22	97.03	98.64	98.26	100.01	100.16

Average analyses of microprobe data; + Standard deviation in parentheses; * Composition obtained from webmineral.com (2010) **.**

The estimated mineral recovery from the feed to the mica concentrate of quartz, kaolinite, muscovite, K-feldspar, zinnwaldite, apatite and topaz were 9%, 60%, 98%, 22%, 99%, 5% and 5% respectively, giving a total of 61% recovery by weight. The recovery from the mica concentrate to the magnetic fraction of quartz, kaolinite, muscovite, K-feldspar, zinnwaldite, apatite and topaz were 38%, 20%, 41%, 30%, 74%, 7% and 6% respectively, achieving a 47.7% recovery by weight. Figure 8.14 shows the overall mineral balance for the mica separation process.

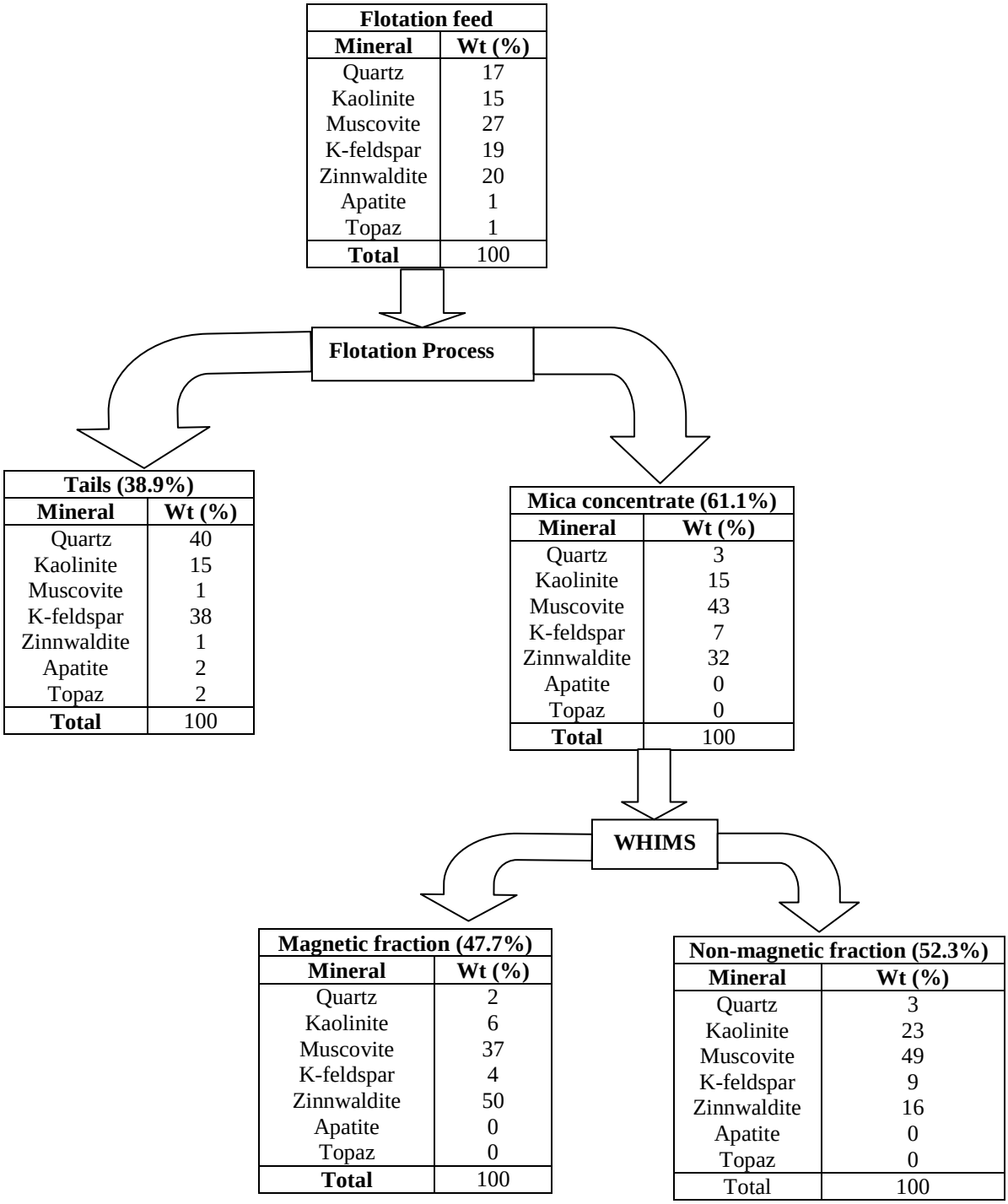

Figure 8.14: Estimated mineral balance of the mica flotation and magnetic separation products.

Table 8.9: Typical chemical analysis of mica feed and separation products.

Chemistry	Feed (%)	Flotation Process (%)		WHIMS Process (%)	
		Concentrate	Tails	Magnetic	Non-magnetic
Si_2O	58.00	49.21	77.69	48.10	50.64
TiO_2	0.16	0.18	0.08	0.27	0.11
Al_2O_3	24.10	29.86	13.1	27.76	32.00
Fe_2O_3*	3.29	4.56	0.45	7.42	2.28
MgO	0.27	0.34	0.12	0.38	0.33
CaO	0.20	0.08	0.07	0.07	0.10
Li_2O	0.89	1.43	0.03	2.07	0.76
Na_2O	0.29	0.15	0.67	0.15	0.14
K_2O	7.63	8.1	5.80	9.56	6.84
P_2O_5	0.19	0.10	0.20	0.06	0.08
F	2.31	2.17	0.87	3.36	1.27
LOI	3.66	5.38	1.16	3.39	6.37
Minus O=F	0.97	0.91	0.37	1.41	0.53
Total	100.4	100.9	99.8	101.2	100.4

*Total Fe as Fe_2O_3

It can be seen from Figure 8.14 that some kaolinite reported to flotation concentrate by entrainment probably due to its fine nature. During magnetic separation most of the zinnwaldite reported to the magnetic fraction while most of the muscovite reported to the non-magnetic fraction, although a substantial amount was present in the magnetic fraction, probably due to the presence of iron. It can be observed from Tables 8.7 and 8.9 that the muscovite found in the magnetic fraction had higher iron content than those found in the non-magnetic, while the zinnwaldite found in the non-magnetic had slightly lower iron content on average.

The presence of zinnwaldite and muscovite in both the magnetic and non-magnetic fraction might be linked to intertwining of the minerals or poor liberation. In trying to upgrade the lithium content in the St Austell micas, Hawkes et al., (1987) performed a magnetic separation process and mentioned that although the separation worked in as far as removing muscovite from the highly contaminated mica flotation concentrate, it was also clear from the lithium content of both fractions that the technique allowed a significant proportion of lithian mica to escape as well. This phenomenon was explained by Figure 8.15 (Hawkes et al., 1987), which shows the composition fields occupied by the St Austell Granite micas. Hawkes et al. (1987) reported that at 'Fe_2O_3' contents of less than 7 – 8 %, the fields for muscovite and the lithian micas overlap in terms of their likely magnetic susceptibility. Therefore, the magnetic field intensity settings appropriate for rejecting muscovite may probably reject any high Li-low Fe mica (polylithionite and lepidolite). Henderson et al., (1989) have also reported the composition and elemental substitution trends in the Fe-bearing Li-mica series as from biotite (siderophyllite) to zinnwaldite to polylithionite.

The Li-micas in the St Austell granites have been identified as zinnwaldite, lepidolite and polylithionite, with zinnwaldite being the predominant (Manning et al. 1996; Henderson et al., 1989; Stone et al. 1988; Hawkes et al., 1987). In their work, Henderson et al., (1989) used a combination of ion-microprobe (for Li) and electron-microprobe (for other major elements) to analyse the Li-rich micas from the S.W. England, mainly the St Austell granite.

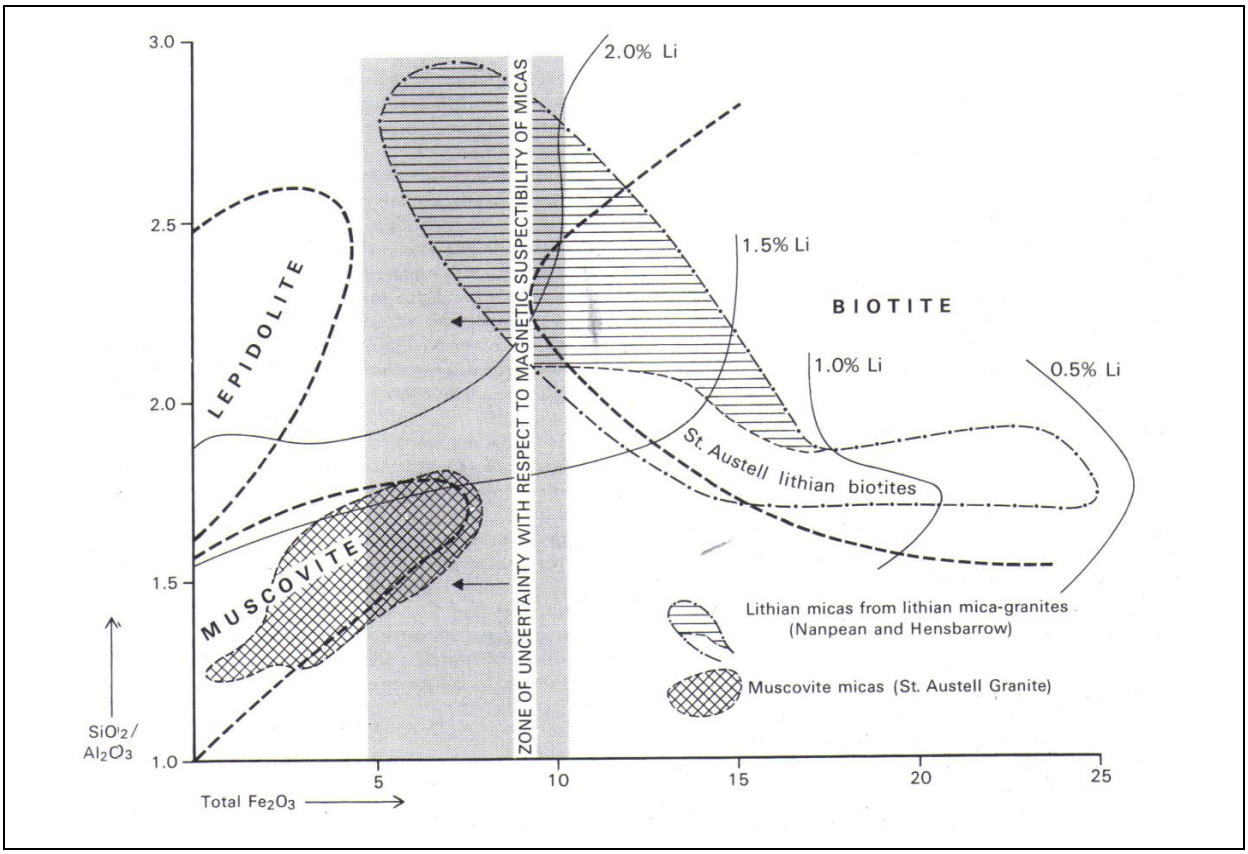

Figure 8.15: Composition diagram showing the overlap in iron content between muscovite and high-Li mica (from Hawkes et al. 1987)

It could be seen from the microprobe data in Appendix F2 that the non-magnetic and magnetic micas consisted predominantly of muscovite and zinnwaldite respectively. Also found in both fractions were grains which appeared to be K-feldspar, quartz and kaolinite, as shown in Tables 8.7 and 8.8.

Figure 8.16 shows the relationship between Si_2O/Al_2O_3 versus Fe_2O_3 of the microprobe data. It can be observed from Figure 8.16 that the lithium-rich micas and muscovite fall in the

regions reported by Hawkes et al. (1987) shown in Figure 8.15. All the lithium contained in the magnetic and non-magnetic fraction appeared to be zinnwaldite. It can be seen from Figure 8.16 that the muscovite present in the magnetic fraction and the zinnwaldite present in the non-magnetic fraction are close to the zone of uncertainity with respect to magnetic susceptibility of micas established by Hawkes et al. (1987).

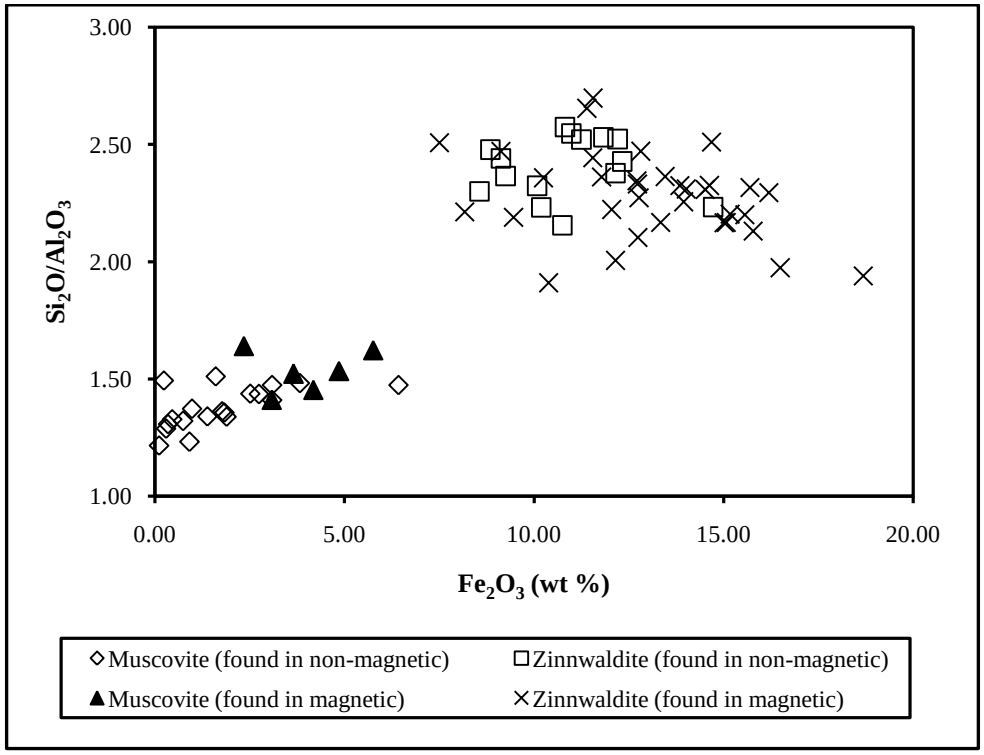

Figure 8.16: Plots of microprobe data for Si_2O/Al_2O_3 versus Fe_2O_3 (wt %)

The lithium-rich micas in the South West of England and in St Austell in particular have been said to define a clear positive correlation between Si_2O and Li_2O (Henderson et al., 1989), and Figure 8.17 shows this relationship in the microprobe data obtained. It could be seen from Figure 8.17 that the Li_2O content in muscovite and zinnwaldite range from 0 to 0.6% and 2.8 to 4.9% respectively. Figure 8.17 could also be used to estimate the lithium content in other micas in these samples based on the Si_2O content. Also muscovite and lithium-rich micas all show clear positive correlation between F and Li_2O (Figure 8.18), and negative correlation between Al_2O_3 and Li_2O (Figure 8.19). Figure 8.18 also shows that fluorine content in muscovite and zinnwaldite ranges from 0 to 2.2% and 2.2 to 7.5% respectively, while the Al_2O_3 content as shown in Figure 8.19 ranges from 28.8 to 37.1% and 18.5 to 22.6% respectively.

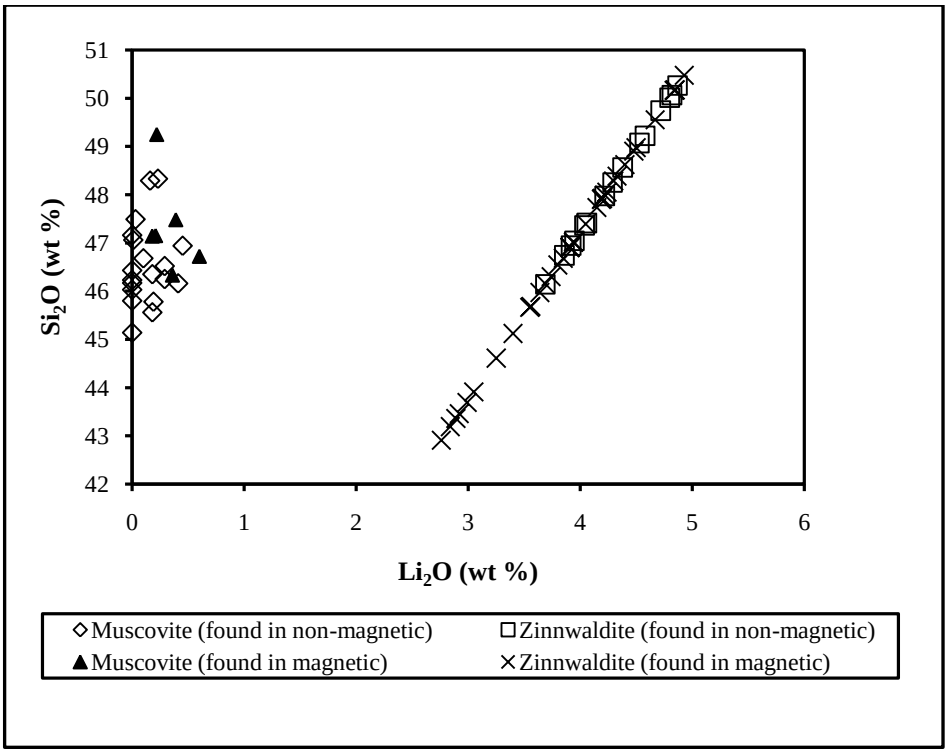

Figure 8.17: Plots of microprobe data for Si_2O versus Li_2O (wt %)

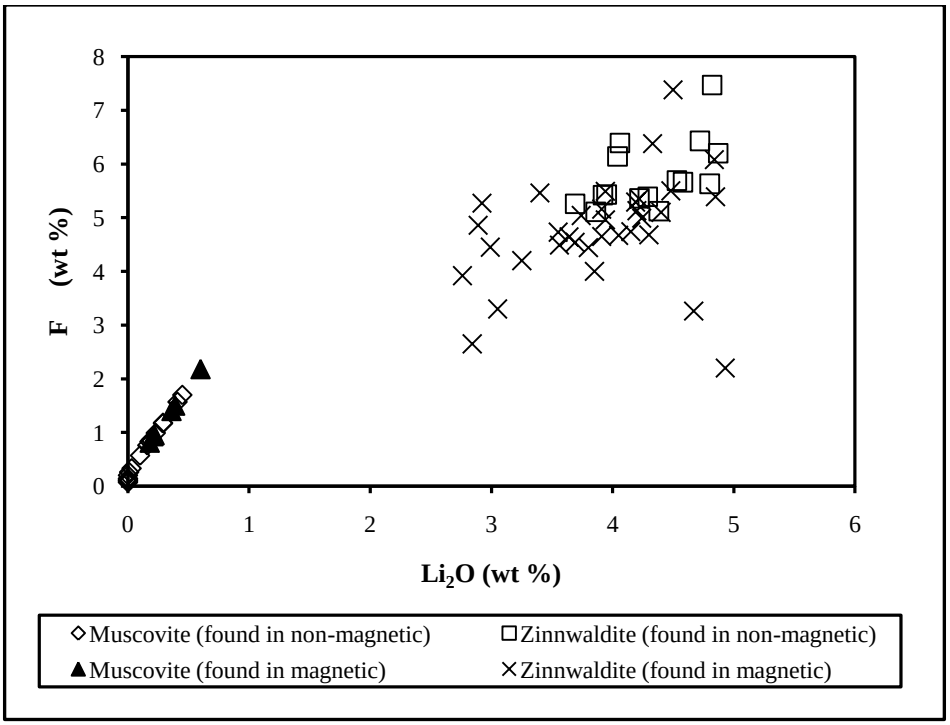

Figure 8.18: Plots of microprobe data for F versus Li_2O (wt %)

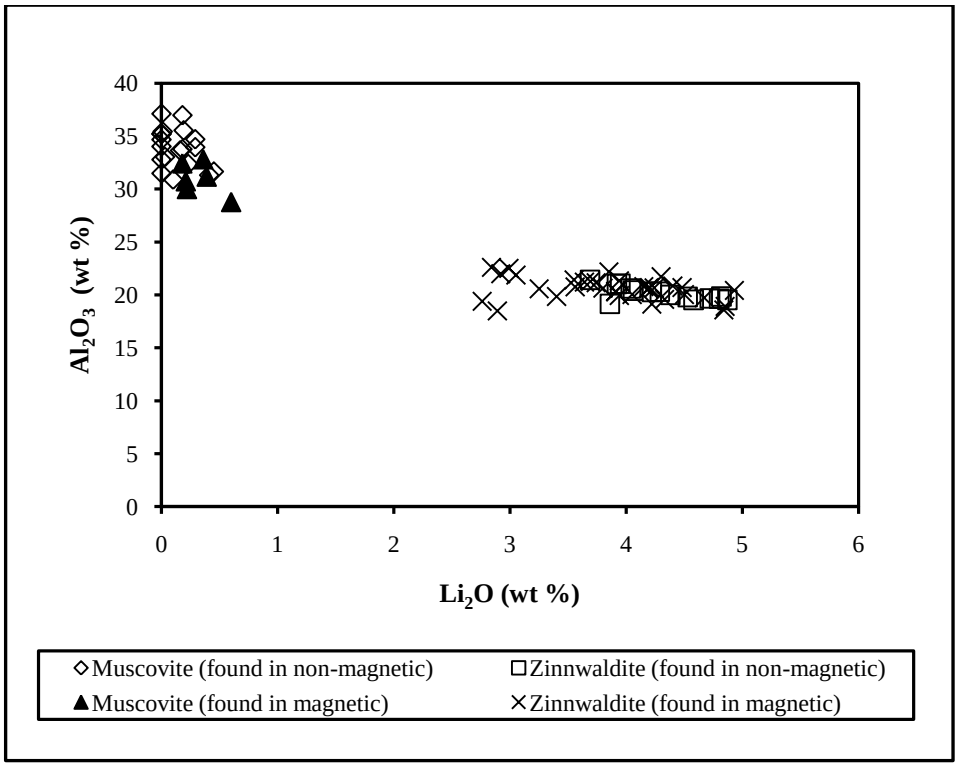

Figure 8.19: Plots of microprobe data for Al_2O_3 versus Li_2O (wt %)

8.6 Lithium Extraction by Roasting and Leaching.

8.6.1 The Gypsum Method

The gypsum lithium extraction test method procedure is given in section 7.6. Figure 8.20 illustrates the effect of roasting temperatures on lithium, rubidium and iron extraction efficiency. Iron is included as it is the major impurity. As can be seen from Figure 8.20, both lithium and rubidium extraction efficiency increased steadily, reaching a maximum of 66 % and 9 % respectively at a roasting temperature of 975^{o}C. These efficiencies were achieved when leaching at the natural pH of the pulp of about 7. Iron co-extraction was very low as could be seen from the figure.

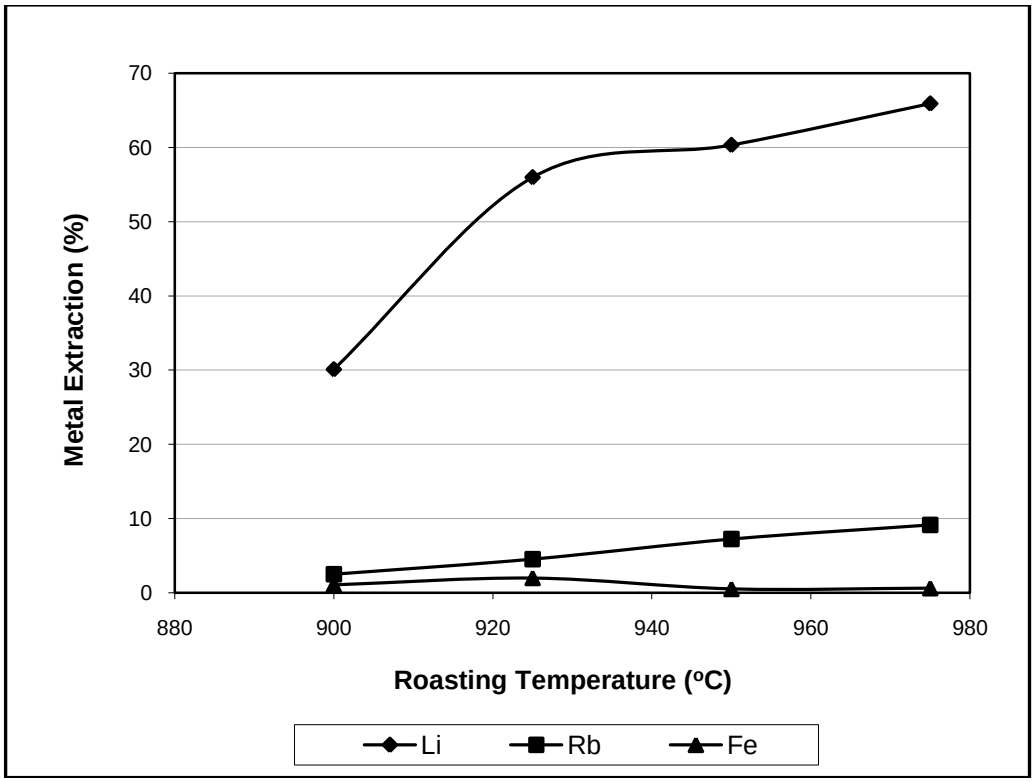

Figure 8.20: Effect of roasting temperature on lithium, rubidium and iron extraction at 85^{o}C, l:s = 10, sinter ratio = 2:1 (gypsum roast).

It is evident from Figure 8.20 that the lithium extraction efficiency increased steadily as the roasting temperature was increased. Generally, the rubidium extraction efficiencies were very low. Table 8.10 shows the chemical composition of roast-products used in the experiments. The loss on ignition gradually increased as the roasting temperature increased.

Table 8.10: Chemical composition of mica-gypsum roasts (ratio = 2:1).

Roasting Temperature [^{o}C]	Grade [%]		LOI
	Li	Rb	
900	0.78	0.50	9.45
925	0.77	0.50	9.79
950	0.78	0.51	10.53
975	0.78	0.50	10.75

The results of leaching in water as shown in Figure 8.20 indicated a steady increase in the extraction efficiency as the roasting temperature was increased. In order to determine the roasting temperatures at which lithium leaching begins and ends, it was decided to extend the roasting temperatures both lower and higher than those shown in Figure 8.20. Leaching was conducted in duplicate and the reported values shown in Figure 8.21 are the average of the two.

It can be seen from Figure 8.21 that lithium extraction begins when materials are roasted above 900^{o}C. Approximately 84% lithium extraction was achieved at 1050^{o}C. Rubidium extraction was very low (14%). A further increase in roasting temperature to 1100^{o}C did not result in significant increase in extraction efficiency for both lithium and rubidium. Iron co-extraction remained very low. This test suggested that different mineral phases were formed at each roasting temperature and that more water soluble lithium mineral compounds were formed when materials were roasted above 900^{o}C. The difference in extraction efficiencies between lithium and rubidium have been assumed to be caused by differential lithium and rubidium binding in zinnwaldite as observed by Jandova and Vu (2008).

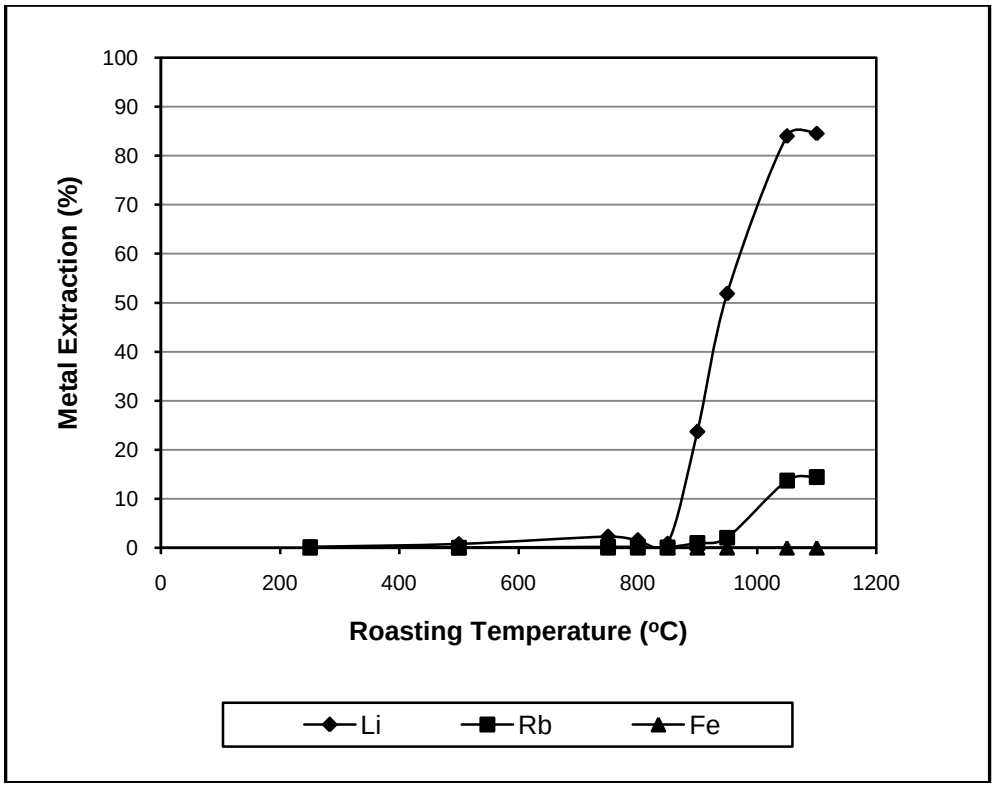

Figure 8.21: Effect of roasting temperature on lithium, rubidium and iron extraction at 85°C, l:s = 10, sinter ratio = 2:1 (gypsum roast).

Figure 8.22 shows the XRD profile of magnetic mica while Figures 8.23 and 8.24 show the XRD profiles for mica-gypsum mixture roasted at 800°C and 1050°C respectively. It can be observed that the XRD profiles of magnetic mica and mica-gypsum roasted at 800°C are similar and this probably explains the low lithium extraction observed at this temperature in Figure 8.21. It is evident from Figure 8.24 that roasting the mica-gypsum mixture at 1050°C resulted in new mineral phases being created, some of which were water-soluble lithium compounds. Figure 8.25 shows the XRD profile for leach residue of mica-gypsum roasted at 1050°C.

During roasting at 1050°C, mica minerals reacted with gypsum to form new mineral phases such as leachable lithium potassium sulphate ($KLiSO_4$). Uvarovite-Aluminian [$Ca_3(Cr_{0.85}Al_{0.15})_2(SiO_4)_3$] and Cuspidine ($Ca_4Si_2O_7F_2$ / $3CaO.2SiO_2.CaF_2$) were new mineral phases identified as shown in Figure 8.24.

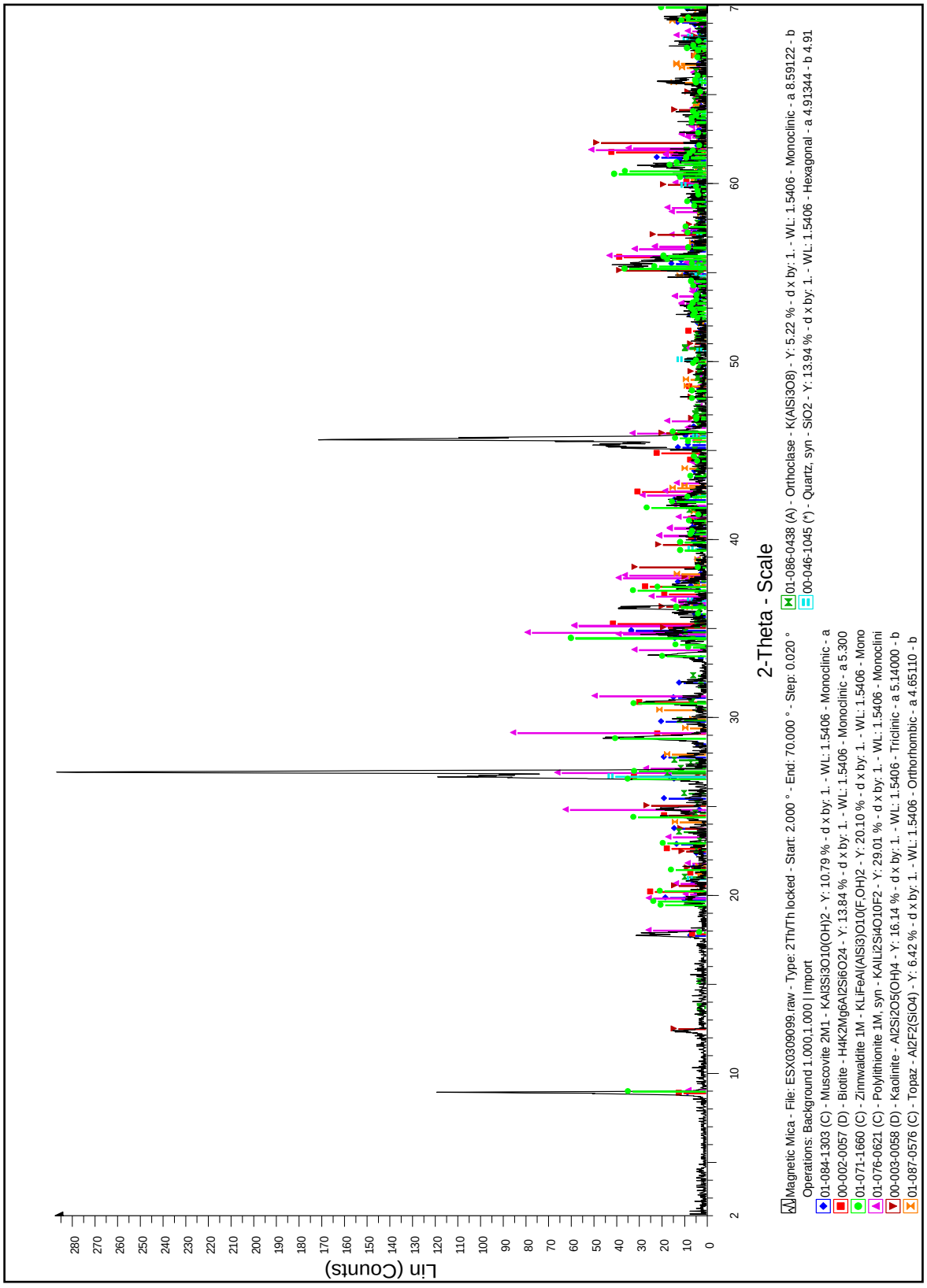

Figure 8.22: XRD profile of magnetic mica.

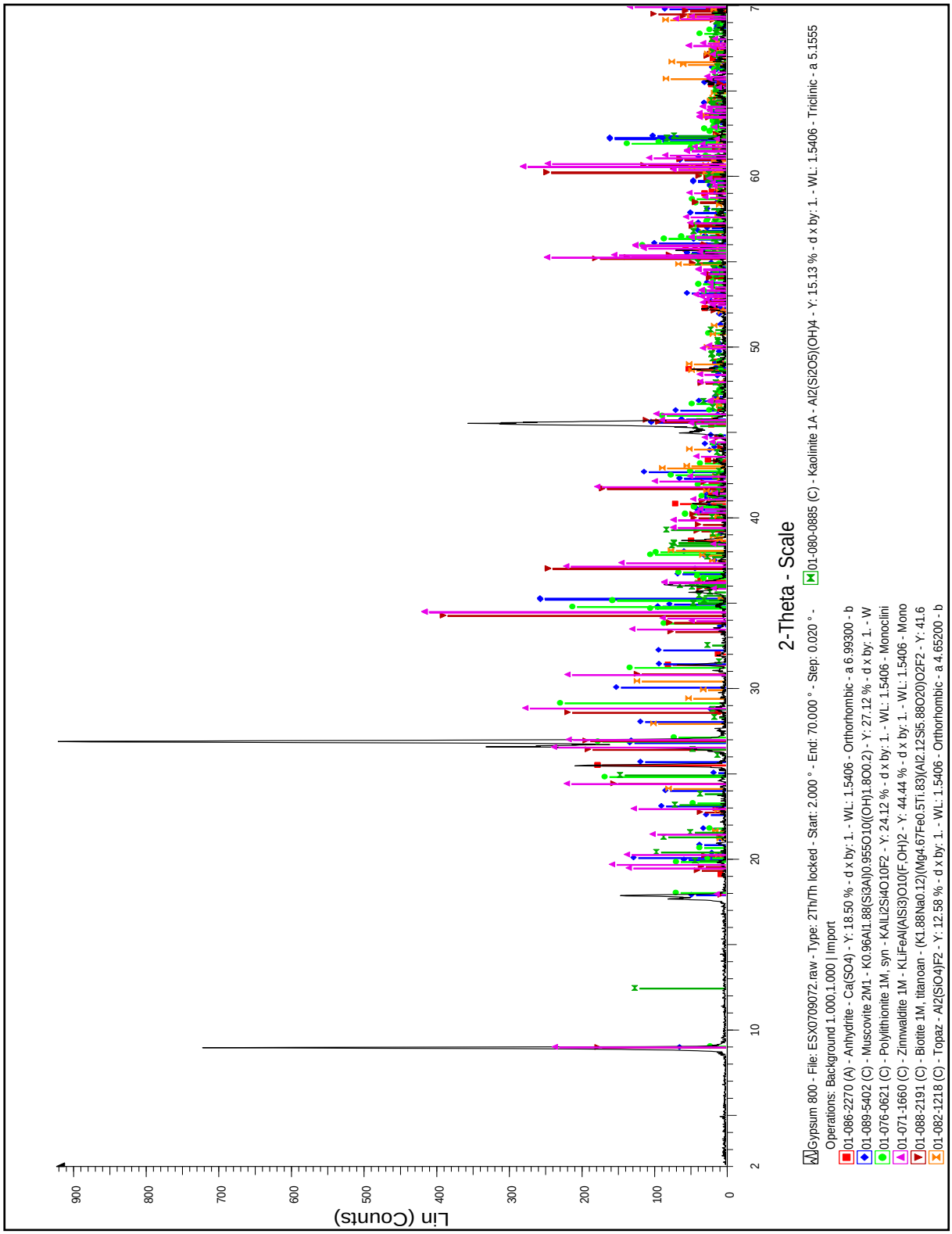

Figure 8.23: XRD profile of mica-gypsum roasted at 800^{o}C.

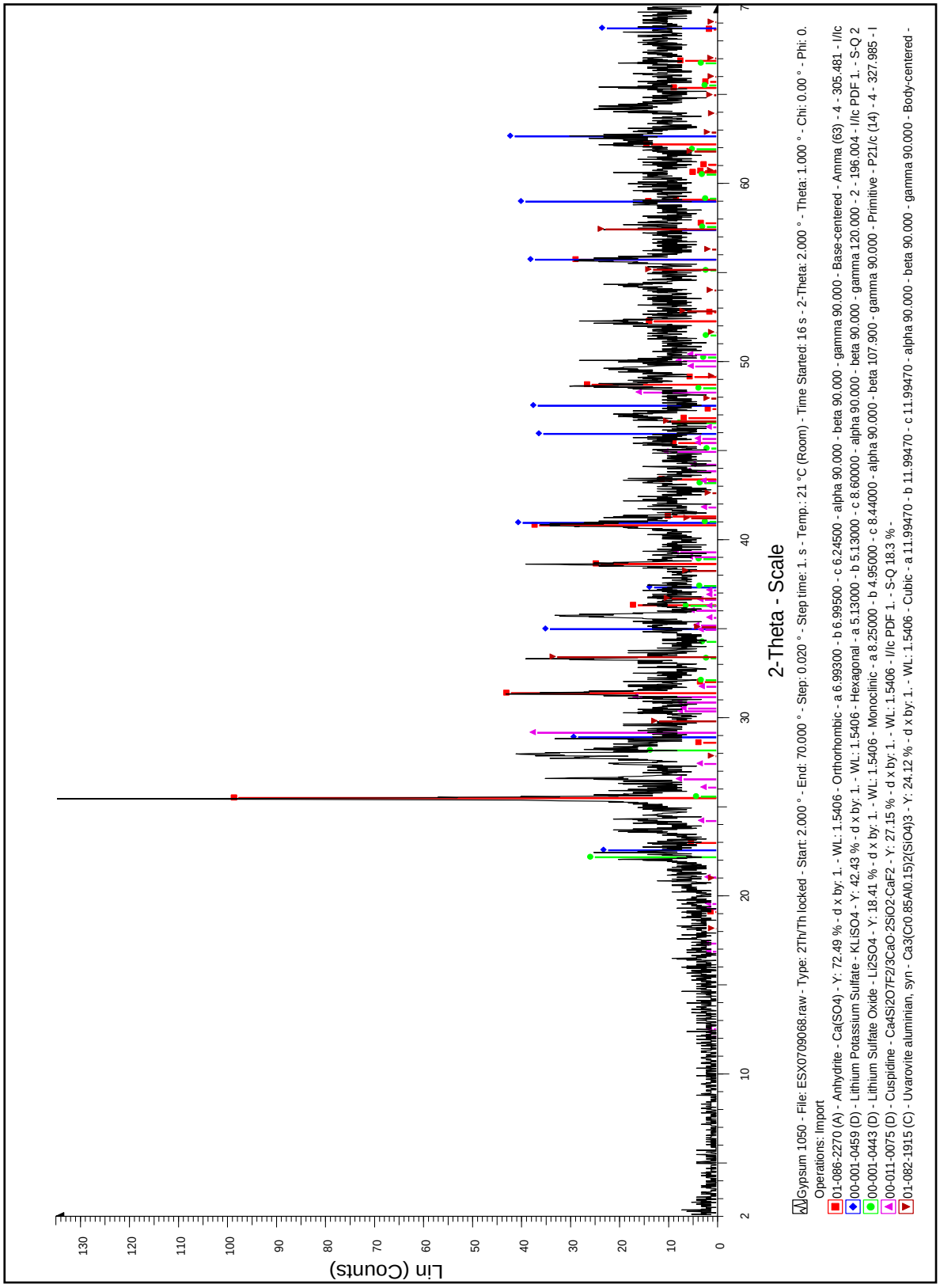

Figure 8.24: XRD profiles of mica-gypsum roasted at 1050°C.

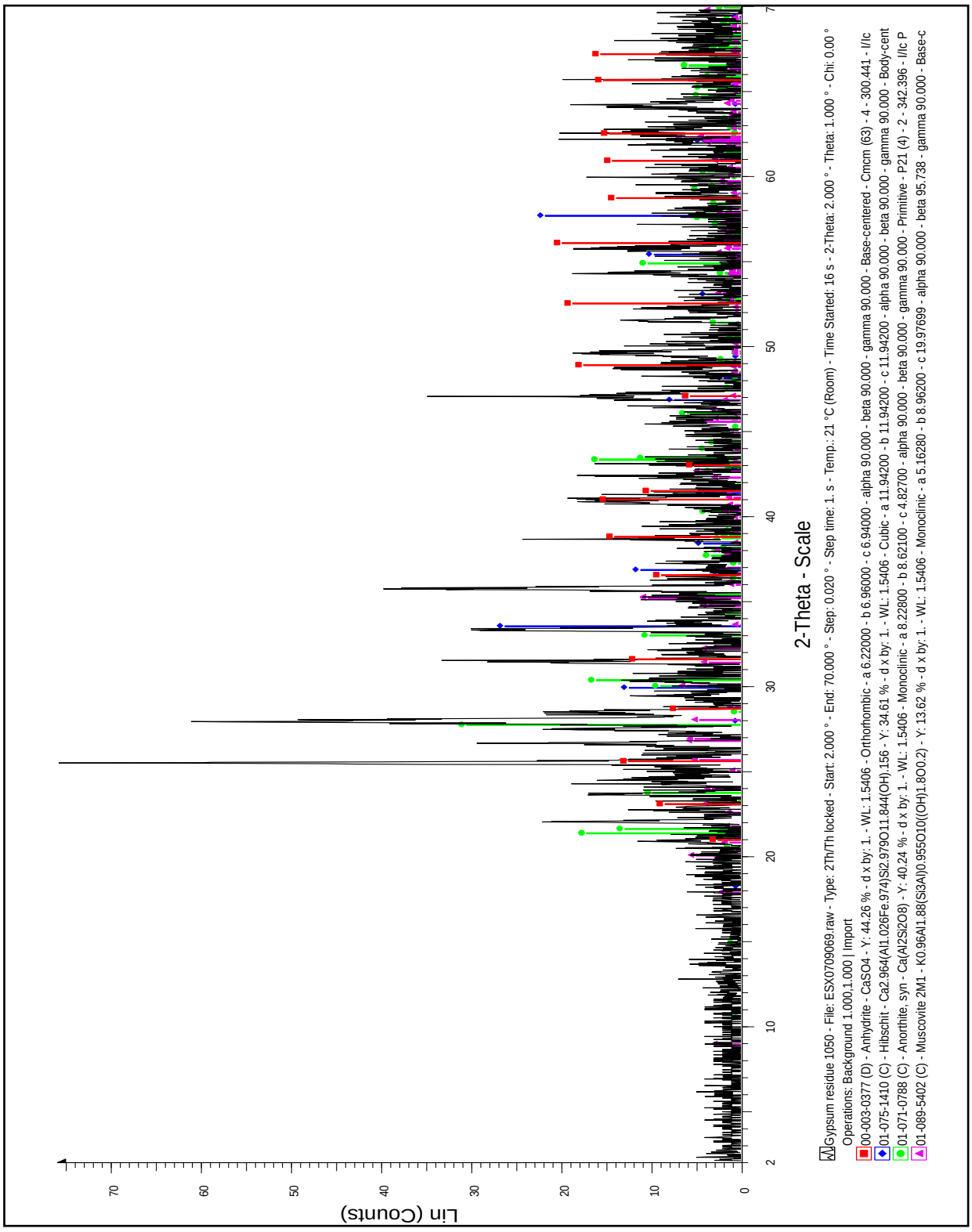

Figure 8.25: XRD profile of leach residue of mica-gypsum roasted at 1050°C.

The effect of leaching bath temperature on lithium and rubidium extraction efficiency for 30 minutes leaching is shown in Figure 8.26. It can be seen that there is a gradual increase in the extraction efficiency of lithium as the leaching bath temperature is increased from 20^{o}C (room temperature) to 85^{o}C. This was the maximum temperature the leaching bath apparatus could reach. This experiment showed that the lithium compounds were slower to dissolve at lower temperatures.

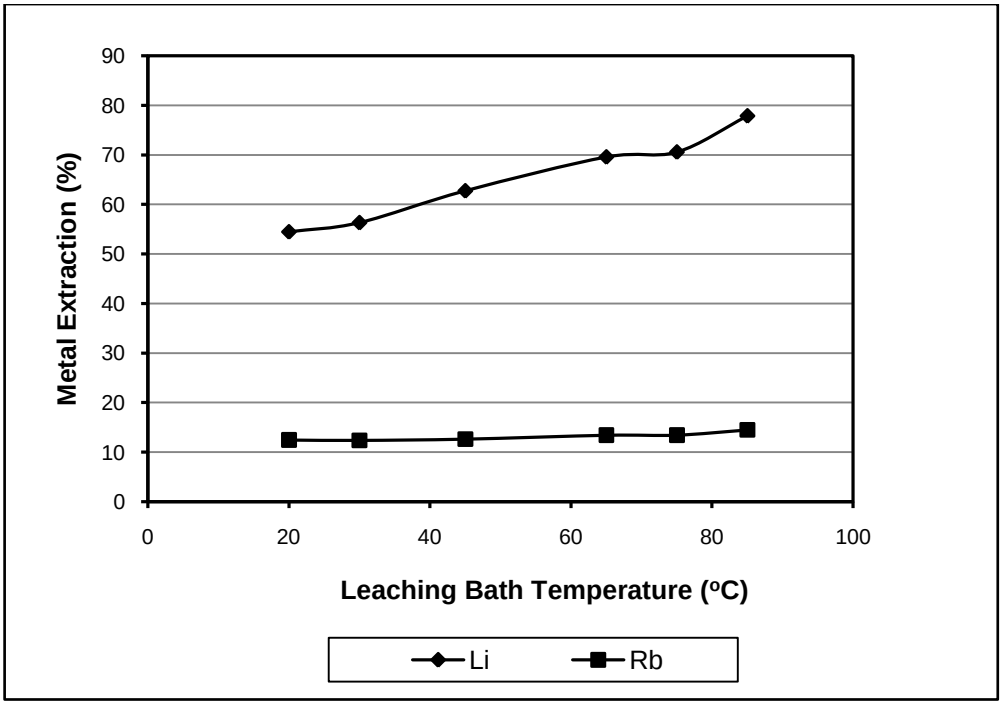

Figure 8.26: Effect of leaching bath temperature on the extractions of lithium and rubidium; ratio = 2:1, roasting temperature 1050^{o}C, l:s = 10 (gypsum roast).

Dissolution kinetics for lithium and rubidium using the material roasted at 1050^{o}C, leaching temperature of 85^{o}C and a liquid to solid ratio of 10:1 are given in Figure 8.27. Both lithium and rubidium dissolution were very fast and were almost completed within 10 minutes.

Figure 8.28 gives the results of the effect of paramagnetic mica concentrate to gypsum ratio in roasted product on lithium and rubidium extraction efficiency. It is evident that increasing the concentrate to gypsum ratio in roast-product results in a gradual decrease in both lithium and rubidium extraction efficiency.

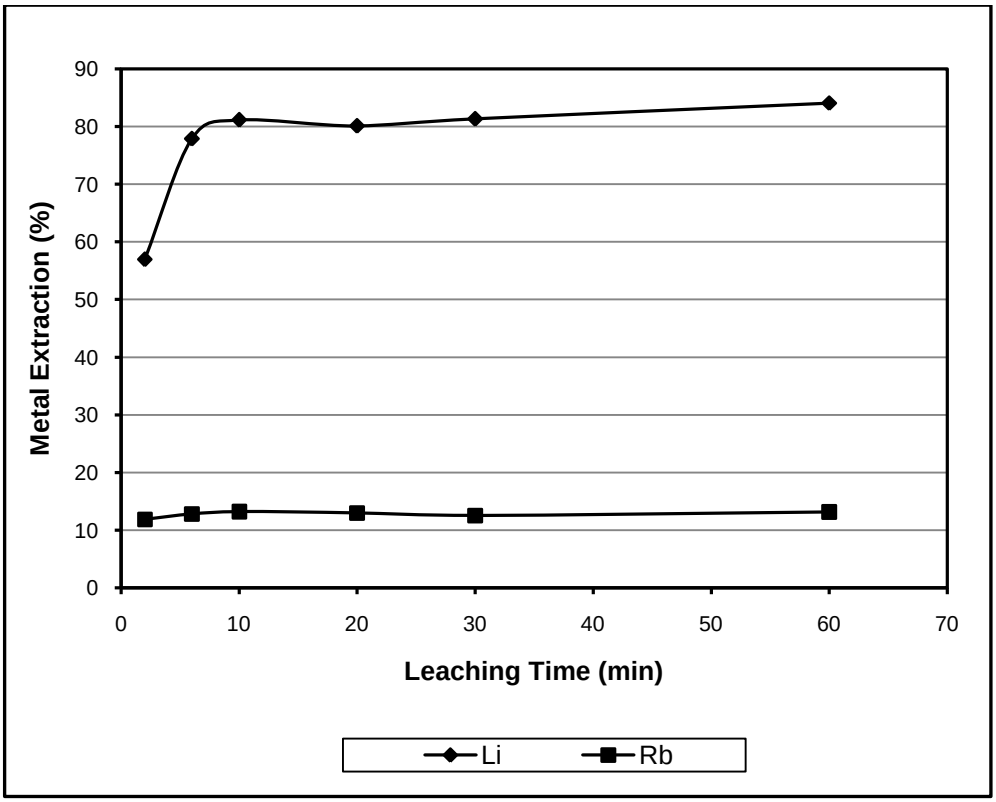

Figure 8.27: Leaching kinetics of lithium and rubidium at 85°C, l:s = 10:1; roasting temperature 1050°C (gypsum roast).

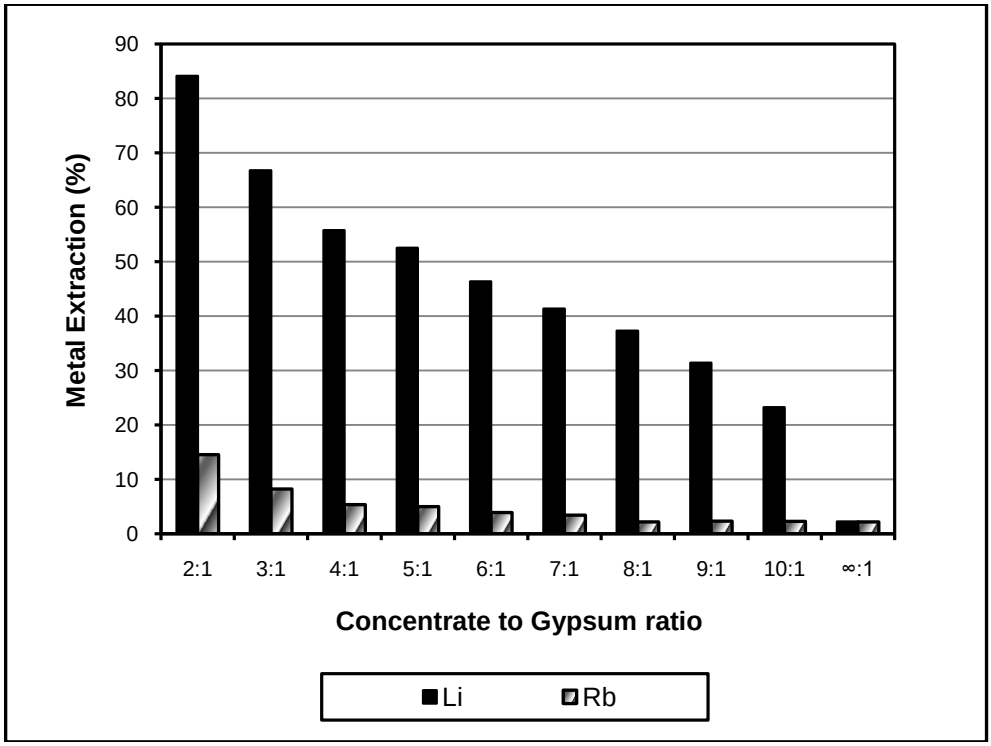

Figure 8.28: Effect of concentrate to gypsum ratio in roast-product on lithium and rubidium extractions at 85°C, l:s = 10:1; roasting temperature 1050°C (gypsum roast).

The typical composition of leach liquors originating from leaching at 85°C and a liquid to solid ratio of 10:1 is shown in Table 8.11. The typical liquor analysis is given to show the impurity concentration as it is important to know this for the lithium precipitation stage.

Table 8.11: Average composition of leach liquors of 1050°C roast leached at 85°C, l:s = 10:1 and ratio = 2:1

Concentration of elements (g/m^3)				
Li	**Rb**	**K**	**Ca**	**Na**
280	30	600	268	7.74

Leaching was also conducted on the mica flotation cleaner concentrate in order to determine the best method to upgrade the lithium content. The results are shown in Table 8.12. Leaching was also conducted on the non-magnetic mica concentrate mixed with gypsum in the ratio 2:1 and roasted at 1050°C. The results of the leaching of non-magnetic-gypsum roast-product are given in Table 8.13. As can be seen from Table 8.13, the non-magnetic mica was difficult to leach. The mica flotation cleaner concentrate contained both the magnetic and non-magnetic mica fractions and this explains why the lithium extraction efficiency was lower than the magnetic mica. This was due to the presence of the non-magnetic mica fraction in the mica flotation cleaner concentrate which is difficult to leach.

Table 8.12: Extraction efficiency of mica cleaner concentrate roasted at 1050°C (sinter ratio=2:1).

Test	**Extraction Efficiency (%)**	
	Li	**Rb**
Run 1	62.4	17.7
Run 2	62.7	17.8
Mean	***62.6***	***17.8***
Standard deviation	***0.2***	***0.1***

Table 8.13: Extraction efficiency of non-magnetic mica concentrate roasted at 1050°C (sinter ratio=2:1).

Test	**Extraction Efficiency (%)**	
	Li	**Rb**
Run 1	15.3	2.1
Run 2	15.0	1.8
Mean	***15.2***	***2.0***
Standard deviation	***0.2***	***0.2***

In these experiments magnetic mica was mixed with gypsum and ground together for 3 minutes to ensure thorough mixing before and after being roasted. In order to show whether the grinding was necessary before roasting at 1050°C, a predetermined amount of un-pulverised magnetic mica and gypsum were mixed in a plastic bag. The roast-product was pulverised and leached. Table 8.14 gives the results. It is evident from the results that un-

pulverised mica resulted in lower lithium extraction efficiency. The variation in the lithium extraction efficiency was too high, probably due to the fact that the mica and gypsum were not thoroughly mixed.

Table 8.14: Extraction efficiency of un-pulverised magnetic-mica/gypsum roasted at 1050^{o}C

Test	Extraction Efficiency (%)	
	Li	**Rb**
Run 1	55.0	12.3
Run 2	32.9	9.3
Mean	***44.0***	***10.8***
Standard deviation	***15.6***	***2.1***

In the lithium extraction by the gypsum method reported by Jandova and Vu (2008), zinnwaldite concentrate was roasted at temperatures ranging from 900 to 975^{o}C together with gypsum and calcium hydroxide [$Ca(OH)_2$] in the ratio 6:4.2:2. The lithium extraction method by the gypsum method reported above did not include calcium hydroxide and therefore it was decided to include it in the concentrate before being roasted at temperatures ranging from 900 to 975^{o}C. The weight ratio of magnetic concentrate to $CaSO_4.2H_2O$ to $Ca(OH)_2$ was 3:2:1. The roast-products were leached in the water-bath maintained at 85^{o}C for 30 minutes at a liquid to solid ratio of 10:1.

The result of the influence of roasting temperature on lithium and rubidium extraction efficiency is illustrated in Figure 8.29. The experiment was performed in duplicate and the reported values are the average of the two tests. It can be seen from the figure that 88% lithium extraction efficiency was achieved if roasting was done at and above the temperature of 950^{o}C. However, at the same temperature, the rubidium extraction efficiency was only 44%. This rubidium extraction was much higher than that obtained without the addition of lime as reported above. The addition of calcium hydroxide to the concentrate not only increased the extraction efficiency, but also decreased the roasting temperature from 1050^{o}C to 950^{o}C. The other attribute of calcium hydroxide is that it makes the roast-product "soft" and thus easy to remove from the crucibles and to grind.

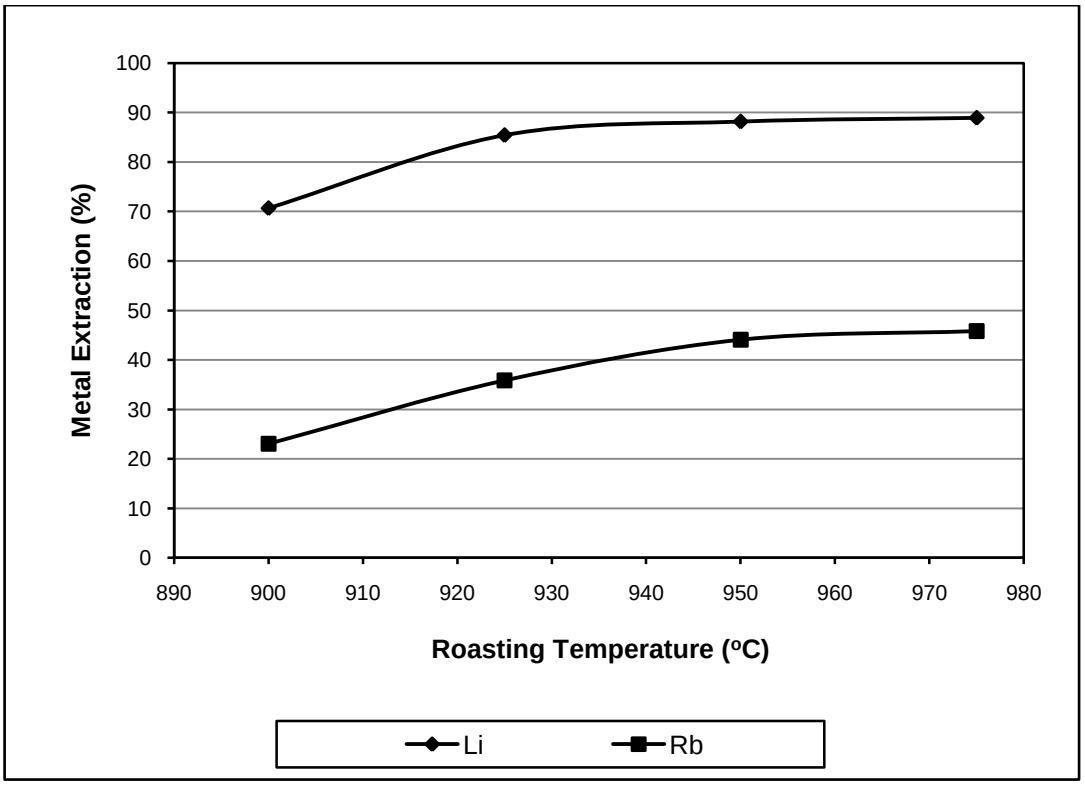

Figure 8.29: Effect of roasting temperature on the extractions of lithium and rubidium; leaching at 85°C, l:s = 10:1; ratio = 3:2:1 (gypsum roast).

Summary of Leaching Results Using the Gypsum Method

The materials tested using the gypsum method of lithium extraction were magnetic mica, non-magnetic mica, mica cleaner concentrate, un-pulverised magnetic mica and magnetic mica mixed with calcium hydroxide. The materials were roasted at 1050°C, except that of the magnetic mica mixed with calcium hydroxide which was roasted at 950°C. Table 8.15 shows a summary of results of the extraction efficiencies. It can be observed from Table 8.15 that roasting the magnetic mica with gypsum and calcium hydroxide drastically increased the rubidium extraction efficiency at a roasting temperature of 950°C (Figure 8.29).

Table 8.15: Summary of the leaching results by the gypsum method.

Material	roasting Temperature (°C)	ratio	Extraction Efficiency (%)	
			Li	Rb
Pulverised magnetic mica : gypsum	1050	2:1	84	14
Pulverised non-magnetic mica : gypsum	1050	2:1	15	2
Pulverised mica cleaner concentrate : gypsum	1050	2:1	63	18
Un-pulverised magnetic mica : gypsum	1050	2:1	44	11
Pulverised magnetic mica : gypsum : calcium hydroxide	950	3:2:1	88	44

8.6.2 The Limestone Method

The limestone lithium extraction test procedure is given in section 7.6. The influence of roasting temperature on lithium, rubidium and iron extraction efficiency is illustrated in Figure 8.30 when leaching is performed at the "natural" pH of about 10 and concentrate to limestone ratio of 5:1. It can be seen from Figure 8.30 that very low extraction efficiencies were achieved, reaching a maximum of 6.1% and 1.9% for lithium and rubidium, respectively, at a roasting temperature of 825^{o}C. Iron co-extraction was also very low.

The low lithium and rubidium extraction efficiencies observed when the concentrate to limestone ratio was 5:1 necessitated the carrying out of an experiment with the reduced amount of concentrate to limestone ratio. It was decided to mix the concentrate and limestone in the ratio 3:1. Figure 8.31 shows the extraction efficiencies of lithium, rubidium and iron at natural pH when the concentrate to limestone ratio was reduced to 3:1. As can be seen from Figure 8.31, the extraction efficiencies of lithium and rubidium decreased with increased roasting temperature. The extraction efficiencies were lower than those observed when the concentrate to limestone ratio was 5:1.

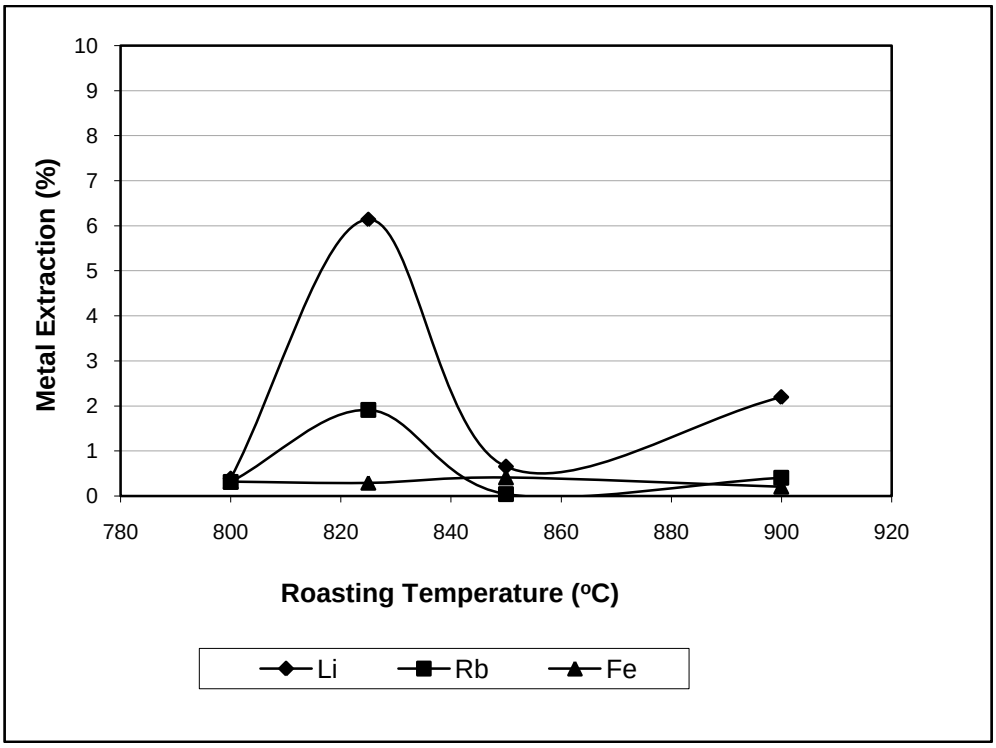

Figure 8.30: Effect of roasting temperature on the extraction of lithium, rubidium and iron at 85^{o}C, l:s = 10, ratio = 5:1(limestone roast).

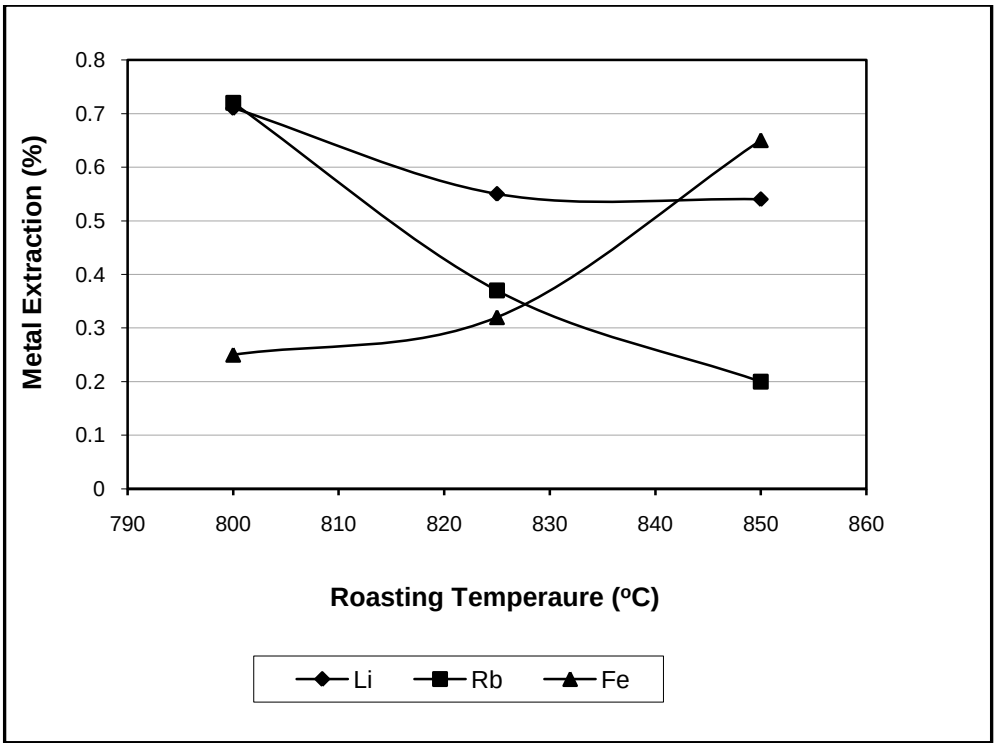

Figure 8.31: Effect of roasting temperature on the extraction of lithium, rubidium and iron at 85°C, l:s = 10, ratio = 3:1 (limestone roast).

The chemical composition of the roast-products used in the experiments is given in Table 8.16.

Table 8.16: Chemical composition of mica-limestone roast-products.

Sintering Temperature [°C]	Ratio	Grade [%]			LOI
		Li	Rb	Fe	
800	5:1	0.92	0.63	6.08	9.70
800	3:1	0.87	0.59	5.54	12.50
825	5:1	0.92	0.62	5.38	9.68
825	3:1	0.87	0.59	5.02	12.89
850	5:1	0.92	0.63	5.89	9.84
850	3:1	0.88	0.59	5.38	13.12
900	5:1	0.94	0.61	7.91	13.91

Generally the lithium extraction efficiencies in the limestone method were very low and, thus, it was also decided to extend the roasting temperatures both lower and higher than those reported above. Roast-products were prepared from 250°C to 1050°C and the reported values in Figure 8.32 are the average of the two leaching experiments. The concentrate to limestone ratio was 5:2. Again it can be seen from Figure 8.32 that the lithium extraction efficiencies were very low and as such further extraction testing with this method was discontinued.

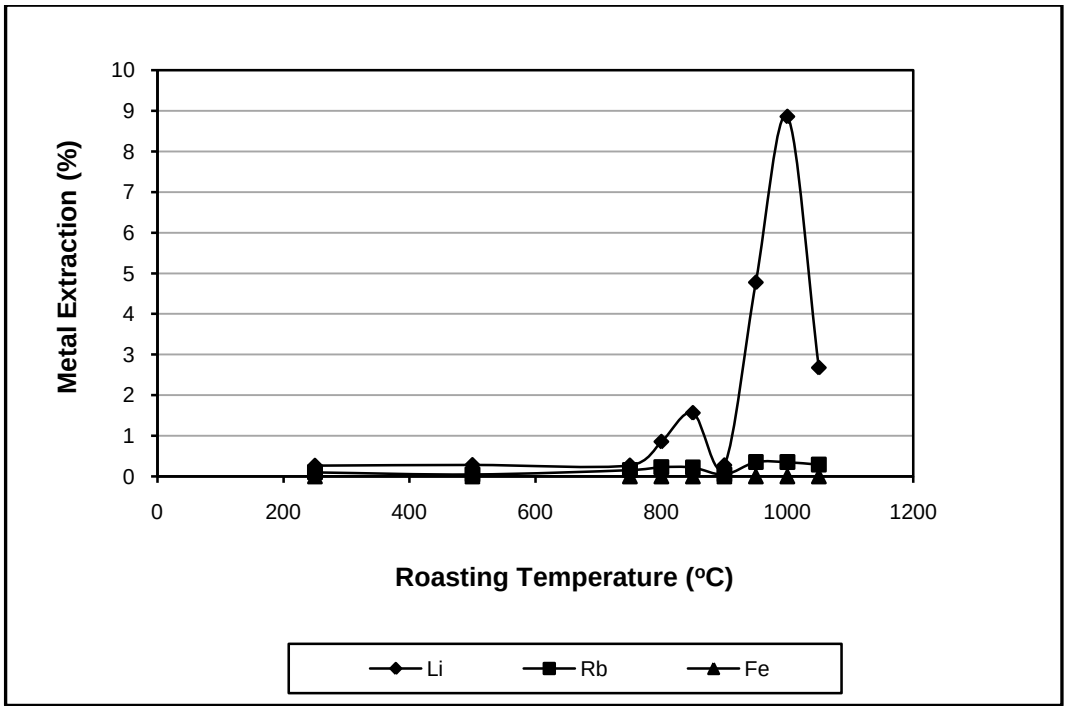

Figure 8.32: Effect of roasting temperature on the extraction of lithium, rubidium and iron at 85°C, L:S = 10, ratio = 5:2 (limestone roast).

The poor results of the limestone method led to speculation that the lithium mineral phases which formed in these roast-products were not water soluble. XRD analysis of the roast-product identified pseudo-eucryptite as the lithium specie, which is sparingly water-soluble.

Although the results in this study were poor, Jandova et al. (2008) have reported lithium and rubidium extraction efficiencies of almost 92% when their zinnwaldite concentrate was roasted with limestone. They reported a concentrate to limestone ratio of 5:1 and calcining temperatures ranging from 800°C to 875°C. The detailed experimental procedure is given in section 6.4.2.

In this study the concentrate to limestone ratios investigated were 3:1, 5:1 and 5:2, and the roasting temperatures ranging from 250°C to 1050°C. The maximum lithium extraction efficiency obtained was about 9% (Figure 8.32).

8.6.3 The Sodium Sulphate Method

The successful leaching results using the gypsum method led to the assumption that the compound that was responsible for lithium leaching in water was a sulphate. It was for this reason that it was decided to roast the mica minerals with another sulphate containing compound, namely sodium sulphate. The gypsum method of lithium extraction had been tried before by Jandova et al. (2008, 2009), but there are no reports of the use of sodium sulphate. Thus the sodium sulphate method was a new route tried in this experimental programme. The same experimental method as described for gypsum and limestone was followed in testing the use of sodium sulphate in lithium extraction. Full details of the test procedure are provided in section 7.6.

The influence of roasting temperature on lithium, rubidium and iron extraction efficiency is illustrated in Figure 8.33.

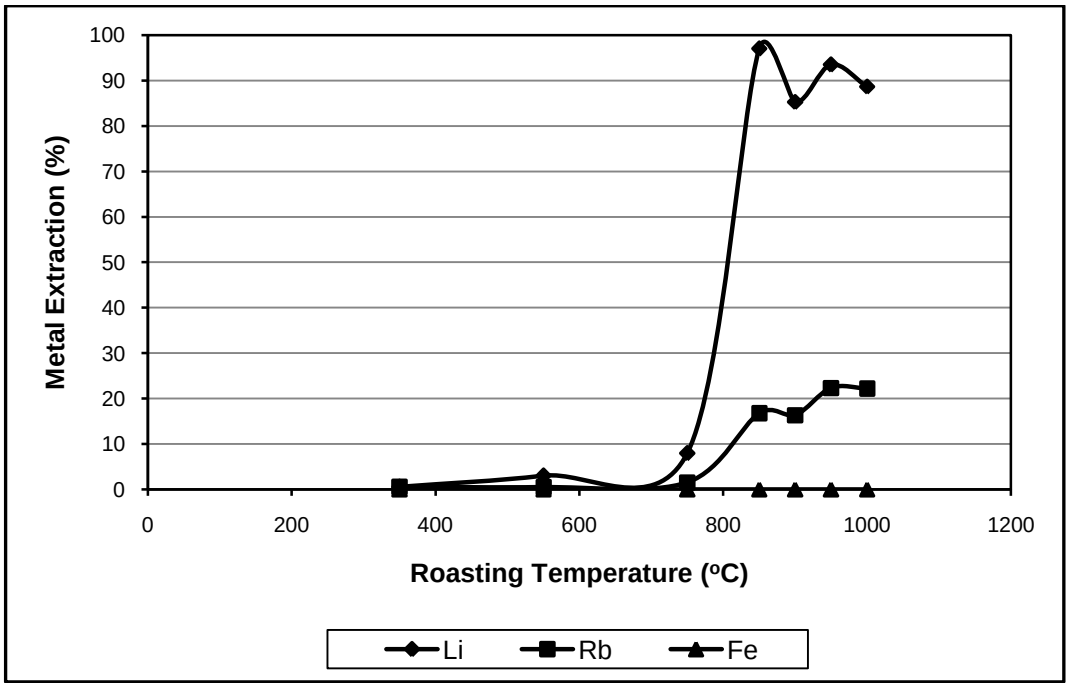

Figure 8.33: Effect of roasting temperature on the extraction of lithium, rubidium and iron at 85°C; l:s = 10; ratio = 2:1(sodium sulphate roast).

The leaching was performed at "natural" pH of the pulp which varied according to the roasting temperature. Leaching was conducted in duplicate and the mean values are shown in Figure 8.33. Water-leaching was carried out for 30 minutes in a stirred beaker immersed in a water bath maintained at a temperature of 85°C. The mica concentrate to sodium sulphate

ratio in the material was 2:1 and leaching was conducted with a liquid to solid ratio of 10:1. It can be seen from Figure 8.33 that very high leaching extraction efficiency was achieved for lithium at a roasting temperature of 850^{o}C. The maximum rubidium extraction efficiency was 22% at a roasting temperature of 950^{o}C. Iron co-extraction was very low.

Figures 8.34 and 8.35 show the XRD profiles of mica-sodium sulphate (2:1) roasted at 750^{o}C and 850^{o}C respectively. It can be observed from Figure 8.34 that the XRD profile of mica-sodium sulphate roasted at 750^{o}C is similar to the paramagnetic mica shown in Figure 8.18. This indicated that the mica and sodium sulphate did not react to form new mineral phases at that temperature and resulted in low lithium extraction efficiency. It can be observed from Figures 8.34 and 8.35 that the two XRD profiles were different. It is evident from Figure 8.35 that new mineral phases were formed when the paramagnetic mica-sodium sulphate mixture was roasted at 850^{o}C. The following mineral phases were among those which were formed and could be identified in roast-product prepared at 850^{o}C: leachable lithium potassium sodium sulphate [$Li_2KNa(SO_4)_2$], anorthite ($CaAl_2Si_2O_8$), fluoroedenite ($NaCa_2(Mg,Fe)_5Si_7AlO_{22}F_2$), tirodite and residual thenardite (Na_2SO_4). Figure 8.36 shows the XRD profile of the mica-sodium sulphate (850^{o}C) leach residue.

Figure 8.37 shows the effect of leaching bath temperature on lithium extraction. The roast-products were water-leached for 30 minutes. It is evident from Figure 8.37 that the leaching temperature has little effect on lithium extraction efficiency. It is interesting to note that materials could be leached in water at room temperature (20^{o}C) and still achieve acceptable lithium extraction efficiency of more than 85%.

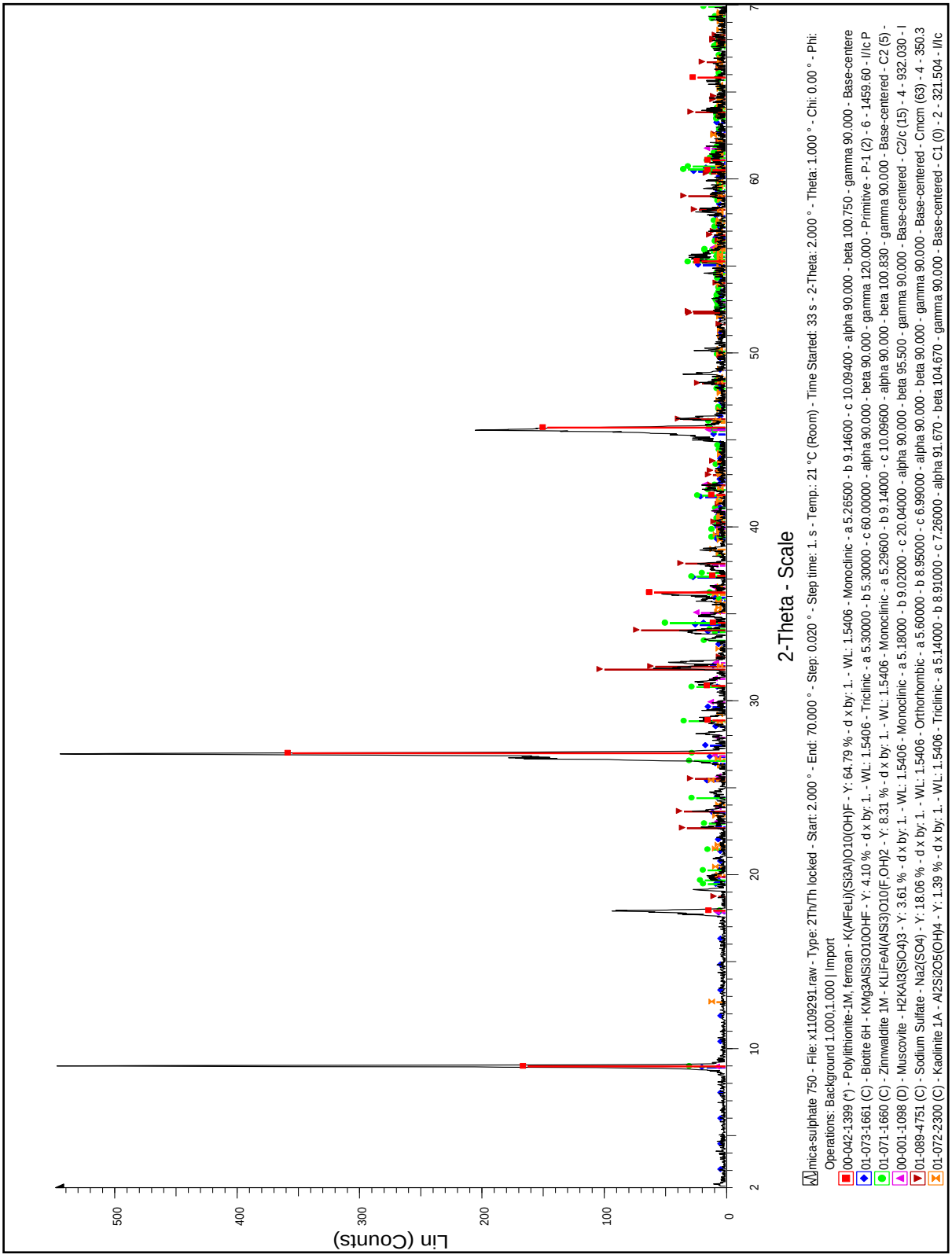

Figure 8.34: XRD profiles of mica-sodium sulphate mixture roasted at 750^{o}C.

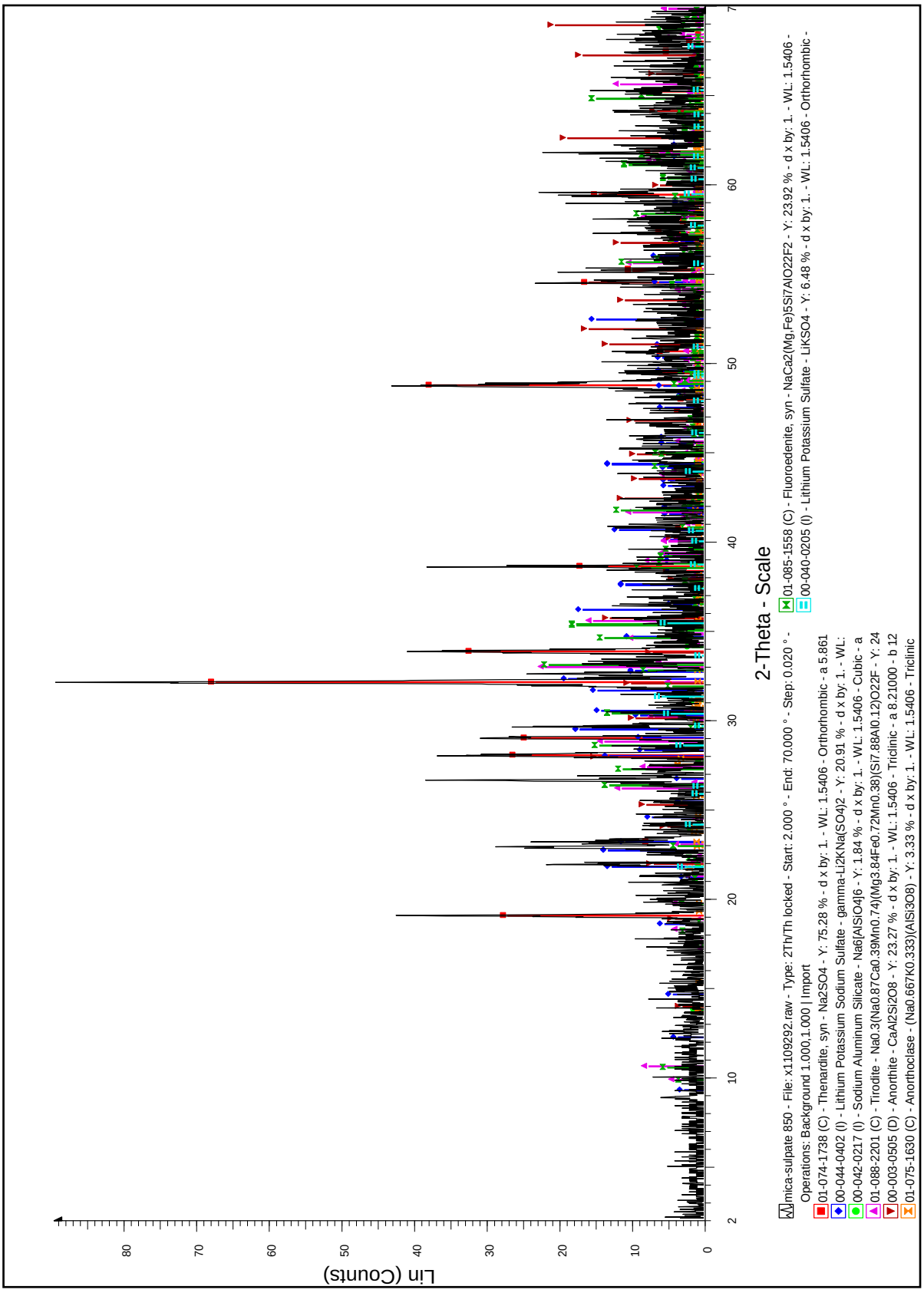

Figure 8.35: XRD profiles of mica-sodium sulphate mixture roasted at 850^{o}C.

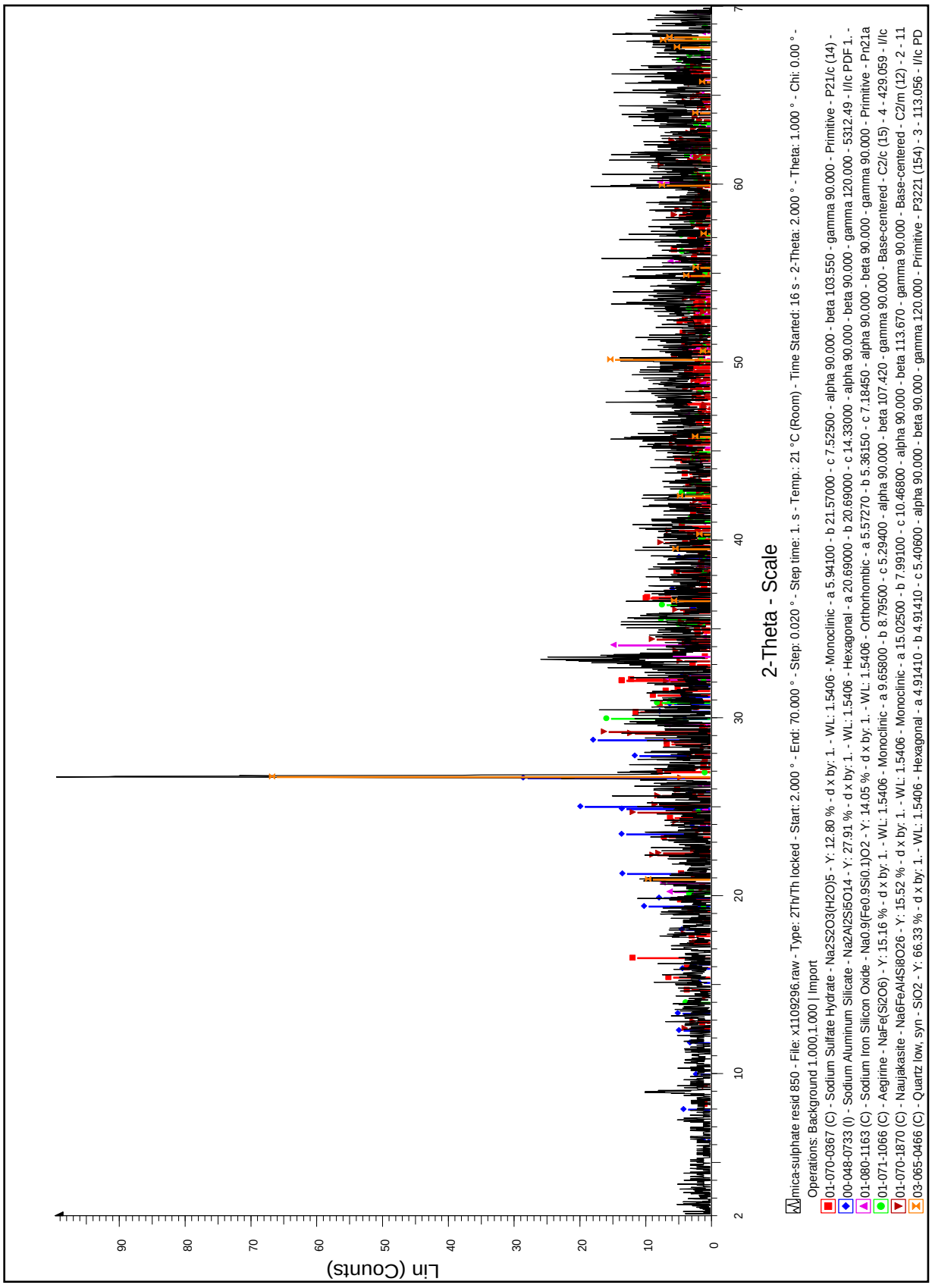

Figure 8.36: XRD profiles of mica-sodium sulphate roast leach residue (850^{o}C).

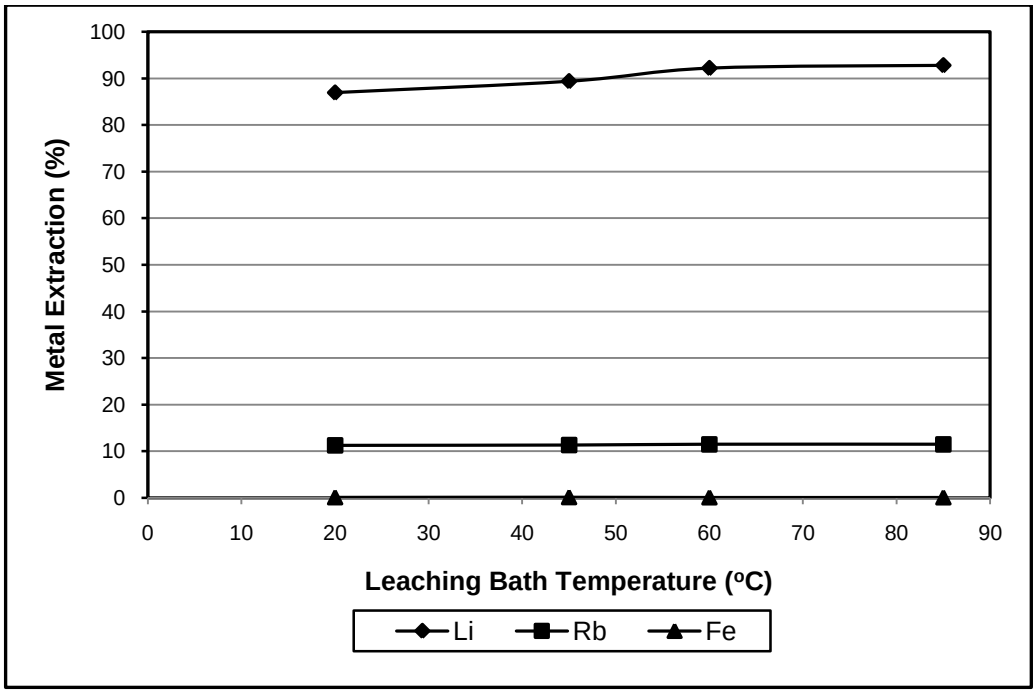

Figure 8.37: Effect of leaching bath temperature on extraction of lithium, rubidium and iron; roasting temperature 850°C, l:s = 10 (sodium sulphate roast).

The kinetics of lithium and rubidium extraction were determined for leaching the roast-product prepared at 850°C, leaching temperature of 85°C and a liquid to solid ratio of 10:1 (see Figure 8.38). It is clear from Figure 8.38 that lithium dissolution is very fast and was almost completed within 10 minutes.

The effect of paramagnetic mica concentrate to sodium sulphate ratio on lithium extraction efficiency is demonstrated in Figure 8.39. Figure 8.39 has shown that the concentrate can be increased up to five times the amount of sodium sulphate while still achieving 80% lithium extraction efficiency. However, increasing the concentrate to sodium sulphate ratio to 7:1 drastically decreased the lithium extraction efficiency to 38%. The low extraction efficiency observed at roast-product ratio 7:1 can be attributed to an insufficient amount of sodium sulphate required to react with the mica in the concentrate. Iron co-extraction was negligible. The ratio 5:1 is backed by stoichiometric calculation which indicated that it was the maximum ratio, which could provide the necessary sulphate ions required to convert the lithium contained in the mica to a water soluble lithium compound [$Li_2KNa(SO_4)_2$] during roasting.

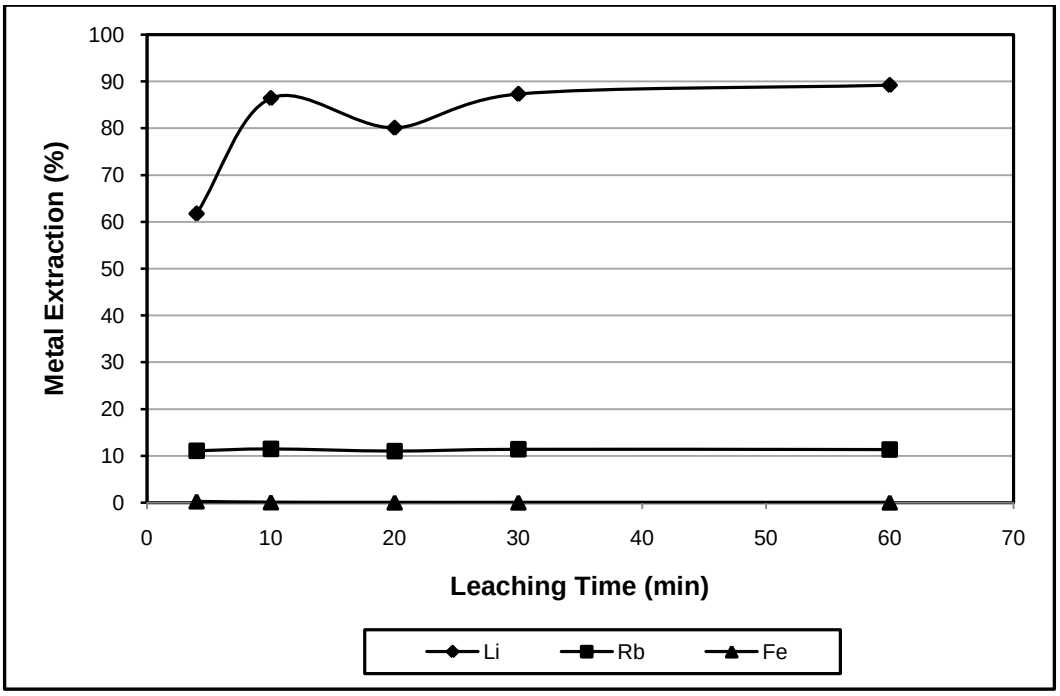

Figure 8.38: Leaching kinetics of lithium and rubidium at 85°C, l:s = 10:1; roasting temperature 850°C (sodium sulphate roast).

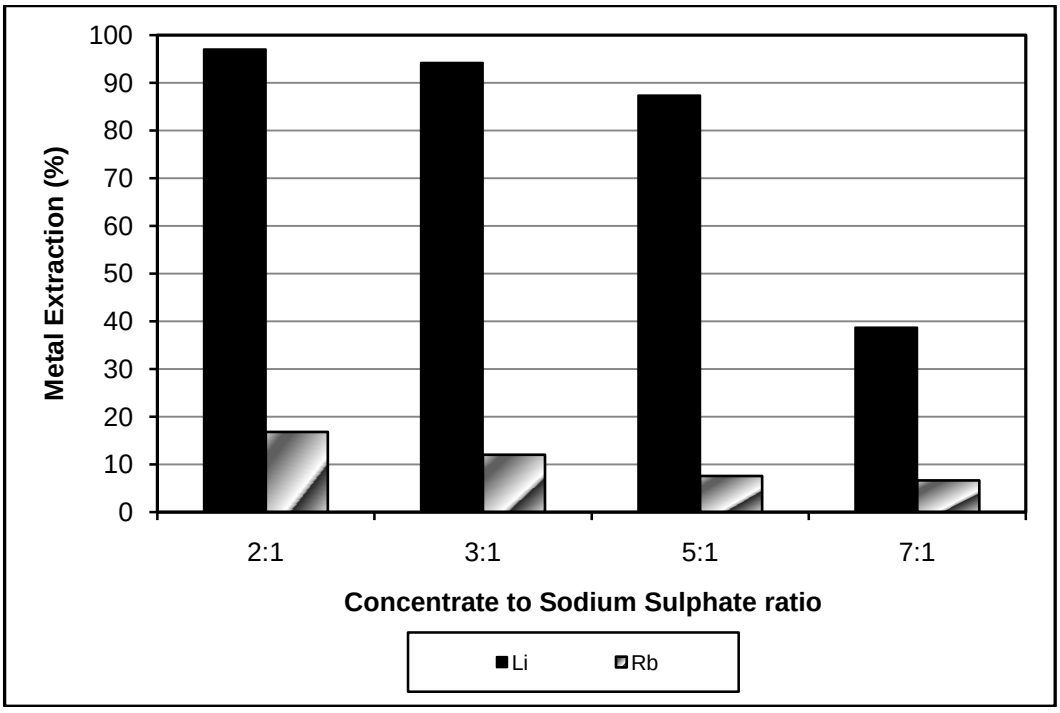

Figure 8.39: Effect of concentrate to sodium sulphate ratio in roast-product on lithium and rubidium extractions at 85°C, l:s = 10:1; roasting temperature 850°C (sodium sulphate roast).

The water soluble lithium compound was determined as $Li_2KNa(SO4)_2$ by the XRD analysis. The ratio of lithium to sulphate in this compound is 1:13.84. Thus, 1 tonne of lithium would require 13.84 tonnes of sulphate ions (20.46 tonnes of sodium sulphate).

The paramagnetic mica contains about 1% Li and therefore, 5 tonnes of paramagnetic mica contains 0.05 tonnes of lithium, which would require about (0.05 x 20.46) 1.02 tonnes of sodium sulphate. This is almost the 5:1 ratio of paramagnetic mica to sodium sulphate. Increasing beyond this ratio would mean less sulphate ions to form the water soluble lithium compound and hence the reason why the lithium extraction efficiency was lower for the 7:1 roast-product ratio reported in Figure 8.39.

Typical composition of leach liquors obtained when leaching at 85^{o}C and l:s = 10:1 is shown in Table 8.17.

Table 8.17: Average composition of leach liquors at 850^{o}C roast and product ratio = 2:1 (sodium sulphate roast)

Concentration of elements (g/m^3)				
Li	**Rb**	**K**	**Ca**	**Na**
264	26	522	18	3627

Leaching was also conducted on the mica cleaner and non-magnetic mica concentrates after they were roasted respectively with sodium sulphate at 850^{o}C in the ratio 2:1. Tables 8.18 and 8.19 show the results. It is evident from Table 8.18 that leaching the mica cleaner concentrate roasted with sodium sulphate at 850^{o}C resulted in almost 80% Li extraction in solution. This has shown that with the sodium sulphate method there may be no need for the magnetic separation stage to recover the lithium mica before roasting and leaching.

Table 8.18: Extraction efficiency of mica flotation cleaner concentrate roasted at 850^{o}C (sinter ratio=2:1).

Test	**Extraction Efficiency (%)**	
	Li	**Rb**
Run 1	80.3	4.2
Run 2	79.4	4.4
Mean	***79.9***	***4.3***
Standard deviation	***0.6***	***0.1***

Table 8.19: Extraction efficiency of non-magnetic mica concentrate roasted at 850^{o}C (sinter ratio=2:1).

Test	**Extraction Efficiency (%)**		
	Li	**Rb**	**Fe**
Run 1	73.2	5.0	1.8
Run 2	74.0	4.8	1.8
Mean	***73.6***	***4.9***	***1.8***
Standard deviation	***0.6***	***0.1***	***0.0***

The extraction efficiencies achieved with the gypsum method in roast-products prepared at 1050^{o}C were slightly lower than those obtained with the sodium sulphate at 850^{o}C. This indicated that with the sodium sulphate method, the water soluble lithium compounds were

formed at a lower temperature. Thus the sodium sulphate method has not only increased the extraction efficiency of lithium but also lead to a reduced roasting temperature being necessary.

The lithium extraction by the sodium sulphate method, which was a new route tried in this research and reported above, did not involve the addition of lime to the roast-product. Thus it was also decided to roast the mica concentrate together with sodium sulphate and calcium hydroxide in the ratio 6:2:1 at temperatures ranging from 800 to 975^{o}C. The roast-products were leached in the water-bath maintained at 85^{o}C for 30 minutes at a liquid to solid ratio of 10:1.

The result of the influence of roasting temperature on lithium and rubidium extraction efficiency is illustrated in Figure 8.40.

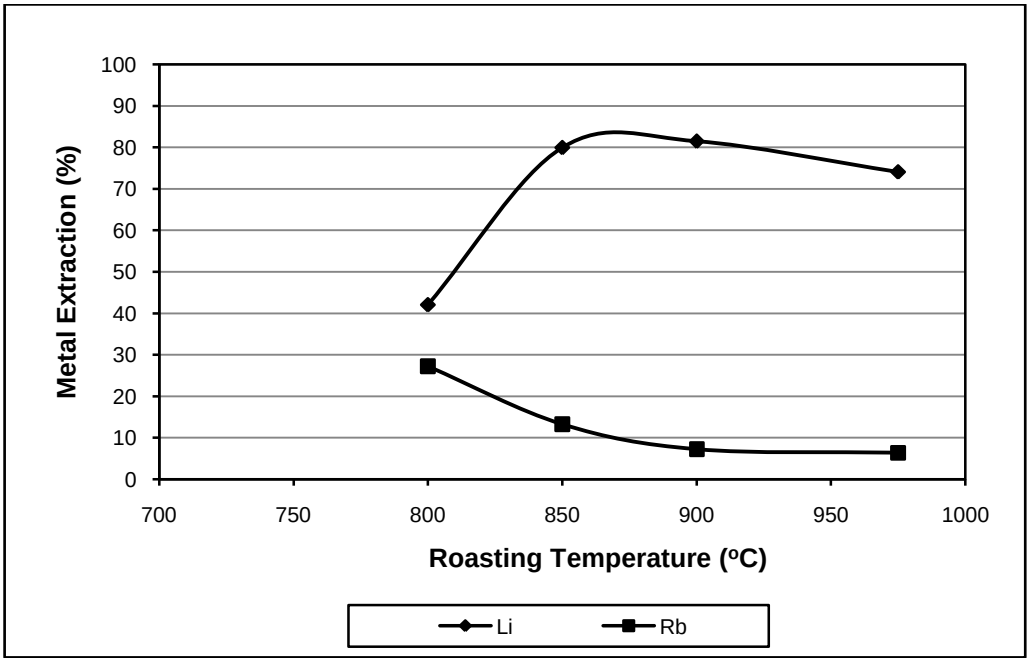

Figure 8.40: Effect of roasting temperature on the extraction of lithium and rubidium at 85^{o}C, l:s = 10:1; ratio = 6:3:1(sodium sulphate roast).

The experiment was performed in duplicate and the reported values are the average of the two. It can be seen from Figure 8.40 that about 80% lithium extraction efficiency was achieved if roasting was carried out at the temperature of 900^{o}C. However, the rubidium extraction efficiency decreased with the increase in roasting temperature. Thus the addition of calcium hydroxide to the concentrate did not increase the extraction efficiency nor decrease

the roasting temperature. The only attribute of calcium hydroxide was that it made the roast-product "soft" and thus easy to remove from the crucibles and to grind.

Comparing these results to those obtained by Jandova et al. (2008, 2009), it can be observed that the sodium sulphate method gives similar lithium extraction efficiency but at a lower roasting temperature. In their experiments, they roasted the zinnwaldite concentrate with gypsum and calcium hydroxide at 950^{o}C in the ratio 6:4.2:2 and achieved about 96% and 25% lithium and rubidium extraction respectively. In the experiments reported here the concentrate was roasted with gypsum only at 1050^{o}C and achieved about 84% and 14% lithium and rubidium extraction respectively. Table 8.20 shows the cost of refined roasting reagents used (Harben, 2002). The cost of roasting reagents may further be reduced by using the impure form of the reagents, which according to Harben (2002) were £59/t for salt cake (impure sodium sulphate containing 90-99% Na_2SO_4) and £6/t for crude gypsum (>50% to < 95% $CaSO_4$, with limestone or insoluble anhydrite being the main contaminant). The cost of crude gypsum appears to be interesting but its efficiency in lithium extraction has to be assessed again because of the impurities contained, which may be deleterious to the lithium extraction during leaching.

Table 8.20: Cost of roasting reagents using data from Harben (2002).

Name	Cost (£/t)
Anhydrous sodium sulphate	82
Calcium sulphate dihydrate	52 - 132

Generally, the sodium sulphate method appears to be interesting both in terms lithium extraction and in energy consumption as the roasting was performed at a lower temperature.

Summary of Leaching Results Using the Sodium Sulphate Method

The summary of the leaching results achieved using the sodium sulphate method is given in Table 8.21. The materials tested under the sodium sulphate method of lithium extraction were magnetic mica, non-magnetic mica, mica cleaner concentrate and magnetic mica mixed with calcium hydroxide. The materials were roasted at 850^{o}C. It can be seen from Table 8.21 that roasting the magnetic mica with sodium sulphate and calcium hydroxide reduced both the lithium and rubidium extraction efficiency. It is interesting to note that 80% lithium extraction

efficiency could be achieved when treating the mica cleaner concentrate by the sodium sulphate method.

Table 8.21: Summary of the leaching results using the sodium sulphate method.

Material	ratio	Extraction Efficiency (%)	
		Li	Rb
Pulverised magnetic mica : sodium sulphate	2:1	94	17
Pulverised non-magnetic mica : sodium sulphate	2:1	74	2
Pulverised mica cleaner concentrate : sodium sulphate	2:1	80	4
Pulverised mag. mica : sodium sulphate: calcium hydroxide	6:3:1	80	13

8.6.4 Recovery of Lithium Carbonate from Leach Solution

After the lithium leaching experiments, attempts were made to recover lithium from the pregnant solution by precipitation. Sodium carbonate was used to try and precipitate lithium as lithium carbonate from the leach solution at 90^{o}C. The solubility of sodium carbonate at room temperature is 7.1g/100 ml and as such 7.1 g was dissolved in 100 ml of deionised water to make the sodium carbonate solution.

In the experiments reported above, only 10g of roast-product was leached at a time, giving a solution containing about 263 g/ml on average, which was too low for lithium carbonate precipitation. According to Jandova et al., (2009), increasing the lithium concentration in solution to at least 9 g/l is necessary to achieve acceptable Li_2CO_3 precipitation efficiency. Therefore, in order to increase the lithium content in solution to accepted level, it was decided to leach about 400g of roast-product split into five fractions of 80g and leached co-currently as shown in Figure 8.41. The material was roasted at 850^{o}C with a ratio of 5:1 (paramagnetic mica concentrate: sodium sulphate). The leaching was conducted at 85^{o}C with a liquid:solid ratio of 10:1 for 30 minutes each. Lithium carbonate was precipitated by the addition of the sodium carbonate solution to the concentrated leach solution (100 ml) at 90^{o}C because its solubility decreases with increasing temperature.

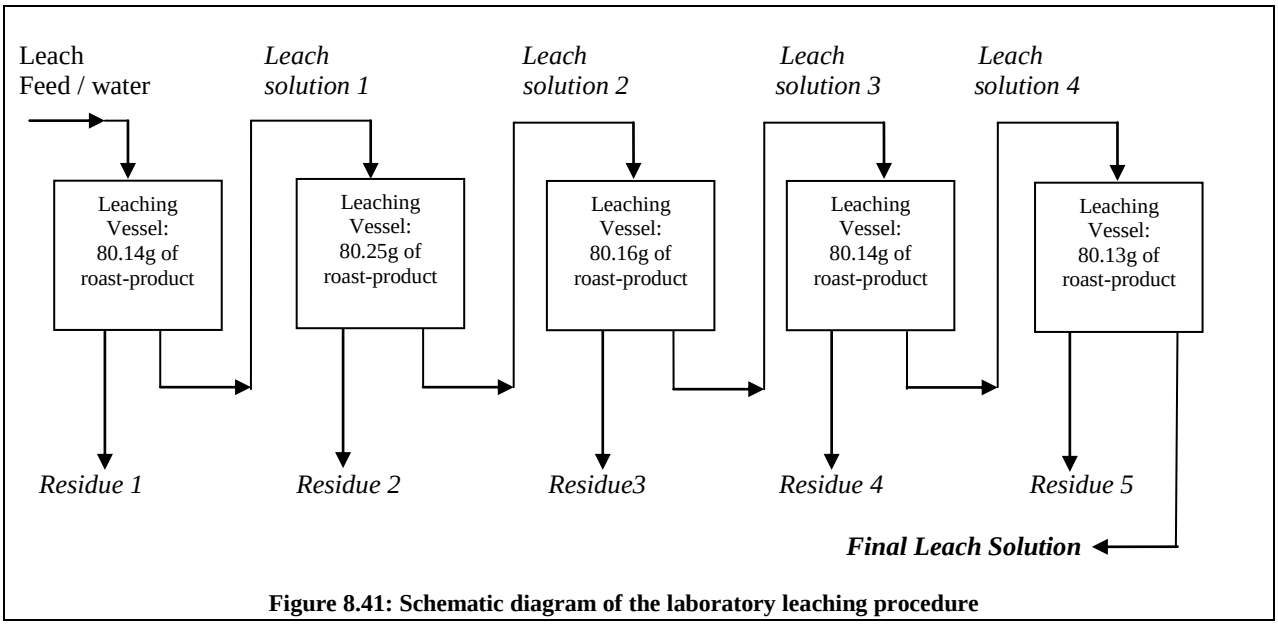

Figure 8.41: Schematic diagram of the laboratory leaching procedure

The content of the final leach solution together with the concentrated leach and mother liquor are shown in Table 8.22. The final leach solution (750 ml) was evaporated to about 150 ml in order to increase the lithium content. In total about 70 ml of sodium carbonate solution was added in 10 ml at a time to the boiling concentrated leach solution until no more precipitate formed. The precipitate was filtered, dried and weighed.

Table: 8.22: Composition of processed leach solution.

Solution	Concentration of elements (mg/l)					
	Li	Rb	Fe	K	Na	Ca
Original leach solution	2324	133.9	1.52	377.7	1422	176
Concentrated leach solution	9348	726.4	1.51	43500	149800	-
Mother leach solution	6588	682.3	0.521	136800	875500	1090

The precipitate was analysed for lithium and other impurity alkali earth metals and the results are given in Table 8.23. The XRD analysis shown in Figure 8.42 indicated that the lithium carbonate precipitate consisted mainly of zabuyelite (Li_2CO_3) with traces of sodium and calcium carbonates.

Table 8.23: Chemical composition of Li_2CO_3 precipitate

Elements (%)					
Li	Rb	Fe	K	Na	Ca
16.94	0.01	0.01	0.55	2.54	2.55

The total lithium carbonate precipitation efficiency achieved was about 30%. As seen from Table 8.23, the lithium carbonate precipitate was contaminated by sodium and calcium. Lithium carbonate contains about 18.79% Li determined from the chemical formula and thus the purity of the precipitate achieved was about 90.1%. The purity of lithium carbonate may be increased by thorough water-washing the precipitate.

Jandova et al. (2009) have reported the total efficiency of lithium carbonate precipitation from leach liquors of about 73% with a purity of 99%. They further mentioned that even the use of excess amount of potassium carbonate during Li_2CO_3 precipitation did not increase the precipitation efficiency. They said this was probably caused by the increase in solubility of Li_2CO_3 in sulphate solutions. Therefore other methods of recovering lithium from the mother leach liquor after lithium carbonate precipitation have to be pursued.

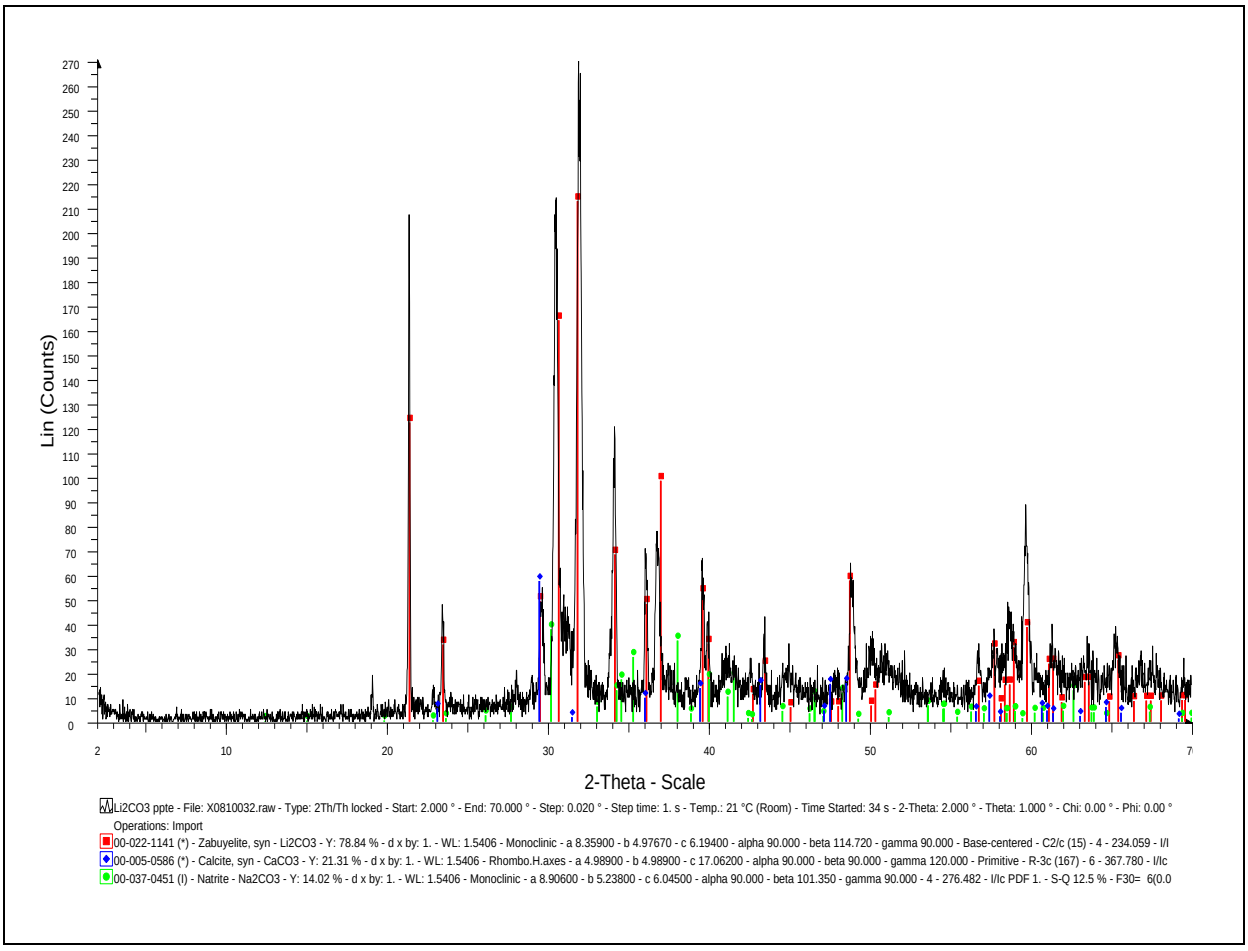

Figure 8.42: XRD analysis of lithium carbonate precipitate

8.7 Thermal Analysis of Leaching Materials

8.7.1 Thermogravimetric Analysis Results

The process description and test method procedure is given in section 7.7. Figure 8.43 shows the thermogravimetric analysis (TGA) curve of gypsum indicating mass loss between 90^{o}C and 150^{o}C. Because TGA measures the mass of a sample, any volatile species that are gained or lost during analysis will be measurable. In the mineral sciences, these species are usually limited to gaseous species, such as CO_2, CO, O_2, H_2O, NH_3, and SO_2. Many reactions seen with TGA can be envisioned as the loss of molecular species from the crystal. Gypsum ($CaSO_4.2H_2O$), for example, undergoes a reaction above 90^{o}C to anhydrite ($CaSO_4$), with the evolution of gaseous H_2O (Figure 8.43). Thus the loss of weight in gypsum is due to dehydration according to the reaction below:

$$CaSO_4.2H_2O \leftrightarrow CaSO_4 + 2H_2O(g)\uparrow. \quad (8.1)$$

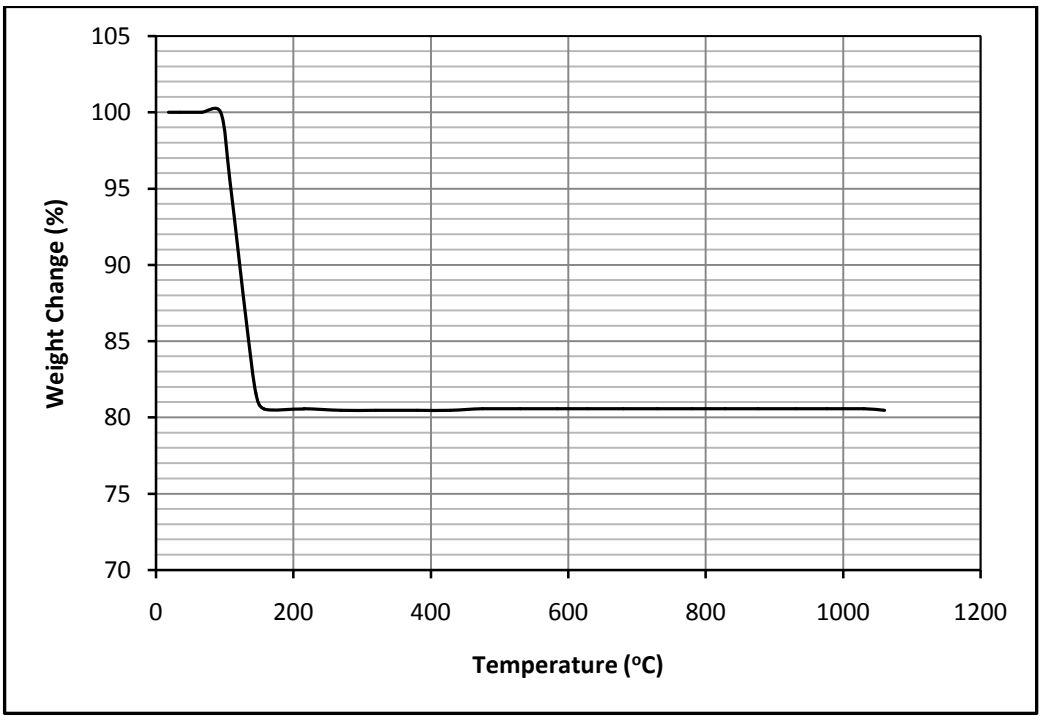

Figure 8.43: Thermogravimetric analysis curves of gypsum showing mass loss due to evolution of H_2O between 90^{o} and 180^{o}C (9.93 mg sample, 10^{o}C/min heating rate).

Figure 8.44 shows the TGA curve of paramagnetic mica. The paramagnetic mica concentrate contained among others zinnwaldite [$KLiFeAl(AlSi_3)O_{10}(F.OH)_2$], muscovite [$KAl_2(AlSi_3)O_{10}(F,OH)_2$], kaolinite [$Al_2Si_2O_5(OH)_4$], polylithionite [$KLi_2AlSi_4O_{10}(F,OH)_2$],

quartz (SiO_2), biotite [$K(Mg,Fe)_3\ AlSi_3O_{10}\ (F,OH)_2$] and topaz [$Al_2SiO_4(F,OH)_2$] in order of decreasing abundance. Thus on heating the sample, each mineral loses the water from the structural hydroxyls at different temperatures and probably produces different species. The example of the production of species different from those contained in a sample is the reaction that takes place on heating kaolinite above the temperature at which the hydroxyl group is stable. Above about 500°C, kaolinite breaks down to an essentially non-crystalline material and H_2O as observed by Bish and Duffy (1990). The reaction can be represented as follows:

$$Al_2Si_2O_5(OH)_4(s) \rightarrow Al_2Si_2O_7(\text{noncrystalline})(s) + 2H_2O(g)\uparrow. \qquad (8.2)$$

Thus, the mass loss observed in Figure 8.44 at about 530°C was partly due to the loss of water from structural hydroxyls through a reaction of $OH + OH = H_2O\ (g)\uparrow + O$. Although some of the oxygen produced by the dehydroxylation of kaolinite remains in the non-crystalline solid, this may not be the case for some reactions, particularly those involving oxidation or reduction. The other contribution to the loss in mass could be the organic matter and probably the evolution of fluorine gas.

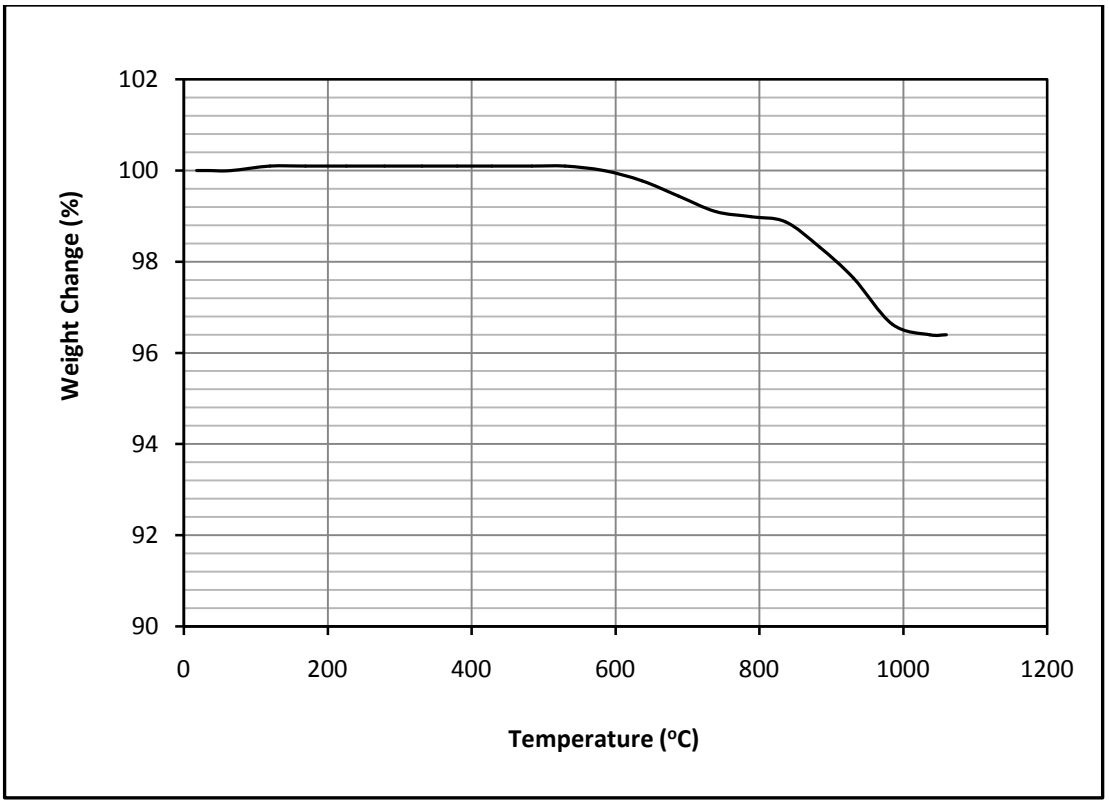

Figure 8.44: Thermogravimetric analysis curves of magnetic-mica (8.9 mg sample, 10°C/min heating rate).

Figure 8.45 shows the thermal gravimetric analysis of the mica-gypsum mixture. The first loss in mass at about 90^{o}C was due to gypsum by reasons explained earlier while the second loss at about 600^{o}C was due to mica also for the reasons mentioned above.

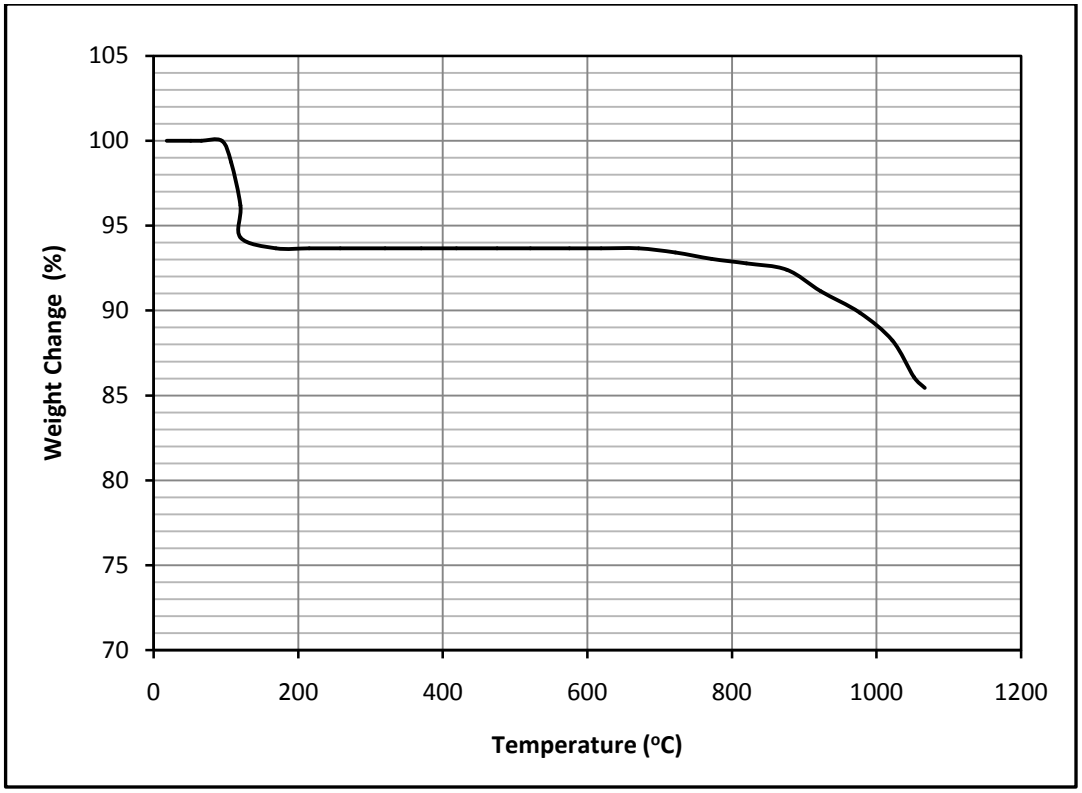

Figure 8.45: Thermogravimetric analysis curves of mica-gypsum (2:1) mixture (7.9 mg sample, 10^{o}C/min heating rate).

Figures 8.46 and 8.47 show the thermal gravimetric analysis of limestone, and paramagnetic mica-limestone mixture respectively. As can be seen from Figure 8.46, the loss in mass at about 700^{o}C was due to the evolution of CO_2 according to the reaction:

$$CaCO_3(s) \leftrightarrow CaO(s) + CO_2(g)\uparrow. \qquad (8.3)$$

The TGA curve for mica-limestone mixture also shows the loss in mass at about 600^{o}C mainly due to the evolution of CO_2 and to a lesser extent due to the mica present.

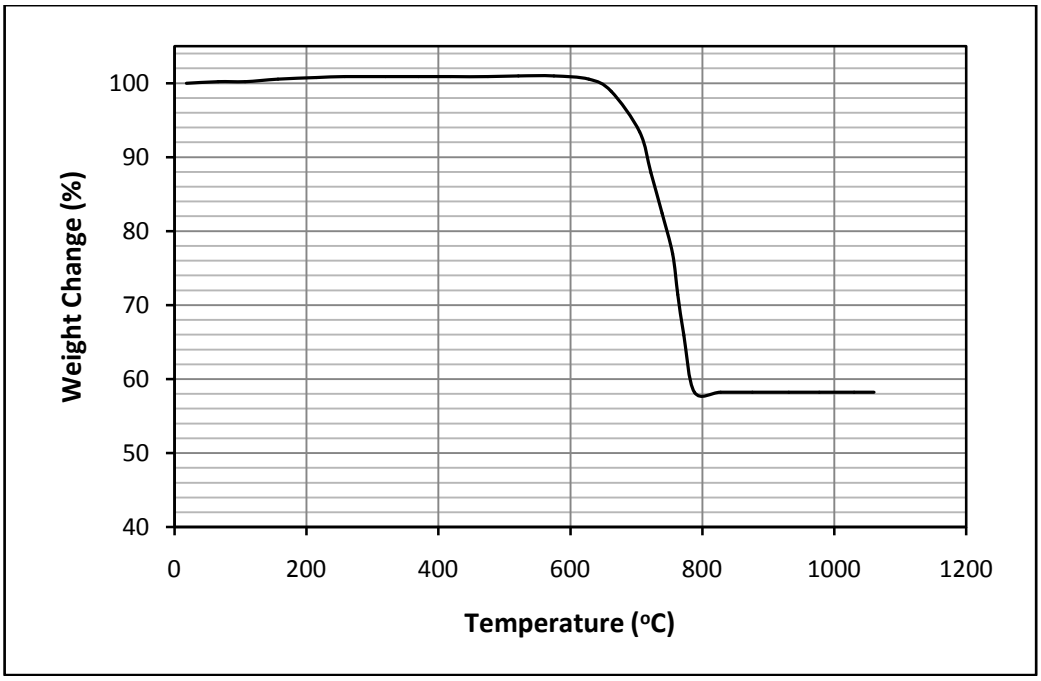

Figure 8.46: Thermogravimetric analysis curve of limestone (9.1 mg sample, 10°C/min heating rate).

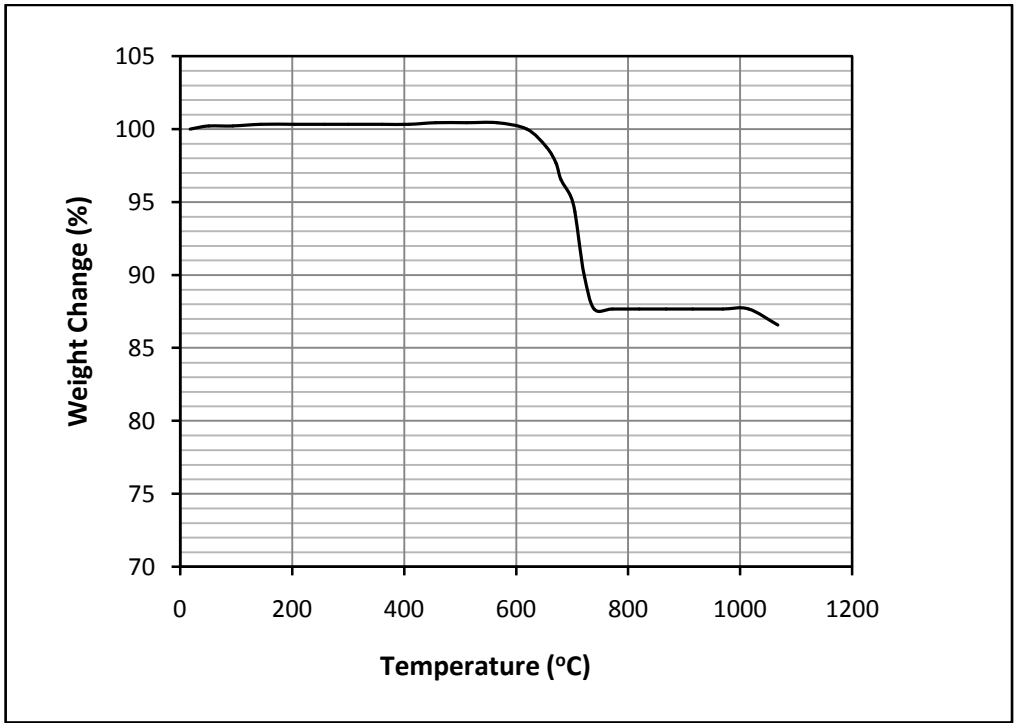

Figure 8.47: Thermogravimetric analysis curve of mica-limestone (5:1) mixture (9.01 mg sample, 10°C/min heating rate).

Figures 8.48 and 8.49 show the thermal gravimetric analysis of sodium sulphate, and paramagnetic mica-sodium sulphate respectively.

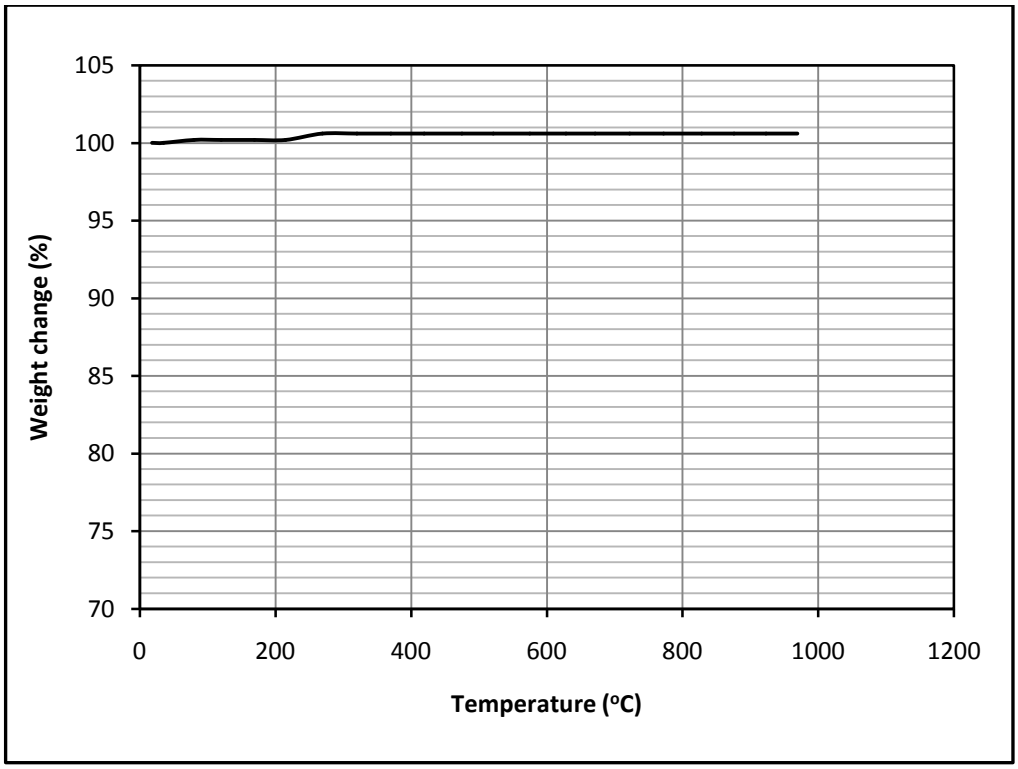

Figure 8.48: Thermogravimetric analysis curve of sodium sulphate (thenardite) [9.04 mg sample, 10°C/min heating rate].

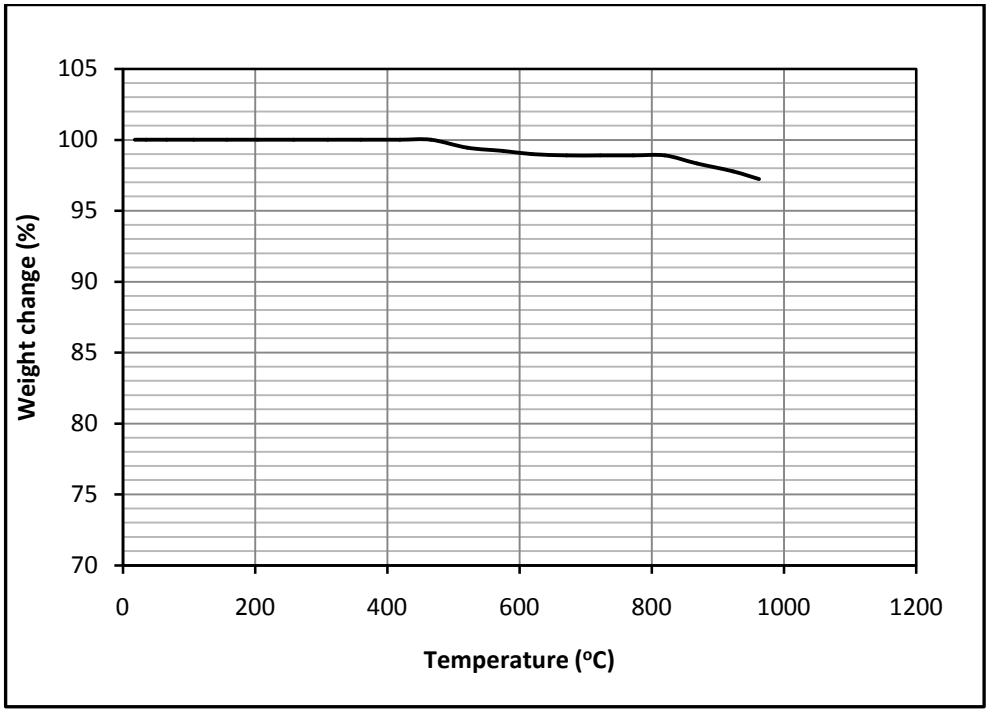

Figure 8.49: Thermogravimetric analysis curve of mica-sodium sulphate mixture (2:1) [8.99 mg sample; 10°C/min heating rate].

Figure 8.50 shows the thermogravimetric analysis of calcium hydroxide. The weight loss observed at 400^{o}C was due to the dehydration of calcium hydroxide. Figures 8.51 and 8.52 give the thermal gravimetric analysis of mica-Na_2SO_4-$Ca(OH)_2$ and mica-gypsum-$Ca(OH)_2$ mixtures respectively.

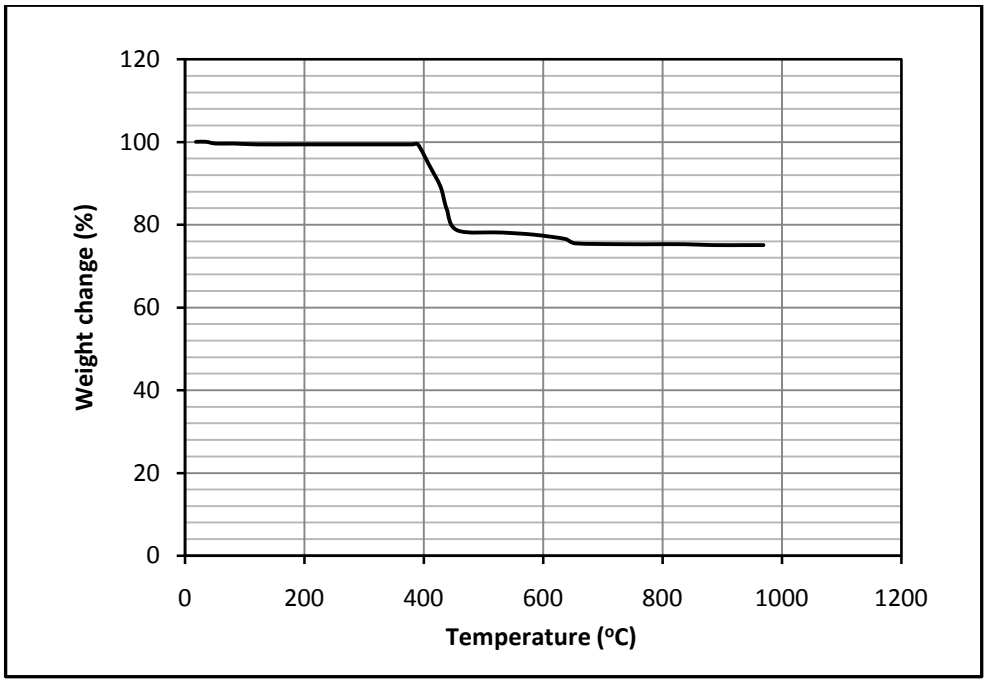

Figure 8.50: Thermogravimetric analysis curve for calcium hydroxide [9.54 mg sample; 10^{o}C/min heating rate].

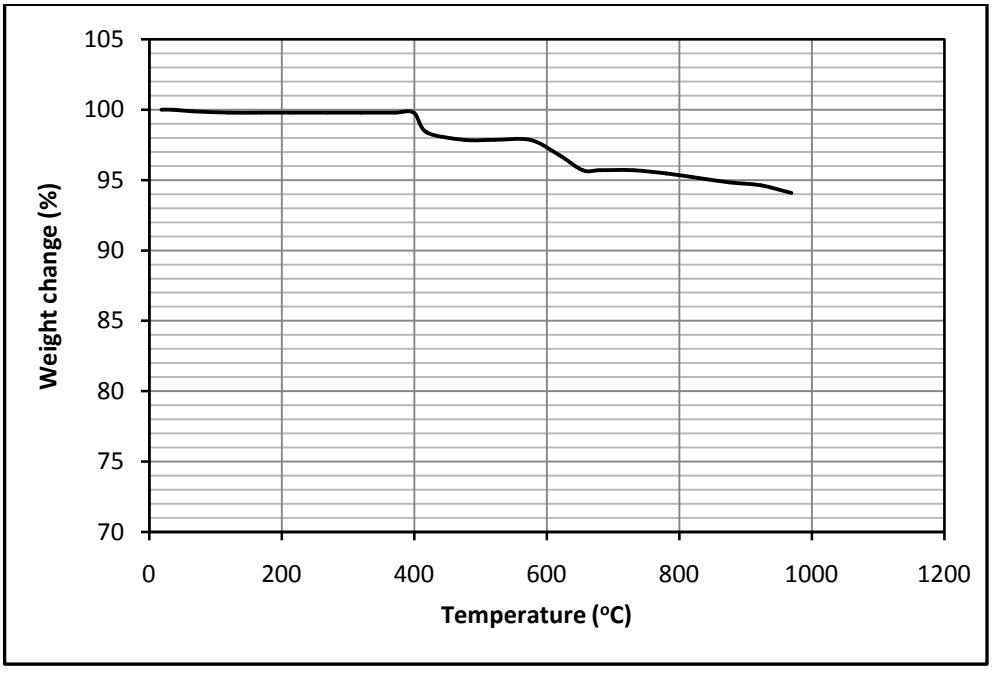

Figure 8.51: Thermogravimetric analysis curve for mica-Na_2SO_4-$Ca(OH)_2$ mixture (6:3:1) [9.26 mg sample; 10^{o}C/min heating rate].

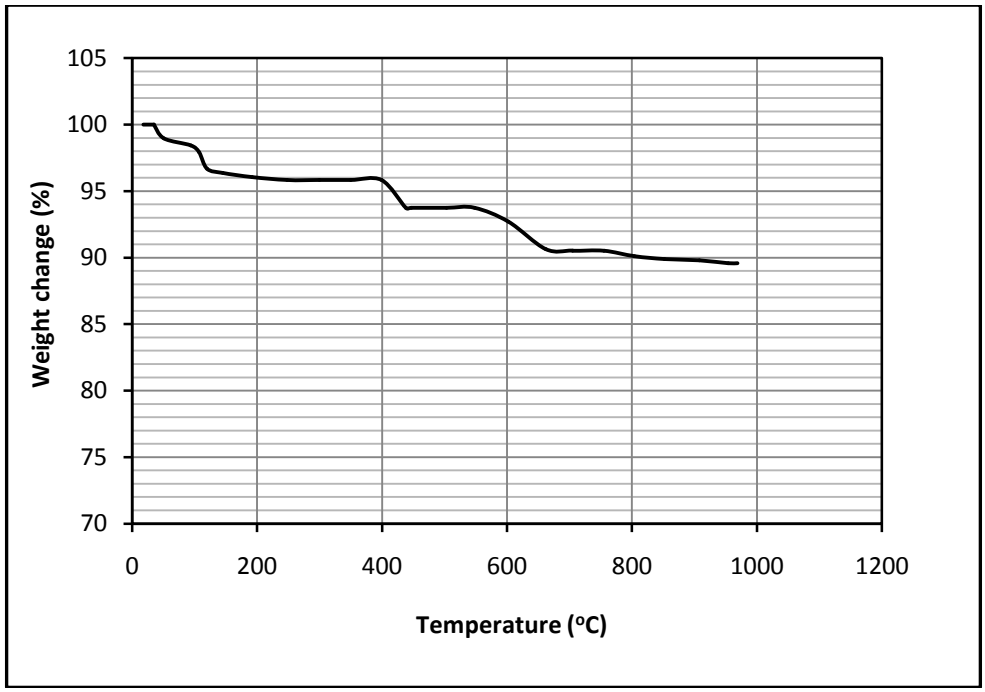

Figure 8.52: Thermogravimetric analysis curve for mica-gypsum-$Ca(OH)_2$ mixture (3:2:1) [9.56 mg sample; 10°C/min heating rate].

8.7.2 Differential Thermal Analysis Results

The detailed test method procedure is given in section 7.7. Figure 9.53 shows the differential thermal analysis (DTA) curve for gypsum ($CaSO_4.2H_2O$), undergoing a single endothermic reaction (in which the sample becomes cooler than the reference and ΔT is negative) due to loss of water (H_2O) between 50°C and 170°C. The loss of water happens in two stages and thus there were supposed to be two endothermic peaks, but they were masked because the pen recorder went off-scale. The two endothermic peaks could be made visible by either reducing the heating rate or by diluting the sample with the reference material. It can also be observed from the figure that there was a small exothermic peak between 300°C and 400°C.

Figure 8.54 shows the DTA curve for the paramagnetic mica heated at 10°C/min. It should be noted that all transformations or reactions involving energy changes in the sample are reflected in the DTA curve. Such reactions may be resolved into five classes: phase transformations, solid-state reactions, decompositions, reactions with an active gas (surface reactions) and second-order transitions (a change in entropy without a change in enthalpy).

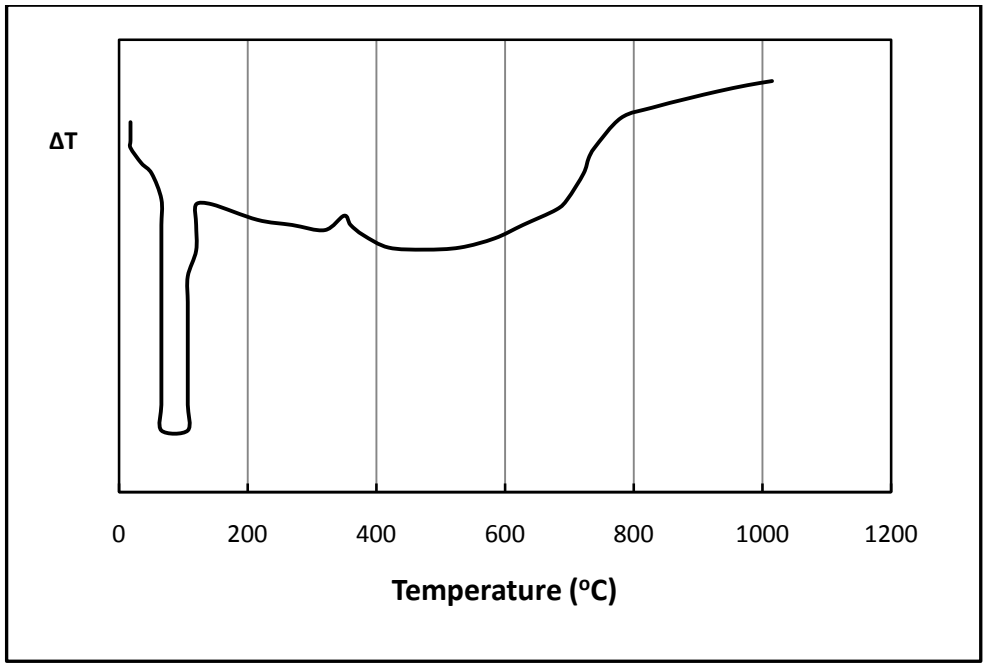

Figure 9.53: DTA curve for gypsum (9.93mg sample, 10°C/min heating rate).

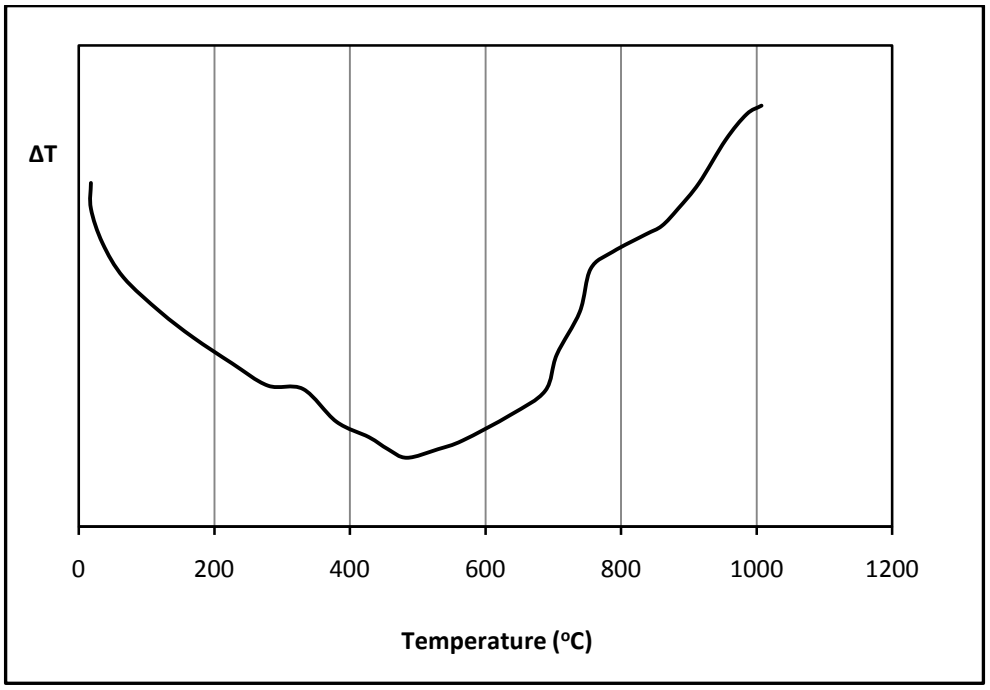

Figure 8.54: DTA curve for paramagnetic-mica (8.9 mg sample, 10°C/min heating rate).

The DTA curve for paramagnetic mica-gypsum mixture is given in Figure 8.55. It can be seen from Figure 8.55 that the double endothermic peaks of gypsum between 90°C and 150°C are visible in this mixture. The first endothermic peak at 80°C represents loss of $1\frac{1}{2}$ H_2O, the second at 94°C loss of $\frac{1}{2}$ H_2O (Mackenzie and Mitchell, 1973). Again it can be observed from

Figure 8.55 that there was a small exothermic peak at about 350^{o}C. This is because certain salts exhibit exothermic effects due to the transformation of an "amorphous" or meta-stable anhydrous phase into a crystalline one as had been observed in the case of dehydrated gypsum, which preserves the structure of the hemi-hydrate, $CaSO_4.\frac{1}{2}H_2O$, until 300^{o}C, when the salt gives out heat and assumes the structure of anhydrite (Berg, 1970).

It was very difficult to ascertain the nature of the endothermic peak at 900^{o}C in Figure 8.55, probably due to the formation of new mineral phases or rather reactions between anhydrite and some minerals present in the mica concentrate. The peak is not present in the DTA curves for gypsum and mica presented above. This probably explains why lithium extraction began when the gypsum-mica mixtures were heated at and above 900^{o}C. Among the new mineral phases formed at and above this temperature were the water-soluble lithium compounds. The endothermic peak at about 90^{o}C observed in Figure 8.55 was accompanied by the loss of weight in gypsum.

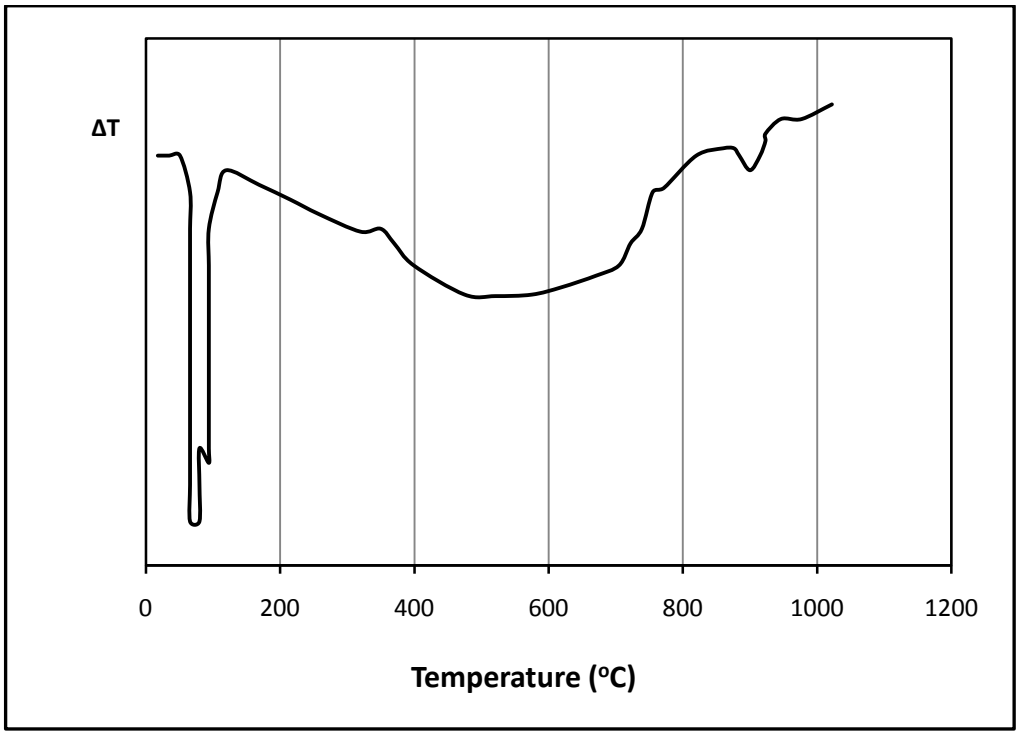

Figure 8.55: DTA curve for mica-gypsum (2:1) mixture (7.9 mg sample, 10^{o}C/min heating rate).

Figure 8.56 shows the DTA curve for limestone ($CaCO_3$). The endothermic peak at about 700^{o}C was due to the evolution of CO_2. The DTA curve for mica-limestone mixture is given

in Figure 8.57. Again the endothermic peak observed at about 688^{o}C was due to the evolution of CO_2.

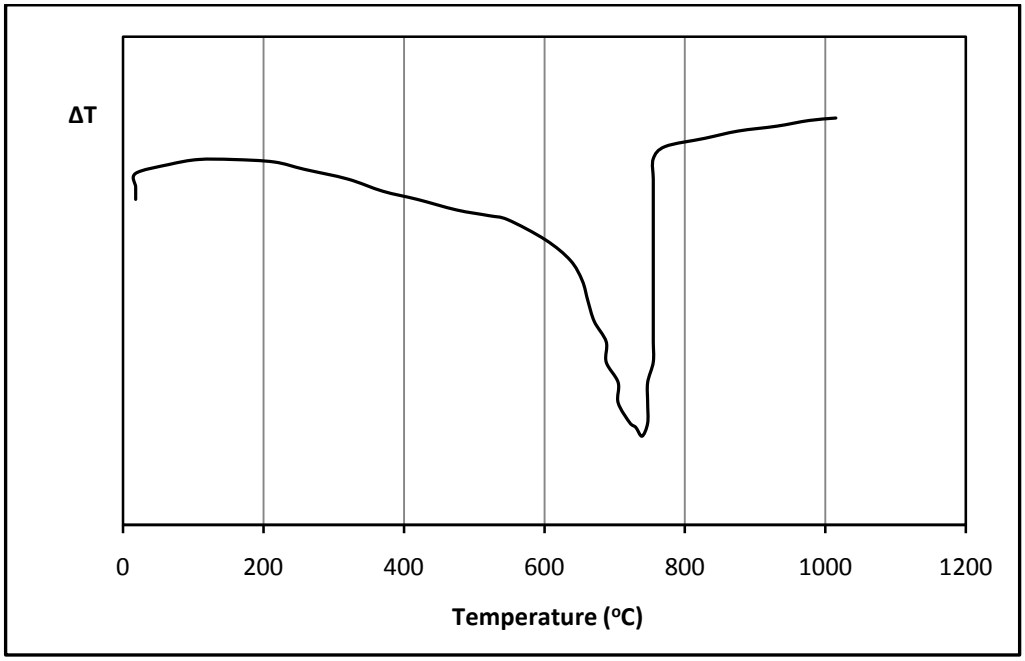

Figure 8.56: DTA curve for limestone (9.1 mg sample, 10^{o}C/min heating rate).

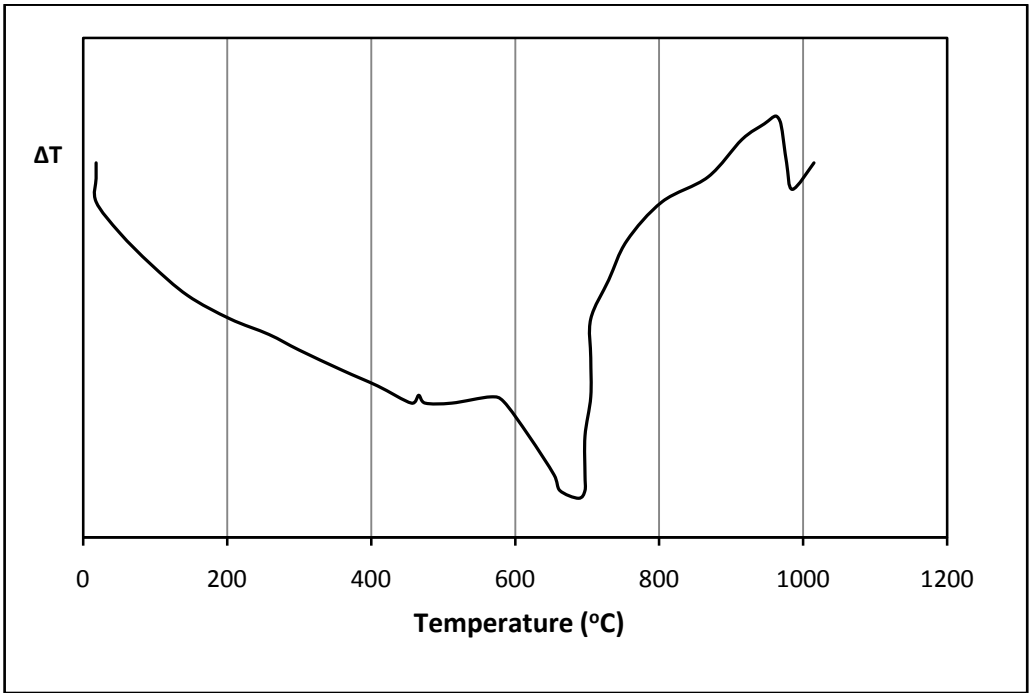

Figure 8.57: DTA curve for mica-limestone (5:1) mixture (9.01 mg sample, 10^{o}C/min heating rate).

Figure 8.58 gives the DTA curves for sodium sulphate (thenardite). The endothermic effect observed between 200^{o}C and 250^{o}C was due to the polymorphic transition of thenardite. Another endothermic effect was observed between 800^{o}C and 900^{o}C due to melting.

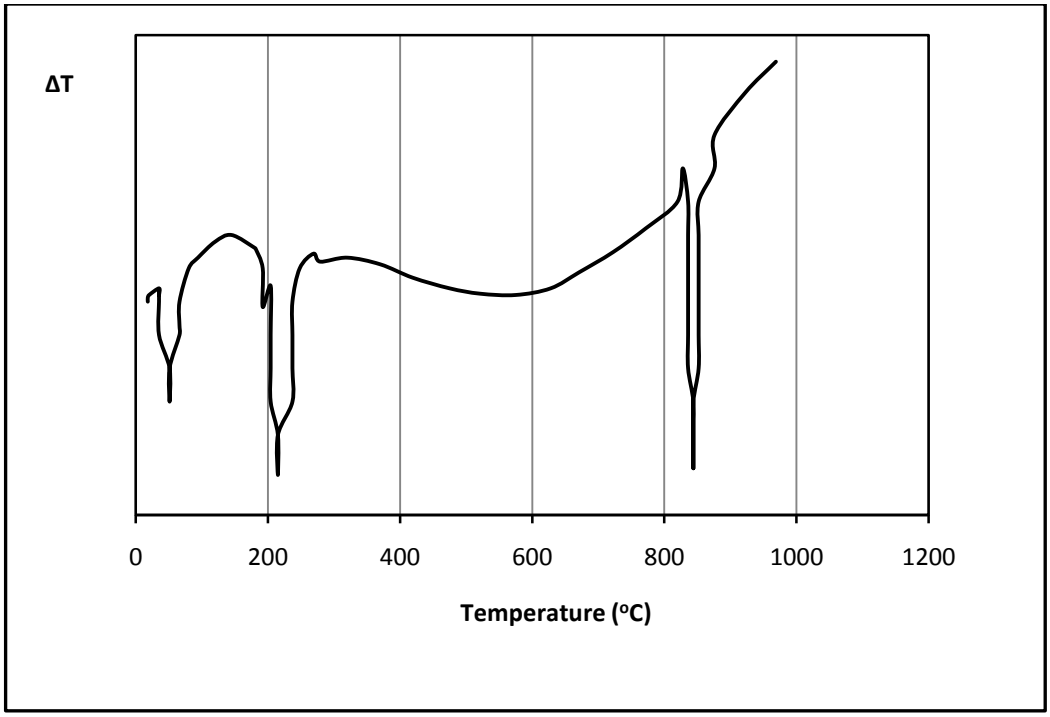

Figure 8.58: DTA curves of sodium sulphate (thenardite) [9.04 mg sample; 10°C/min heating rate]

The DTA curve for paramagnetic mica-sodium sulphate mixture (2:1) is shown in Figure 8.59. Again the endothermic effect at about 200^{o}C was due to the polymorphic transition of thenardite. The melting of thenardite at about 800^{o}C was accompanied by a small endothermic effect. This probably explains why the lithium extraction was higher in mica-sodium sulphate roast-products prepared at 850^{o}C. This is the temperature at which sodium sulphate melts and reacts with mica minerals to form other mineral phases among which were water soluble lithium compounds.

The DTA curve of calcium hydroxide [$Ca(OH)_2$] is given in Figure 8.60. The endothermic effect observed at 400^{o}C was due to dehydration of calcium hydroxide. Figure 8.61 shows the DTA curves for mica-Na_2SO_4-$Ca(OH)_2$ mixture (6:3:1). Again, the endothermic peaks observed between 200^{o}C and 250^{o}C, and at about 400^{o}C were due to the polymorphic transition of sodium sulphate (thenardite) and the dehydration of calcium hydroxide respectively. The endothermic peak close to 800^{o}C was due to the melting of thenardite.

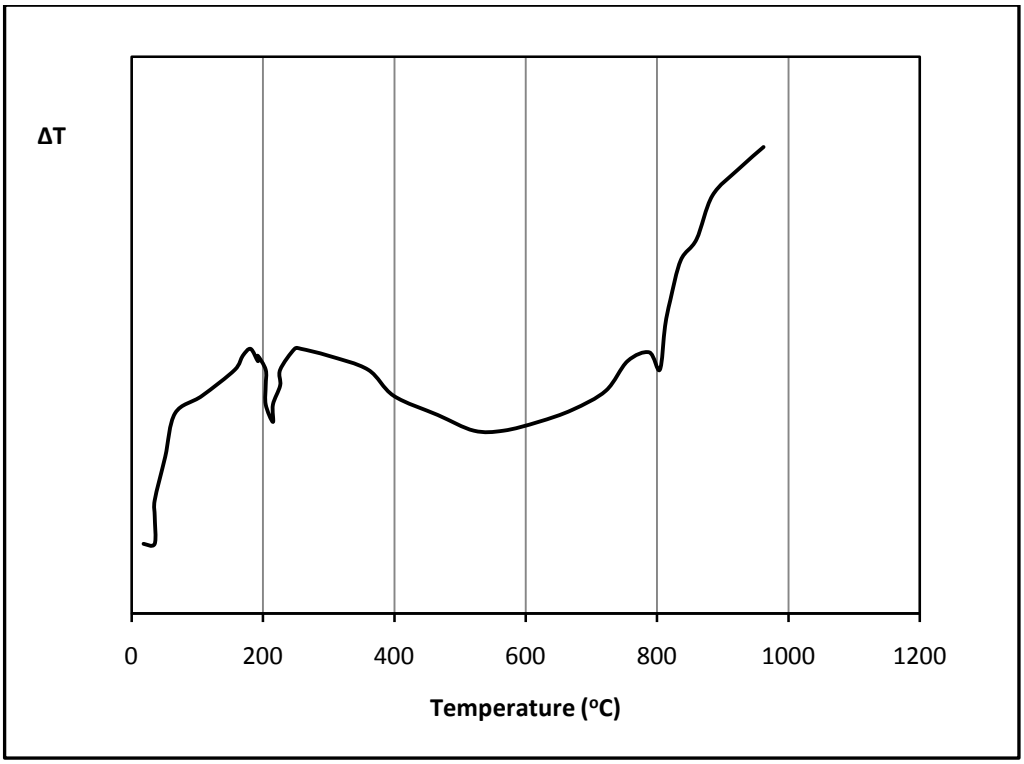

Figure 8.59: DTA curves for mica-sodium sulphate mixture (2:1) [8.99 mg sample; 10°C/min heating rate]

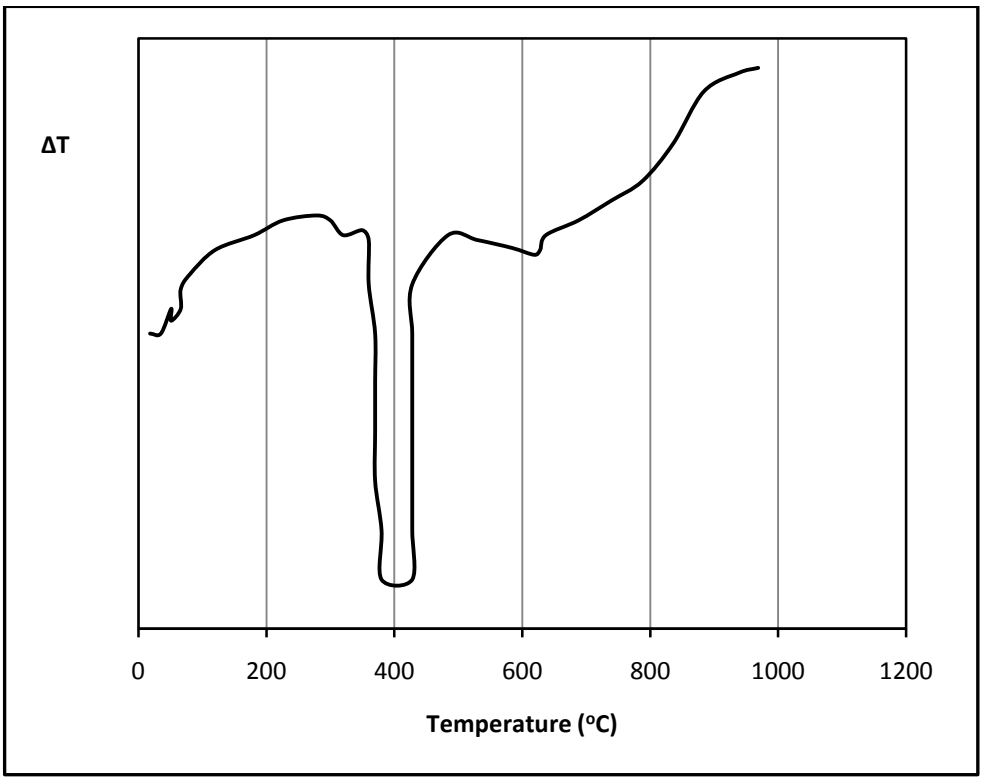

Figure 8.60: DTA curves for calcium hydroxide [9.54 mg sample; 10°C/min heating rate]

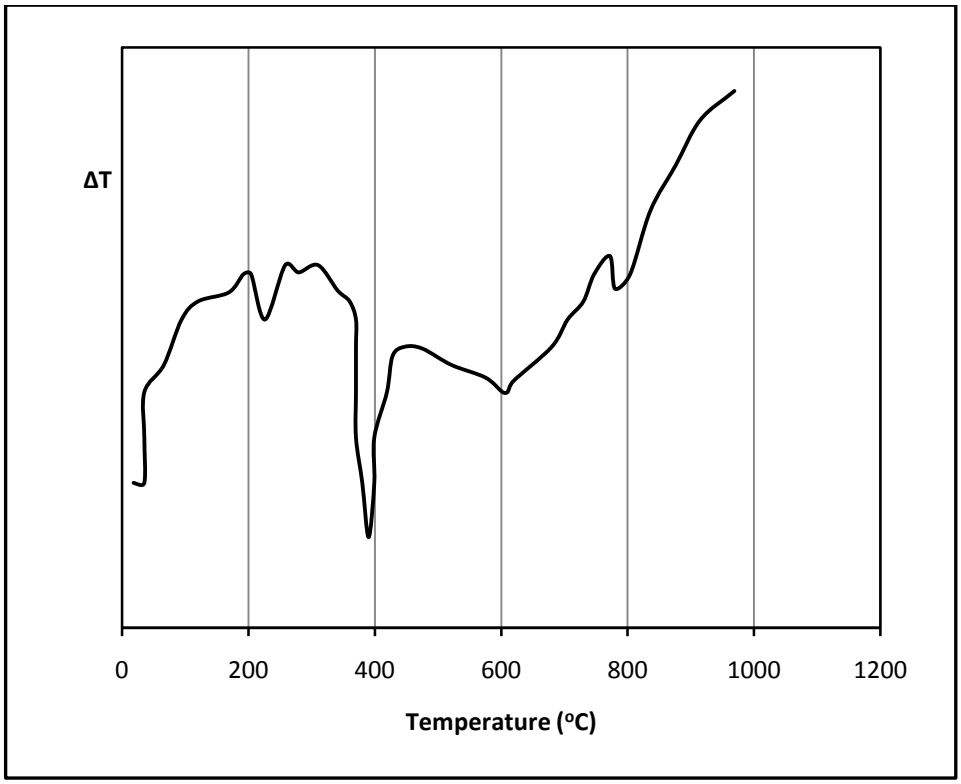

Figure 8.61: DTA curves for mica-Na_2SO_4-$Ca(OH)_2$ mixture (6:3:1) [9.26 mg sample; 10°C/min heating rate].

Figures 8.62 shows the DTA curve for paramagnetic mica-gypsum-$Ca(OH)_2$ mixture (3:2:1). The DTA curve demonstrates the endothermic peaks arising from dehydration. It shows two effects at 94°C and 169°C due to the loss of $1\frac{1}{2}$ molecules H_2O and then $\frac{1}{2}$ molecule H_2O due to the presence of gypsum as explained earlier. The next endothermic peak exhibited at 400°C was again due to the dehydration of calcium hydroxide.

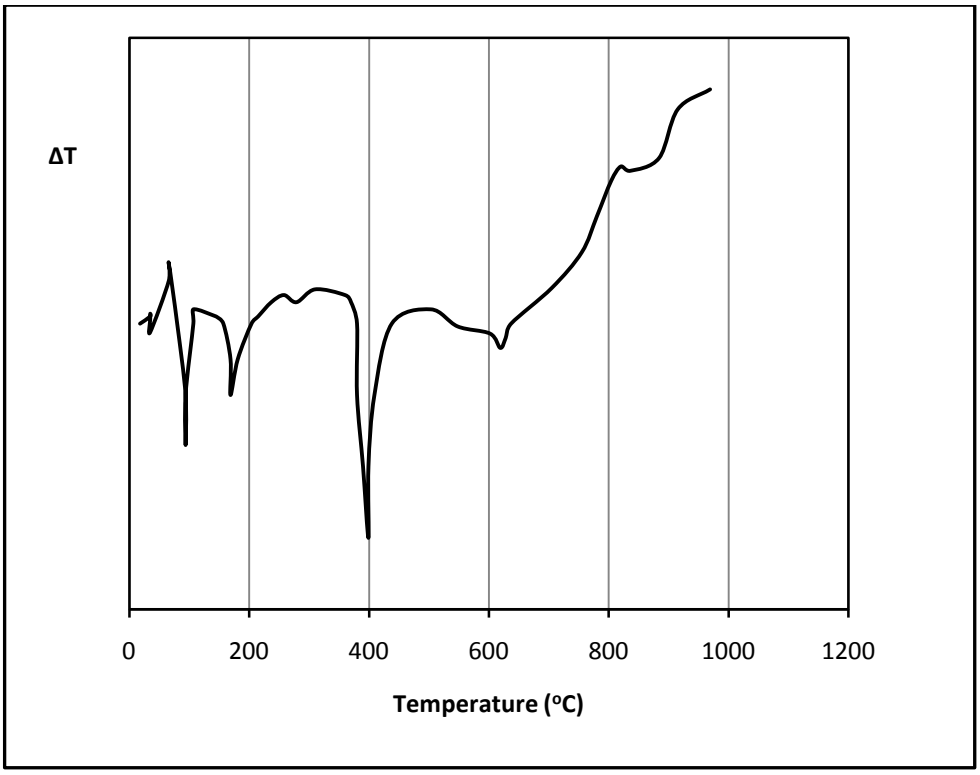

Figure 8.62: DTA curves for mica-gypsum-$Ca(OH)_2$ mixture (3:2:1) [9.56 mg sample; 10°C/min heating rate]

8.7.3 Summary of the TGA and DTA Results

The TGA and DTA analytical results indicated the reactions which resulted from roasting. The loss in weight of the material indicated the loss of volatile species in gaseous form. For example, gypsum loses its molecular water from the crystal when heated above 90°C. The loss of weight in mica was partly due to the loss of H_2O as the material was heated above the temperature at which the hydroxyl group is stable and to the loss of any other volatile species such as fluorine. The DTA has indicated the reason why the water soluble lithium compounds in the sodium sulphate and gypsum sinters were formed only when the materials were heated above 800°C and 900°C respectively. These were the temperatures above which the two compounds decomposed and reacted with the mica minerals to form new mineral species, as evidenced by the presence of endothermic peaks. The study has indicated that structural water and any other volatile species had to be released from the materials before they can react and form new mineral species.

9. ECONOMIC APPRAISAL FOR THE PRODUCTION OF LITHIUM CARBONATE

Before carrying out a preliminary economic feasibility for the production of lithium carbonate, a proposed process flow diagram is given showing the unit operations and materials required.

9.1 Process Flow Diagrams

Flow diagrams are used to show the sequence of equipment and unit operations in the overall process, to simplify visualisation of the manufacturing procedures and to indicate the quantities of materials. These diagrams may be divided into three general types: (1) qualitative, (2) quantitative, and (3) combined-detail. A qualitative flow diagram indicates the flow of materials, unit operations involved, equipment necessary, and special information on operating temperatures and pressures etc., while a quantitative flow diagram shows the quantities of materials required for process operation. Figure 9.1 shows a suggested qualitative flow diagram for the production of lithium carbonate while Figure 9.2 presents a quantitative flow diagram for the same process. The dotted lines in Figure 9.1 indicate bypass routes when the unit operation is not needed.

It must be mentioned that Figures 9.1 and 9.2 are preliminary flow diagrams and thus are subject to modification. As the design proceeds toward completion and the detailed information on flow quantities and equipment specifications become available, then a combined-detail flow diagram can be prepared. This type of diagram shows the qualitative flow pattern and thus serves as a base reference for giving equipment specifications, quantitative data, and sample calculations.

Table 9.1 gives the densities of the materials as determined by the Gas Pycometer (AccuPyc 1330 V3.03). The densities were used in material balances and in determining the capacity of unit processing equipments.

Table 9.1: Densities of flotation and leaching materials (g/cm^3).

Run Number	Flotation Feed	Flotation Concentrate	Magnetic Mica	Gypsum-mica Sinter (1050°C)	Na_2SO_4-mica Sinter (850°C)
1	2.6925	2.8245	2.8807	2.7064	2.6488
2	2.6912	2.8184	2.8752	2.7017	2.6295
3	2.6883	2.8147	2.8731	2.6943	2.6274
Average	**2.6906**	**2.8192**	**2.8763**	**2.7008**	**2.6352**
SD	**0.0022**	**0.0050**	**0.0040**	**0.0061**	**0.0118**

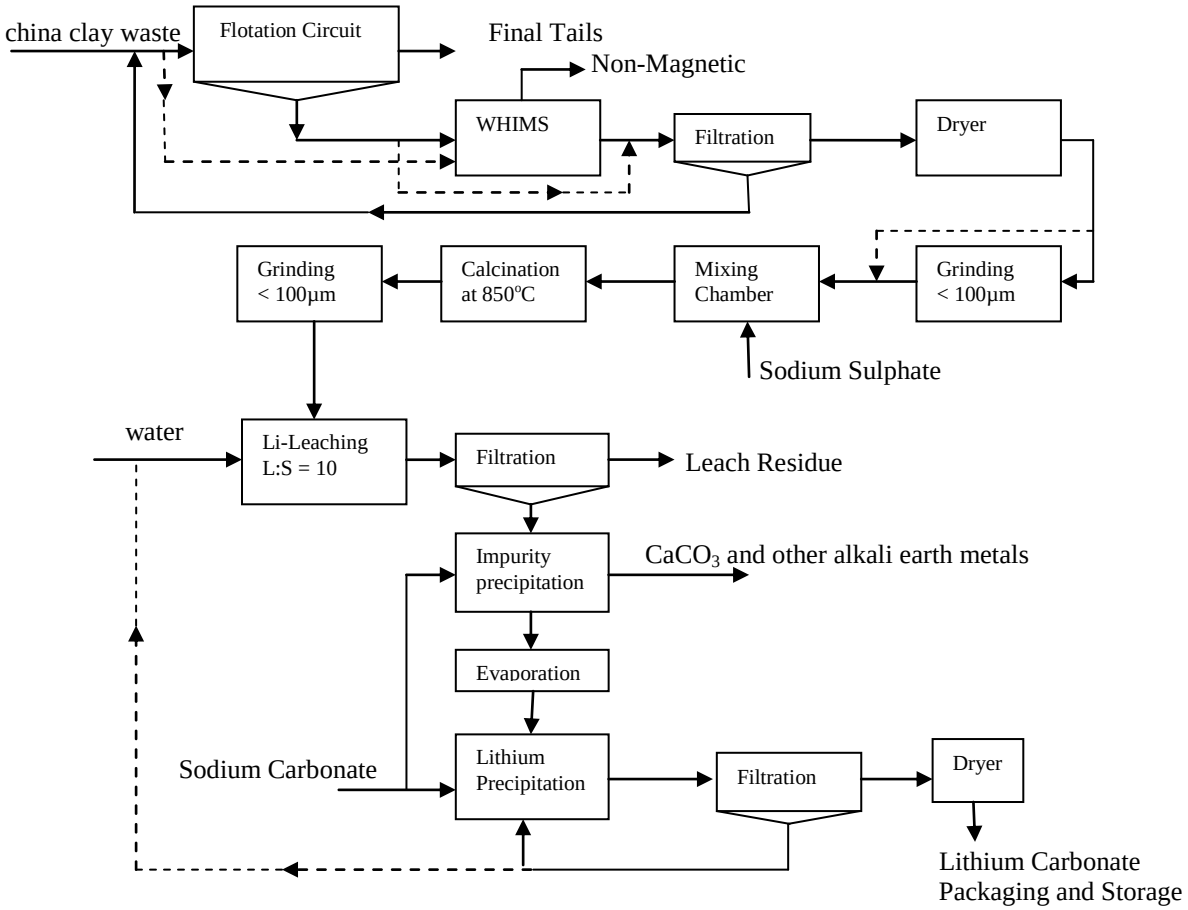

Figure 9.1: Proposed qualitative flow diagram for the production of lithium carbonate by the sodium sulphate method.

Key

——— Main processing route

- - - - - - - - - Bypass route

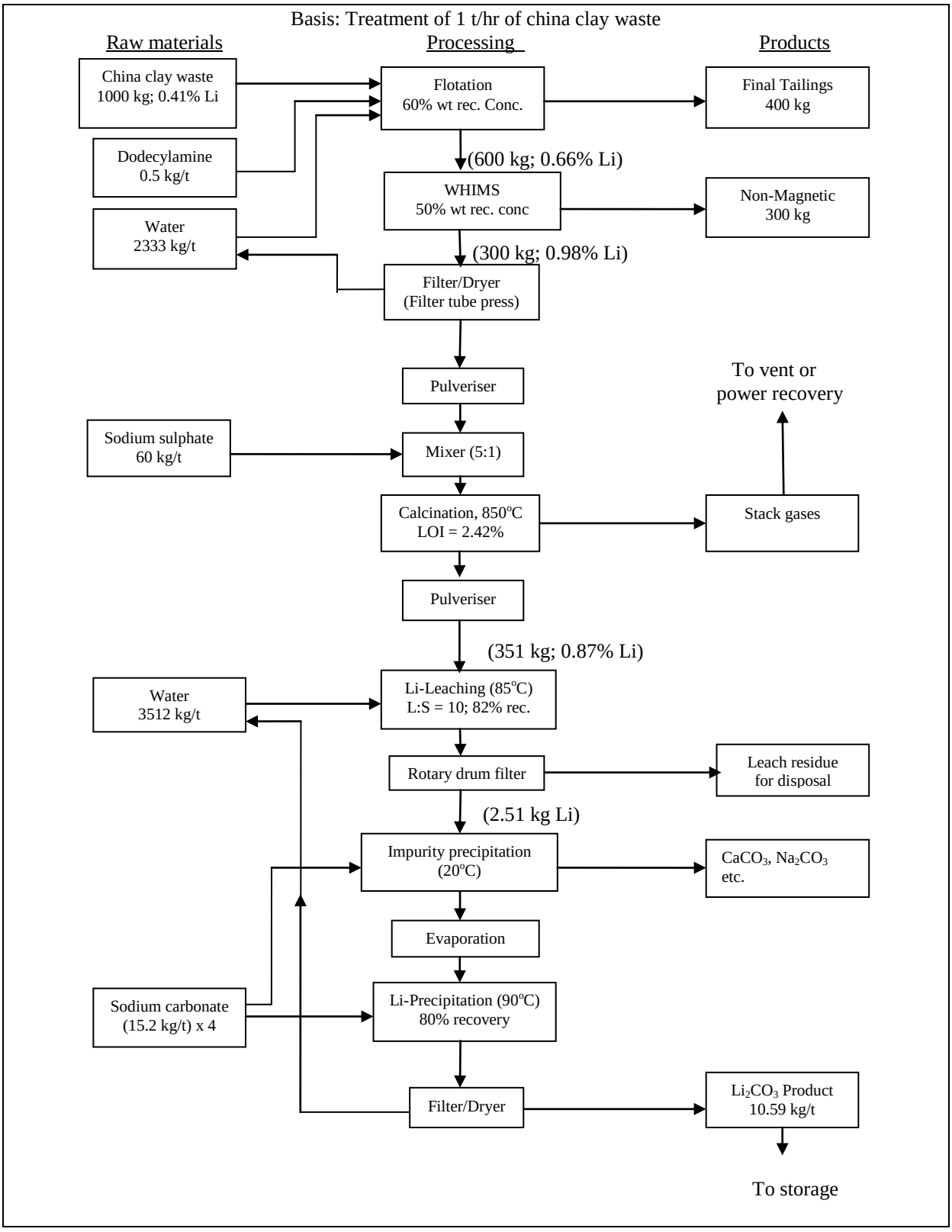

Figure 9.2: Proposed quantitative flow diagram for the production of lithium carbonate by the sodium sulphate method.

9.2 Process Description

As described by Figure 9.1, the primary feed material in the process of lithium carbonate production is the china clay waste. The china clay waste could first be treated by flotation followed by magnetic separation to separate a lithium-rich mica product from the bulk mica concentrate. The material will have to be filtered, dried and ground to more than 80% passing 100 μm before being roasted together with sodium sulphate and calcium hydroxide in the kiln. The roast-products will be pulverised and water leached in a closed tank reactor maintained at 90^{o}C. The leaching time will have to be re-examined in the plant depending on the amount of material to be treated although any time between 30 and 60 minutes will suffice. Laboratory experiments had shown that leaching is almost complete within 10 minutes of commencement of the leaching process. Solid-liquid separations could be achieved by rotary drum filters.

The leach liquor obtained would be contaminated by mainly Ca, Rb and Na, and, as such, the liquor has to be purified before lithium carbonate precipitation. This can be achieved by adding potassium carbonate to the leach liquor at room temperature. After the separation of the impurity as carbonate precipitates, the leach liquor has to be heated to 90^{o}C to increase the lithium concentration by evaporation of H_2O. According to experimental work carried out by Jandova and others (2008, 2009), and in this work, increasing the lithium concentration in solution to at least 9g/l before lithium carbonate precipitation is necessary to achieve an acceptable precipitation efficiency. The precipitated crystals of calcium and potassium sulphates during the evaporation process have to be filtered off and may probably be used to supply the SO_4^{2-} ions in the roasting / calcination process. The purified solution has to be heated to 90^{o}C before lithium carbonate is precipitated by the addition of stoichiometric amount of potassium or sodium carbonate because its solubility decreases with increasing temperature. The precipitated lithium carbonate has to be filtered off, water-washed and dried in an indirect fired rotary dryer. According to Jandova and others (2008, 2009), about 70% lithium carbonate precipitation efficiency could be achieved. They performed experiments with model solutions and found that using stoichiometric excess amounts of potassium carbonate during lithium carbonate precipitation did not result in increased precipitation efficiency.

9.3 Cost Estimation

A plant design obviously must present a process that is capable of operating under conditions which will yield a profit. Since net profit equals total income minus all expenses, it is essential that all the different types of costs involved in the manufacturing process are evaluated. Money must be paid out for direct plant expenses, such as raw materials, labour, and equipment. In addition, many other indirect expenses are incurred, and these must be included if a complete analysis of the total cost is to be obtained. Some examples of these direct expenses are administrative salaries, product-distribution cost etc.

A capital investment is required for any industrial process, and determination of the necessary investment is an important part of a plant-design project. The total investment for any process consists of the fixed-capital investment for the physical equipment and facilities in the plant plus the working capital for money which must be available to pay salaries, keep raw materials and products on hand, and handle other special items requiring a direct cash outlay. Thus, in an analysis of costs in industrial processes, capital-investment costs, manufacturing costs, and general expenses including taxes must be taken into consideration.

On the basis of this case, the cost of mining is covered by the sale of china clay by Goonvean Ltd. The material being treated is regarded as waste and as such only cost incurred in setting up and running the processing plant will be evaluated. Therefore, the produced lithium carbonate only has to cover the costs of processing the china clay waste. Costs for the purchasing and installation of the processing equipment have been estimated based on the process flow sheets designed above. The capital cost is based on information obtained from a Handbook for Estimating Mining and Mineral Processing Equipment Cost and Capital Expenditures and Aiding Mineral Project Evaluations (Mular and Poulin, 1998).

9.3.1 Capital Costs

The capital costs in setting up the processing plant are derived mainly from the purchase of the processing units. The Plant Component Cost Ratio Method was used as elaborated in the Handbook for Estimating Mining and Mineral Processing Equipment Cost and Capital Expenditures and Aiding Mineral Project Evaluations (Mular and Poulin, 1998). This method is said to provide considerable flexibility and involves a breakdown of fixed capital costs into plant components whose costs are a ratio of major equipment costs. These ratios are

sometimes referred to as factors and hence the name factored estimates. The method has been used in chemical engineering for process plants with success. The accuracy of the estimate by this method is $\mp 20\%$ of the determined cost.

In the process of producing lithium carbonate, fluorine will be discharged to the atmosphere. There is need to recover the fluorine to prevent pollution and, thus, the costs of the scrubber or the method given in section 10 for the recovery of fluorine should be included in the actual total capital investment determined in the future.

Equipment costs were estimated from graphs of $(Cost)_{1400}$ versus Cost Parameter of various equipments as contained in the Handbook, where $(Cost)_{1400}$ is the base cost in US dollars. The current Marshall and Swift Cost Index (Mining & Milling) of 1573 (www.che.com, 2010) was employed for updating equipment costs. The costs were estimated in British pounds as follows: First estimated $(Cost)_{now}$ in US dollars from graphs by using the index ratio, $\frac{IndexNow}{1400}$, and then converted to British pounds via the current exchange ratio.

The following assumptions were used to arrive at the expected unit treatment capacity in tonnages:

- A total annual production of 55,000 tonnes of china clay by Goonvean Ltd.
- A ratio of micaceous residues to china clay production of 1:1.
- 365 working days of 24 hours.
- 60% mica recovery by weight at the flotation stage.
- 50% magnetic mica recovery by weight at the WHIMS stage.

Table 9.2 gives the breakdown of the total capital investment for a plant treating 150 t/day of china clay waste. The purchased equipment costs based on an M&S(Mine/Mill) index of 1573 amount to about £1,756,021. The fixed capital cost is estimated as £6,733,542 and the total capital investment is £7,541,567. It should be noted that the working capital is taken as 12 percent of the fixed capital cost. Detailed determination of unit treatment capacity and costs is given in Appendix I.

Table 9.2: Total Capital Investment For a 150 TPD Plant

1. Purchased equipment cost (M&S = 1573).....**£1,756,021**
    - Mica Flotation (eight-0.71 m^3-cell): £65,864
    - WHIMS (6.71kW): £70,514
    - Vertical Plate and Frame Pressure Filters (3): £121,725
    - Rotary Gas Dryers (2): £202,348
    - Rotary Dry Blender: £17,356
    - Direct-fired rotary kiln: £1,184,119
    - Pulveriser (Two-11.19kW): £52,980
    - Leaching (1-open tank mixers): £8,223
    - Evaporator (2-closed tank mixers): £16,446
    - Precipitation (2-closed tank mixers): £16,446
2. Installed equipment costs (1.43 times Item 1) £2,511,110
3. Process piping (20 percent of Item 2) £502,222
4. Instrumentation (8 percent of Item 2) £200,889
5. Building and site development (35 percent of Item 2) £878,889
6. Auxiliaries (5 percent of Item 2) £125,556
7. Outside lines (5 percent of Item 2) £125,556
8. Total physical plant costs (2+3+4+5+6+7) £4,344,220
9. Engineering and construction (25 percent of Item 8) £1,086,055
10. Contingencies (20 percent of Item 8) £868,844
11. Size factor (10 percent of Item 8) £434,422
12. **Fixed Capital Costs** (8+9+10+11) **£6,733,542**
13. **Working Capital** (12 percent of Item 12) **£808,025**
14. **Total Capital Investment** (12+13) **£7,541,567**

9.3.2 Operating Costs

Determination of the necessary capital investment is only one part of a complete cost estimate. The estimation of costs for operating the plant and selling the products is another equally important part. These costs can be grouped under the general heading of total product cost, which is generally divided into the categories of manufacturing costs and general expenses. Manufacturing costs are also known as operating or production costs.

The total product costs are commonly calculated on one of three bases: namely, daily basis, unit-of-product basis, or annual basis. It has been reported that the annual cost basis is probably the best for estimation of total product cost and will be used in this analysis. The advantages are that the effect of seasonal variations is smoothed out and plant on-stream time or equipment-operating factor is considered.

All expenses directly connected with the manufacturing operation or the physical equipment of a process plant itself are included in the manufacturing costs. These expenses are divided into three classifications as follows: (a) direct production costs, (b) fixed charges, and (c) plant-overhead costs. The direct production costs would include expenses directly connected with the manufacturing operation such as expenditures for raw materials, power and clerical labour etc. The amount of raw materials which would be supplied per unit of product would be determined from the process material balances. The operating labour may be divided into the two classes of skilled and unskilled labour. Fixed charges include cost for depreciation, local taxes, insurance, and rent while plant-overhead costs may include hospital and medical services, safety and general plant maintenance. The fixed charges may be taken as 10-20% of the total product cost while the plant-overhead cost may be taken as 50 to 70 percent of cost for operating labour.

In this analysis, only the costs of raw materials, energy and labour would be considered for simplicity. The industrial electricity price of £0.1077/ kWh was obtained from the UK Trade and Investment web site (www.ukti.gov.uk, 2010), while the wage rate of £8.87 for a labourer employed permanently at the shop was obtained from the Joint Industrial Board web site (www.jib.org.uk, 2010). The process considered here would involve flotation, magnetic separation and leaching therefore would assume unskilled labour manning these unit processes. The operating labour was estimated from an analysis of the work to be done based

on the flow sheet of the process provided. A total of 6 personnel would be required for the entire process and the total operating cost of the plant was based on 80% plant availability operating. Figure 9.2 above gives the proposed quantitative flow diagram for lithium carbonate production by the so called sodium sulphate method. Due to lack of information on the operating cost of the process units, the following are taken into consideration:

- 365 working days of 24 hours.
- 80% plant availability.
- 70% overhead on the salary.
- A staff of 6 persons costing £53.22/hour excluding 70% overhead.
- Fixed operating cost of £60/hour for the kiln.
- Sodium carbonate, sodium sulphate and lithium carbonate prices of £161.06, £74.28 and £3,484 respectively.
- A total annual production of 55,000 tonnes of china clay by Goonvean Ltd.
- Magnetic mica to sodium sulphate ratio of 5:1.

The amount of lithium carbonate produced would be dependent on the amount of china clay waste treated and this has a direct bearing on the amount and cost of collector (dodecylamine), sodium sulphate, calcium hydroxide and sodium carbonate consumed in the process. According to Figure 9.2, 10.59 kg of lithium carbonate could be produced per tonne of china clay waste treated and that 60 kg of sodium sulphate would be consumed. The consumption of sodium carbonate was determined based on the following reaction:

$$Na_2CO_3 + Li_2SO_4 = Na_2SO_4 + Li_2CO_3 \quad (9.1)$$

Thus based upon this reaction about 15.17 kg of sodium carbonate would be required to produce 10.59 kg of lithium carbonate. This amount was multiplied by 4 to allow for the precipitation of other alkali earth metals. Therefore about 61 kg of sodium carbonate per tonne of china clay waste would be required. This was just an estimate which can be changed in actual plant trials. The prices of sodium carbonate and lithium carbonate are those reported in the January 2010 Industrial Minerals issue. The following exchange rate was used: 1 British pound = 1.5212 U.S. dollars. The estimated operating costs for the lithium carbonate production process are given in Table 9.3.

9.3.3 Revenue

Goonvean Ltd produces about 90,000-100,000 tonnes per year of china clay. Since the china clay to micaceous waste production ratio is 1:1, it produces the same amount in terms of china clay waste. Assuming the treatment of about 55000 tonnes per year of china clay waste, this would translate into the production of about 646 tonnes of lithium carbonate per year resulting into an annual income of about £2,250,664 ($3,423,800).

Table 9.3: Operating costs for the lithium carbonate production

Stage	Equipment	Rated		Units needed	Other Cost (£/h)	Total operation cost (£)
		kW	Cost (£/kWh)			
Flotation	Flotation cells			8		
	Electric motors	1.49	0.1077	8	-	8,997
	Centrifugal pump	2.24	0.1077	2		3,381
Magnetic separation	WHIMS	6.71	0.1077	1		5,064
	Centrifugal pump	2.24	0.1077	1	-	1,691
Filtration	Vertical plate and frame pressure filter	-	-	1	0.70	4,906
Drying	Rotary gas dryers					
	Electric motor	2.24	0.1077	2	-	3,381
Blending	Rotary dry blender					
	Electric motor	2.24	0.1077	1	-	3,381
Calcination	Directly-fired rotary kiln	-	-	1	60	420,480
grinding	Pulveriser	11.19	0.1077	2		16,892
	Electric motor	2.24	0.1077	1	-	1,691
Leaching	Closed tank mixer			1		
	Electric motor	2.24	0.1077	1	-	1,691
	Centrifugal pump	2.24	0.1077	1		1,691
Filtration	Vertical plate and frame pressure filter	-	-	1	0.70	4,906
Evaporation	Closed tank mixer			2		
	Electric motor	2.24	0.1077	2	-	3.381
	Centrifugal pump	2.24	0.1077	2		3,381
Precipitation	Closed tank mixer			2		
	Electric motor	1.49	0.1077	2	-	2,249
	Centrifugal pump	2.24	0.1077	2		3,381
Filtration	Vertical plate and frame pressure filter	-	-	1	0.70	4906
Others	Staff			6 persons	8.87	155,402
Raw materials	Na_2CO_3	£161.06/t		3355t		451,773
	Na_2SO_4	£74.28/t	-	5500t	-	408,540
Plant-overhead costs	-	-	-	70% of labour cost	-	108,782
Total operating costs						**£1,708,530**

9.4 Evaluating the Project Profitability

It is said that total profit alone cannot be used as the deciding profitability factor in determining if an investment should be made. The profit goal of a company is to maximise income above the cost of the capital which must be invested to generate the income. The rate of return, rather than the total amount of profit is the important profitability factor among others, in determining if the investment should be made. The yearly profit divided by the total initial investment necessary represents the fractional return, and this fraction times 100 is the standard percent return on investment. The profit is defined as the difference between income and expense. It must be realised that the amount of profit is affected by the economic efficiency of the operation, and increased profits could be obtained by use of effective methods which reduce operating expenses. To determine the profit, estimates must be made of direct production costs, plant overhead costs, fixed charges, and general expenses. The profits may be expressed on a before-tax or after-tax basis, but the conditions should be indicated. Both working capital and fixed capital should be considered in determining the total investment.

The proposed lithium carbonate production requires an initial fixed-capital investment of £6,733,542 and £808,025 of working capital. It has been estimated that the annual income would be £2,250,664 and the annual operating cost would be £1,708,530 before income taxes. Considering an income tax of 30%:

1. The annual percent return on the total investment before income tax:
   Annual profit before income taxes = £2,250,664 – £1,708,530 = £542,134.
   Annual percent return on the total initial investment before income tax = [542,134/(6,733,542 + 808,025)](100) = **7.2%**

2. The annual percent return on the total investment after income tax:
   Annual profit after income tax = (£542,134)(0.7) = £379,494.
   Annual percent return on the total initial investment after income tax = [379,494/(6,733,542 + 808,025)](100) = **5.0%**

3. The annual percent return on the average investment before income tax assuming straight-line depreciation and zero salvage value:

The average investment assuming straight-line depreciation and zero salvage value = £6,733,542 / 2 + £808,025 = £4,174,796.

Annual percent return on average investment before income tax = (542,134/4,174,796)(100) = **13.0%**

Although the annual rate of return on the investment is low, the demand for lithium carbonate and reduction in operation costs especially if the magnetic separation is bypassed could probably make this a worthwhile investment to make in the future. The other determining factor is the selling price of lithium carbonate: a higher selling price could mean a higher rate of return on the investment. The major contributions to the operating costs are the kiln and raw materials. Others are from the pulveriser, flotation and magnetic separation apart from the salaries for the operating personnel. The cost of sodium sulphate could probably be low as some could be recovered during the lithium carbonate precipitation and recycled to the roasting process. Furthermore, actual quotes from similar operating plants could probably bring the annual operating costs down and would make the investment attractive.

10. LIFE CYCLE ASSESSMENT – ENVIRONMENTAL ISSUES

Life Cycle Assessment (LCA) is a tool for assessing the environmental impacts of a product, process or service from design to disposal i.e. across its entire lifecycle, a so called cradle to grave approach. The impacts may be beneficial or adverse. These impacts are sometimes referred to as the "environmental footprint" of a product or service.

The major environmental problems associated with any pyrometallurgical process come from gases and particulate solids while those associated with hydrometallurgical processes are from waste liquors and unwanted solid products. Reactions involving gases play a major role in pyrometallurgical processes and an inevitable consequence of these methods is the production of harmful vapours and fine air-borne particles. Dust and smoke which are solid particles are distinguished from fog, which is composed of liquid droplets formed by condensation or chemical reaction. Just like in any hydrometallurgical processes, the disposal of solid leach or treatment residues can present problems, since leaching reactions may continue within the materials by reaction with natural waters.

Although the china clay wastes pose an environmental risk as they are dumped, reprocessing them to recover lithium and other by products will only mitigate the risk to a certain extent. During roasting, fluorine from the mica concentrate will be released to the atmosphere, posing another environmental threat. The advantage of the leaching process is that it will be performed in water thus, eliminating the use of acids. The disposal of solid leach or treatment residues should be treated with caution because the long term stability of the solids is a problem which must be seriously considered. Aqueous waste solutions also present problems. Solutions containing metals in particular should be handled with care. Although the concentrations of elements in the discharge solutions may be low, these elements can become concentrated in the food chains of animals and fish. Thus a comprehensive environmental impact assessment should be carried out before large scale lithium carbonate production could commence.

Fluorine from stack gases may be recovered by a process of passing the stack gases in a bed of lump limestone at temperatures above the dew point of the stack gases (Hignett and Siegel, 1949). The calcium fluoride reaction product separates from the limestone lumps in the form

of fines. The portions of the bed are withdrawn from the tower at intervals, screened to remove the fines, and the oversize (partially reacted limestone) is recycled to the tower together with fresh make-up limestone. According to Hignett and Siegel (1949), the product contains about 80-95% CaF, which is comparable in grade to commercial fluorspar. This process is expected to reduce drastically the amount of fluorine discharged directly to the atmosphere. The product could probably be sold to industries producing hydrofluoric acid and other related fluorine containing products.

11. DISCUSSION

11.1 Flotation Process

Mica minerals can be successfully separated from china clay waste by flotation with or without the addition of frother in the pH range 2.5-5.5, with dodecylamine as collector at a dosage of 500g/t. The collector dosage can be drastically reduced from 500g/t to 300g/t when added in six stages during the mica flotation process. The average flotation recovery and grade of Fe_2O_3 in the concentrates was 93.6% and 4.2% respectively. The flotation concentrates contained about 1.43% Li_2O and 0.52% Rb_2O while the tailings assayed 0.03% Li_2O and 0.14% Rb_2O, giving a recovery on average of 98.87% and 87.21% respectively.

The statistical analysis performed on the flotation results suggests that all the variables studied (impeller speed, aeration rate and frother dosage) and their respective combination did not significantly affect the recovery and grade of mica minerals. Another statistical analysis performed on the flotation results suggests that collector dosage had a greater effect on both recovery and grade of the concentrates than the pH over the ranges studied.

11.2 Magnetic Separation Process

The lithium-rich mica minerals could be separated from the bulk mica concentrate by using the wet high intensity magnetic separator. The recovery and grades of Li_2O, Rb_2O and Fe_2O_3 at 1.95 Tesla were 73.4%, 66.9%, 76.7% and 2.1%, 0.7%, 7.4% respectively. Furthermore, the size by size recovery of Li_2O, Rb_2O and Fe_2O_3 obtained as diluents in the magnetic product indicated that a material of varying particle size distribution could be successfully treated at a magnetic field strength of 1.95 Tesla.

During magnetic separation most of the zinnwaldite reported to the magnetic fraction while most of the muscovite reported to the non-magnetic fraction although a substantial amount was present in the magnetic fraction probably due to the presence of iron. Microprobe analysis has indicated the presence of zinnwaldite and muscovite in both the magnetic and non-magnetic fraction and this shows that the magnetic separation may probably not be the best option to upgrade the lithium mica. The reason for this phenomenon, according to Hawkes et al. (1987), is that the composition fields in which the St Austell micas lie tend to overlap. Hawkes et al. (1987) reported two overlapping fields for muscovite resulting from

alteration of either biotite or lithian mica (zinnwaldite, lepidolite, polylithionite etc.) and that these muscovites tended to be less rich in iron.

11.3 Lithium Extraction by Roasting and Leaching.

11.3.1 The Gypsum Method

The leaching results obtained from this study have shown that it is possible to extract about 84% of lithium into solution when the zinnwaldite concentrate was reacted with gypsum at 1050^{o}C. Generally, rubidium extraction was very low at less than 20%. The leaching kinetics indicated that the lithium extraction was almost completed within 10 minutes. The XRD analysis showed that the water soluble lithium species in the gypsum roast-products was potassium lithium sulphate [$KLiSO_4$]. Increasing the zinnwaldite concentrate to gypsum ratio from 2:1 to 10:1 resulted in a gradual decrease in lithium extraction whilst increasing the leaching temperature from 20^{o}C to 85^{o}C resulted in an increased lithium extraction rate. Leaching the mica cleaner concentrate roasted with gypsum showed that only about 62% of lithium extraction efficiency could be achieved.

In lithium extraction by the gypsum method reported by Jandova and others (2008, 2009), zinnwaldite concentrate was roasted at temperatures ranging from 900 to 975 together with gypsum and calcium hydroxide in the ratio 6:4.2:2 and achieved about 96% and 25% lithium and rubidium extraction respectively. The lithium extraction by the gypsum method reported above did not include calcium hydroxide and, therefore, it was decided to include it in the concentrate before being roasted at temperatures ranging from 900 to 975^{o}C. The results showed that 88% lithium and 44% rubidium extraction efficiencies could be achieved if the roasting was carried out at and above 950^{o}C. This rubidium extraction efficiency was much higher than that reported by Jandova et al. (2008, 2009) and the one achieved without the addition of lime as reported above. Thus the addition of calcium hydroxide to the concentrate did not only increase the extraction efficiency but also decreased the roasting temperature. Thus comparing these results to those obtained by Jandova et al. (2008, 2009), it can be concluded that the gypsum method gave slightly lower lithium extraction efficiency and at a higher roasting temperature.

11.3.2 The Limestone Method

The limestone lithium extraction method gave poor results, indicating that the lithium compounds formed during roasting were not water soluble. XRD analysis of the roasting-product identified the lithium phase as pseudo-eucryptite, which is sparingly water soluble. Further tests with this method were discontinued.

11.3.3 The Sodium Sulphate Method

The results from this study indicated that it was possible to extract about 90% of lithium into solution when the zinnwaldite concentrate was roasted with sodium sulphate at 850^{o}C. The rubidium extraction was much lower at 13%. The dissolution kinetics showed that the lithium extraction was almost complete within 10 minutes. Increasing the zinnwaldite concentrate to sodium sulphate ratio from 2:1 to 7:1 resulted in a gradual decrease of lithium extraction efficiency. The XRD analysis of the sodium sulphate roast-products showed that the water soluble lithium species was lithium potassium sodium sulphate [$Li_2KNa(SO_4)_2$].

The main advantages of the sodium sulphate method, which was the new route of lithium extraction tried in this study, were the increase in lithium extraction in solution to more than 90% and the reduction in the roasting temperature to 850^{o}C. Furthermore, the concentrate could be increased up to five times the amount of sodium sulphate while still achieve 84% lithium extraction efficiency. The stoichiometric calculation had indicated that the ratio 5:1 of paramagnetic mica to sodium sulphate was the maximum which could provide the necessary sulphate ions required to convert the lithium contained in the mica to a water soluble lithium compound during the calcination process. Additionally, upgrading the lithium content in the flotation concentrate by wet high intensity magnetic separation before roasting and leaching may not be necessary with the sodium sulphate method. Leaching the mica cleaner concentrate roasted with sodium sulphate gave a lithium extraction efficiency of about 80%.

Thus comparing these results to those obtained by Jandova et al. (2008, 2009), it can be concluded that the sodium sulphate method gives similar lithium extraction efficiency but at a lower roasting temperature.

11.3.4 Recovery of Lithium Carbonate from Leach Solution

The sodium sulphate sinters with a sinter ratio of 5:1 (paramagnetic mica to sodium sulphate) were leached at 85^{o}C co-currently in order to increase the lithium concentration in solution to 9 g/l. According to Jandova et al. (2009) increasing the lithium concentration in solution to at least 9 g/l is necessary to achieve acceptable lithium carbonate precipitation efficiency. Lithium was recovered from the concentrated sulphate leach solution by precipitation as lithium carbonate with Li_2CO_3 content of about 90% using sodium carbonate. Only about 30% lithium carbonate precipitation efficiency was achieved. The lithium carbonate obtained with Li_2CO_3 content of about 90% is still suitable for use in the glass and ceramic industries, and as feedstock for the production of other high-purity lithium compounds, although more work is required to reach the industrial target of >99%.

11.4 Thermal Analysis of Leaching Materials

Thermal analysis of the leaching materials such as differential thermal analysis (DTA) has indicated the reason why the water soluble lithium compounds in the sodium sulphate and gypsum sinters were formed only when the samples were heated above 800^{o}C and 900^{o}C respectively. These were temperatures above which the two compounds decomposed and reacted with the mica minerals to form new mineral species. This process was evidenced by the presence of endothermic peaks in the DTA curves at these temperatures.

11.5 Economic Analysis of the Lithium Carbonate Production Process

The proposed lithium carbonate production requires an initial fixed-capital investment of £6,733,542 and £808,025 of working capital. The estimated annual income would be £2,250,664 and the annual operating cost would be £1,708,530 before taxes. The annual rate of return on the investment before and after tax has been determined as 7.2% and 5.0 % respectively. The estimated annual income is dependent on the selling price of lithium carbonate. Although the annual rate of return on the investment is low, the demand for lithium carbonate and reduction in operation costs, especially if the magnetic separation is bypassed could probably make this a worthwhile investment to make in the future.

12. CONCLUSIONS

This study has demonstrated that it is possible to recover lithium from the Goonvean's china clay waste through flotation, magnetic separation, roasting with sulphates followed by leaching. Thus based on the experimental results, the following conclusions are drawn:

- The china clay waste contained the following minerals in order of increasing abundance: muscovite, zinnwaldite, K-feldspar, quartz and kaolinite while accessory minerals were apatite and topaz.

- Mica concentrate containing 1.43% Li_2O and 0.52% Rb_2O with the corresponding recovery of 98% and 85% could be successfully separated from china clay waste assaying 0.84% Li_2O and 0.36% Rb_2O by flotation using dodecylamine as collector at a dosage of 500 g/t.

- The collector dosage could be drastically reduced from 500 g/t to 300 g/t when added in six stages during the mica flotation process.

- A statistical analysis performed on the flotation results suggested that collector dosage had a greater effect on both the recovery and grade of the concentrates than the pH over the ranges studied.

- The predominant minerals in the flotation concentrate were muscovite, zinnwaldite and kaolinite while the tailings contained quartz and K-feldspar as the main minerals.

- The size by assay analysis of the mica concentrate indicated that a product with Li_2O content of approximately 3% could be produced from the coarser mica fraction.

- Further upgrading of the concentrate might be possible using a wet high intensity magnetic separator to produce a magnetic fraction containing 2.07% Li_2O, 0.74% Rb_2O and 7.4% Fe_2O_3, with a recovery of 73%, 67% and 77% respectively.

- Zinnwaldite and muscovite were identified as the predominant minerals in the magnetic and non-magnetic fractions respectively.

- Microprobe analysis of the individual mica grains showed that lithium is drawn mainly from zinnwaldite (3.88% Li_2O) and a lesser to minor amounts being contributed by muscovite (0.13% Li_2O).

- It would be possible to extract about 84 and 90% of lithium into solution when the zinnwaldite concentrate is roasted with gypsum and sodium sulphate at 1050^oC and 850^oC respectively. Rubidium extraction would be much lower at 14 and 23% respectively.

- Roasting the zinnwaldite concentrate with limestone did not produce better lithium and rubidium extraction results as those obtained by Jandova et al. (2009). XRD

analysis of the roast-product indentified pseudo-eucryptite as the lithium-containing species, which is sparingly water soluble.

- Dissolution kinetics indicated that the lithium extraction was almost complete within 10 minutes in both the gypsum and sodium sulphate roast-products.

- The XRD analysis of the gypsum- and sodium sulphate-roasting products identified the water-soluble lithium species as $KLiSO_4$ and $Li_2KNa(SO_4)_2$ respectively.

- DTA analysis indicated the temperature at which the water-soluble species formed with an endothermic peak, and for the gypsum- and sodium sulphate-roasting methods, this occurred at 900^oC and 800^oC respectively.

- Lithium could be recovered from the concentrated leach solution by precipitation as a carbonate with Li_2CO_3 content of >90%.

- The sodium sulphate method offers a promising way of extracting lithium from mica by roasting and leaching.

- Precautions would have to be taken against the emission of fluorine during the roasting process. The TGA results indicated loss of weight of materials during heating probably due to the emission of fluorine, H_2O and other volatile matter.

- The economic analysis of the proposed lithium carbonate production plant has indicated the annual rate of return on the investment before and after tax of 7.2% and 5.0% respectively.

- The St Austell lithium mica indeed represents a strategic and potential source of lithium. When the current cheaper sources of lithium from brines start to dwindle, coupled with the increase in demand for lithium, there is no doubt that lithium recovery from other sources such as the Goonvean china clay waste explored in this research would be an alternative.

13. RECOMMENDATIONS FOR FUTURE WORK

- Other methods of recovering lithium from the mother leach solution after precipitation such as ion exchange should be tried in future.

- Further precipitation experiments should focus on increasing the recovery and purity of lithium carbonate precipitate (>99%) using stage wise evaporation of leach solution and impurity precipitation.

- Leaching experiments should be scaled-up with larger samples in order to increase the lithium concentration in solution to acceptable levels before the precipitation process.

- The effect of using crude gypsum in the roasting process on lithium and rubidium extraction efficiency should be tested. The cost of crude gypsum is cheaper than the other materials tested in this research.

- Lithium extraction should be concentrated on the coarser sized mica fraction. The size by assay analysis of lithium, rubidium and iron oxides in the mica concentrate increased from finer to coarser size fractions.

REFERENCES

Alderton, D.H.M. 1990. *Mineralisation associated with the Cornubian granite batholiths.* In: Pattrick R.A.D. & Polya D.A. (Eds) Mineralisation in the British Isles. Chapman and Hall, London, pp. 270-354.

Alex, P., Suri, A.K. 1996. *Processing of low grade zinnwaldite (lithium-mica) concentrate*. In: Light Metals, ed. W. Hale (Warrendale, PA: TMS), pp. 1165-1168.

Asmatulu, R. 2002. *Removal of the Discolouring Contaminants of an East Georgia Kaolin Clay and its Dewatering.* In: Turkish J. Eng. Env. Sci., Vol. 26, pp. 447-453.

Atomic absorption spectroscopy; Wikipedia; http://en.wikipedia.org/wiki/Atomic_absorption_spectroscopy; accessed on 13th December, 2010, 14:00.

Bacon, F.C. 1987. *Froth flotation treatment of clay.* Pat. Spec. (Aust.) A.U. 567, 110 (C BO3 DI/02), 12 November 1987. US Appl., 25 August 1982, pp. 411-587.

Banks, M.K., McDaniel W.T. and Sales P.N. 1953. *A Method for Concentration of North Carolina Spodumene Ores*. Mining Engineering, vol. 5, 2, pp. 181-186.

Basilio, C. I. 1997. *Recent Advances in the Processing of Kaolin.* Thiele Kaolin Company, special presentation at Virginia Tech.

Bayat, O., Arslan, V., Cebeci, Y., 2006. *Combined application of different collectors in the flotation concentration of Turkish feldspars*. Minerals Engineering 19, pp. 98-101.

Bayraktar, I., Ersayin, S. and Gulsoy, O.Y. 1997. *Upgrading titanium bearing Na-feldspar by flotation using sulphonates, succinamate and soaps of vegetable oils.* Minerals Engineering, Vol. 1, No. 12, pp. 1363-1374.

Bayraktar, I., Ersayin, S. and Gulsoy, O.Y. 1998. *Magnetic separation and flotation of albite ore.* In: Atak S., Onal G., Celik M.S. (Eds.), Proc. 7th International Mineral Processing Symposium, Turkey, pp. 315-318.

Berg, L.G. 1970. Simple salts. In: *Differential thermal analysis* (ed. R.C. Mackenzie), Fundamental Aspects, Vol. 1, pp. 343-359.

Bhadeshia, H.K.D.H. "*Thermal analyses techniques. Differential thermal analysis*". University of Cambridge, Material Science and Metallurgy. www.msm.cam.ac.uk/phase-trans/2002/Thermal1.pdf; accessed on 10th August, 2009, 10:25.

Billimoria, B.M. 1984. *Beneficiation of china clay by froth flotation.* Braz. Pedide Pedido P1 BR, 8307: pp. 515.

Bish, L.D., Duffy, C.J. 1990. *Thermogravimetric analysis of minerals*. In: cms workshop lectures, Thermal Analysis in Clay Science, vol. 3, pp. 96-157.

Botula, J., Rucky, P., Repka, V. 2005. *Extraction of zinnwaldite from mining and processing wastes*. Technical University of Ostrava – geologicka Volume LI, No. 2, pp. 9-16.

Celik, M.S., Can, I. and Eren, R.H. 1998. *Removal of titanium impurities from feldspar ores by new flotation collectors.* Minerals Engineering, Vol. 11, No. 12, pp. 1201-1208.

Celik, M.S., Pehlivanoglu, B., Aslanbas, A. and Asmatulu, R. 2001. *Flotation of coloured impurities from feldspar ores.* Minerals & Metallurgical Processing 18 (2), pp. 101-105.

Chemical Engineering – Chemical processing intelligence for Chemical Engineers; www.chem.com/; accessed on 5th February, 2010, 14:00.

Cho, Y.S., Laskowski, J.S., 2002. *Effect of flotation frothers on bubble size and foam stability*. Int. J. Min. Process., 64 (2-3), pp. 69-80.

Christie, T., Brathwaite, B. 2008. *Mineral Commodity Report 19 – Beryllium, Gallium, Lithium, Magnesium, Uranium and Zirconium*. Institute of Geological and Nuclear Sciences Ltd, pp. 4-6.

Crozier, R.D. 1990. *Non-metallic mineral flotation – reagent technology.* Industrial Minerals, February, pp. 55-65.

Crozier, R.D. 1992. *Flotation, Theory, Reagents and Ore Testing*. Pergamon Press,UK, pp. 279.

D'Assumpcao, L.F.G., Neto, J.D., Oliveira, J.A., and Resende, A.K.L. 1995. *High Gradient Magnetic Separation of Kaolin Clay.* The SME Annual Meeting, Denver-Colorado, March 6 - 9, pp. 95-119.

Degner, V.R. 1986. *Flotation machine selection for sulphide and non-sulphide application.* In Design and Installation of Concentration and Dewatering Circuits, ed. A.L. Mular and M.A. Anderson, SME Inc., Littleton, Colorado, pp. 57-75.

Delon, J.F., Lietard O., Cases J.M., Richard M., Sauret G. and Maume J.P. 1982. *Possibilite d'emploi des kaolins des Charentes dans le couchage des papiers et des cartons.* Bull. Mineral. 105 (5), pp. 571-581.

Dobby, G.S. and Savassi, O.N. 2005. *An Advanced Modelling Technique for Scale-Up of Batch Flotation Results to Plant Metallurgical Performance*. In: Centenary of Flotation Symposium, Brisbane, Australia, pp. 1-6.

Dresler, W., Jena, B.C., Reilly, I.G., Laffin, S. and Egab, E. 1998. *The extraction of lithium carbonate from a pegmatite deposit in Manitoba, Canada*. In: Light Metals, The minerals, Metals & Materials Society, pp. 1303-1308.

Eddy, W.H., Collins, E.W., Browning, J.S. and Sullivan, G.V. 1972. *Recovery of feldspar and glass sand from South Carolina waste granite fines.* US Bureau of Mines, Report of Investigations 7651, Washington.

Evans, R.K. 2008. An Abundance of Lithium. Report, USA.

Exley, C.S., Stone, M. and Floyd, P.A. 1983. *Composition and petrogenesis of the Cornubian granite batholiths and post-orogenic volcanic rocks in southwest England.* In Hancock P.L. (ed.) The Variscan Fold Belt in the British Isles. Adam Hilger, Bristol, pp. 153-177.

Floyd, P.A., Exley, C.S. and Styles, M.T. 1993. *Igneous rocks of south-west England.* Chapman and Hall, London.

Fuerstenau, D.W. 1982. *Mineral-Water Interfaces and the Electrical Double Layer*. In: Principles of flotation (R.P. King, Ed.), SAIMM, Monograph Series No. 3, Johannesburg, pp. 17-30.

Fuerstenau, D.W. and Fuerstenau, M.C. (1982). *The Flotation of Oxide and Silicate Minerals*. In: Principles of flotation (R.P. King, Ed.), SAIMM, Monograph Series No. 3, Johannesburg, pp. 109-158.

Fuerstenau, M.C, Jameson, G.J. and Yoon, R.H. (2007). *Flotation chemistry and technology of nonsulphide minerals*. In Froth Flotation: A century of Innovation, SME, pp. 481-487.

Fuerstenau, M.C., Miller, J.D. and Kuhn, M.C. (1985). *Chemistry of flotation*, SME, AIMMPE., pp. 1-33.

Garret, E.D. 2004. *Handbook of Lithium and Natural Calcium Chloride*, Part 1, 1st Edition, Elsevier, pp. 1-196.

Global and China Lithium Carbonate Industry Report, 2008-2010, (3rd Edition) – http//www.researchandmarkets.com/research; accessed on 12th January, 2010, 15:00.

Grau, R.A., Heiskanen, K., 2005. *Bubble size distribution in laboratory scale flotation cells*. Minerals Engineering, 18, pp. 1164-1172.

Harben, W.P. 1999. *Lithium Minerals and Brines*. In: The Industrial Minerals Handbook, 3rd Edition, Published by Industrial Minerals Information Ltd, UK., pp. 113-116.

Harben, W.P. 2002. *Lithium Minerals and Compounds*. In: The Industrial Minerals Handbook , 4th Edition, Published by Industrial Minerals Information Ltd, UK., pp. 184-192.

Harris, C.C. 1976. *Flotation machines.* In Flotation, A.M. Gaudin Memorial Volume, ed. M.C. Fuerstenau, American Institute of Mining and Metallurgical Engineers, New York, Vol. 2, pp. 753-815.

Hawkes, J.R., Harris, P.M., Dangerfield, J., Strong, G.E., Davis, A.E. and Nancarrow, P.H.A. 1987. *The lithium potential of the St Austell Granite*. In: British Geological Survey (BGS) report, Vol. 19, No. 4, London, pp. 1-54.

Henderson, C.M.B, Martin, J.S. and Mason, R.A. 1989. *Composition relations in Li-micas from S.W. England and France: an ion- and electron microprobe study*. In: Mineralogical Magazine, Vol. 53, pp. 427-449.

Highley, D., Bloodworth, A., Bate, R., Cameron, D., Lusty, P. and Rayner, D. 2006. *Kaolin*. In: British Geological Survey Report, Mineral Planning Factsheet, pp. 1-7.

Hignett, T.P. and Siegel, M.R. 1949. *Recovery of fluorine from stack gases*. In. Industrial and engineering chemistry journal, Vol. 41, No. 11, pp. 2493-2498.

Hill, P.I. and Manning, D.A.C. 1987. *Multiple intrusions and pervasive hydrothermal activity in the St Austell Granite, Cornwall.* Proceedings of the Ussher Society, 6, pp. 447-453.

Hu, Y. and Liu, X. 2003. *Chemical composition and surface property of kaolins.* Min. Eng. Vol. 16, No. 3, pp. 1279-1284.

Hu, Y., Jiang, H. and Wang, D. 2003. *Electrokinetic behaviour and flotation of kaolinite in CTAB solution.* Min. Eng. Vol. 16, No. 3, pp. 1221-1223.

Hu, Y., Wei, S., Hao, J., Miller, D.J. and Fa, K. 2005. *The anomalous behaviour of kaolinite flotation with dodecylamine collector as explained from crystal structure considerations.* Min. Eng. Vol. 76, No. 3, pp. 163-172.

Hykawy, J. 2010. *Looking at lithium: Discussing market demand for lithium in electronics*. In: Materials World – Ceramics and lithium, Vol. 18, No. 5, pp. 34-35.

Jandova, J. and Vu, H.N. 2008. *Processing of zinnwaldite wastes to obtain lithium and rubidium compounds.* Global Symposium on Recycling, Waste Treatment and Clean Technology, Mexico, pp. 923-930.

Jandova, J., Vu, H.N, Dvorak, P. 2007. *Utilisation of gypsum and limestone method for lithium and rubidium separation from zinnwaldite wastes*. Proceedings of the 9th Conference of Waste Recycling, Kosice, Slovak Republic, vol. 1, pp. 83-88.

Jandova, J., Vu, H.N., Kondas, J., Dvorak, P. 2007. *Lithium recovery from wastes after mining of Sn-W ore*. Proceedings of EMC 2007, Dusseldorf, vol. 2, pp. 667-677.

Jandova, J., Vu, H.N., Belkova, T., Dvorak, P., Kondas, J. 2009. *Obtaining Li_2CO_3 from zinnwaldite wastes*. In: Ceramics – Silikaty 53 (2) pp. 108-112.

Jepson, W.B. 1984. *Kaolins: their properties and uses.* Philos. Trans. R. Soc. London A311, pp. 411-432.

Jepson, W.B. 1988. *Structural iron in kaolinites and in associated ancillary minerals.* In: Stucki, J.W. et al. (Eds), Iron in Soils and Clay Minerals. D. Reidel, Dordrecht, pp. 467-536.

Joint Industry Board for the Electrical Contracting Industry. www.jib.org.uk; accessed on 13th October, 2010, 12:25.

Karavaiko, G.I., Krutsko, V.S., Mel'nikova, E.O., Avakyan, Z.A. and Ostroushko, Y.I. 1980. *Role of microorganisms in spodumene degradation.* Mikrobiologiya 49, pp. 547-551.

Kesler, T.L. 1960. Lithium raw materials. Ind. Miner. Rocks, Am. Inst. Min. Eng., Sect. 24, pp. 521-531.

Khalek, K.N.A., Arafa, M.A., and Hassan, F. 1996. *Froth Flotation of Ultrafine Egyptian Kaolin Clay*. Proceedings of the 6th International Mineral Processing Symposium, Kusadasi-Turkey, September 24-26, pp. 395-400.

Koh, P. T. L., Manickam, M. and Schwarz, M. P. 2000. *CFD Simulation of Bubble-Particle Collisions in Mineral Flotation Cells.* Minerals Engineering, Vol. 13, No. 14-15, pp. 1455-1463.

Kunasz, I,A. 1994. *Lithium Resources*. "Mono., Ind. Minerals, Rocks". (D. D. Carr ed.), Soc. Min. Met. Explor., pp. 631-642.

Levich, V.G., 1962. *Physico chemical hydrodynamics*, Prentice-Hall, Englewood-Cliffs, N.J.

London, D. and Manning, D.A.C. 1995. *Chemical variation and significance of tourmaline from southwest England.* Economic Geology, 90, pp. 495-519.

Luz, A.B., Yildirim, I., and Yoon, R.H. 2000. *Purification of Brazilian Kaolin Clay by Flotation.* Proceedings of the XXI International Mineral Processing Congress, Rome-Italy, Volume C, July 23-27, pp. 79-83.

Mackenzie, R.C., 1973. *Differential Thermal Analysis*. Fundamental Aspects, Vol. 1, Academic Press, London.

Mackenzie, R.C. and Mitchell, B.D. 1973. *Technique.* In: Differential Thermal Analysis, (Ed. R.C. Mackenzie), Fundamental Aspects, Vol. 1, Academic Press, London, pp. 101-120.

Manning, D.A.C. 1996. *Granite and associated igneous activity.* In: Durrance E.M. and Selwood E.B. (ed.) The Geology of Cornwall. University of Exeter Press, Exeter.

Manning, D.A.C., Hill, P.I. and Howe, J.H. 1996. *Primary lithological variation in the kaolinized St Austell Granite, Cornwall, England.* Journal of the Geological Society, London, Vol. 153, pp. 827-838.

Manser, R.M., 1975. *Handbook of Silicate Flotation*. Warren Spring Laboratory, Stevanage, England, pp. 206.

MinnovEX Technologies, 2004. MinnovEX flotation test: standard procedure and parameter extraction (http://www.minnovex.com).

Mineral Compositions. http://webmineral.com, accessed on 12th July, 2010, 10:55.

Monier, G. And Robert, J.L. 1986a. *Muscovite solid solutions in the system K_2O-MgO-FeO-Al_2O_3-Si_2O-H_2O: an experimental study at 2 kbar P_{H_2O} and comparison with natural Li-free white micas*. In: Mineral. Mag. Vol. 50, pp. 257-266.

Moores, S. 2010. *Li-Ion in the driving seat – Auto battery development sees increased mineral and chemical opportunities*. In Industrial Minerals, January issue, pp. 52.

Mular, A. and Poulin, R. 1998. *CAPCOSTS – A Handbook for Estimating Mining and Mineral Processing Equipment Costs and Capital Expenditures and Aiding Mineral Project Evaluations*. CIM Special Volume 47, published by Canadian Mineral Processors Division of Canadian Institute of Mining, Metallurgy and Petroleum, Canada.

Mullary, M.B. 1974. *Purification of kaolin clay by froth flotation.* US Patent, 3, 827, pp.556.

Nagaraj, D.R. (2005). *Reagent selection and optimization – the case for a holistic approach*. In Minerals Engineering Vol. 18, pp. 151-158.

Nelson, M.G. and Lelinski, D. 2000. *Hydrodynamic Design of Self-Aerated Flotation Machines.* In Minerals Engineering, Vol. 13, No. 10-11, pp. 991-998.

Nesse, W.D. 2000. *Introduction to Mineralogy*. Oxford University Press, pp. 208-209.

Norrgran, D.A., Mankosa, M.J. 2002. *Bench Scale and Pilot Plant Test for Magnetic Concentration Circuit Design.* In: Andrew L. Mular, Doug N. Halbe, Derek J. Barratt (Eds.), Mineral Processing Plant Design, Practice, and Control: Proceedings Volume 1, pp. 176 -200.

Nott, A.J. 1976. *Treatment of kaolin ore.* US Patent Appl. 51, pp. 315-408.

Orhan, E.C. and Bayraktar, I. 2006. *Amine-oleate interactions in feldspar flotation.* Minerals Engineering, Vol. 19, pp. 48-55.

Patent – WO/2007/103083. *Extraction of lithium from lithium bearing minerals by Caustic Leaching*. World Intellectual Property Organisation, IP Services.

Peres, A.E.C, Leonel, C.M.L. and Valadao, G.E.S. 1985. *Floatability of Beryl and Lithium Minerals*. Proc. 2nd Latin-American Congress on Froth Flotation, Conception, Chile, S.H. Castro Flores and J.A. Moisan Eds., Elsevier, pp. 165-174.

Physical Separation – Outotec; www.outotec.com/36904.epibrw; accessed on 5th October, 2010, 11:00.

Raghavan, P., Chandrasekhar, S. and Damodaran, A.D. 1997. *Value addition of paper coating grade kaolins by the removal of ultra-fine colouring impurities.* Int. J. Miner. Process. Vol. 50, pp. 307-316.

Redecker, H.I. 1981. *Flotation of Feldspar, Spodumene, Quartz and Mica from Pegmatites in North Carolina, USA*. Proc.13th Annual Meeting of the Canadian Mineral Processors, Canadian Centre for Mineral and Energy Technology, Energy, Mines and Resources, Canada, Ottawa, January 20, Paper No. 8, pp. 136-153.

Rezza, I., Salinas, E., Calvente, V. Benuzzi, D., and Sanz de Tosetti, M.I. 1997. *Extraction of lithium from spodumene by bioleaching.* The Society for Applied Bacteriology, Letters in Applied Microbiology, 25, pp. 172-176.

Richardson, W.A. 1923. *A micrometric study of the St Austell granite*. Q.J. geol. Soc. London, 79, pp. 546-576.

Rossi, G. and Ehrlich, H. 1990. *Other bioleaching processes.* In Microbial Mineral Recovery (eds.) Ehrlich E. and Brierley C.L. McGraw-Hill Inc, USA, pp. 158-159.

Samkova, R. 2009. *Recovering lithium mica from the waste after mining tin-tungsten ores through the use of flotation*. In: GeoScience Engineering, Vol. LV, No. 1, pp. 33-37.

Smith, L. 2010. *Demand not to be taken lightly: While future lithium markets appear promising*. In: Industrial Minerals, January issue, pp. 45-46.

Solubility Table; Wikipedia; http://en.wikipedia.org/wiki/solubility_table; accessed on 12th November, 2009, 10:45.

Stone, M., Exley, C.S. and George, M.C. 1988. *Composition of trioctahedral micas in the Cornubian batholiths*. In: Mineralogical Magazine, vol. 52, pp. 175-192.

Subrahmanyam, T.V. and Forssberg, E. (1988). *Froth stability, particle entrainment and drainage in flotation – A Review*. In Int. J. Min Proc., Vol. 23, pp. 33-53.

Thurlow, C. 2001. *China Clay from Cornwall and Devon*. 3rd Edition, Cornish Hillside Publications, St Austell, Cornwall, pp. 4-5.

Tindle, A.G. and Webb, P.C. 1990. *Estimation of lithium contents in trioctahedral micas using microprobe data: application to micas from granitic rocks*. In: Europ. J. Mineral., Vol. 2, pp. 595-610.

USGS, 2002. *Lithium*. U.S. Geological Survey Minerals Yearbook, Minerals Commodity Report, pp. 2-10.

Utility Costs in the UK. www.ukti.gov.uk; visited on 13th October, 2010, 09:40.

Vandevivere, P., Welch, S.A. Ullman, W.J. and Kirchman, D.L. 1994. *Enhanced dissolution of silicate minerals by bacterial at near-neutral pH.* Microbial Ecology, 27, pp. 241-251.

Wietelmann, U., Bauer, R.J. 2008. *Ullmann's Encyclopedia of Industrial Chemistry* (WILEY-VCH Verlag GmbH & Co., Weinheim, Germany), 7th ed. Vol. 20, pp. 33-60.

Volborth, A. (1954). *Phosphate Minerals from the lithium Pegmatite in the Viitaniemi, Eraejaevi, Central Finland*. Geologica Geographia, Series A3, pp. 90.

Wills, B.A. and Napier-Munn, T.J. 2006. *Froth Flotation*. Mineral Processing Technology (Ed. T.J Napier-Munn), 7th Edition, Butterworth-Heinemann, Great Britain.

Yoon, R.H. and Shi, J. 1986. *Processing of Kaolin Clay.* Advances in Mineral Processing, (Ed. P. Somasundaran), Published by the Society of Mining Engineers, Inc., March 3-5, pp. 366-379.

Appendix A: Particle Size Analysis of China Clay Waste Data.

Table 1: Particle Size Analysis of China Clay Waste obtained by Malvern Mastersizer.

Particle Size (μm)	Cumulative Undersize (%)			
	Run 1	Run2	Run 3	Average
0.67	0	0	0	0
0.71	0	0	0	0
0.75	0	0	0	0
0.82	0.02	0.02	0.01	0.02
0.88	0.05	0.05	0.04	0.05
0.94	0.1	0.1	0.07	0.09
1	0.16	0.16	0.12	0.15
1.15	0.34	0.35	0.26	0.32
1.2	0.4	0.41	0.31	0.37
1.3	0.51	0.53	0.41	0.48
1.4	0.61	0.64	0.5	0.58
1.42	0.63	0.65	0.51	0.6
1.5	0.71	0.74	0.58	0.68
1.6	0.8	0.83	0.66	0.76
1.7	0.89	0.92	0.74	0.85
1.8	0.97	1	0.81	0.93
2	1.12	1.16	0.94	1.07
2.1	1.19	1.23	1.01	1.14
2.3	1.33	1.37	1.13	1.28
2.5	1.45	1.5	1.25	1.4
2.6	1.51	1.57	1.3	1.46
2.8	1.63	1.68	1.41	1.57
3	1.74	1.79	1.5	1.68
3.25	1.87	1.93	1.62	1.81
3.5	1.99	2.05	1.74	1.93
3.75	2.11	2.18	1.84	2.04
4	2.22	2.29	1.95	2.15
4.25	2.33	2.41	2.05	2.26
4.5	2.44	2.52	2.15	2.37
5	2.65	2.73	2.34	2.57
5.3	2.78	2.86	2.45	2.7
5.6	2.9	2.99	2.56	2.82
6	3.07	3.15	2.71	2.98
6.5	3.28	3.36	2.9	3.18
7	3.49	3.57	3.09	3.38
7.5	3.71	3.79	3.28	3.59
8	3.93	4.01	3.48	3.81
8.5	4.15	4.23	3.68	4.02
9	4.38	4.45	3.88	4.24
9.5	4.62	4.68	4.09	4.46
10	4.85	4.92	4.29	4.69
11	5.34	5.39	4.72	5.15
12	5.83	5.87	5.15	5.62
13	6.32	6.36	5.58	6.09
14	6.82	6.84	6.02	6.56
15	7.31	7.32	6.45	7.03

Table 1, Continued

Particle Size (μm)	Cumulative Undersize (%)			Average
	Run 1	Run2	Run 3	
16	7.8	7.81	6.88	7.5
17	8.29	8.28	7.3	7.96
18	8.77	8.75	7.72	8.41
19	9.25	9.22	8.14	8.87
20	9.73	9.68	8.55	9.32
21	10.2	10.14	8.95	9.76
23	11.13	11.04	9.75	10.64
25	12.06	11.95	10.56	11.52
27	12.99	12.86	11.36	12.4
29	13.93	13.78	12.19	13.3
31	14.89	14.72	13.03	13.95
33	15.87	15.69	13.9	15.15
35	16.87	16.69	14.81	16.12
37	17.91	17.72	15.74	17.12
40	19.51	19.33	17.22	18.69
45	22.31	22.17	19.84	21.44
47	23.48	23.35	20.95	22.59
50	25.26	25.18	22.67	24.37
53	27.09	27.05	24.45	26.2
58	30.21	30.27	27.52	29.33
63	33.39	33.56	30.7	32.55
66	35.31	35.55	32.63	34.5
70	37.87	38.21	35.24	37.11
75	41.06	41.52	38.5	40.36
80	44.21	44.79	41.75	43.58
85	47.3	47.99	44.95	46.75
90	50.32	51.11	48.08	49.84
100	56.05	57.03	54.09	55.72
105	58.76	59.82	56.93	58.5
115	63.85	65.02	62.29	63.72
125	68.48	69.72	67.18	68.46
130	70.63	71.88	69.46	70.66
140	74.61	75.86	73.66	74.71
150	78.17	79.4	77.42	78.33
160	81.37	82.53	80.79	81.56
170	84.21	85.29	83.77	84.42
180	86.75	87.73	86.42	86.97
200	90.94	91.71	90.77	91.14
210	92.65	93.31	92.53	92.83
230	95.44	95.88	95.39	95.57
250	97.47	97.73	97.44	97.55
260	98.21	98.4	98.2	98.27
280	99.24	99.32	99.23	99.26
300	99.95	99.95	99.95	99.95

Table 2: Results of Dry Sieve Analysis on China Clay Waste

Sieve Size Range (μm)	Sieve Fractions		Nominal Aperture Size (μm)	Cumulative %	
	wt (g)	wt (%)		Oversize	Undersize
710	0.00	0.000	710	0.000	100.000
-710 + 500	0.00	0.000	500	0.000	100.000
-500 + 355	0.00	0.000	355	0.000	100.000
-355 + 250	1.15	0.325	250	0.325	99.675
-250 + 180	5.40	1.528	180	1.853	98.147
-180 + 125	75.05	21.231	125	23.083	76.917
-125 + 90	94.35	26.690	90	49.774	50.226
-90 + 63	126.35	35.743	63	85.516	14.484
-63 + 45	33.65	9.519	45	95.035	4.965
-45 +38	11.25	3.182	38	98.218	1.782
-38	6.30	1.782		100.000	0.000

Appendix B1: Flotation Results Balance Sheets.

Table 1a: Metallurgical Balance Sheet for the Treatment Combinations (1) – Run 1

Flotation Time (sec)	Fraction	Weight (g)	Weight (%)	Content (%) SiO_2	Al_2O_3	Fe_2O_3	TiO_2	MgO	CaO	K_2O	Na_2O	P_2O_5	F	LOI
480	Conc.	707.00	59.83	50.420	29.350	4.200	0.193	0.337	0.076	7.852	0.159	0.058	2.170	5.420
	Tail	474.60	40.17	77.220	13.660	0.522	0.086	0.123	0.055	5.658	0.665	0.126	1.000	1.060
	Head Cal.	1181.60	100.00	**61.184**	**23.048**	**2.723**	**0.150**	**0.251**	**0.067**	**6.971**	**0.362**	**0.085**	**1.700**	**3.669**
Time		**Weight**	**Weight**	**Recovery %**										
(sec)	Fraction	(g)	(%)	SiO_2	Al_2O_3	Fe_2O_3	TiO_2	MgO	CaO	K_2O	Na_2O	P_2O_5	F	LOI
480	Conc.	707.00	59.83	49.31	76.19	92.30	76.98	80.32	67.56	67.40	26.26	40.68	76.37	5.420
	Tail	474.60	40.17	50.69	23.81	7.70	23.02	19.68	32.44	32.60	73.74	59.32	23.63	1.060
				100.00	100.00	100.00	100.00	100.00	100.00	100.00	100.00	100.00	100.00	3.669

Table 1b: Metallurgical Balance Sheet for the Treatment Combinations (1) – Run 2

Flotation Time (sec)	Fraction	Weight (g)	Weight (%)	Content (%) SiO_2	Al_2O_3	Fe_2O_3	TiO_2	MgO	CaO	K_2O	Na_2O	P_2O_5	F	LOI
480	Conc. 1	710.40	60.35	50.290	29.200	4.421	0.197	0.337	0.056	8.102	0.157	0.038	2.400	5.100
	Tail	466.80	39.65	77.760	13.500	0.497	0.077	0.124	0.040	5.606	0.659	0.128	1.000	1.260
	Head Cal.	1177.20	100.00	**61.183**	**22.974**	**2.865**	**0.149**	**0.253**	**0.050**	**7.112**	**0.356**	**0.074**	**1.845**	**3.577**
Time		**Weight**	**Weight**	**Recovery %**										
(sec)	Fraction	(g)	(%)	SiO_2	Al_2O_3	Fe_2O_3	TiO_2	MgO	CaO	K_2O	Na_2O	P_2O_5	F	LOI
480	Conc. 1	710.40	60.35	49.60	76.70	93.12	79.52	80.53	68.06	68.74	26.61	31.12	78.51	5.100
	Tail	466.80	39.65	50.40	23.30	6.88	20.48	19.47	31.94	31.26	73.39	68.88	21.49	1.260
				100.00	100.00	100.00	100.00	100.00	100.00	100.00	100.00	100.00	100.00	3.577

Table 2a: Metallurgical Balance Sheet for the Treatment Combinations (*a*) – Run 1

Flotation Time (sec)	Fraction	Weight (g)	Weight (%)	Content (%) SiO_2	Al_2O_3	Fe_2O_3	TiO_2	MgO	CaO	K_2O	Na_2O	P_2O_5	F	LOI
480	Conc. 1	714.60	60.87	50.830	29.030	4.279	0.197	0.332	0.086	8.009	0.164	0.070	2.320	4.990
	Tail	459.40	39.13	76.460	13.970	0.546	0.085	0.125	0.059	5.738	0.660	0.135	1.100	1.340
	Head Cal.	1174.00	100.00	**60.859**	**23.137**	**2.818**	**0.153**	**0.251**	**0.076**	**7.120**	**0.358**	**0.095**	**1.843**	**3.562**
Time		**Weight**	**Weight**	**Recovery %**										
(sec)	Fraction	(g)	(%)	SiO_2	Al_2O_3	Fe_2O_3	TiO_2	MgO	CaO	K_2O	Na_2O	P_2O_5	F	LOI
480	Conc. 1	714.60	60.87	50.84	76.37	92.42	78.25	80.51	69.32	68.47	27.88	44.65	76.64	4.990
	Tail	459.40	39.13	49.16	23.63	7.58	21.75	19.49	30.68	31.53	72.12	55.35	23.36	1.340
				100.00	100.00	100.00	100.00	100.00	100.00	100.00	100.00	100.00	100.00	3.562

Table 2b: Metallurgical Balance Sheet for the Treatment Combinations (*a*) – Run 2

Flotation Time (sec)	Fraction	Weight (g)	Weight (%)	Content (%)										
				SiO_2	Al_2O_3	Fe_2O_3	TiO_2	MgO	CaO	K_2O	Na_2O	P_2O_5	F	LOI
480	Conc. 1	709.50	59.93	50.000	29.110	4.395	0.201	0.327	0.120	8.099	0.159	0.095	2.440	5.360
	Tail	474.40	40.07	77.210	13.570	0.484	0.076	0.125	0.065	5.550	0.637	0.132	1.100	1.280
	Head Cal.	1183.90	100.00	**60.903**	**22.883**	**2.828**	**0.151**	**0.246**	**0.098**	**7.078**	**0.351**	**0.110**	**1.903**	**3.725**
Time		**Weight**	**Weight**	**Recovery %**										
(sec)	Fraction	(g)	(%)	SiO_2	Al_2O_3	Fe_2O_3	TiO_2	MgO	CaO	K_2O	Na_2O	P_2O_5	F	LOI
480	Conc. 1	709.50	59.93	49.20	76.24	93.14	79.80	79.64	73.44	68.58	27.18	51.81	76.84	5.360
	Tail	474.40	40.07	50.80	23.76	6.86	20.20	20.36	26.56	31.42	72.82	48.19	23.16	1.280
				100.00	100.00	100.00	100.00	100.00	100.00	100.00	100.00	100.00	100.00	3.725

Table 3a: Metallurgical Balance Sheet for the Treatment Combinations (*b*) – Run 1

Flotation Time (sec)	Fraction	Weight (g)	Weight (%)	Content (%)										
				SiO_2	Al_2O_3	Fe_2O_3	TiO_2	MgO	CaO	K_2O	Na_2O	P_2O_5	F	LOI
480	Conc. 1	726.40	61.54	50.580	29.040	4.215	0.196	0.333	0.084	8.004	0.164	0.068	2.450	5.220
	Tail	454.00	38.46	78.440	12.670	0.417	0.074	0.115	0.061	5.516	0.708	0.140	1.000	1.060
	Head Cal.	1180.40	100.00	**61.295**	**22.744**	**2.754**	**0.149**	**0.249**	**0.075**	**7.047**	**0.373**	**0.096**	**1.892**	**3.620**
Time		**Weight**	**Weight**	**Recovery %**										
(sec)	Fraction	(g)	(%)	SiO_2	Al_2O_3	Fe_2O_3	TiO_2	MgO	CaO	K_2O	Na_2O	P_2O_5	F	LOI
480	Conc. 1	726.40	61.54	50.78	78.57	94.18	80.95	82.25	68.73	69.89	27.04	43.73	79.67	5.220
	Tail	454.00	38.46	49.22	21.43	5.82	19.05	17.75	31.27	30.11	72.96	56.27	20.33	1.060
				100.00	100.00	100.00	100.00	100.00	100.00	100.00	100.00	100.00	100.00	3.620

Table 3b: Metallurgical Balance Sheet for the Treatment Combinations (*b*) – Run 2

Flotation Time (sec)	Fraction	Weight (g)	Weight (%)	Content (%)										
				SiO_2	Al_2O_3	Fe_2O_3	TiO_2	MgO	CaO	K_2O	Na_2O	P_2O_5	F	LOI
480	Conc. 1	727.20	61.32	50.600	28.920	4.432	0.195	0.339	0.122	8.138	0.161	0.098	2.310	5.020
	Tail	458.80	38.68	78.660	12.380	0.454	0.098	0.103	0.074	5.400	0.695	0.146	1.100	1.110
	Head Cal.	1186.00	100.00	**61.455**	**22.522**	**2.893**	**0.157**	**0.248**	**0.103**	**7.079**	**0.368**	**0.117**	**1.842**	**3.507**
Time		**Weight**	**Weight**	**Recovery %**										
(sec)	Fraction	(g)	(%)	SiO_2	Al_2O_3	Fe_2O_3	TiO_2	MgO	CaO	K_2O	Na_2O	P_2O_5	F	LOI
480	Conc. 1	727.20	61.32	50.49	78.74	93.93	75.96	83.91	72.32	70.49	26.86	51.55	76.90	5.020
	Tail	458.80	38.68	49.51	21.26	6.07	24.04	16.09	27.68	29.51	73.14	48.45	23.10	1.110
				100.00	100.00	100.00	100.00	100.00	100.00	100.00	100.00	100.00	100.00	3.507

Table 4a: Metallurgical Balance Sheet for the Treatment Combinations (*ab*) – Run 1

Flotation Time (sec)	Fraction	Weight (g)	Weight (%)	Content (%) SiO_2	Al_2O_3	Fe_2O_3	TiO_2	MgO	CaO	K_2O	Na_2O	P_2O_5	F	LOI
480	Conc. 1	807.90	68.61	50.980	28.630	3.836	0.201	0.320	0.092	7.652	0.169	0.091	2.430	5.960
	Tail	369.60	31.39	81.970	9.973	0.303	0.021	0.095	0.037	5.374	0.697	0.120	1.000	1.070
	Head Cal.	1177.50	100.00	**60.707**	**22.774**	**2.727**	**0.145**	**0.250**	**0.074**	**6.937**	**0.335**	**0.100**	**1.981**	**4.425**
Time		**Weight**	**Weight**	**Recovery %**										
(sec)	Fraction	(g)	(%)	SiO_2	Al_2O_3	Fe_2O_3	TiO_2	MgO	CaO	K_2O	Na_2O	P_2O_5	F	LOI
480	Conc. 1	807.90	68.61	57.62	86.25	96.51	95.44	88.00	84.40	75.68	34.64	62.27	84.16	5.960
	Tail	369.60	31.39	42.38	13.75	3.49	4.56	12.00	15.60	24.32	65.36	37.73	15.84	1.070
				100.00	100.00	100.00	100.00	100.00	100.00	100.00	100.00	100.00	100.00	4.425

Table 4b: Metallurgical Balance Sheet for the Treatment Combinations (*ab*) – Run 2

Flotation Time (sec)	Fraction	Weight (g)	Weight (%)	Content (%) SiO_2	Al_2O_3	Fe_2O_3	TiO_2	MgO	CaO	K_2O	Na_2O	P_2O_5	F	LOI
480	Conc. 1	731.90	61.88	50.840	28.960	4.242	0.199	0.338	0.129	7.984	0.160	0.105	2.280	5.080
	Tail	450.80	38.12	77.990	12.950	0.484	0.109	0.120	0.080	5.385	0.644	0.161	1.100	1.170
	Head Cal.	1182.70	100.00	**61.189**	**22.858**	**2.810**	**0.165**	**0.255**	**0.110**	**6.993**	**0.344**	**0.126**	**1.830**	**3.590**
Time		**Weight**	**Weight**	**Recovery %**										
(sec)	Fraction	(g)	(%)	SiO_2	Al_2O_3	Fe_2O_3	TiO_2	MgO	CaO	K_2O	Na_2O	P_2O_5	F	LOI
480	Conc. 1	731.90	61.88	51.42	78.41	93.43	74.77	82.06	72.44	70.65	28.74	51.43	77.09	5.080
	Tail	450.80	38.12	48.58	21.59	6.57	25.23	17.94	27.56	29.35	71.26	48.57	22.91	1.170
				100.00	100.00	100.00	100.00	100.00	100.00	100.00	100.00	100.00	100.00	3.590

Table 5a: Metallurgical Balance Sheet for the Treatment Combinations (*c*) – Run 1

Flotation Time (sec)	Fraction	Weight (g)	Weight (%)	Content (%) SiO_2	Al_2O_3	Fe_2O_3	TiO_2	MgO	CaO	K_2O	Na_2O	P_2O_5	F	LOI
480	Conc. 1	713.00	59.93	50.430	29.220	4.255	0.202	0.337	0.101	8.046	0.169	0.077	2.370	5.110
	Tail	476.70	40.07	77.450	13.370	0.491	0.093	0.116	0.055	5.495	0.644	0.127	1.160	1.230
	Head Cal.	1189.70	100.00	**61.257**	**22.869**	**2.747**	**0.158**	**0.248**	**0.082**	**7.024**	**0.359**	**0.097**	**1.885**	**3.555**
Time		**Weight**	**Weight**	**Recovery %**										
(sec)	Fraction	(g)	(%)	SiO_2	Al_2O_3	Fe_2O_3	TiO_2	MgO	CaO	K_2O	Na_2O	P_2O_5	F	LOI
480	Conc. 1	713.00	59.93	49.34	76.57	92.84	76.48	81.29	73.45	68.65	28.19	47.56	75.34	5.110
	Tail	476.70	40.07	50.66	23.43	7.16	23.52	18.71	26.55	31.35	71.81	52.44	24.66	1.230
				100.00	100.00	100.00	100.00	100.00	100.00	100.00	100.00	100.00	100.00	3.555

Table 5b: Metallurgical Balance Sheet for the Treatment Combinations (*c*) – Run 2

Flotation Time (sec)	Fraction	Weight (g)	Weight (%)	Content (%) SiO_2	Al_2O_3	Fe_2O_3	TiO_2	MgO	CaO	K_2O	Na_2O	P_2O_5	F	LOI
480	Conc. 1	768.60	65.01	51.290	28.670	4.094	0.193	0.333	0.116	7.900	0.179	0.104	2.340	5.110
	Tail	413.70	34.99	78.700	12.300	0.450	0.060	0.101	0.050	5.516	0.698	0.132	1.000	1.180
	Head Cal.	1182.30	100.00	**60.881**	**22.942**	**2.819**	**0.146**	**0.252**	**0.093**	**7.066**	**0.361**	**0.114**	**1.871**	**3.735**
Time		**Weight**	**Weight**	**Recovery %**										
(sec)	Fraction	(g)	(%)	SiO_2	Al_2O_3	Fe_2O_3	TiO_2	MgO	CaO	K_2O	Na_2O	P_2O_5	F	LOI
480	Conc. 1	768.60	65.01	54.77	81.24	94.41	85.64	85.97	81.17	72.68	32.27	59.41	81.30	5.110
	Tail	413.70	34.99	45.23	18.76	5.59	14.36	14.03	18.83	27.32	67.73	40.59	18.70	1.180
				100.00	100.00	100.00	100.00	100.00	100.00	100.00	100.00	100.00	100.00	3.735

Table 6a: Metallurgical Balance Sheet for the Treatment Combinations (*ac*) – Run 1

Flotation Time (sec)	Fraction	Weight (g)	Weight (%)	Content (%) SiO_2	Al_2O_3	Fe_2O_3	TiO_2	MgO	CaO	K_2O	Na_2O	P_2O_5	F	LOI
480	Conc. 1	666.50	56.78	49.960	29.130	4.577	0.195	0.332	0.081	8.227	0.156	0.062	2.460	5.170
	Tail	507.40	43.22	75.820	14.630	0.620	0.122	0.143	0.083	5.520	0.588	0.160	1.100	1.390
	Head Cal.	1173.90	100.00	**61.138**	**22.863**	**2.866**	**0.163**	**0.250**	**0.082**	**7.057**	**0.343**	**0.104**	**1.872**	**3.536**
Time		**Weight**	**Weight**	**Recovery %**										
(sec)	Fraction	(g)	(%)	SiO_2	Al_2O_3	Fe_2O_3	TiO_2	MgO	CaO	K_2O	Na_2O	P_2O_5	F	LOI
480	Conc. 1	666.50	56.78	46.40	72.34	90.66	67.74	75.31	56.06	66.19	25.84	33.73	74.60	5.170
	Tail	507.40	43.22	53.60	27.66	9.34	32.26	24.69	43.94	33.81	74.16	66.27	25.40	1.390
				100.00	100.00	100.00	100.00	100.00	100.00	100.00	100.00	100.00	100.00	3.536

Table 6b: Metallurgical Balance Sheet for the Treatment Combinations (*ac*) – Run 2

Flotation Time (sec)	Fraction	Weight (g)	Weight (%)	Content (%) SiO_2	Al_2O_3	Fe_2O_3	TiO_2	MgO	CaO	K_2O	Na_2O	P_2O_5	F	LOI
480	Conc. 1	785.20	66.06	51.580	28.550	3.956	0.206	0.331	0.128	7.856	0.177	0.109	2.470	5.000
	Tail	403.50	33.94	79.310	11.990	0.448	0.065	0.101	0.047	5.487	0.674	0.127	0.850	1.020
	Head Cal.	1188.70	100.00	**60.993**	**22.929**	**2.765**	**0.158**	**0.253**	**0.101**	**7.052**	**0.346**	**0.115**	**1.920**	**3.649**
Time		**Weight**	**Weight**	**Recovery %**										
(sec)	Fraction	(g)	(%)	SiO_2	Al_2O_3	Fe_2O_3	TiO_2	MgO	CaO	K_2O	Na_2O	P_2O_5	F	LOI
480	Conc. 1	785.20	66.06	55.86	82.25	94.50	86.03	86.45	84.10	73.59	33.82	62.55	84.97	5.000
	Tail	403.50	33.94	44.14	17.75	5.50	13.97	13.55	15.90	26.41	66.18	37.45	15.03	1.020
				100.00	100.00	100.00	100.00	100.00	100.00	100.00	100.00	100.00	100.00	3.649

Table 7a: Metallurgical Balance Sheet for the Treatment Combinations (*bc*) – Run 1

Flotation Time (sec)	Fraction	Weight (g)	Weight (%)	Content (%)										
				SiO_2	Al_2O_3	Fe_2O_3	TiO_2	MgO	CaO	K_2O	Na_2O	P_2O_5	F	LOI
480	Conc. 1	703.10	60.43	50.370	29.090	4.265	0.183	0.342	0.067	8.101	0.163	0.045	2.490	5.240
	Tail	460.40	39.57	77.110	13.420	0.508	0.087	0.126	0.103	5.718	0.666	0.178	0.930	1.270
	Head Cal.	1163.50	100.00	**60.951**	**22.889**	**2.778**	**0.145**	**0.257**	**0.081**	**7.158**	**0.362**	**0.098**	**1.873**	**3.669**
Time		**Weight**	**Weight**	**Recovery %**										
(sec)	Fraction	(g)	(%)	SiO_2	Al_2O_3	Fe_2O_3	TiO_2	MgO	CaO	K_2O	Na_2O	P_2O_5	F	LOI
480	Conc. 1	703.10	60.43	49.94	76.80	92.76	76.18	80.56	49.87	68.39	27.21	27.85	80.35	5.240
	Tail	460.40	39.57	50.06	23.20	7.24	23.82	19.44	50.13	31.61	72.79	72.15	19.65	1.270
				100.00	100.00	100.00	100.00	100.00	100.00	100.00	100.00	100.00	100.00	3.669

Table 7b: Metallurgical Balance Sheet for the Treatment Combinations (*bc*) – Run 2

Flotation Time (sec)	Fraction	Weight (g)	Weight (%)	Content (%)										
				SiO_2	Al_2O_3	Fe_2O_3	TiO_2	MgO	CaO	K_2O	Na_2O	P_2O_5	F	LOI
480	Conc. 1	769.90	65.17	51.120	28.780	4.156	0.208	0.330	0.125	8.007	0.167	0.099	2.270	4.990
	Tail	411.40	34.83	78.910	12.060	0.448	0.069	0.102	0.053	5.633	0.709	0.133	1.000	1.060
	Head Cal.	1181.30	100.00	**60.798**	**22.957**	**2.865**	**0.160**	**0.251**	**0.100**	**7.180**	**0.356**	**0.111**	**1.828**	**3.621**
Time		**Weight**	**Weight**	**Recovery %**										
(sec)	Fraction	(g)	(%)	SiO_2	Al_2O_3	Fe_2O_3	TiO_2	MgO	CaO	K_2O	Na_2O	P_2O_5	F	LOI
480	Conc. 1	769.90	65.17	54.80	81.70	94.55	84.94	85.82	81.56	72.68	30.59	58.31	80.95	4.990
	Tail	411.40	34.83	45.20	18.30	5.45	15.06	14.18	18.44	27.32	69.41	41.69	19.05	1.060
				100.00	100.00	100.00	100.00	100.00	100.00	100.00	100.00	100.00	100.00	3.621

Table 8a: Metallurgical Balance Sheet for the Treatment Combinations (*abc*) – Run 1

Flotation Time (sec)	Fraction	Weight (g)	Weight (%)	Content (%)										
				SiO_2	Al_2O_3	Fe_2O_3	TiO_2	MgO	CaO	K_2O	Na_2O	P_2O_5	F	LOI
480	Conc. 1	770.00	65.25	52.240	27.900	4.186	0.192	0.316	0.062	8.040	0.185	0.047	2.330	4.780
	Tail	410.10	34.75	76.530	14.050	0.549	0.136	0.123	0.081	5.482	0.623	0.144	1.100	1.350
	Head Cal.	1180.10	100.00	**60.681**	**23.087**	**2.922**	**0.173**	**0.249**	**0.069**	**7.151**	**0.337**	**0.081**	**1.903**	**3.588**
Time		**Weight**	**Weight**	**Recovery %**										
(sec)	Fraction	(g)	(%)	SiO_2	Al_2O_3	Fe_2O_3	TiO_2	MgO	CaO	K_2O	Na_2O	P_2O_5	F	LOI
480	Conc. 1	770.00	65.25	56.17	78.85	93.47	72.61	82.83	59.00	73.36	35.80	38.00	79.91	4.780
	Tail	410.10	34.75	43.83	21.15	6.53	27.39	17.17	41.00	26.64	64.20	62.00	20.09	1.350
				100.00	100.00	100.00	100.00	100.00	100.00	100.00	100.00	100.00	100.00	3.588

Table 8b: Metallurgical Balance Sheet for the Treatment Combinations (*abc*) – Run 2

Flotation Time (sec)	Fraction	Weight (g)	Weight (%)	Content (%)										
				SiO_2	Al_2O_3	Fe_2O_3	TiO_2	MgO	CaO	K_2O	Na_2O	P_2O_5	F	LOI
480	Conc. 1	781.00	65.90	51.310	28.830	4.045	0.200	0.329	0.135	7.815	0.168	0.118	2.090	5.210
	Tail	404.20	34.10	78.850	12.340	0.383	0.058	0.116	0.053	5.532	0.765	0.146	0.930	1.020
	Head Cal.	1185.20	100.00	**60.702**	**23.206**	**2.796**	**0.152**	**0.256**	**0.107**	**7.036**	**0.372**	**0.128**	**1.694**	**3.781**
Time		**Weight**	**Weight**	**Recovery %**										
(sec)	Fraction	(g)	(%)	SiO_2	Al_2O_3	Fe_2O_3	TiO_2	MgO	CaO	K_2O	Na_2O	P_2O_5	F	LOI
480	Conc. 1	781.00	65.90	55.70	81.87	95.33	86.87	84.57	83.01	73.19	29.79	60.96	81.28	5.210
	Tail	404.20	34.10	44.30	18.13	4.67	13.13	15.43	16.99	26.81	70.21	39.04	18.72	1.020
				100.00	100.00	100.00	100.00	100.00	100.00	100.00	100.00	100.00	100.00	3.781

Appendix B2: Statistical Analysis of the Flotation Results.

The experimental design used in this work was a factorial design 2^3 with two replicas for each experiment. The notation used to establish the experimental conditions for each test is presented in Table B2-1.

Table B2-1: Analysis of Contrasts and notation used to establish the experimental conditions for each test

Number of Test	Factors			Treatment combinations
	Impeller Speed (*A*)	Frother Dosage (*B*)	Aeration Rate (*C*)	
1	-	-	-	(1)
2	+	-	-	*a*
3	-	+	-	*b*
4	+	+	-	*ab*
5	-	-	+	*c*
6	+	-	+	*ac*
7	-	+	+	*bc*
8	+	+	+	*abc*

+ = High level.

- = Low level.

Valuation of the contrast values: The statistical analysis of the values of the contrasts for the main effects as well as its interactions (or its combinations), allow to know which of these values significantly affect the variable of answer.

Values of the contrasts for the main effects of the factors impeller speed, frother dosage and aeration rate (factors *A*,*B*, and *C*, respectively), and contrasts values of its interactions (*AB*, *AC*, *BC*, and *ABC*), are obtained following Yates' method shown in Table B2-2 and are given by dividing entries in column (iii) by 4n, where *n* is the number of replicas (*n* = 2, in the present case). Finally the sum of squares for the main effects and interactions are obtained by squaring the entries in column (iii) and dividing by 8*n*.

Table B2-2: Yates Technique for a 2^3 Factorial Experiment

Treatment Combination	(i)	(ii)	(iii)	Identification
(1)	(1) +*a*	(1)+ *a*+*b*+*ab*	(1)+*a* +*b* + *ab* + *c* +*ac* + *bc* + *abc*	Total
a	*b* +*ab*	*b*+ *ac* + *bc*+*abc*	*a* – (1) + *ab* – *b* +*ac* – *c* + *abc* – *bc*	*A* contrast
b	*c*+ *ac*	*a* – (1) +*ab* – *b*	*b* + *ab* – (1) – *a* + *bc* +*abc* – *c* – *ac*	*B* contrast
ab	*bc* + *abc*	*ac* – *c*+*abc* – *bc*	*ab* – *b* – *a* + (1) + *abc* – *bc* – *ac* + *c*	*AB* contrast
c	*a* – (1)	*b*+*ab* – (1) – *a*	*c* + *ac* +*bc* + *abc* – (1) – *a* – *b* – *ab*	*C* contrast
ac	*ab* – *b*	*bc*+*abc* – *c* – *ac*	*ac* - *c* +*abc* – *bc* – *a* + (1) – *ab* +*b*	*AC* contrast
bc	*ac* – *c*	*ab* – *b* – *a* + (1)	*bc* + *abc* – *c* – *ac* – *b* – *ab* + (1) + *a*	*BC* contrast
abc	*abc* - *bc*	*abc* – *bc* – *ac* +*c*	*abc* – *bc* – *ac* +*c* – *ab* +*b* + *a* – (1)	*ABC* contrast

These expressions were evaluated in terms of grade and recovery of Fe_2O_3 in the concentrate in order to obtain the values of the contrasts for the main effects and its interactions. The obtained results are presented in Table B2-3.

Table B2-3: Values of the contrasts for the main effects and its combinations

Contrasts	Fe_2O_3 grade, %	Fe_2O_3 recovery, %
A	- 0.07	0.17
B	- 0.1	1.35
AB	- 0.13	0.66
C	- 0.06	- 0.06
AC	0.06	- 0.32
BC	0.04	- 0.42
ABC	0.03	0.24

Tables B2-4 and B2-5 show the analysis of variance (ANOVA) of the obtained results as a function of Fe_2O_3 recovery and grade in the concentrate, respectively.

Table B2-4: Analysis of variance of the results expressed in recovery of Fe_2O_3 in the concentrate

Source of Variation	**Sum of Squares**	**Degrees of freedom**	**Mean Square**	**Computed *f***	**Theoretical *f* α = 0.05**
Main effects					
A (*impeller speed*)	0.1173	1	0.1173	0.054	*5.32*
B (*frother dosage*)	7.2496	1	7.2496	3.351	*5.32*
C (*aeration rate*)	0.0163	1	0.0163	0.008	*5.32*
Two-factor interaction					
AB	1.7358	1	1.7358	0.802	*5.32*
AC	0.4128	1	0.4128	0.191	*5.32*
BC	0.7098	1	0.7098	0.328	*5.32*
Three-factor interaction					
ABC	0.2233	1	0.2233	0.103	*5.32*
Error	17.3070	8	2.1634		
Total	27.7717	15	-		

Table B2-5: Analysis of variance of the results expressed in grade of Fe_2O_3 in the concentrate

Source of Variation	**Sum of Squares**	**Degrees of freedom**	**Mean Square**	**Computed *f***	**Theoretical *f* α = 0.05**
Main effects					
A (*impeller speed*)	0.0170	1	0.0170	0.380	*5.32*
B (*frother dosage*)	0.0400	1	0.0400	0.892	*5.32*
C (*aeration rate*)	0.0148	1	0.0148	0.329	*5.32*
Two-factor interaction					
AB	0.0620	1	0.0620	1.383	*5.32*
AC	0.0163	1	0.0163	0.362	*5.32*
BC	0.0072	1	0.0072	0.161	*5.32*
Three-factor interaction					
ABC	0.0038	1	0.0038	0.086	*5.32*
Error	0.3588	8	0.0449		
Total	0.5199	7	-		

Appendix C1: Flotation Results Balance Sheets.

Table 1a: Metallurgical Balance Sheet of Test A1B1 Run 1

Flotation Time (sec)	Fraction	Weight (g)	Weight (%)	Content (%)										
				SiO_2	Al_2O_3	Fe_2O_3	TiO_2	MgO	CaO	K_2O	Na_2O	P_2O_5	F	LOI
480	Conc. 1	575.60	49.35	49.170	29.550	4.947	0.194	0.337	0.101	8.414	0.143	0.074	2.240	5.072
	Tail	590.70	50.65	71.980	16.800	1.003	0.126	0.167	0.221	6.005	0.536	0.270	1.270	1.899
	Head Cal.	1166.30	100.00	**60.723**	**23.092**	**2.949**	**0.160**	**0.251**	**0.162**	**7.194**	**0.342**	**0.173**	**1.749**	**3.465**
Time (sec)	**Fraction**	**Water Recovery** Weight (g)	Rate (g/s)	**Recovery %** SiO_2	Al_2O_3	Fe_2O_3	TiO_2	MgO	CaO	K_2O	Na_2O	P_2O_5	F	LOI
480	Conc. 1	1674.10	3.49	39.96	63.15	82.78	60.01	66.29	30.81	57.72	20.63	21.08	63.22	5.072
	Tail			60.04	36.85	17.22	39.99	33.71	69.19	42.28	79.37	78.92	36.78	1.899
	Head Cal.			100.00	100.00	100.00	100.00	100.00	100.00	100.00	100.00	100.00	100.00	3.465

Table 1b: Metallurgical Balance Sheet of Test A1B1 Run 2

Flotation Time (sec)	Fraction	Weight (g)	Weight (%)	Content (%)										
				SiO_2	Al_2O_3	Fe_2O_3	TiO_2	MgO	CaO	K_2O	Na_2O	P_2O_5	F	LOI
480	Conc. 1	350.70	29.45	47.540	30.770	4.849	0.170	0.346	0.067	8.267	0.122	0.036	2.490	5.729
	Tail	840.20	70.55	64.670	20.740	2.188	0.156	0.223	0.212	7.084	0.387	0.193	1.740	2.768
	Head Cal.	1190.90	100.00	**59.626**	**23.694**	**2.972**	**0.160**	**0.259**	**0.169**	**7.432**	**0.309**	**0.147**	**1.961**	**3.640**
Time (sec)	**Fraction**	**Water Recovery** Weight (g)	Rate (g/s)	**Recovery %** SiO_2	Al_2O_3	Fe_2O_3	TiO_2	MgO	CaO	K_2O	Na_2O	P_2O_5	F	LOI
480	Conc. 1	1024.80	2.14	23.48	38.24	48.05	31.26	39.31	11.70	32.76	11.63	7.22	37.39	5.729
	Tail			76.52	61.76	51.95	68.74	60.69	88.30	67.24	88.37	92.78	62.61	2.768
	Head Cal.			100.00	100.00	100.00	100.00	100.00	100.00	100.00	100.00	100.00	100.00	3.640

Table 1c: Metallurgical Balance Sheet of Test A1B1 Run 3

Flotation Time (sec)	Fraction	Weight (g)	Weight (%)	Content (%)										
				SiO_2	Al_2O_3	Fe_2O_3	TiO_2	MgO	CaO	K_2O	Na_2O	P_2O_5	F	LOI
480	Conc. 1	477.00	40.18	47.330	30.430	4.854	0.172	0.330	0.074	8.183	0.127	0.047	2.020	5.393
	Tail	710.20	59.82	69.430	18.220	1.460	0.130	0.194	0.211	6.259	0.493	0.246	1.420	2.237
	Head Cal.	1187.20	100.00	**60.551**	**23.126**	**2.824**	**0.147**	**0.249**	**0.156**	**7.032**	**0.346**	**0.166**	**1.661**	**3.505**
Time (sec)	**Fraction**	**Water Recovery** Weight (g)	Rate (g/s)	**Recovery %** SiO_2	Al_2O_3	Fe_2O_3	TiO_2	MgO	CaO	K_2O	Na_2O	P_2O_5	F	LOI
480	Conc. 1	1333.90	2.78	31.41	52.87	69.07	47.05	53.33	18.98	46.75	14.75	11.37	48.86	5.393
	Tail			68.59	47.13	30.93	52.95	46.67	81.02	53.25	85.25	88.63	51.14	2.237
	Head Cal.			100.00	100.00	100.00	100.00	100.00	100.00	100.00	100.00	100.00	100.00	3.505

Table 2a: Metallurgical Balance Sheet of Test A2B1 Run 1

Flotation Time (sec)	Fraction	Weight (g)	Weight (%)	Content (%)										
				SiO_2	Al_2O_3	Fe_2O_3	TiO_2	MgO	CaO	K_2O	Na_2O	P_2O_5	F	LOI
480	Conc. 1	553.70	47.12	48.240	29.660	4.912	0.191	0.335	0.080	8.525	0.147	0.056	2.610	5.666
	Tail	621.30	52.88	70.990	17.340	1.086	0.123	0.182	0.245	6.056	0.518	0.285	1.250	2.161
	Head Cal.	1175.00	100.00	**60.269**	**23.146**	**2.889**	**0.155**	**0.254**	**0.167**	**7.219**	**0.343**	**0.177**	**1.891**	**3.813**
Time (sec)	**Fraction**	**Water Recovery**		**Recovery %**										
		Weight (g)	Rate (g/s)	SiO_2	Al_2O_3	Fe_2O_3	TiO_2	MgO	CaO	K_2O	Na_2O	P_2O_5	F	LOI
480	Conc. 1	1532.80	3.19	37.72	60.39	80.12	58.05	62.13	22.43	55.64	20.19	14.90	65.04	5.666
	Tail			62.28	39.61	19.88	41.95	37.87	77.57	44.36	79.81	85.10	34.96	2.161
	Head Cal.			100.00	100.00	100.00	100.00	100.00	100.00	100.00	100.00	100.00	100.00	3.813

Table 2b: Metallurgical Balance Sheet of Test A2B1 Run 2

Flotation Time (sec)	Fraction	Weight (g)	Weight (%)	Content (%)										
				SiO_2	Al_2O_3	Fe_2O_3	TiO_2	MgO	CaO	K_2O	Na_2O	P_2O_5	F	LOI
480	Conc. 1	366.60	30.86	47.470	30.570	5.026	0.175	0.340	0.064	8.423	0.119	0.036	2.470	5.634
	Tail	821.50	69.14	65.860	20.230	2.010	0.147	0.222	0.199	6.746	0.412	0.206	1.720	2.607
	Head Cal.	1188.10	100.00	**60.186**	**23.421**	**2.941**	**0.156**	**0.258**	**0.157**	**7.263**	**0.322**	**0.154**	**1.951**	**3.541**
Time (sec)	**Fraction**	**Water Recovery**		**Recovery %**										
		Weight (g)	Rate (g/s)	SiO_2	Al_2O_3	Fe_2O_3	TiO_2	MgO	CaO	K_2O	Na_2O	P_2O_5	F	LOI
480	Conc. 1	1132.60	2.36	24.34	40.28	52.74	34.69	40.60	12.46	35.78	11.42	7.23	39.06	5.634
	Tail			75.66	59.72	47.26	65.31	59.40	87.54	64.22	88.58	92.77	60.94	2.607
	Head Cal.			100.00	100.00	100.00	100.00	100.00	100.00	100.00	100.00	100.00	100.00	3.541

Table 2c: Metallurgical Balance Sheet of Test A2B1 Run 3

Flotation Time (sec)	Fraction	Weight (g)	Weight (%)	Content (%)										
				SiO_2	Al_2O_3	Fe_2O_3	TiO_2	MgO	CaO	K_2O	Na_2O	P_2O_5	F	LOI
480	Conc. 1	572.30	48.29	48.880	29.820	4.826	0.184	0.336	0.077	8.413	0.146	0.061	2.460	5.169
	Tail	612.80	51.71	69.660	16.300	0.901	0.110	0.171	0.185	5.727	0.538	0.226	1.230	1.818
	Head Cal.	1185.10	100.00	**59.625**	**22.829**	**2.797**	**0.146**	**0.251**	**0.133**	**7.024**	**0.349**	**0.146**	**1.824**	**3.436**
Time (sec)	**Fraction**	**Water Recovery**		**Recovery %**										
		Weight (g)	Rate (g/s)	SiO_2	Al_2O_3	Fe_2O_3	TiO_2	MgO	CaO	K_2O	Na_2O	P_2O_5	F	LOI
480	Conc. 1	1696.50	3.53	39.59	63.08	83.34	60.97	64.73	27.99	57.84	20.22	20.13	65.13	5.169
	Tail			60.41	36.92	16.66	39.03	35.27	72.01	42.16	79.78	79.87	34.87	1.818
	Head Cal.			100.00	100.00	100.00	100.00	100.00	100.00	100.00	100.00	100.00	100.00	3.436

Table 3a: Metallurgical Balance Sheet of Test A3B1 Run 1

Flotation Time (sec)	Fraction	Weight (g)	Weight (%)	Content (%)										
				SiO_2	Al_2O_3	Fe_2O_3	TiO_2	MgO	CaO	K_2O	Na_2O	P_2O_5	F	LOI
480	Conc. 1	758.80	64.73	50.040	28.090	4.142	0.186	0.322	0.149	7.930	0.170	0.117	2.270	4.750
	Tail	413.40	35.27	77.690	13.100	0.445	0.075	0.117	0.074	5.803	0.666	0.166	0.870	1.156
	Head Cal.	1172.20	100.00	**59.791**	**22.803**	**2.838**	**0.147**	**0.250**	**0.123**	**7.180**	**0.345**	**0.134**	**1.776**	**3.483**
		Water Recovery		**Recovery %**										
Time (sec)	Fraction	Weight (g)	Rate (g/s)	SiO_2	Al_2O_3	Fe_2O_3	TiO_2	MgO	CaO	K_2O	Na_2O	P_2O_5	F	LOI
480	Conc. 1	2285.70	4.76	54.18	79.74	94.47	82.01	83.48	78.70	71.50	31.90	56.40	82.73	4.750
	Tail			45.82	20.26	5.53	17.99	16.52	21.30	28.50	68.10	43.60	17.27	1.156
	Head Cal.			100.00	100.00	100.00	100.00	100.00	100.00	100.00	100.00	100.00	100.00	3.483

Table 3b: Metallurgical Balance Sheet of Test A3B1 Run 2

Flotation Time (sec)	Fraction	Weight (g)	Weight (%)	Content (%)										
				SiO_2	Al_2O_3	Fe_2O_3	TiO_2	MgO	CaO	K_2O	Na_2O	P_2O_5	F	LOI
480	Conc. 1	704.90	59.34	49.990	29.420	4.574	0.181	0.338	0.121	8.239	0.159	0.096	2.100	5.020
	Tail	483.10	40.66	76.620	13.980	0.494	0.093	0.130	0.136	5.589	0.628	0.216	1.070	1.280
	Head Cal.	1188.00	100.00	**60.819**	**23.141**	**2.915**	**0.145**	**0.253**	**0.127**	**7.161**	**0.350**	**0.145**	**1.681**	**3.499**
		Water Recovery		**Recovery %**										
Time (sec)	**Fraction**	Weight (g)	Rate (g/s)	SiO_2	Al_2O_3	Fe_2O_3	TiO_2	MgO	CaO	K_2O	Na_2O	P_2O_5	F	LOI
480	Conc. 1	2161.30	4.50	48.77	75.43	93.11	73.92	79.14	56.49	68.26	26.98	39.31	74.12	5.020
	Tail			51.23	24.57	6.89	26.08	20.86	43.51	31.74	73.02	60.69	25.88	1.280
	Head Cal.			100.00	100.00	100.00	100.00	100.00	100.00	100.00	100.00	100.00	100.00	3.499

Table 3c: Metallurgical Balance Sheet of Test A3B1 Run 3

Flotation Time (sec)	Fraction	Weight (g)	Weight (%)	Content (%)										
				SiO_2	Al_2O_3	Fe_2O_3	TiO_2	MgO	CaO	K_2O	Na_2O	P_2O_5	F	LOI
480	Conc. 1	659.30	55.58	49.240	29.510	4.694	0.189	0.327	0.092	8.397	0.154	0.064	2.350	5.046
	Tail	527.00	44.42	75.630	14.510	0.599	0.105	0.141	0.172	5.700	0.620	0.228	1.000	1.468
	Head Cal.	1186.30	100.00	**60.963**	**22.846**	**2.875**	**0.152**	**0.244**	**0.128**	**7.199**	**0.361**	**0.137**	**1.750**	**3.457**
		Water Recovery		**Recovery %**										
Time (sec)	**Fraction**	Weight (g)	Rate (g/s)	SiO_2	Al_2O_3	Fe_2O_3	TiO_2	MgO	CaO	K_2O	Na_2O	P_2O_5	F	LOI
480	Conc. 1	1930.00	4.02	44.89	71.79	90.74	69.25	74.37	40.19	64.83	23.71	25.99	74.62	5.046
	Tail			55.11	28.21	9.26	30.75	25.63	59.81	35.17	76.29	74.01	25.38	1.468
	Head Cal.			100.00	100.00	100.00	100.00	100.00	100.00	100.00	100.00	100.00	100.00	3.457

Table 4a: Metallurgical Balance Sheet of Test A1B3 Run 1

Flotation Time (sec)	Fraction	Weight (g)	Weight (%)	Content (%)										
				SiO_2	Al_2O_3	Fe_2O_3	TiO_2	MgO	CaO	K_2O	Na_2O	P_2O_5	F	LOI
480	Conc. 1	481.80	40.48	48.730	29.710	4.973	0.180	0.345	0.051	8.455	0.138	0.046	2.390	5.314
	Tail	708.30	59.52	68.540	18.490	1.610	0.146	0.197	0.275	6.579	0.467	0.285	1.490	2.244
	Head Cal.	1190.10	100.00	**60.520**	**23.032**	**2.971**	**0.160**	**0.257**	**0.184**	**7.338**	**0.334**	**0.188**	**1.854**	**3.487**

Time (sec)	Fraction	Water Recovery		Recovery %										
		Weight (g)	Rate (g/s)	SiO_2	Al_2O_3	Fe_2O_3	TiO_2	MgO	CaO	K_2O	Na_2O	P_2O_5	F	LOI
480	Conc. 1	1415.90	2.95	32.60	52.22	67.75	45.61	54.36	11.14	46.64	16.74	9.89	52.18	5.314
	Tail			67.40	47.78	32.25	54.39	45.64	88.86	53.36	83.26	90.11	47.82	2.244
	Head Cal.			100.00	100.00	100.00	100.00	100.00	100.00	100.00	100.00	100.00	100.00	3.487

Table 4b: Metallurgical Balance Sheet of Test A1B3 Run 2

Flotation Time (sec)	Fraction	Weight (g)	Weight (%)	Content (%)										
				SiO_2	Al_2O_3	Fe_2O_3	TiO_2	MgO	CaO	K_2O	Na_2O	P_2O_5	F	LOI
480	Conc. 1	475.00	39.92	48.340	30.510	4.864	0.166	0.347	0.046	8.243	0.130	0.045	2.130	5.41
	Tail	714.90	60.08	68.490	18.540	1.665	0.145	0.197	0.272	6.510	0.455	0.279	1.560	2.25
	Head Cal.	1189.90	100.00	**60.446**	**23.318**	**2.942**	**0.153**	**0.257**	**0.182**	**7.202**	**0.325**	**0.186**	**1.788**	**3.51**

Time (sec)	Fraction	Water Recovery		Recovery %										
		Weight (g)	Rate (g/s)	SiO_2	Al_2O_3	Fe_2O_3	TiO_2	MgO	CaO	K_2O	Na_2O	P_2O_5	F	LOI
480	Conc. 1	1516.30	3.16	31.92	52.23	66.00	43.20	53.92	10.16	45.69	15.95	9.68	47.57	5.41
	Tail			68.08	47.77	34.00	56.80	46.08	89.84	54.31	84.05	90.32	52.43	2.25
	Head Cal.			100.00	100.00	100.00	100.00	100.00	100.00	100.00	100.0	100	100	3.51

Table 4c: Metallurgical Balance Sheet of Test A1B3 Run 3

Flotation Time (sec)	Fraction	Weight (g)	Weight (%)	Content (%)										
				SiO_2	Al_2O_3	Fe_2O_3	TiO_2	MgO	CaO	K_2O	Na_2O	P_2O_5	F	LOI
480	Conc. 1	244.70	20.51	47.230	30.860	5.012	0.165	0.339	0.033	8.189	0.114	0.035	2.420	5.95
	Tail	948.60	79.49	62.950	21.810	2.531	0.157	0.241	0.206	7.201	0.369	0.202	1.930	2.78
	Head Cal.	1193.30	100.00	**59.726**	**23.666**	**3.040**	**0.159**	**0.261**	**0.171**	**7.404**	**0.317**	**0.168**	**2.030**	**3.43**

Time (sec)	Fraction	Water Recovery		Recovery %										
		Weight (g)	Rate (g/s)	SiO_2	Al_2O_3	Fe_2O_3	TiO_2	MgO	CaO	K_2O	Na_2O	P_2O_5	F	LOI
480	Conc. 1	835.40	1.74	16.22	26.74	33.81	21.33	26.62	3.97	22.68	7.38	4.28	24.44	5.95
	Tail			83.78	73.26	66.19	78.67	73.38	96.03	77.32	92.62	95.72	75.56	2.78
	Head Cal.			100.00	100.00	100.00	100.00	100.00	100.00	100.00	100.0	100.0	100.0	3.43

Table 5a: Metallurgical Balance Sheet of Test A3B2 Run 1

Flotation Time (sec)	Fraction	Weight (g)	Weight (%)	Content (%)										
				SiO_2	Al_2O_3	Fe_2O_3	TiO_2	MgO	CaO	K_2O	Na_2O	P_2O_5	F	LOI
480	Conc. 1	725.90	60.92	50.590	29.140	4.292	0.176	0.329	0.058	8.129	0.160	0.070	2.360	5.122
	Tail	465.70	39.08	76.910	13.440	0.470	0.102	0.121	0.261	5.679	0.647	0.321	1.100	1.224
	Head Cal.	1191.60	100.00	**60.876**	**23.004**	**2.798**	**0.147**	**0.248**	**0.137**	**7.171**	**0.350**	**0.168**	**1.868**	**3.599**
		Water Recovery		**Recovery %**										
Time (sec)	**Fraction**	Weight (g)	Rate (g/s)	SiO_2	Al_2O_3	Fe_2O_3	TiO_2	MgO	CaO	K_2O	Na_2O	P_2O_5	F	LOI
480	Conc. 1	2166.90	4.51	50.62	77.17	93.44	72.90	80.91	25.79	69.05	27.82	25.37	76.98	5.122
	Tail			49.38	22.83	6.56	27.10	19.09	74.21	30.95	72.18	74.63	23.02	1.224
	Head Cal.			100	100	100	100	100	100	100	100	100	100	3.59

Table 5b: Metallurgical Balance Sheet of Test A3B2 Run 2

Flotation Time (sec)	Fraction	Weight (g)	Weight (%)	Content (%)										
				SiO_2	Al_2O_3	Fe_2O_3	TiO_2	MgO	CaO	K_2O	Na_2O	P_2O_5	F	LOI
480	Conc. 1	650.80	54.63	49.490	29.280	4.687	0.173	0.332	0.047	8.363	0.150	0.045	2.620	5.30
	Tail	540.50	45.37	74.530	15.150	0.646	0.114	0.153	0.238	5.903	0.597	0.282	1.110	1.50
	Head Cal.	1191.30	100.00	**60.851**	**22.869**	**2.853**	**0.146**	**0.251**	**0.133**	**7.247**	**0.353**	**0.153**	**1.935**	**3.58**
		Water Recovery		**Recovery %**										
Time (sec)	**Fraction**	Weight (g)	Rate (g/s)	SiO_2	Al_2O_3	Fe_2O_3	TiO_2	MgO	CaO	K_2O	Na_2O	P_2O_5	F	LOI
480	Conc. 1	1885.90	3.93	44.43	69.94	89.74	64.63	72.32	19.08	63.04	23.23	16.12	73.97	5.30
	Tail			55.57	30.06	10.26	35.37	27.68	80.92	36.96	76.77	83.88	26.03	1.50
	Head Cal.			100.00	100.00	100.00	100.00	100.00	100.00	100.00	100.0	100.0	100.0	3.58

Table 5c: Metallurgical Balance Sheet of Test A3B2 Run 3

Flotation Time (sec)	Fraction	Weight (g)	Weight (%)	Content (%)										
				SiO_2	Al_2O_3	Fe_2O_3	TiO_2	MgO	CaO	K_2O	Na_2O	P_2O_5	F	LOI
480	Conc. 1	704.60	59.28	50.340	28.700	4.561	0.184	0.328	0.061	8.426	0.172	0.057	2.650	5.01
	Tail	484.00	40.72	75.780	14.620	0.526	0.125	0.143	0.268	5.505	0.604	0.325	1.110	1.26
	Head Cal.	1188.60	100.00	**60.699**	**22.967**	**2.918**	**0.160**	**0.253**	**0.146**	**7.237**	**0.348**	**0.166**	**2.023**	**3.48**
		Water Recovery		**Recovery %**										
Time (sec)	**Fraction**	Weight (g)	Rate (g/s)	SiO_2	Al_2O_3	Fe_2O_3	TiO_2	MgO	CaO	K_2O	Na_2O	P_2O_5	F	LOI
480	Conc. 1	2070.60	4.31	49.16	74.08	92.66	68.18	76.95	25.01	69.02	29.31	20.34	77.66	5.01
	Tail			50.84	25.92	7.34	31.82	23.05	74.99	30.98	70.69	79.66	22.34	1.26
	Head Cal.			100.00	100.00	100.00	100.00	100.00	100.00	100.00	100.0	100.0	100.0	3.48

Table 6a: Metallurgical Balance Sheet of Test A2B2 Run 1

Flotation Time (sec)	Fraction	Weight (g)	Weight (%)	Content (%)										
				SiO_2	Al_2O_3	Fe_2O_3	TiO_2	MgO	CaO	K_2O	Na_2O	P_2O_5	F	LOI
480	Conc. 1	507.50	42.60	48.070	30.900	4.670	0.163	0.345	0.041	8.101	0.129	0.041	2.170	5.65
	Tail	683.70	57.40	69.700	18.140	1.451	0.143	0.187	0.228	6.277	0.471	0.253	1.380	2.06
	Head Cal.	1191.20	100.00	**60.485**	**23.576**	**2.822**	**0.152**	**0.254**	**0.148**	**7.054**	**0.325**	**0.163**	**1.717**	**3.59**
Time (sec)	**Fraction**	**Water Recovery**		**Recovery %**										
		Weight (g)	Rate (g/s)	SiO_2	Al_2O_3	Fe_2O_3	TiO_2	MgO	CaO	K_2O	Na_2O	P_2O_5	F	LOI
480	Conc. 1	1402.10	2.92	33.86	55.84	70.49	45.83	57.80	11.65	48.93	16.90	10.74	53.86	5.65
	Tail			66.14	44.16	29.51	54.17	42.20	88.35	51.07	83.10	89.26	46.14	2.06
	Head Cal.			100.00	100.00	100.00	100.00	100.00	100.00	100.00	100.0	100.0	100.0	3.59

Table 6b: Metallurgical Balance Sheet of Test A2B2 Run 2

Flotation Time (sec)	Fraction	Weight (g)	Weight (%)	Content (%)										
				SiO_2	Al_2O_3	Fe_2O_3	TiO_2	MgO	CaO	K_2O	Na_2O	P_2O_5	F	LOI
480	Conc. 1	685.10	57.43	49.640	30.100	4.491	0.170	0.334	0.067	7.978	0.141	0.067	2.050	5.25
	Tail	507.90	42.57	75.900	14.260	0.554	0.127	0.136	0.341	5.489	0.608	0.370	1.250	1.27
	Head Cal.	1193.00	100.00	**60.820**	**23.356**	**2.815**	**0.152**	**0.250**	**0.184**	**6.918**	**0.340**	**0.196**	**1.709**	**3.56**
Time (sec)	Fraction	**Water Recovery**		**Recovery %**										
		Weight (g)	Rate (g/s)	SiO_2	Al_2O_3	Fe_2O_3	TiO_2	MgO	CaO	K_2O	Na_2O	P_2O_5	F	LOI
480	Conc. 1	1934.10	4.03	46.87	74.01	91.62	64.36	76.81	21.05	66.22	23.83	19.63	68.87	5.25
	Tail			53.13	25.99	8.38	35.64	23.19	78.95	33.78	76.17	80.37	31.13	1.27
	Head Cal.			100.00	100.00	100.00	100.00	100.00	100.00	100.00	100.0	100.0	100.0	3.56

Table 6c: Metallurgical Balance Sheet of Test A2B2 Run 3

Flotation Time (sec)	Fraction	Weight (g)	Weight (%)	Content (%)										
				SiO_2	Al_2O_3	Fe_2O_3	TiO_2	MgO	CaO	K_2O	Na_2O	P_2O_5	F	LOI
480	Conc. 1	650.20	54.54	49.280	29.840	4.768	0.180	0.341	0.062	8.197	0.144	0.062	2.130	5.24
	Tail	541.90	45.46	74.990	14.810	0.642	0.132	0.141	0.339	5.606	0.589	0.399	1.190	1.44
	Head Cal.	1192.10	100.00	**60.967**	**23.008**	**2.893**	**0.158**	**0.250**	**0.188**	**7.019**	**0.346**	**0.215**	**1.703**	**3.51**
Time (sec)	**Fraction**	**Water Recovery**		**Recovery %**										
		Weight (g)	Rate (g/s)	SiO_2	Al_2O_3	Fe_2O_3	TiO_2	MgO	CaO	K_2O	Na_2O	P_2O_5	F	LOI
480	Conc. 1	1917.30	3.99	44.09	70.74	89.91	62.07	74.37	17.90	63.69	22.68	15.71	68.23	5.24
	Tail			55.91	29.26	10.09	37.93	25.63	82.10	36.31	77.32	84.29	31.77	1.44
	Head Cal.			100.00	100.00	100.00	100.00	100.00	100.00	100.00	100.0	100.0	100.0	3.51

Table 7a: Metallurgical Balance Sheet of Test A1B2 Run 1

Flotation Time (sec)	Fraction	Weight (g)	Weight (%)	Content (%)										
				SiO_2	Al_2O_3	Fe_2O_3	TiO_2	MgO	CaO	K_2O	Na_2O	P_2O_5	F	LOI
480	Conc. 1	667.00	55.92	49.910	29.350	4.549	0.181	0.335	0.065	8.276	0.151	0.060	2.340	5.15
	Tail	525.80	44.08	74.840	14.750	0.663	0.113	0.146	0.338	5.821	0.624	0.389	1.190	1.41
	Head Cal.	1192.80	100.00	**60.899**	**22.914**	**2.836**	**0.151**	**0.252**	**0.186**	**7.194**	**0.360**	**0.205**	**1.833**	**3.50**
		Water Recovery		**Recovery %**										
Time (sec)	**Fraction**	Weight (g)	Rate (g/s)	SiO_2	Al_2O_3	Fe_2O_3	TiO_2	MgO	CaO	K_2O	Na_2O	P_2O_5	F	LOI
480	Conc. 1	1946.70	4.06	45.83	71.62	89.70	67.02	74.43	19.71	64.33	23.49	16.36	71.38	5.15
	Tail			54.17	28.38	10.30	32.98	25.57	80.29	35.67	76.51	83.64	28.62	1.41
	Head Cal.			100.00	100.00	100.00	100.00	100.00	100.00	100.00	100.0	100.0	100.0	3.50

Table 7b: Metallurgical Balance Sheet of Test A1B2 Run 2

Flotation Time (sec)	Fraction	Weight (g)	Weight (%)	Content (%)										
				SiO_2	Al_2O_3	Fe_2O_3	TiO_2	MgO	CaO	K_2O	Na_2O	P_2O_5	F	LOI
480	Conc. 1	603.20	50.54	49.390	29.710	4.633	0.181	0.343	0.095	8.268	0.157	0.072	2.100	5.27
	Tail	590.20	49.46	72.980	16.070	0.898	0.116	0.168	0.297	5.996	0.579	0.342	1.180	1.62
	Head Cal.	1193.40	100.00	**61.057**	**22.964**	**2.786**	**0.149**	**0.256**	**0.195**	**7.144**	**0.366**	**0.206**	**1.645**	**3.47**
		Water Recovery		**Recovery %**										
Time (sec)	**Fraction**	Weight (g)	Rate (g/s)	SiO_2	Al_2O_3	Fe_2O_3	TiO_2	MgO	CaO	K_2O	Na_2O	P_2O_5	F	LOI
480	Conc. 1	1697.60	3.54	40.89	65.39	84.06	61.46	67.60	24.60	58.49	21.70	17.71	64.52	5.27
	Tail			59.11	34.61	15.94	38.54	32.40	75.40	41.51	78.30	82.29	35.48	1.62
	Head Cal.			100.00	100.00	100.00	100.00	100.00	100.00	100.00	100.0	100.0	100.0	3.47

Table 7c: Metallurgical Balance Sheet of Test A1B2 Run 3

Flotation Time (sec)	Fraction	Weight (g)	Weight (%)	Content (%)										
				SiO_2	Al_2O_3	Fe_2O_3	TiO_2	MgO	CaO	K_2O	Na_2O	P_2O_5	F	LOI
480	Conc. 1	678.30	56.88	50.070	29.130	4.703	0.186	0.329	0.077	8.296	0.150	0.067	2.180	5.08
	Tail	514.20	43.12	75.690	14.100	0.593	0.112	0.134	0.357	5.697	0.636	0.407	1.190	1.36
	Head Cal.	1192.50	100.00	**61.117**	**22.649**	**2.931**	**0.154**	**0.245**	**0.198**	**7.175**	**0.360**	**0.214**	**1.753**	**3.48**
		Water Recovery		**Recovery %**										
Time (sec)	**Fraction**	Weight (g)	Rate (g/s)	SiO_2	Al_2O_3	Fe_2O_3	TiO_2	MgO	CaO	K_2O	Na_2O	P_2O_5	F	LOI
480	Conc. 1	1985.50	4.14	46.60	73.16	91.28	68.66	76.41	22.22	65.76	23.73	17.84	70.73	5.08
	Tail			53.40	26.84	8.72	31.34	23.59	77.78	34.24	76.27	82.16	29.27	1.36
	Head Cal.			100.00	100.00	100.00	100.00	100.00	100.00	100.00	100.0	100.0	100.0	3.48

Table 8a: Metallurgical Balance Sheet of Test A3B3 Run 1

Flotation Time (sec)	Fraction	Weight (g)	Weight (%)	Content (%)										
				SiO_2	Al_2O_3	Fe_2O_3	TiO_2	MgO	CaO	K_2O	Na_2O	P_2O_5	F	LOI
480	Conc. 1	578.20	49.73	48.580	30.090	4.854	0.180	0.341	0.041	8.368	0.137	0.044	2.290	5.39
	Tail	584.50	50.27	72.700	16.190	0.956	0.128	0.160	0.242	5.926	0.556	0.257	1.180	1.94
	Head Cal.	1162.70	100.00	**60.705**	**23.102**	**2.895**	**0.154**	**0.250**	**0.142**	**7.140**	**0.348**	**0.151**	**1.732**	**3.66**
		Water Recovery		**Recovery %**										
Time (sec)	**Fraction**	Weight (g)	Rate (g/s)	SiO_2	Al_2O_3	Fe_2O_3	TiO_2	MgO	CaO	K_2O	Na_2O	P_2O_5	F	LOI
480	Conc. 1	1666.00	3.47	39.80	64.77	83.39	58.18	67.83	14.32	58.28	19.60	14.48	65.75	5.39
	Tail			60.20	35.23	16.61	41.82	32.17	85.68	41.72	80.40	85.52	34.25	1.94
	Head Cal.			100.00	100.00	100.00	100.00	100.00	100.00	100.00	100.0	100.0	100.0	3.66

Table 8b: Metallurgical Balance Sheet of Test A3B3 Run 2

Flotation Time (sec)	Fraction	Weight (g)	Weight (%)	Content (%)										
				SiO_2	Al_2O_3	Fe_2O_3	TiO_2	MgO	CaO	K_2O	Na_2O	P_2O_5	F	LOI
480	Conc.	730.40	61.25	50.560	29.230	4.456	0.184	0.329	0.063	8.050	0.148	0.063	2.210	5.00
	Tail	462.00	38.75	77.230	13.360	0.456	0.124	0.114	0.300	5.402	0.612	0.355	1.110	1.20
	Head Cal.	1192.40	100.00	**60.893**	**23.081**	**2.906**	**0.161**	**0.246**	**0.155**	**7.024**	**0.328**	**0.176**	**1.784**	**3.53**
		Water Recovery		**Recovery %**										
Time (sec)	**Fraction**	Weight (g)	Rate (g/s)	SiO_2	Al_2O_3	Fe_2O_3	TiO_2	MgO	CaO	K_2O	Na_2O	P_2O_5	F	LOI
480	Conc.	2196.80	4.58	50.86	77.57	93.92	70.11	82.02	25.04	70.20	27.66	21.91	75.89	5.00
	Tail			49.14	22.43	6.08	29.89	17.98	74.96	29.80	72.34	78.09	24.11	1.20
	Head Cal.			100.00	100.00	100.00	100.00	100.00	100.00	100.00	100.0	100.0	100.0	3.53

Table 8c: Metallurgical Balance Sheet of Test A3B3 Run 3

Flotation Time (sec)	Fraction	Weight (g)	Weight (%)	Content (%)										
				SiO_2	Al_2O_3	Fe_2O_3	TiO_2	MgO	CaO	K_2O	Na_2O	P_2O_5	F	LOI
480	Conc.	578.70	48.73	48.660	30.340	4.745	0.172	0.341	0.042	8.170	0.128	0.039	2.180	5.47
	Tail	608.90	51.27	71.610	16.550	0.850	0.131	0.174	0.256	5.587	0.522	0.275	1.090	1.81
	Head Cal.	1187.60	100.00	**60.427**	**23.270**	**2.748**	**0.151**	**0.255**	**0.152**	**6.846**	**0.330**	**0.160**	**1.621**	**3.60**
		Water Recovery		**Recovery %**										
Time (sec)	**Fraction**	Weight (g)	Rate (g/s)	SiO_2	Al_2O_3	Fe_2O_3	TiO_2	MgO	CaO	K_2O	Na_2O	P_2O_5	F	LOI
480	Conc.	1632.20	3.40	39.24	63.53	84.14	55.51	65.07	13.43	58.16	18.90	11.88	65.53	5.47
	Tail			60.76	36.47	15.86	44.49	34.93	86.57	41.84	81.10	88.12	34.47	1.81
	Head Cal.			100.00	100.00	100.00	100.00	100.00	100.00	100.00	100.0	100.0	100.0	3.60

Table 9a: Metallurgical Balance Sheet of Test A2B3 Run 1

Flotation Time (sec)	Fraction	Weight (g)	Weight (%)	Content (%) SiO_2	Al_2O_3	Fe_2O_3	TiO_2	MgO	CaO	K_2O	Na_2O	P_2O_5	F	LOI
480	Conc.	625.20	52.55	49.270	29.750	4.588	0.173	0.334	0.047	8.101	0.147	0.051	2.300	5.57
	Tail	564.50	47.45	73.990	15.460	0.776	0.133	0.152	0.313	5.665	0.560	0.328	1.200	1.68
	Head Cal.	1189.70	100.00	**60.999**	**22.970**	**2.779**	**0.154**	**0.248**	**0.173**	**6.945**	**0.343**	**0.182**	**1.778**	**3.73**
		Water Recovery		**Recovery %**										
Time (sec)	**Fraction**	Weight (g)	Rate (g/s)	SiO_2	Al_2O_3	Fe_2O_3	TiO_2	MgO	CaO	K_2O	Na_2O	P_2O_5	F	LOI
480	Conc.	1824.40	3.80	42.45	68.06	86.75	59.03	70.88	14.26	61.30	22.52	14.69	67.98	5.57
	Tail			57.55	31.94	13.25	40.97	29.12	85.74	38.70	77.48	85.31	32.02	1.68
	Head Cal.			100.00	100.00	100.00	100.00	100.00	100.00	100.00	100.0	100.0	100.0	3.73

Table 9b: Metallurgical Balance Sheet of Test A2B3 Run 2

Flotation Time (sec)	Fraction	Weight (g)	Weight (%)	Content (%) SiO_2	Al_2O_3	Fe_2O_3	TiO_2	MgO	CaO	K_2O	Na_2O	P_2O_5	F	LOI
480	Conc.	650.20	54.47	49.430	30.050	4.545	0.179	0.341	0.065	8.060	0.141	0.057	1.950	5.37
	Tail	543.40	45.53	74.800	14.870	0.681	0.123	0.137	0.294	5.747	0.586	0.348	1.100	1.57
	Head Cal.	1193.60	100.00	**60.980**	**23.139**	**2.786**	**0.154**	**0.248**	**0.169**	**7.007**	**0.344**	**0.189**	**1.563**	**3.64**
		Water Recovery		**Recovery %**										
Time (sec)	Fraction	Weight (g)	Rate (g/s)	SiO_2	Al_2O_3	Fe_2O_3	TiO_2	MgO	CaO	K_2O	Na_2O	P_2O_5	F	LOI
480	Conc.	1889.40	3.94	44.16	70.74	88.88	63.52	74.86	20.82	62.66	22.35	16.39	67.96	5.37
	Tail			55.84	29.26	11.12	36.48	25.14	79.18	37.34	77.65	83.61	32.04	1.57
	Head Cal.			100.00	100.00	100.00	100.00	100.00	100.00	100.00	100.0	100.0	100.0	3.64

Table 9c: Metallurgical Balance Sheet of Test A2B3 Run 3

Flotation Time (sec)	Fraction	Weight (g)	Weight (%)	Content (%) SiO_2	Al_2O_3	Fe_2O_3*	TiO_2	MgO	CaO	K_2O	Na_2O	P_2O_5	F	LOI
480	Conc.	740.60	62.13	50.680	28.770	4.258	0.178	0.329	0.074	8.045	0.171	0.067	2.450	5.41
	Tail	451.40	37.87	77.030	13.180	0.455	0.121	0.117	0.323	5.500	0.649	0.363	1.100	1.42
	Head Cal.	1192.00	100.00	**60.659**	**22.866**	**2.818**	**0.156**	**0.249**	**0.168**	**7.081**	**0.352**	**0.179**	**1.939**	**3.90**
		Water Recovery		**Recovery %**										
Time (sec)	**Fraction**	Weight (g)	Rate (g/s)	SiO_2	Al_2O_3	Fe_2O_3	TiO_2	MgO	CaO	K_2O	Na_2O	P_2O_5	F	LOI
480	Conc.	2242.30	4.67	51.91	78.17	93.89	70.71	82.19	27.29	70.59	30.18	23.24	78.51	5.41
	Tail			48.09	21.83	6.11	29.29	17.81	72.71	29.41	69.82	76.76	21.49	1.42
	Head Cal.			100.00	100.00	100.00	100.00	100.00	100.00	100.00	100.0	100.0	100.0	3.90

*** Total Fe as Fe_2O_3**

Appendix C2: Statistical Analysis of the Floatability Results.

This was a two-factor factorial experiment using repeated observations in a completely randomised design of n (3) replications of treatment combinations determined by "*a*" levels of factor *A* (collector dosage) and "*b*" levels of factor *B* (pH) as shown in Table C2-1. In Table 8.5, a_1, a_2 and a_3 represent the collector dosage of 150 g/t, 250 g/t and 500 g/t respectively while b_1, b_2 and b_3 represent the pH of 2.5, 3.5 and 5 respectively.

Table C2-1: Two-factor experiment with three replications.

Collector Dosage, *A*	**pH, *B***		
	b_1	b_2	b_3
a_1	$a_1b_1^1$ $a_1b_1^2$ $a_1b_1^3$	$a_1b_2^1$ $a_1b_2^2$ $a_1b_2^3$	$a_1b_3^1$ $a_1b_3^2$ $a_1b_3^3$
a_2	$a_2b_1^1$ $a_2b_1^2$ $a_2b_1^3$	$a_2b_2^1$ $a_2b_2^2$ $a_2b_2^3$	$a_2b_3^1$ $a_2b_3^2$ $a_2b_3^3$
a_3	$a_3b_1^1$ $a_3b_1^2$ $a_3b_1^3$	$a_3b_2^1$ $a_3b_2^2$ $a_3b_2^3$	$a_3b_3^1$ $a_3b_3^2$ $a_3b_3^3$

The computations in an analysis-of-variance, for a two-factor experiment with n replications, are summarized as in Table C2-3.

The sum-of-squares (SS) are usually obtained by constructing the following table of totals for the flotation results and presented as shown in Table C2-2:

Table C2-2: Table of Totals

	B				
A	1	2	⋯	b	Total
1	T11.	T12.	⋯	T1b.	T1..
2	T21.	T22.	⋯	T2b.	T2..
⋮	⋮	⋮		⋮	⋮
a	Ta1.	Ta2.	⋯	Tab.	Ta..
Total	T.1.	T.2.	⋯	T.b.	T...

and using the following formulas (Sum-of-Square Computing Formulas):

$$SST = \sum_{i=1}^{a}\sum_{j=1}^{b}\sum_{k=1}^{n} y_{ijk}^2 - \frac{T^2...}{abn}$$

$$SSA = \frac{\sum_{i=1}^{a} T_{i..}^2}{bn} - \frac{T^2...}{abn}$$

$$SSB = \frac{\sum_{j=1}^{b} T_{.j.}^2}{an} - \frac{T^2...}{abn}$$

$$SS(AB) = \frac{\sum_{i=1}^{a}\sum_{j=1}^{b} T_{ij.}^2}{n} - \frac{\sum_{i=1}^{a} T_{i..}^2}{bn} - \frac{\sum_{j=1}^{b} T_{.j.}^2}{an} + \frac{T^2...}{abn}$$

$$SSE = SST - SSA - SSB - SS(AB).$$

Table C2-3: Analysis of Variance for the Two-Factor Experiment with *n* Replications

Source of Variation	Sum of Squares	Degrees of Freedom	Mean Square	Computed f
Main effects A	SSA	$a-1$	$s_1^2 = \frac{SSA}{a-1}$	$f_1 = \frac{s_1^2}{s^2}$
B	SSB	$b-1$	$s_2^2 = \frac{SSB}{b-1}$	$f_2 = \frac{s_2^2}{s^2}$
Two-factor interactions AB	SS(AB)	$(a-1)(b-1)$	$s_3^2 = \frac{SS(AB)}{(a-1)(b-1)}$	$f_3 = \frac{s_3^2}{s^2}$
Error	SSE	$ab(n-1)$	$s^2 = \frac{SSE}{ab(n-1)}$	
Total	SST	$abn-1$		

Sample calculations

(a) Analysis of variance for mica concentrate grade

Table C2-4: Grade of Fe_2O_3 in concentrate

Collector dosage (g/t) (A)	pH (B)		
	2.5 (b_1)	**3.5 (b_2)**	**5 (b_3)**
150 (a_1)	4.95 4.85 4.85	4.55 4.63 4.70	4.97 4.86 5.01
250 (a_2)	4.91 5.03 4.83	4.67 4.49 4.77	4.59 4.55 4.26
500 (a_3)	4.14 4.57 4.69	4.29 4.69 4.56	4.85 4.46 4.75

Table C2-5: Table of totals

Collector (g/t)	**pH**			***Total***
	2.5	3.5	5	
150	14.65	13.88	14.84	***43.37***
250	14.77	13.93	13.40	***42.10***
500	13.40	13.54	14.06	***41.00***
Total	***42.82***	***41.35***	***42.30***	**126.47**

Using the formulas for the sum-of-squares given above:

SST = 593.77 – 592.40 = 1.37;
SSA = 592.71 – 592.40 = 0.31;
SSB = 592.52 – 592.40 = 0.12;
SS(AB) = 593.28 – 592.71 – 592.52 + 592.40 = 0.45;
SSE = 1.37 – 0.31 – 0.12 – 0.45 = 0.49

These data are used to construct a table for the analysis of variance as shown in Table C2-6.

Table C2-6: Analysis of variance of the results expressed in grade of Fe_2O_3 in concentrate

Source of variation	Sum of squares	Degrees of freedom	Mean square	Computed *f*
Main effects				
Collector dosage (*A*)	0.31	2	0.1562	5.77
pH (*B*)	0.12	2	0.0617	2.28
Two factor interactions				
Collector-pH (AB)	0.45	4	0.1118	4.13
Error	0.49	18	0.0271	
Total	1.37	26		

The theoretical *f* values from the table for the 99% and 95% confidence levels are:

$f_{0.01}$ (2,18) = 6.01; $f_{0.01}$ (4,18) = 4.58;
$f_{0.05}$ (2,18) = 3.55; $f_{0.05}$ (4,18) = 2.93

(b) Analysis of variance for mica concentrate recovery.

Table C2-7: Recovery of Fe_2O_3 in concentrate

Collector dosage (g/t) (*A*)	pH (*B*)		
	2.5 (b_1)	**3.5 (b_2)**	**5 (b_3)**
150 (a_1)	82.78 48.05 69.07	89.7 84.06 91.28	67.75 66.00 33.81
250 (a_2)	80.12 52.74 83.34	70.49 91.62 89.91	86.75 88.88 93.89
500 (a_3)	94.47 93.11 90.74	93.44 89.74 92.66	83.39 93.92 84.14

Table C2-8: Table of totals

Collector (g/t)	**pH**			***Total***
	2.5	3.5	5	
150	199.90	265.04	167.56	***632.50***
250	216.20	252.02	269.52	***737.74***
500	278.32	275.84	261.45	***815.61***
Total	***694.42***	***792.90***	***698.53***	**2185.85**

Again using the sum-of-square computing formulas:

SST = 183351.5 – 176960.7 = 6390.71
SSA = 178837.4 – 176960.7 = 1876.61
SSB = 177650.4 – 176960.7 = 689.66
SS(AB) = 181028.6 – 178837.4 – 177650.4 + 176960.7 = 1501.63
SSE = 6390.71 – 1876.61 – 689.66 – 1501.63 = 2322.81

Table C2-9: Analysis of variance of the results expressed in recovery of Fe_2O_3 in concentrate

Source of variation	Sum of squares	Degrees of freedom	Mean square	Computed f
Main effects				
Collector dosage (*A*)	1876.61	2	938.31	7.27
pH (*B*)	689.66	2	344.83	2.67
Two factor interactions				
Collector-pH (AB)	1501.63	4	375.41	2.91
Error	2322.81	18	129.05	
Total	6390.71	26		

The theoretical *f* values for the 99% and 95% confidence level are given above.

Appendix D: Results of the Effect of Stage Wise Addition of Collector.

Table 1 a: Metallurgical Balance Sheet for Six-Stage Collector Addition - Run 1

Flotation Time (sec)	Fraction	Weight (g)	Weight (%)	Content (%)										
				SiO_2	Al_2O_3	Fe_2O_3	TiO_2	MgO	CaO	K_2O	Na_2O	P_2O_5	F	LOI
120	Conc. 1	44.80	3.88	47.130	30.690	5.127	0.160	0.334	0.029	8.412	0.113	0.000	2.630	5.81
120	Conc.2	162.80	14.11	47.380	31.030	4.900	0.163	0.337	0.047	8.218	0.114	0.034	2.360	5.78
120	Conc. 3	125.20	10.85	47.120	30.930	5.205	0.178	0.334	0.056	8.411	0.125	0.036	2.520	5.50
120	Conc. 4	96.60	8.37	47.210	30.480	5.485	0.202	0.332	0.088	8.762	0.124	0.053	2.460	5.12
120	Conc. 5	146.90	12.73	47.830	30.480	4.666	0.264	0.355	0.350	8.399	0.163	0.285	2.160	5.28
120	Conc. 6	46.60	4.04	49.000	32.820	2.386	0.550	0.386	0.541	6.651	0.143	0.494	1.970	5.34
	Tail	531.20	46.03	77.670	13.290	0.452	0.061	0.128	0.062	5.649	0.673	0.130	0.850	1.25
	Head Cal.	1154.10	100.00	**61.392**	**22.797**	**2.812**	**0.149**	**0.244**	**0.116**	**7.069**	**0.381**	**0.129**	**1.660**	**3.53**

Flotation Time (sec)	Fraction	Water Recovery		Recovery %										
		Weight (g)	Rate (g/s)	SiO_2	Al_2O_3	Fe_2O_3	TiO_2	MgO	CaO	K_2O	Na_2O	P_2O_5	F	LOI
120	Conc. 1	265.70	2.21	2.98	5.23	7.08	4.16	5.31	0.97	4.62	1.15	0.00	6.15	5.81
120	Conc.2	390.90	3.26	10.89	19.20	24.58	15.40	19.47	5.74	16.40	4.22	3.71	20.05	5.78
120	Conc. 3	337.10	2.81	8.33	14.72	20.08	12.94	14.84	5.24	12.91	3.56	3.02	16.47	5.50
120	Conc. 4	292.40	2.44	6.44	11.19	16.32	11.33	11.38	6.33	10.37	2.73	3.43	12.40	5.12
120	Conc. 5	466.20	3.89	9.92	17.02	21.12	22.51	18.50	38.30	15.12	5.45	28.08	16.56	5.28
120	Conc. 6	289.10	2.41	3.22	5.81	3.43	14.88	6.38	18.78	3.80	1.52	15.44	4.79	5.34
	Tail			58.23	26.83	7.40	18.78	24.12	24.65	36.78	81.37	46.31	23.57	1.25
Head Cal.				100.00	100.00	100.00	100.00	100.00	100.00	100.00	100.0	100.0	100.0	3.53

Table 1b: Metallurgical Balance Sheet Six-Stage Collector Addition - Run 2

Flotation Time (sec)	Fraction	Weight (g)	Weight (%)	Content (%)										
				SiO_2	Al_2O_3	Fe_2O_3	TiO_2	MgO	CaO	K_2O	Na_2O	P_2O_5	F	LOI
120	Conc. 1	60.90	5.17	47.220	31.260	4.799	0.150	0.345	0.039	8.030	0.114	0.032	2.230	6.096
120	Conc.2	85.00	7.22	46.950	30.940	5.241	0.163	0.333	0.048	8.331	0.108	0.000	2.430	5.760
120	Conc. 3	279.20	23.70	47.970	30.490	4.941	0.182	0.342	0.115	8.309	0.150	0.067	2.310	5.443
120	Conc. 4	163.80	13.90	48.200	29.860	4.864	0.236	0.349	0.255	8.595	0.171	0.198	2.450	5.184
120	Conc. 5	62.80	5.33	49.350	33.330	2.097	0.536	0.386	0.606	6.112	0.151	0.539	2.530	4.958
120	Conc. 6	36.20	3.07	51.720	34.590	1.869	0.396	0.375	0.121	4.096	0.192	0.207	3.500	3.947
	Tail	490.10	41.60	80.860	10.810	0.293	0.000	0.096	0.047	5.625	0.734	0.134	0.000	1.065
	Head Cal.	1178.00	100.00	**61.762**	**22.564**	**2.765**	**0.136**	**0.244**	**0.124**	**6.973**	**0.392**	**0.136**	**1.421**	**3.570**

Time (sec)	Fraction	Water Recovery		Recovery %										
		Weight (g)	Rate (g/s)	SiO_2	Al_2O_3	Fe_2O_3	TiO_2	MgO	CaO	K_2O	Na_2O	P_2O_5	F	LOI
120	Conc. 1	278.60	2.32	3.95	7.16	8.97	5.69	7.32	1.61	5.95	1.50	1.22	8.11	6.096
120	Conc.2	241.20	2.01	5.49	9.89	13.68	8.63	9.86	2.77	8.62	1.99	0.00	12.34	5.760
120	Conc. 3	643.20	5.36	18.41	32.03	42.36	31.67	33.28	22.00	28.24	9.06	11.68	38.52	5.443
120	Conc. 4	491.70	4.10	10.85	18.40	24.46	24.09	19.92	28.62	17.14	6.06	20.26	23.97	5.184
120	Conc. 5	353.90	2.95	4.26	7.87	4.04	20.98	8.45	26.08	4.67	2.05	21.14	9.49	4.958
120	Conc. 6	322.50	2.69	2.57	4.71	2.08	8.93	4.73	3.00	1.81	1.50	4.68	7.57	3.947
	Tail			54.47	19.93	4.41	0.00	16.43	15.92	33.56	77.83	41.02	0.00	1.065
Head Cal.				100	100	100	100	100	100	100	100	100	100	3.57

Table 1c: Metallurgical Balance Sheet Six-Stage Collector Addition - Run 3

Flotation Time (sec)	Fraction	Weight (g)	Weight (%)	Content (%)										
				SiO_2	Al_2O_3	Fe_2O_3	TiO_2	MgO	CaO	K_2O	Na_2O	P_2O_5	F	LOI
120	Conc. 1	87.20	7.45	47.38	31.29	4.863	0.164	0.344	0.043	8.179	0.114	0.036	2.320	5.58
120	Conc.2	176.50	15.08	47.17	30.96	4.944	0.169	0.340	0.061	8.288	0.122	0.038	2.390	5.89
120	Conc. 3	170.50	14.57	47.31	30.52	5.249	0.195	0.344	0.097	8.548	0.126	0.059	2.340	5.51
120	Conc. 4	142.20	12.15	48.14	30.18	4.815	0.227	0.357	0.253	8.410	0.135	0.203	2.120	5.42
120	Conc. 5	47.10	4.03	49.04	31.98	2.581	0.380	0.396	0.655	7.073	0.116	0.520	1.530	5.88
120	Conc. 6	37.20	3.18	51.38	34.25	1.393	0.651	0.370	0.325	4.691	0.144	0.337	3.140	4.21
	Tail	509.40	43.53	78.94	12.43	0.390	0.041	0.117	0.050	5.549	0.712	0.125	0.780	0.99
	Head Cal.	1170.10	100.00	**61.36**	**22.90**	**2.776**	**0.148**	**0.249**	**0.116**	**6.977**	**0.381**	**0.128**	**1.633**	**3.57**

Time (sec)	Fraction	Water Recovery		Recovery %										
		Weight (g)	Rate (g/s)	SiO_2	Al_2O_3	Fe_2O_3	TiO_2	MgO	CaO	K_2O	Na_2O	P_2O_5	F	LOI
120	Conc. 1	331.30	2.76	5.75	10.18	13.05	8.28	10.29	2.80	8.74	2.23	2.10	10.59	5.588
120	Conc.2	414.00	3.45	11.60	20.39	26.86	17.26	20.59	8.01	17.92	4.83	4.49	22.08	5.893
120	Conc. 3	383.30	3.19	11.23	19.42	27.55	19.24	20.12	12.26	17.85	4.82	6.73	20.88	5.515
120	Conc. 4	406.50	3.39	9.53	16.01	21.08	18.68	17.42	26.58	14.65	4.31	19.31	15.78	5.425
120	Conc. 5	307.40	2.56	3.22	5.62	3.74	10.36	6.40	22.79	4.08	1.23	16.39	3.77	5.889
120	Conc. 6	290.20	2.42	2.66	4.75	1.60	14.01	4.72	8.93	2.14	1.20	8.39	6.11	4.212
	Tail			56.00	23.63	6.12	12.17	20.45	18.63	34.62	81.38	42.60	20.79	0.998
Head Cal.				100	100	100	100	100	100	100	100	100.	100.	3.57

Table 1d: Metallurgical Balance Sheet Six-Stage Collector Addition - Run 4

Flot Time (sec)	Fraction	Weight (g)	Weight (%)	Content (%)										
				SiO_2	Al_2O_3	Fe_2O_3	TiO_2	MgO	CaO	K_2O	Na_2O	P_2O_5	F	LOI
120	Conc. 1	176.10	14.92	47.82	31.12	4.508	0.159	0.345	0.043	8.015	0.120	0.037	2.170	5.99
120	Conc.2	286.30	24.26	47.74	30.24	5.156	0.186	0.331	0.104	8.497	0.134	0.067	2.380	5.47
120	Conc. 3	95.60	8.10	47.37	30.39	5.194	0.221	0.346	0.249	8.619	0.133	0.196	2.320	5.26
120	Conc. 4	66.90	5.67	47.96	31.20	3.660	0.346	0.372	0.784	7.716	0.137	0.709	1.760	5.55
120	Conc. 5	36.10	3.06	50.89	33.36	1.555	0.658	0.382	0.507	5.468	0.136	0.468	2.910	5.56
120	Conc. 6	15.10	1.28	52.07	34.26	1.383	0.417	0.385	0.116	4.486	0.153	0.194	3.100	4.38
	Tail	504.10	42.71	79.35	11.93	0.394	0.035	0.110	0.056	5.702	0.721	0.137	0.000	1.03
	Head Cal.	1180.20	100.00	**61.38**	**22.76**	**2.785**	**0.147**	**0.244**	**0.137**	**7.053**	**0.383**	**0.153**	**1.318**	**3.63**

Time (sec)	Fraction	Water Recovery		Recovery %										
		Weight (g)	Rate (g/s)	SiO_2	Al_2O_3	Fe_2O_3	TiO_2	MgO	CaO	K_2O	Na_2O	P_2O_5	F	LOI
120	Conc. 1	542.00	4.52	11.62	20.40	24.15	16.16	21.06	4.63	16.96	4.67	3.60	24.58	5.996
120	Conc.2	661.90	5.52	18.87	32.23	44.91	30.74	32.84	18.43	29.23	8.49	10.61	43.82	5.478
120	Conc. 3	329.20	2.74	6.25	10.81	15.11	12.20	11.46	14.73	9.90	2.81	10.37	14.26	5.266
120	Conc. 4	300.20	2.50	4.43	7.77	7.45	13.36	8.63	32.46	6.20	2.03	26.24	7.57	5.559
120	Conc. 5	257.40	2.15	2.54	4.48	1.71	13.71	4.78	11.33	2.37	1.09	9.35	6.76	5.569
120	Conc. 6	223.60	1.86	1.09	1.93	0.64	3.64	2.01	1.08	0.81	0.51	1.62	3.01	4.387
	Tail			55.21	22.38	6.04	10.19	19.22	17.34	34.53	80.40	38.21	0.00	1.032
Head Cal.				100	100	100	100	100	100	100	100	100	100	3.63

Table 1: Metallurgical Balance Sheet for Two-Stage Collector Addition of 250 g/t each – Run 1

Flotation Time (sec)	Fraction	Weight (g)	Weight (%)	Content (%)										
				SiO_2	Al_2O_3	Fe_2O_3	TiO_2	MgO	CaO	K_2O	Na_2O	P_2O_5	F	LOI
240	Conc. 1	510.90	43.69	48.540	30.040	4.910	0.181	0.337	0.060	8.291	0.134	0.041	2.250	5.440
240	Conc.2	157.30	13.45	49.040	30.950	3.765	0.437	0.361	0.204	7.558	0.149	0.153	2.660	5.120
	Tail	501.20	42.86	78.280	12.830	0.427	0.030	0.126	0.044	5.694	0.679	0.127	0.000	1.150
	Head Cal.	1169.40	100.00	**61.354**	**22.786**	**2.835**	**0.151**	**0.250**	**0.073**	**7.079**	**0.370**	**0.093**	**1.341**	**3.558**
				Recovery %										
				SiO_2	Al_2O_3	Fe_2O_3	TiO_2	MgO	CaO	K_2O	Na_2O	P_2O_5	F	LOI
240	Conc. 1			34.56	57.60	75.68	52.47	58.94	36.15	51.17	15.84	19.28	73.31	5.440
240	Conc.2			10.75	18.27	17.87	39.00	19.44	37.84	14.36	5.42	22.15	26.69	5.120
	Tail			54.68	24.13	6.46	8.53	21.62	26.01	34.47	78.74	58.58	0.00	1.150
	Head Cal.			100.00	100.00	100.00	100.00	100.00	100.00	100.00	100.00	100.00	100.00	3.558
Cum Flot Time (sec)	Fraction			**Cumulative Grade %**										
				SiO_2	Al_2O_3	Fe_2O_3	TiO_2	MgO	CaO	K_2O	Na_2O	P_2O_5	F	LOI
240	Conc. 1			48.54	30.04	4.91	0.18	0.34	0.06	8.29	0.13	0.04	2.25	5.440
480	Conc.2			48.66	30.25	4.64	0.24	0.34	0.09	8.12	0.14	0.07	2.35	5.365

Table 2: Metallurgical Balance Sheet for Two-Stage Collector Addition of 250 g/t each – Run 2

Flotation Time (sec)	Fraction	Weight (g)	Weight (%)	Content (%)										
				SiO_2	Al_2O_3	Fe_2O_3	TiO_2	MgO	CaO	K_2O	Na_2O	P_2O_5	F	LOI
240	Conc. 1	415.70	35.34	48.680	30.150	4.580	0.172	0.350	0.044	8.101	0.137	0.034	2.340	5.710
240	Conc.2	252.70	21.48	48.750	30.140	4.510	0.350	0.357	0.144	8.168	0.157	0.092	2.490	5.130
	Tail	507.80	43.17	78.100	13.100	0.414	0.035	0.128	0.042	5.421	0.676	0.131	0.920	1.170
	Head Cal.	1176.20	100.00	**61.397**	**22.787**	**2.766**	**0.151**	**0.256**	**0.064**	**6.958**	**0.374**	**0.088**	**1.759**	**3.625**
Flotation Time (sec)				**Recovery %**										
	Fraction			SiO_2	Al_2O_3	Fe_2O_3	TiO_2	MgO	CaO	K_2O	Na_2O	P_2O_5	F	LOI
120	Conc. 1			28.02	46.76	58.51	40.23	48.38	24.11	41.15	12.95	13.60	47.01	5.710
120	Conc.2			17.06	28.42	35.03	49.77	30.00	47.97	25.22	9.02	22.37	30.41	5.130
	Tail			54.92	24.82	6.46	10.00	21.62	27.92	33.63	78.03	64.02	22.58	1.170
	Head Cal.			100.00	100.00	100.00	100.00	100.00	100.00	100.00	100.00	100.00	100.00	3.625
Cum Flot Time (sec)	Fraction			**Cumulative Grade %**										
				SiO_2	Al_2O_3	Fe_2O_3	TiO_2	MgO	CaO	K_2O	Na_2O	P_2O_5	F	LOI
240	Conc. 1			48.68	30.15	4.58	0.17	0.35	0.04	8.10	0.14	0.03	2.34	5.710
480	Conc.2			48.71	30.15	4.55	0.24	0.35	0.08	8.13	0.14	0.06	2.40	5.491
				Cumulative Recovery										
				SiO_2	Al_2O_3	Fe_2O_3	TiO_2	MgO	CaO	K_2O	Na_2O	P_2O_5	F	
240	Conc. 1			28.02	46.76	58.51	40.23	48.38	24.11	41.15	12.95	13.60	47.01	
480	Conc.2			45.08	75.18	93.54	90.00	78.38	72.08	66.37	21.97	35.98	77.42	

Table 3: Metallurgical Balance Sheet for Two-Stage Collector Addition of 150 g/t each – Run 1

Flotation Time (sec)	Fraction	Weight (g)	Weight (%)	Content (%) SiO_2	Al_2O_3	Fe_2O_3	TiO_2	MgO	CaO	K_2O	Na_2O	P_2O_5	F	LOI
240	Conc. 1	247.90	20.95	47.640	30.880	4.731	0.166	0.348	0.033	8.184	0.120	0.028	2.230	5.870
240	Conc.2	292.10	24.69	48.490	29.770	5.046	0.227	0.344	0.092	8.543	0.132	0.044	2.410	5.160
	Tail	643.10	54.36	72.120	16.900	1.034	0.136	0.176	0.089	5.895	0.527	0.127	1.220	1.970
	Head Cal.	1183.10	100.00	**61.157**	**23.007**	**2.799**	**0.165**	**0.254**	**0.078**	**7.028**	**0.344**	**0.086**	**1.725**	**3.575**
Flotation Time (sec)	Fraction			**Recovery %** SiO_2	Al_2O_3	Fe_2O_3	TiO_2	MgO	CaO	K_2O	Na_2O	P_2O_5	F	LOI
120	Conc. 1			16.32	28.12	35.41	21.11	28.76	8.87	24.40	7.31	6.84	27.08	5.870
120	Conc.2			19.58	31.95	44.51	34.02	33.50	29.03	30.01	9.47	12.67	34.48	5.160
	Tail			64.10	39.93	20.08	44.87	37.74	62.10	45.59	83.23	80.49	38.43	1.970
	Head Cal.			100.00	100.00	100.00	100.00	100.00	100.00	100.00	100.00	100.00	100.00	3.575
Cum Flot Time (sec)	Fraction			**Cumulative Grade %** SiO_2	Al_2O_3	Fe_2O_3	TiO_2	MgO	CaO	K_2O	Na_2O	P_2O_5	F	LOI
240	Conc. 1			47.64	30.88	4.73	0.17	0.35	0.03	8.18	0.12	0.03	2.23	5.870
480	Conc.2			48.10	30.28	4.90	0.20	0.35	0.06	8.38	0.13	0.04	2.33	5.486

Table 4: Metallurgical Balance Sheet for Two-Stage Collector Addition of 150 g/t each – Run 1

Flotation Time (sec)	Fraction	Weight (g)	Weight (%)	Content (%) SiO_2	Al_2O_3	Fe_2O_3	TiO_2	MgO	CaO	K_2O	Na_2O	P_2O_5	F	LOI
240	Conc. 1	253.20	21.55	47.780	30.710	4.781	0.169	0.352	0.034	8.171	0.119	0.000	2.360	5.800
240	Conc.2	331.00	28.17	48.160	30.160	4.931	0.239	0.348	0.104	8.524	0.137	0.054	2.400	5.190
	Tail	590.90	50.29	74.500	15.590	0.737	0.136	0.152	0.059	5.554	0.566	0.126	1.100	1.640
	Head Cal.	1175.10	100.00	**61.323**	**22.952**	**2.790**	**0.172**	**0.250**	**0.066**	**6.954**	**0.349**	**0.079**	**1.738**	**3.536**
Flotation Time (sec)	Fraction			**Recovery %** SiO_2	Al_2O_3	Fe_2O_3	TiO_2	MgO	CaO	K_2O	Na_2O	P_2O_5	F	LOI
120	Conc. 1			16.79	28.83	36.93	21.16	30.30	11.08	25.32	7.35	0.00	29.26	5.800
120	Conc.2			22.12	37.01	49.79	39.11	39.16	44.29	34.52	11.06	19.36	38.90	5.190
	Tail			61.09	34.16	13.29	39.73	30.54	44.63	40.16	81.59	80.64	31.83	1.640
	Head Cal.			100.00	100.00	100.00	100.00	100.00	100.00	100.00	100.00	100.00	100.00	3.536
Cum Flot Time (sec)	Fraction			**Cumulative Grade %** SiO_2	Al_2O_3	Fe_2O_3	TiO_2	MgO	CaO	K_2O	Na_2O	P_2O_5	F	LOI
240	Conc. 1			47.78	30.71	4.78	0.17	0.35	0.03	8.17	0.12	0.00	2.36	5.800
480	Conc.2			48.00	30.40	4.87	0.21	0.35	0.07	8.37	0.13	0.03	2.38	5.454
				Cumulative Recovery										
				SiO_2	Al_2O_3	Fe_2O_3	TiO_2	MgO	CaO	K_2O	Na_2O	P_2O_5	F	
240	Conc. 1			16.79	28.83	36.93	21.16	30.30	11.08	25.32	7.35	0.00	29.26	
480	Conc.2			38.91	65.84	86.71	60.27	69.46	55.37	59.84	18.41	19.36	68.17	

Appendix E: Induced Roll Magnetic Separation Results.

Table 1: 1 Amp - Dry Magnetic Separation of +150µm Mica Concentrate Particles

Test	Fraction	wt %	Grade [%]			Recovery [%]		
			Li_2O	Rb_2O	FeO	Li_2O	Rb_2O	FeO
	Magnetic	15.47	3.44	1.15	8.14	19.92	18.55	20.10
	Non-mag.	84.53	2.53	0.92	5.92	80.08	81.45	79.90
Run 1	Head	100.00	2.67	0.96	6.26	100.00	100.00	100.00
	Magnetic	18.85	3.39	1.20	8.66	24.83	24.85	26.82
	Non-mag.	81.15	2.38	0.85	5.49	75.17	75.15	73.18
Run 2	Head	100.00	2.57	0.91	6.09	100.00	100.00	100.00
	Magnetic	***17.16***	***3.41***	1.18	***8.40***	***22.38***	21.70	***23.46***
	Non-mag.	***82.84***	***2.46***	0.89	***5.71***	***77.62***	78.30	***76.54***
Average	Head	***100.00***	***2.62***	0.94	***6.18***	***100.00***	100.00	***100.00***

Table 2: 1 Amp - Dry Magnetic Separation of +125µm Mica Concentrate Particles

Test	Fraction	wt %	Grade [%]			Recovery [%]		
			Li_2O	Rb_2O	FeO	Li_2O	Rb_2O	FeO
	Magnetic	19.83	2.79	1.04	6.41	25.99	25.76	25.76
	Non-mag.	80.17	1.97	0.74	4.57	74.01	74.24	74.24
Run 1	Head	100.00	2.13	0.80	4.94	100.00	100.00	100.00
	Magnetic	18.68	2.82	1.08	6.43	24.86	25.51	23.80
	Non-mag.	81.32	1.96	0.72	4.73	75.14	74.49	76.20
Run 2	Head	100.00	2.12	0.79	5.05	100.00	100.00	100.00
	Magnetic	***19.26***	***2.81***	***1.06***	***6.42***	***25.43***	***25.63***	***24.78***
	Non-mag.	***80.74***	***1.96***	***0.73***	***4.65***	***74.57***	***74.37***	***75.22***
Average	Head	***100.00***	***2.12***	***0.80***	***4.99***	***100.00***	***100.00***	***100.00***

Table 3: 1 Amp - Dry Magnetic Separation of +106µm Mica Concentrate Particles

Test	Fraction	wt %	Grade [%]			Recovery [%]		
			Li_2O	Rb_2O	FeO	Li_2O	Rb_2O	FeO
	Magnetic	12.93	2.66	0.95	5.94	18.92	18.01	17.28
	Non-mag.	87.07	1.69	0.64	4.22	81.08	81.99	82.72
Run 1	Head	100.00	1.82	0.68	4.44	100.00	100.00	100.00
	Magnetic	12.28	2.59	0.98	6.07	17.68	17.79	17.38
	Non-mag.	87.72	1.69	0.63	4.04	82.32	82.21	82.62
Run 2	Head	100.00	1.80	0.68	4.29	100.00	100.00	100.00
	Magnetic	***12.60***	***2.63***	***0.96***	***6.00***	***18.30***	***17.90***	***17.33***
	Non-mag.	***87.40***	***1.69***	***0.64***	***4.13***	***81.70***	***82.10***	***82.67***
Average	Head	***100.00***	***1.81***	***0.68***	***4.37***	***100.00***	***100.00***	***100.00***

Table 4: 1 Amp - Dry Magnetic Separation of +90µm Mica Concentrate Particles

Test	Fraction	wt %	Grade [%]			Recovery [%]		
			Li_2O	Rb_2O	FeO	Li_2O	Rb_2O	FeO
	Magnetic	10.62	2.40	0.89	5.68	16.33	16.36	15.57
	Non-mag.	89.38	1.46	0.54	3.66	83.67	83.64	84.43
Run 1	Head	100.00	1.56	0.58	3.87	100.00	100.00	100.00
	Magnetic	9.11	2.42	0.90	5.59	14.80	15.11	13.49
	Non-mag.	90.89	1.39	0.51	3.60	85.20	84.89	86.51
Run 2	Head	100.00	1.49	0.54	3.78	100.00	100.00	100.00
	Magnetic	***9.87***	***2.41***	***0.90***	***5.63***	***15.56***	***15.74***	***14.53***
	Non-mag.	***90.13***	***1.43***	***0.53***	***3.63***	***84.44***	***84.26***	***85.47***
Average	Head	***100.00***	***1.52***	***0.56***	***3.82***	***100.00***	***100.00***	***100.00***

Table 5: 1 Amp - Dry Magnetic Separation of +75µm Mica Concentrate Particles

Test	Fraction	wt %	Grade [%]			Recovery [%]		
			Li_2O	Rb_2O	FeO	Li_2O	Rb_2O	FeO
	Magnetic	17.28	1.94	0.69	4.70	24.52	24.08	24.59
	Non-mag.	82.72	1.25	0.45	3.01	75.48	75.92	75.41
Run 1	Head	100.00	1.37	0.49	3.30	100.00	100.00	100.00
	Magnetic	18.71	1.96	0.67	4.73	25.82	24.21	25.13
	Non-mag.	81.29	1.30	0.48	3.24	74.18	75.79	74.87
Run 2	Head	100.00	1.42	0.52	3.52	100.00	100.00	100.00
	Magnetic	***17.99***	***1.95***	***0.68***	***4.71***	***25.17***	***24.14***	***24.86***
	Non-mag.	***82.01***	***1.27***	***0.47***	***3.13***	***74.83***	***75.86***	***75.14***
Average	Head	***100.00***	***1.40***	***0.50***	***3.41***	***100.00***	***100.00***	***100.00***

Table 6: 1 Amp - Dry Magnetic Separation of +63µm Mica Concentrate Particles

Test	Fraction	wt %	Grade [%]			Recovery [%]		
			Li_2O	Rb_2O	FeO	Li_2O	Rb_2O	FeO
	Magnetic	31.37	1.32	0.28	1.91	35.85	25.34	24.86
	Non-mag.	68.63	1.08	0.38	2.63	64.15	74.66	75.14
Run 1	Head	100.00	1.16	0.34	2.41	100.00	100.00	100.00
	Magnetic	31.37	1.37	0.42	3.36	37.00	33.51	33.51
	Non-mag.	68.63	1.07	0.38	3.05	63.00	66.49	66.49
Run 2	Head	100.00	1.16	0.39	3.15	100.00	100.00	100.00
	Magnetic	***31.37***	***1.35***	***0.35***	***2.64***	***36.43***	***29.43***	***29.18***
	Non-mag.	***68.63***	***1.08***	***0.38***	***2.84***	***63.57***	***70.57***	***70.82***
Average	Head	***100.00***	***1.16***	***0.37***	***2.78***	***100.00***	***100.00***	***100.00***

Table 7: 1 Amp - Dry Magnetic Separation of +53µm Mica Concentrate Particles

Test	Fraction	wt %	Grade [%]			Recovery [%]		
			Li_2O	Rb_2O	FeO	Li_2O	Rb_2O	FeO
	Magnetic	52.67	1.05	0.36	2.72	57.68	61.79	63.06
	Non-mag.	47.33	0.86	0.24	1.77	42.32	38.21	36.94
Run 1	Head	100.00	0.96	0.30	2.27	100.00	100.00	100.00
	Magnetic	51.87	1.06	0.35	2.57	57.65	46.08	55.55
	Non-mag.	48.13	0.84	0.45	2.22	42.35	53.92	44.45
Run 2	Head	100.00	0.95	0.40	2.40	100.00	100.00	100.00
	Magnetic	***52.27***	***1.05***	***0.35***	***2.65***	***57.67***	***53.93***	***59.30***
	Non-mag.	***47.73***	***0.85***	***0.35***	***2.00***	***42.33***	***46.07***	***40.70***
Average	Head	***100.00***	***0.95***	***0.35***	***2.34***	***100.00***	***100.00***	***100.00***

Table 8: 3 Amps - Dry Magnetic Separation of +150µm Mica Concentrate Particles

Test	Fraction	wt %	Grade [%]			Recovery [%]		
			Li_2O	Rb_2O	FeO	Li_2O	Rb_2O	FeO
	Magnetic	20.22	3.00	1.23	7.57	25.32	24.42	27.23
	Non-mag.	79.78	2.25	0.97	5.13	74.68	75.58	72.77
Run 1	Head	100.00	2.40	1.02	5.62	100.00	100.00	100.00
	Magnetic	22.75	3.09	1.24	7.57	28.73	27.55	30.73
	Non-mag.	77.25	2.26	0.96	5.02	71.27	72.45	69.27
Run 2	Head	100.00	2.45	1.02	5.60	100.00	100.00	100.00
	Magnetic	***21.48***	***3.05***	***1.24***	***7.57***	***27.03***	***25.98***	***28.98***
	Non-mag.	***78.52***	***2.25***	***0.96***	***5.07***	***72.97***	***74.02***	***71.02***
Average	Head	***100.00***	***2.42***	***1.02***	***5.61***	***100.00***	***100.00***	***100.00***

Table 9: 3 Amps - Dry Magnetic Separation of +125µm Mica Concentrate Particles

Test	Fraction	wt %	Grade [%]			Recovery [%]		
			% Li_2O	Rb_2O	FeO	% Li_2O	Rb_2O	FeO
	Magnetic	19.57	2.73	1.22	5.97	25.73	25.50	24.46
	Non-mag.	80.43	1.92	0.87	4.49	74.27	74.50	75.54
Run 1	Head	100.00	2.08	0.94	4.78	100.00	100.00	100.00
	Magnetic	16.98	2.79	1.18	6.07	21.29	20.28	20.40
	Non-mag.	83.02	2.11	0.95	4.85	78.71	79.72	79.60
Run 2	Head	100.00	2.23	0.98	5.06	100.00	100.00	100.00
	Magnetic	***18.28***	***2.76***	***1.20***	***6.02***	***23.51***	***22.89***	***22.43***
	Non-mag.	***81.72***	***2.01***	***0.91***	***4.67***	***76.49***	***77.11***	***77.57***
Average	Head	***100.00***	***2.15***	***0.96***	***4.92***	***100.00***	***100.00***	***100.00***

Table 10: 3 Amps - Dry Magnetic Separation of +106µm Mica Concentrate Particles

Test	Fraction	wt %	Grade [%]			Recovery [%]		
			Li_2O	Rb_2O	FeO	Li_2O	Rb_2O	FeO
	Magnetic	17.84	2.60	1.15	5.73	26.10	24.90	24.29
	Non-mag.	82.16	1.60	0.75	3.88	73.90	75.10	75.71
Run 1	Head	100.00	1.78	0.82	4.21	100.00	100.00	100.00
	Magnetic	16.12	2.55	1.11	5.70	24.44	22.30	21.75
	Non-mag.	83.88	1.51	0.75	3.94	75.56	77.70	78.25
Run 2	Head	100.00	1.68	0.81	4.22	100.00	100.00	100.00
	Magnetic	***16.98***	***2.57***	***1.13***	***5.72***	***25.27***	***23.60***	***23.02***
	Non-mag.	***83.02***	***1.55***	***0.75***	***3.91***	***74.73***	***76.40***	***76.98***
Average	Head	***100.00***	***1.73***	***0.81***	***4.22***	***100.00***	***100.00***	***100.00***

Table 11: 3 Amps - Dry Magnetic Separation of +90µm Mica Concentrate Particles

Test	Fraction	wt %	Grade [%]			Recovery [%]		
			Li_2O	Rb_2O	FeO	Li_2O	Rb_2O	FeO
	Magnetic	15.39	2.18	1.04	5.29	23.39	23.26	23.22
	Non-mag.	84.61	1.30	0.62	3.18	76.61	76.74	76.78
Run 1	Head	100.00	1.43	0.69	3.50	100.00	100.00	100.00
	Magnetic	17.82	2.30	1.02	5.17	27.68	26.43	26.49
	Non-mag.	82.18	1.30	0.62	3.11	72.32	73.57	73.51
Run 2	Head	100.00	1.48	0.69	3.48	100.00	100.00	100.00
	Magnetic	***16.60***	***2.24***	***1.03***	***5.23***	***25.54***	***24.85***	***24.86***
	Non-mag.	***83.40***	***1.30***	***0.62***	***3.15***	***74.46***	***75.15***	***75.14***
Average	Head	***100.00***	***1.46***	***0.69***	***3.49***	***100.00***	***100.00***	***100.00***

Table 12: 3 Amps - Dry Magnetic Separation of +75µm Mica Concentrate Particles

Test	Fraction	wt %	Grade [%]			Recovery [%]		
			Li_2O	Rb_2O	FeO	Li_2O	Rb_2O	FeO
	Magnetic	28.88	1.85	0.82	4.28	41.54	38.26	39.82
	Non-mag.	71.12	1.06	0.53	2.62	58.46	61.74	60.18
Run 1	Head	100.00	1.29	0.62	3.10	100.00	100.00	100.00
	Magnetic	29.50	1.90	0.81	4.25	40.27	38.52	39.32
	Non-mag.	70.50	1.18	0.54	2.74	59.73	61.48	60.68
Run 2	Head	100.00	1.40	0.62	3.19	100.00	100.00	100.00
	Magnetic	***29.19***	***1.88***	***0.81***	***4.26***	***40.91***	***38.39***	***39.57***
	Non-mag.	***70.81***	***1.12***	***0.54***	***2.68***	***59.09***	***61.61***	***60.43***
Average	Head	***100.00***	***1.34***	***0.62***	***3.14***	***100.00***	***100.00***	***100.00***

Table 13: 3 Amps - Dry Magnetic Separation of +63µm Mica Concentrate Particles

Test	Fraction	wt %	Grade [%]			Recovery [%]		
			Li_2O	Rb_2O	FeO	Li_2O	Rb_2O	FeO
	Magnetic	41.30	1.36	0.56	3.15	48.33	45.00	48.02
	Non-mag.	58.70	1.02	0.48	2.40	51.67	55.00	51.98
Run 1	Head	100.00	1.16	0.51	2.71	100.00	100.00	100.00
	Magnetic	39.78	1.36	0.56	3.13	100.00	43.97	40.53
	Non-mag.	60.22	0.00	0.47	3.04	0.00	56.03	59.47
Run 2	Head	100.00	0.54	0.50	3.08	100.00	100.00	100.00
	Magnetic	***40.54***	***1.36***	***0.56***	***3.14***	***74.17***	***44.48***	***44.27***
	Non-mag.	***59.46***	***0.51***	***0.48***	***2.72***	***25.83***	***55.52***	***55.73***
Average	Head	***100.00***	***0.85***	***0.51***	***2.89***	***100.00***	***100.00***	***100.00***

Table 14: 3 Amps - Dry Magnetic Separation of +53µm Mica Concentrate Particles

Test	Fraction	wt %	Grade [%]			Recovery [%]		
			Li_2O	Rb_2O	FeO	Li_2O	Rb_2O	FeO
	Magnetic	69.13	0.85	0.46	3.10	71.05	70.93	73.48
	Non-mag.	30.87	0.78	0.42	2.51	28.95	29.07	26.52
Run 1	Head	100.00	0.83	0.45	2.92	100.00	100.00	100.00
	Magnetic	61.82	1.00	0.46	2.57	64.97	63.75	59.03
	Non-mag.	38.18	0.88	0.42	2.88	35.03	36.25	40.97
Run 2	Head	100.00	0.95	0.44	2.69	100.00	100.00	100.00
	Magnetic	***65.48***	***0.93***	***0.46***	***2.83***	***68.01***	***67.34***	***66.25***
	Non-mag.	***34.52***	***0.83***	***0.42***	***2.70***	***31.99***	***32.66***	***33.75***
Average	Head	***100.00***	***0.89***	***0.45***	***2.80***	***100.00***	***100.00***	***100.00***

Table 15: 5 Amps - Dry Magnetic Separation of +150µm Mica Concentrate Particles

Test	Fraction	wt %	Grade [%]			Recovery [%]		
			Li_2O	Rb_2O	FeO	Li_2O	Rb_2O	FeO
	Magnetic	16.99	3.07	1.09	8.82	21.36	21.46	24.37
	Non-mag.	83.01	2.31	0.81	5.60	78.64	78.54	75.63
Run 1	Head	100.00	2.44	0.86	6.15	100.00	100.00	100.00
	Magnetic	17.11	3.15	1.11	9.25	21.98	21.87	25.66
	Non-mag.	82.89	2.31	0.82	5.53	78.02	78.13	74.34
Run 2	Head	100.00	2.45	0.87	6.17	100.00	100.00	100.00
	Magnetic	***17.05***	***3.11***	***1.10***	***9.03***	***21.67***	***21.66***	***25.01***
	Non-mag.	***82.95***	***2.31***	***0.82***	***5.57***	***78.33***	***78.34***	***74.99***
Average	Head	***100.00***	***2.45***	***0.87***	***6.16***	***100.00***	***100.00***	***100.00***

Table 16: 5 Amps - Dry Magnetic Separation of +125µm Mica Concentrate Particles

Test	Fraction	wt %	Grade [%]			Recovery [%]		
			Li_2O	Rb_2O	FeO	Li_2O	FeO	Li_2O
	Magnetic	15.65	2.84	1.06	8.16	20.51	20.94	22.29
	Non-mag.	84.35	2.04	0.74	5.28	79.49	79.06	77.71
Run 1	Head	100.00	2.17	0.79	5.73	100.00	100.00	100.00
	Magnetic	13.12	2.90	1.07	8.52	18.04	18.13	20.46
	Non-mag.	86.88	1.99	0.73	5.00	81.96	81.87	79.54
Run 2	Head	100.00	2.11	0.77	5.46	100.00	100.00	100.00
	Magnetic	***14.38***	***2.87***	***1.07***	***8.34***	***19.27***	***19.54***	***21.38***
	Non-mag.	***85.62***	***2.02***	***0.74***	***5.14***	***80.73***	***80.46***	***78.62***
Average	Head	***100.00***	***2.14***	***0.78***	***5.59***	***100.00***	***100.00***	***100.00***

Table 17: 5 Amps - Dry Magnetic Separation of +106µm Mica Concentrate Particles

Test	Fraction	wt %	Grade [%]			Recovery [%]		
			Li_2O	Rb_2O	FeO	Li_2O	Rb_2O	FeO
	Magnetic	12.38	2.68	0.99	6.30	19.15	18.78	17.53
	Non-mag.	87.62	1.60	0.60	4.18	80.85	81.22	82.47
Run 1	Head	100.00	1.73	0.65	4.44	100.00	100.00	100.00
	Magnetic	12.50	2.68	1.00	6.30	18.34	18.32	16.79
	Non-mag.	87.50	1.70	0.64	4.46	81.66	81.68	83.21
Run 2	Head	100.00	1.82	0.68	4.69	100.00	100.00	100.00
	Magnetic	***12.44***	***2.68***	***0.99***	***6.30***	***18.74***	***18.55***	***17.16***
	Non-mag.	***87.56***	***1.65***	***0.62***	***4.32***	***81.26***	***81.45***	***82.84***
Average	Head	***100.00***	***1.78***	***0.67***	***4.57***	***100.00***	***100.00***	***100.00***

Table 18: 5 Amps - Dry Magnetic Separation of +90µm Mica Concentrate Particles

Test	Fraction	wt %	Grade [%]			Recovery [%]		
			Li_2O	Rb_2O	FeO	Li_2O	Rb_2O	FeO
	Magnetic	20.84	2.30	0.81	5.57	32.28	28.75	30.92
	Non-mag.	79.16	1.27	0.53	3.28	67.72	71.25	69.08
Run 1	Head	100.00	1.49	0.59	3.76	100.00	100.00	100.00
	Magnetic	17.31	2.19	0.82	5.52	26.87	24.44	26.82
	Non-mag.	82.69	1.25	0.53	3.16	73.13	75.56	73.18
Run 2	Head	100.00	1.41	0.58	3.57	100.00	100.00	100.00
	Magnetic	***19.07***	***2.25***	***0.82***	***5.55***	***29.58***	***26.60***	***28.87***
	Non-mag.	***80.93***	***1.26***	***0.53***	***3.22***	***70.42***	***73.40***	***71.13***
Average	Head	***100.00***	***1.45***	***0.58***	***3.66***	***100.00***	***100.00***	***100.00***

Table 19: 5 Amps - Dry Magnetic Separation of +75µm Mica Concentrate Particles

Test	Fraction	wt %	Grade [%]			Recovery [%]		
			Li_2O	Rb_2O	FeO	Li_2O	Rb_2O	FeO
Run 1	Magnetic	34.83	1.65	0.62	4.25	47.58	41.70	45.71
	Non-mag.	65.17	0.97	0.46	2.70	52.42	58.30	54.29
	Head	100.00	1.21	0.52	3.24	100.00	100.00	100.00
Run 2	Magnetic	35.71	1.71	0.64	4.42	49.99	43.42	48.82
	Non-mag.	64.29	0.95	0.46	2.57	50.01	56.58	51.18
	Head	100.00	1.22	0.52	3.23	100.00	100.00	100.00
Average	Magnetic	***35.27***	***1.68***	***0.63***	***4.34***	***48.79***	***42.56***	***47.27***
	Non-mag.	***64.73***	***0.96***	***0.46***	***2.64***	***51.21***	***57.44***	***52.73***
	Head	***100.00***	***1.22***	***0.52***	***3.24***	***100.00***	***100.00***	***100.00***

Table 20: Five Amps - Dry Magnetic Separation of +63µm Mica Concentrate Particles

Test	Fraction	wt %	Grade [%]			Recovery [%]		
			Li_2O	Rb_2O	FeO	Li_2O	Rb_2O	FeO
Run 1	Magnetic	49.68	1.15	0.49	3.14	54.45	52.13	54.65
	Non-mag.	50.32	0.95	0.44	2.57	45.55	47.87	45.35
	Head	100.00	1.05	0.47	2.86	100.00	100.00	100.00
Run 2	Magnetic	50.03	1.16	0.49	3.13	54.65	52.55	54.75
	Non-mag.	49.97	0.97	0.44	2.59	45.35	47.45	45.25
	Head	100.00	1.06	0.46	2.86	100.00	100.00	100.00
Average	Magnetic	***49.85***	***1.15***	***0.49***	***3.14***	***54.55***	***52.34***	***54.70***
	Non-mag.	***50.15***	***0.96***	***0.44***	***2.58***	***45.45***	***47.66***	***45.30***
	Head	***100.00***	***1.06***	***0.46***	***2.86***	***100.00***	***100.00***	***100.00***

Table 21: 5 Amps - Dry Magnetic Separation of +53µm Mica Concentrate Particles

Test	Fraction	wt %	Grade [%]			Recovery [%]		
			Li_2O	Rb_2O	FeO	Li_2O	Rb_2O	FeO
Run 1	Magnetic	80.85	0.94	0.42	2.52	82.53	81.68	82.55
	Non-mag.	19.15	0.84	0.40	2.25	17.47	18.32	17.45
	Head	100.00	0.92	0.42	2.47	100.00	100.00	100.00
Run 2	Magnetic	78.99	0.95	0.43	2.52	81.03	80.10	80.63
	Non-mag.	21.01	0.84	0.40	2.28	18.97	19.90	19.37
	Head	100.00	0.93	0.42	2.47	100.00	100.00	100.00
Average	Magnetic	***79.92***	***0.95***	***0.42***	***2.52***	***81.78***	***80.89***	***81.59***
	Non-mag.	***20.08***	***0.84***	***0.40***	***2.26***	***18.22***	***19.11***	***18.41***
	Head	***100.00***	***0.93***	***0.42***	***2.47***	***100.00***	***100.00***	***100.00***

Appendix F1: Wet High intensity magnetic separation balance sheets.

Table 1: 5 Amps - Wet High Intensity Magnetic Separation

Test	Fraction	wt %	Grade %			Recovery %		
			Li_2O	Rb_2O	FeO	Li_2O	Rb_2O	FeO
	Magnetic	14.40	2.172353	0.79368	5.306655	21.853	21.218	20.637
	Non-Magnetic	85.60	1.306823	0.495751	3.433055	78.147	78.782	79.363
Run 1	Head Cal	100.00	1.431459	0.538653	3.702854	100.000	100.000	100.000
	Magnetic	19.67	2.24664	0.795802	5.400904	30.153	28.759	29.861
	Non-Magnetic	80.33	1.2743	0.482715	3.106397	69.847	71.241	70.139
Run 2	Head Cal	100.00	1.46556	0.544299	3.557726	100.000	100.000	100.000
	Magnetic	***17.04***	***2.209496***	***0.794741***	***5.35378***	***26.003***	***24.988***	***25.249***
	Non-Magnetic	***82.97***	***1.290562***	***0.489233***	***3.269726***	***73.997***	***75.012***	***74.751***
Average	Head Cal	***100.00***	***1.44851***	***0.541476***	***3.63029***	***100.000***	***100.000***	***100.000***

Table 2: 10 Amps - Wet High Intensity Magnetic Separation

Test	Fraction	wt %	Grade %			Recovery %		
			Li_2O	Rb_2O	FeO	Li_2O	Rb_2O	FeO
	Magnetic	27.67	2.358371	0.833606	5.598689	45.341	42.100	42.445
	Non-Magnetic	72.33	1.087591	0.438582	2.904243	54.659	57.900	57.555
Run 1	Head Cal	100.00	1.439216	0.547885	3.649796	100.000	100.000	100.000
	Magnetic	26.39	2.237245	0.742757	5.625892	40.358	36.056	39.122
	Non-Magnetic	73.61	1.185338	0.47224	3.138645	59.642	63.944	60.878
Run 2	Head Cal	100.00	1.462936	0.543629	3.79503	100.000	100.000	100.000
	Magnetic	***27.03***	***2.297808***	***0.788181***	***5.612291***	***42.850***	***39.078***	***40.783***
	Non-Magnetic	***72.97***	***1.136465***	***0.455411***	***3.021444***	***57.150***	***60.922***	***59.217***
Average	Head Cal	***100.00***	***1.451076***	***0.545757***	***3.722413***	***100.000***	***100.000***	***100.000***

Table 3: 15 Amps- Wet High Intensity Magnetic Separations

Test	Fraction	wt %	Grade %			Recovery %		
			Li_2O	Rb_2O	FeO	Li_2O	Rb_2O	FeO
	Magnetic	35.00	2.340323	0.781055	5.429377	55.317	52.657	54.237
	Non-Magnetic	65.00	1.017921	0.378124	2.466719	44.683	47.343	45.763
Run 1	Head Cal	100.00	1.480762	0.51915	3.50365	100.000	100.000	100.000
	Magnetic	35.18	2.329374	0.777457	5.487639	56.094	54.093	53.682
	Non-Magnetic	64.82	0.989554	0.358099	2.569744	43.906	45.907	46.318
Run 2	Head Cal	100.00	1.460903	0.505629	3.59626	100.000	100.000	100.000
	Magnetic	***35.09***	***2.334848***	***0.779256***	***5.458508***	***55.705***	***53.375***	***53.960***
	Non-Magnetic	***64.91***	***1.003738***	***0.368112***	***2.518232***	***44.295***	***46.625***	***46.040***
Average	Head Cal	***100.00***	***1.470832***	***0.51239***	***3.549955***	***100.000***	***100.000***	***100.000***

Table 4: 20 Amps - Wet High Intensity Magnetic Separations

Test	Fraction	wt %	Grade %			Recovery %		
			Li_2O	Rb_2O	FeO	Li_2O	Rb_2O	FeO
	Magnetic	46.84	2.207247	0.767934	5.399012	72.114	67.344	68.465
	Non-Magnetic	53.16	0.752068	0.328117	2.191126	27.886	32.656	31.535
Run 1	Head Cal	100.00	1.433674	0.534127	3.6937	100.000	100.000	100.000
	Magnetic	47.25	2.165166	0.706654	5.328667	71.663	67.845	68.965
	Non-Magnetic	52.75	0.766868	0.299998	2.147922	28.337	32.155	31.035
Run 2	Head Cal	100.00	1.427564	0.492143	3.650824	100.000	100.000	100.000
	Magnetic	***47.05***	***2.186206***	***0.737294***	***5.36384***	***71.889***	***67.594***	***68.715***
	Non-Magnetic	***52.96***	***0.759468***	***0.314057***	***2.169524***	***28.111***	***32.406***	***31.285***
Average	Head Cal	***100.00***	***1.430619***	***0.513135***	***3.672262***	***100.000***	***100.000***	***100.000***

Table 5: 25 Amps - Wet High Intensity Magnetic Separations

Test	Fraction	wt %	Grade %			Recovery %		
			Li_2O	Rb_2O	FeO	Li_2O	Rb_2O	FeO
	Magnetic	43.54	2.039298	0.734128	5.344051	68.042	63.698	65.743
	Non-Magnetic	56.46	0.738629	0.322641	2.147385	31.958	36.302	34.257
Run 1	Head Cal	100.00	1.30494	0.501803	3.539213	100.000	100.000	100.000
	Magnetic	48.26	2.20404	0.714035	5.218804	77.755	72.723	72.877
	Non-Magnetic	51.74	0.588149	0.249802	1.811698	22.245	27.277	27.123
Run 2	Head Cal	100.00	1.367978	0.473841	3.455967	100.000	100.000	100.000
	Magnetic	***45.90***	***2.121669***	***0.724082***	***5.281427***	***72.899***	***68.211***	***69.310***
	Non-Magnetic	***54.10***	***0.663389***	***0.286222***	***1.979541***	***27.101***	***31.789***	***30.690***
Average	Head Cal	***100.00***	***1.336459***	***0.487822***	***3.49759***	***100.000***	***100.000***	***100.000***

Size by Assay Recovery of Lithium, Rubidium and Iron in the Magnetic and Non-Magnetic Fractions

Table 1: 10 Amps - Wet High Intensity Magnetic Separation Screen Products

Mag. Separation		Sieve Analysis		Grade %			Recovery %		
Fraction	**wt %**	**Size(µm)**	**wt %**	**Li_2O**	**Rb_2O**	**FeO**	**Li_2O**	**Rb_2O**	**FeO**
Mag.	27.03	+150	5.83	3.033	1.061	9.413	***42.453***	***45.541***	***48.825***
Non-Mag.	72.97	+150	3.66	2.426	0.748	5.821	57.547	54.459	51.175
Mag.	27.03	+106	16.1	2.682	1.025	6.292	***44.856***	***45.125***	***43.237***
Non-Mag.	72.97	+106	10.43	1.885	0.713	4.723	55.144	54.875	56.763
Mag.	27.03	+75	25.98	2.410	0.914	5.848	***44.964***	***43.199***	***42.833***
Non-Mag.	72.97	+75	20.92	1.357	0.553	3.591	55.036	56.801	57.167
Mag.	27.03	+53	26.58	2.195	0.803	5.404	***46.340***	***42.410***	***44.576***
Non-Mag.	72.97	+53	25.95	0.964	0.414	2.549	53.660	57.590	55.424
Mag.	27.03	+38	12.69	2.075	0.746	5.148	***45.943***	***40.048***	***40.293***
Non-Mag.	72.97	+38	15.3	0.750	0.343	2.344	54.057	59.952	59.707
Mag.	27.03	-38	12.82	1.758	0.602	4.508	***43.392***	***35.121***	***36.743***
Non-Mag.	72.97	-38	23.74	0.459	0.222	1.552	56.608	64.879	63.257

Table 2: 15 Amps - Wet High Intensity Magnetic Separation Screen Products

Mag. Separation		Sieve Analysis		Grade %			Recovery %		
Fraction	**wt %**	**Size (µm)**	**wt %**	**Li_2O**	**Rb_2O**	**FeO**	**Li_2O**	**Rb_2O**	**FeO**
Mag.	35.09	+150	5.81	2.981	1.044	8.910	***59.123***	***59.237***	***64.016***
Non-Mag.	64.91	+150	3.38	1.915	0.668	4.654	40.877	40.763	35.984
Mag.	35.09	+106	15.92	2.663	1.020	6.224	***59.579***	***59.339***	***58.196***
Non-Mag.	64.91	+106	8.84	1.759	0.680	4.352	40.421	40.661	41.804
Mag.	35.09	+75	25.33	2.087	0.870	5.043	***54.590***	***54.616***	***52.139***
Non-Mag.	64.91	+75	18.85	1.261	0.525	3.363	45.410	45.384	47.861
Mag.	35.09	+53	26.83	2.159	0.784	5.447	***57.680***	***52.708***	***54.531***
Non-Mag.	64.91	+53	25.06	0.917	0.407	2.629	42.320	47.292	45.469
Mag.	35.09	+38	12.46	1.989	0.718	5.098	***55.818***	***49.683***	***51.069***
Non-Mag.	64.91	+38	15.12	0.701	0.324	2.176	44.182	50.317	48.931
Mag.	35.09	-38	13.66	1.622	0.553	4.384	***49.112***	***41.088***	***42.860***
Non-Mag.	64.91	-38	28.75	0.432	0.204	1.501	50.888	58.912	57.140

Table 3: 20 Amps - Wet High Intensity Magnetic Separation Screen Products

Mag. Separation		Sieve Analysis		Grade %			Recovery %		
Fraction	**wt %**	**Size(µm)**	**wt %**	**Li_2O**	**Rb_2O**	**FeO**	**Li_2O**	**Rb_2O**	**FeO**
Mag.	46.84	+150	5.64	2.938	1.132	9.049	***78.505***	***76.020***	***81.142***
Non-Mag.	53.16	+150	2.73	1.464	0.650	3.828	21.495	23.980	18.858
Mag.	46.84	+106	15.81	2.531	1.030	5.659	***75.214***	***73.211***	***73.870***
Non-Mag.	53.16	+106	7.99	1.454	0.657	3.490	24.786	26.789	26.130
Mag.	46.84	+75	25.36	2.268	0.963	5.609	***75.587***	***70.227***	***73.095***
Non-Mag.	53.16	+75	18.2	0.900	0.501	2.535	24.413	29.773	26.905
Mag.	46.84	+53	26.74	2.032	0.834	5.272	***73.486***	***67.054***	***71.281***
Non-Mag.	53.16	+53	25.66	0.673	0.376	1.950	26.514	32.946	28.719
Mag.	46.84	+38	12.56	1.805	0.760	4.892	***71.242***	***72.979***	***70.157***
Non-Mag.	53.16	+38	15.43	0.522	0.202	1.492	28.758	27.021	29.843
Mag.	46.84	-38	13.89	1.477	0.571	4.091	***64.122***	***55.678***	***58.382***
Non-Mag.	53.16	-38	29.99	0.337	0.185	1.190	35.878	44.322	41.618

Table 4: 25 Amps - Wet High Intensity Magnetic Separation Screen Products

Mag. Separation		Sieve Analysis		Grade %			Recovery %		
Fraction	**wt %**	**Size(µm)**	**wt %**	**Li_2O**	**Rb_2O**	**FeO**	**Li_2O**	**Rb_2O**	**FeO**
Mag.	43.54	+150	5.34	2.963	0.390	8.227	***73.984***	***75.564***	***80.208***
Non-Mag	56.46	+150	3.17	1.354	0.410	2.637	26.016	24.436	19.792
Mag.	43.54	+106	14.8	2.622	0.993	6.068	***74.357***	***74.177***	***73.571***
Non-Mag.	56.46	+106	7.52	1.373	0.525	3.308	25.643	25.823	26.429
Mag.	43.54	+75	24.53	2.296	0.876	5.390	***73.503***	***67.538***	***71.260***
Non-Mag.	56.46	+75	16.82	0.931	0.474	2.445	26.497	32.462	28.740
Mag.	43.54	+53	26.23	2.104	0.803	5.116	***74.012***	***69.895***	***73.311***
Non-Mag.	56.46	+53	24.2	0.617	0.289	1.557	25.988	30.105	26.689
Mag.	43.54	+38	12.91	1.925	0.635	4.587	***71.528***	***63.897***	***67.350***
Non-Mag.	56.46	+38	15.61	0.489	0.229	1.418	28.472	36.103	32.650
Mag.	43.54	-38	16.2	1.504	0.492	3.826	***63.916***	***59.888***	***62.846***
Non-Mag.	56.46	-38	32.68	0.325	0.126	0.865	36.084	40.112	37.154

Appendix F2: Electron-Microprobe Analysis of Magnetic Separation Products.

Table 1: Microprobe data of non-magnetic mica

Muscovites

Ident. No.[#]	2	4	7	12	15	17	19	25	26	28	30	31	34	36	38	39	40	41	44	Average
SiO_2	46.9	47.1	46.1	45.1	48.3	45.8	47.0	46.6	45.5	45.7	46.2	48.2	47.4	46.1	46.0	46.3	46.2	46.4	46.5	***46.55 (0.8)***[+]
TiO_2	0.38	0.05	0.01	0.20	0.14	0.22	0.02	0.01	0.01	0.16	0.04	0.02	0.10	0.04	0.12	0.23	0.16	0.00	0.21	***0.11 (0.1)***
Al_2O_3	31.6	35.2	31.3	37.1	32.3	34.6	35.4	30.9	36.9	35.5	32.7	33.6	33.0	34.0	35.2	33.7	33.9	31.4	34.7	***33.89 (1.8)***
FeO*	3.44	1.70	5.78	0.10	0.21	0.67	0.41	1.44	0.82	0.26	2.78	2.47	2.26	1.65	0.31	0.88	1.59	2.78	1.24	***1.62 (1.4)***
MnO	0.02	0.07	0.16	0.00	0.02	0.07	0.00	0.01	0.09	0.00	0.12	0.04	0.07	0.02	0.00	0.00	0.02	0.02	0.10	***0.04 (0.0)***
MgO	0.96	0.09	0.01	0.09	2.00	0.60	0.67	1.32	0.02	0.18	0.10	0.05	0.25	0.33	0.31	0.61	0.30	0.42	0.33	***0.45 (0.5)***
CaO	0.01	0.01	0.00	0.00	0.00	0.00	0.01	0.08	0.02	0.01	0.00	0.00	0.01	0.01	0.00	0.00	0.00	0.00	0.00	***0.01 (0.0)***
Na_2O	0.21	0.07	0.23	0.35	0.29	0.27	0.36	0.14	0.31	0.28	0.18	0.08	0.17	0.20	0.27	0.24	0.22	0.21	0.28	***0.23 (0.0)***
K_2O	10.30	5.52	10.17	10.41	10.31	10.43	10.07	9.11	10.24	10.55	10.56	9.03	10.06	9.59	10.37	10.24	10.61	10.02	10.44	***9.90 (1.1)***
F	1.70	0.08	1.57	0.11	0.99	0.14	0.26	0.57	0.83	0.86	0.07	0.76	0.33	0.10	0.13	0.83	1.17	0.20	1.18	***0.63 (0.5)***
Cl	0.00	0.00	0.42	0.00	0.00	0.12	0.33	0.00	0.00	0.27	0.99	0.57	0.00	0.21	0.27	0.00	0.00	0.21	0.00	***0.18 (0.2)***
Li_2O*	0.45	0.00	0.41	0.00	0.23	0.00	0.01	0.10	0.18	0.19	0.00	0.16	0.03	0.00	0.00	0.18	0.29	0.00	0.29	***0.13 (0.1)***
H_2O*	3.62	4.37	3.52	4.40	4.02	4.31	4.29	4.02	4.09	3.95	4.08	3.98	4.27	4.28	4.29	4.01	3.87	4.16	3.91	***4.08 (0.2)***
Subtotal	99.69	94.34	99.74	97.92	98.91	97.30	98.93	94.36	99.15	98.05	97.92	99.08	98.08	96.62	97.30	97.34	98.42	95.94	99.18	***97.80***
O=F,Cl	0.72	0.03	0.75	0.05	0.42	0.09	0.18	0.24	0.35	0.42	0.25	0.45	0.14	0.09	0.12	0.35	0.49	0.13	0.49	***0.30***
Total	98.97	94.30	98.99	97.87	98.49	97.22	98.74	94.12	98.80	97.62	97.67	98.63	97.94	96.53	97.19	96.99	97.93	95.80	98.69	***97.50***
Cell formulae (to 22 oxygen)																				
Si	6.357	6.409	6.338	6.077	6.460	6.233	6.276	6.524	6.092	6.197	6.357	6.461	6.428	6.318	6.247	6.313	6.276	6.460	6.247	***6.32***
Al [iv]	1.643	1.591	1.662	1.923	1.540	1.767	1.724	1.476	1.908	1.803	1.643	1.539	1.572	1.682	1.753	1.687	1.724	1.540	1.753	***1.68***
Al [vi]	3.411	4.053	3.407	3.968	3.560	3.796	3.848	3.614	3.921	3.869	3.674	3.769	3.701	3.806	3.880	3.734	3.707	3.626	3.740	***3.74***
Ti	0.039	0.005	0.001	0.021	0.014	0.022	0.002	0.001	0.001	0.016	0.004	0.002	0.011	0.004	0.012	0.024	0.016	0.000	0.021	***0.01***
Fe	0.390	0.193	0.664	0.012	0.023	0.076	0.046	0.169	0.092	0.029	0.319	0.276	0.256	0.189	0.035	0.100	0.181	0.323	0.139	***0.18***
Mn	0.003	0.008	0.018	0.000	0.002	0.008	0.001	0.001	0.010	0.000	0.014	0.004	0.008	0.003	0.000	0.000	0.003	0.002	0.011	***0.01***
Mg	0.194	0.017	0.003	0.019	0.399	0.121	0.134	0.274	0.004	0.036	0.019	0.010	0.050	0.068	0.064	0.125	0.060	0.088	0.065	***0.09***
Li*	0.247	0.000	0.227	0.000	0.125	0.000	0.003	0.058	0.097	0.105	0.000	0.086	0.014	0.000	0.000	0.101	0.157	0.000	0.157	***0.07***
Ca	0.001	0.001	0.000	0.000	0.000	0.000	0.001	0.013	0.000	0.000	0.000	0.000	0.001	0.001	0.000	0.000	0.000	0.000	0.000	***0.00***
Na	0.054	0.019	0.060	0.090	0.075	0.070	0.092	0.038	0.081	0.075	0.048	0.020	0.044	0.053	0.071	0.062	0.058	0.058	0.073	***0.06***
K	1.779	0.956	1.781	1.787	1.758	1.811	1.713	1.624	1.747	1.822	1.853	1.540	1.738	1.673	1.795	1.779	1.836	1.778	1.787	***1.71***
OH*	3.272	3.965	3.223	3.953	3.581	3.913	3.815	3.747	3.651	3.569	3.741	3.550	3.860	3.907	3.882	3.641	3.500	3.861	3.501	***3.69***
F	0.72	0.03	0.68	0.04	0.41	0.05	0.11	0.25	0.34	0.36	0.03	0.32	0.14	0.04	0.05	0.35	0.50	0.09	0.49	***0.27***
Cl	0.00	0.00	0.09	0.00	0.00	0.02	0.07	0.00	0.00	0.06	0.23	0.12	0.00	0.04	0.06	0.00	0.00	0.04	0.00	***0.04***
TOTAL	18.116	17.252	18.161	17.896	17.955	17.904	17.839	17.790	17.955	17.952	17.931	17.706	17.823	17.797	17.857	17.924	18.024	17.874	17.994	***17.88***
Y total	4.283	4.276	4.320	4.019	4.123	4.023	4.033	4.116	4.124	4.054	4.035	4.146	4.040	4.069	3.991	4.083	4.124	4.034	4.133	***4.11***
X total	1.833	0.976	1.841	1.877	1.833	1.881	1.806	1.673	1.831	1.898	1.901	1.560	1.783	1.727	1.866	1.841	1.894	1.835	1.861	***1.77***
Al total	5.054	5.644	5.069	5.891	5.100	5.563	5.572	5.090	5.828	5.672	5.316	5.307	5.272	5.488	5.633	5.421	5.431	5.166	5.494	***5.42***
Fe/Fe+Mg	0.668	0.918	0.996	0.381	0.055	0.386	0.256	0.381	0.958	0.448	0.943	0.966	0.836	0.736	0.356	0.444	0.751	0.787	0.679	***0.63***

Identification number; + Standard deviations in parentheses (1σ); * Total Fe as FeO

Table 1 (continued)

zinnwaldite																
Ident. No.	**1**	**5**	**6**	**8**	**9**	**11**	**13**	**16**	**20**	**23**	**24**	**33**	**35**	**42**	**43**	**Average**
SiO_2	50.014	50.26	48.245	48.558	49.223	47.044	49.071	46.941	46.74	47.359	50.064	47.412	49.743	47.971	46.143	***48.32 (1.36)***
TiO_2	0.26	0.25	0.29	0.208	0.342	0.171	0.308	0.464	0.085	0.287	0.279	0.105	0.275	0.253	0.042	***0.24 (0.11)***
Al_2O_3	19.626	19.52	20.288	20.002	19.523	21.062	19.796	21.031	19.154	20.585	19.836	20.395	19.649	20.279	21.407	***20.14 (0.66)***
FeO	9.882	9.727	10.934	11.09	10.117	13.245	7.959	9.171	8.211	7.702	10.983	9.067	10.635	8.322	9.67	***9.78 (1.48)***
MnO	0.15	0.24	0.138	0.276	0.312	0.168	0.193	0.126	0.193	0.138	0.18	0.138	0.186	0.187	0.108	***0.18 (0.06)***
MgO	0.344	0.373	0.339	0.215	0.165	0.109	0.233	0.334	0.286	0.218	0.168	0.204	0.258	0.321	0.146	***0.25 (0.08)***
CaO	0	0	0	0	0	0	0	0	0.015	0	0	0	0	0	0.003	***0.00***
Na_2O	0.121	0.125	0.194	0.099	0.202	0.164	0.216	0.155	0.112	0.189	0.113	0.14	0.148	0.14	0.193	***0.15 (0.04)***
K_2O	9.83	9.89	9.648	9.513	9.613	9.692	9.66	9.871	9.253	9.88	9.497	9.756	9.787	9.737	10.115	***9.72 (0.2)***
F	5.628	6.199	5.388	5.118	5.656	5.433	5.686	5.422	5.112	6.143	7.466	6.39	6.426	5.358	5.258	***5.78 (0.64)***
Cl	0.325	0	0.915	0	0.856	0.206	0.059	0	0	0.207	0.089	0	0	0	0.826	***0.23 (0.34)***
Li_2O*	4.80	4.87	4.29	4.38	4.58	3.95	4.53	3.92	3.86	4.04	4.82	4.06	4.72	4.22	3.69	***4.32 (0.39)***
H_2O*	1.61	1.44	1.51	1.87	1.41	1.66	1.55	1.64	1.63	1.21	0.83	1.16	1.31	1.67	1.46	***1.46 (0.26)***
Subtotal	102.59	102.89	102.18	101.33	101.99	102.90	99.26	99.07	94.65	97.95	104.32	98.82	103.14	98.46	99.06	***100.57***
O=F,Cl	2.44	2.61	2.47	2.15	2.57	2.33	2.41	2.28	2.15	2.63	3.16	2.69	2.71	2.26	2.40	***2.48***
Total	100.15	100.28	99.71	99.18	99.42	100.57	96.85	96.79	92.50	95.32	101.16	96.13	100.44	96.20	96.66	***98.09***
Cell formulae (to 22 oxygen)																
Si	6.874	6.888	6.737	6.778	6.855	6.582	6.909	6.690	6.914	6.808	6.839	6.793	6.841	6.827	6.650	***6.80***
Al ^{iv}	1.126	1.112	1.263	1.222	1.145	1.418	1.091	1.310	1.086	1.192	1.161	1.207	1.159	1.173	1.350	***1.20***
Al ^{vi}	2.054	2.041	2.077	2.069	2.059	2.055	2.194	2.223	2.254	2.296	2.032	2.237	2.027	2.228	2.286	***2.14***
Ti	0.027	0.026	0.030	0.022	0.036	0.018	0.033	0.050	0.009	0.031	0.029	0.011	0.028	0.027	0.005	***0.03***
Fe	1.136	1.115	1.277	1.295	1.178	1.550	0.937	1.093	1.016	0.926	1.255	1.086	1.223	0.990	1.165	***1.15***
Mn	0.017	0.028	0.016	0.033	0.037	0.020	0.023	0.015	0.024	0.017	0.021	0.017	0.022	0.023	0.013	***0.02***
Mg	0.070	0.076	0.071	0.045	0.034	0.023	0.049	0.071	0.063	0.047	0.034	0.044	0.053	0.068	0.031	***0.05***
Li*	2.655	2.686	2.412	2.461	2.563	2.223	2.566	2.247	2.298	2.336	2.646	2.337	2.613	2.413	2.139	***2.44***
Na	0.032	0.033	0.053	0.027	0.055	0.044	0.059	0.043	0.032	0.053	0.030	0.039	0.039	0.039	0.054	***0.04***
K	1.723	1.729	1.719	1.694	1.708	1.730	1.735	1.794	1.746	1.812	1.655	1.783	1.717	1.767	1.859	***1.74***
OH*	1.478	1.313	1.404	1.741	1.307	1.547	1.454	1.556	1.608	1.157	0.754	1.105	1.205	1.589	1.402	***1.37***
F	2.446	2.687	2.380	2.259	2.491	2.404	2.532	2.444	2.392	2.793	3.225	2.895	2.795	2.411	2.396	***2.57***
Cl	0.076	0.000	0.217	0.000	0.202	0.049	0.014	0.000	0.000	0.050	0.021	0.000	0.000	0.000	0.202	***0.06***
TOTAL	19.714	19.734	19.654	19.645	19.669	19.662	19.596	19.536	19.446	19.517	19.701	19.553	19.722	19.555	19.554	***19.62***
Y total	5.959	5.972	5.883	5.925	5.907	5.888	5.802	5.699	5.664	5.653	6.017	5.732	5.966	5.749	5.640	***5.83***
X total	1.756	1.762	1.771	1.721	1.762	1.774	1.794	1.837	1.780	1.864	1.685	1.822	1.756	1.806	1.914	***1.79***
Al total	3.179	3.153	3.339	3.291	3.205	3.473	3.285	3.533	3.340	3.488	3.194	3.444	3.185	3.401	3.636	***3.34***
Fe/Fe+Mg	0.942	0.936	0.948	0.967	0.972	0.986	0.950	0.939	0.942	0.952	0.973	0.961	0.959	0.936	0.974	***0.96***

Table 2: Microprobe data of non-magnetic mica

Other minerals													
Ident. No.	**3**	**10**	**18**	**29**	**32**	**Average**	**14**	**21**	**37**	**Average**	**22**	**27**	**Average**
SiO_2	98.66	98.73	99.21	99.19	97.23	***98.61 (0.81)***	63.81	64.22	64.41	***64.15 (0.31)***	46.13	45.57	***45.85 (0.40)***
TiO_2	0.00	0.00	0.02	0.00	0.02	***0.01 (0.01)***	0.01	0.00	0.00	***0.00***	0.01	0.00	***0.00***
Al_2O_3	0.03	0.10	0.04	0.00	0.08	***0.05 (0.04)***	18.35	18.88	18.71	***18.65 (0.27)***	36.87	36.51	***36.69 (0.26)***
FeO	0.05	0.00	0.00	0.05	0.00	***0.02 (0.03)***	0.00	0.05	0.05	***0.03 (0.03)***	0.77	0.16	***0.46 (0.44)***
MnO	0.02	0.00	0.00	0.09	0.00	***0.02 (0.04)***	0.00	0.06	0.00	***0.02 (0.03)***	0.00	0.00	***0.00***
MgO	0.00	0.00	0.00	0.00	0.00	***0.00***	0.01	0.01	0.00	***0.01 (0.01)***	0.05	0.02	***0.03 (0.02)***
CaO	0.01	0.01	0.01	0.01	0.00	***0.01 (0.00)***	0.00	0.00	0.00	***0.00***	0.02	0.01	***0.01 (0.00)***
Na_2O	0.00	0.03	0.00	0.00	0.02	***0.01 (0.01)***	0.39	0.55	0.35	***0.43 (0.10)***	0.09	0.01	***0.05 (0.06)***
K_2O	0.01	0.00	0.02	0.01	0.01	***0.01 (0.01)***	15.75	15.32	14.94	***15.34 (0.40***	3.92	0.12	***2.02 (2.69)***
F	0.00	0.06	0.09	0.09	0.02	***0.05 (0.04)***	0.01	0.00	0.00	***0.00***	0.32	0.01	***0.17 (0.21)***
Cl	0.00	0.00	0.09	0.00	0.16	***0.05 (0.07)***	0.00	0.00	0.03	***0.01 (0.02)***	0.18	0.09	***0.14 (0.06)***
Total	98.79	98.88	99.43	99.41	97.48	***98.80***	98.33	99.09	98.49	***98.64***	88.19	82.47	***85.33***

Note: In Table 2, the microprobe analysis of identification numbers 3, 10, 18, 29 and 32 appears to be grains of quartz; that of 14, 21 and 37 appears to be K-feldspar; 22 and 27 are kaolinite.

Table 3: Microprobe data of magnetic mica

Magnetic mica (Zinnwaldite)

Ident. No.	46	49	53	54	55	58	59	60	61	62	63	69	70	71	72	76
SiO_2	48.38	47.02	46.30	45.66	42.91	48.28	47.01	46.54	43.46	43.69	45.12	47.39	48.97	47.99	43.36	50.16
TiO_2	0.05	0.08	0.32	0.14	0.06	0.01	0.03	0.10	0.27	0.26	0.18	0.10	0.07	0.03	0.07	0.08
Al_2O_3	19.58	19.94	21.15	21.43	19.39	21.72	21.34	20.63	22.01	22.52	19.85	20.05	20.04	19.14	18.49	18.59
FeO	8.21	9.22	8.51	14.20	7.35	10.84	13.65	12.55	14.84	16.81	11.49	12.11	10.39	6.75	11.44	10.40
MnO	0.14	0.17	0.18	0.22	0.17	0.25	0.20	0.17	0.16	0.02	0.18	0.08	0.11	0.08	0.18	0.13
MgO	0.71	0.01	0.29	0.28	0.32	0.13	0.12	0.33	0.36	0.39	0.27	0.20	0.10	0.23	0.16	0.21
CaO	0.00	0.00	0.00	0.00	0.02	0.00	0.00	0.00	0.00	0.00	0.00	0.00	0.00	0.01	0.00	0.00
Na_2O	0.16	0.16	0.16	0.22	0.10	0.27	0.17	0.20	0.24	0.26	0.17	0.11	0.15	0.15	0.17	0.14
K_2O	9.89	9.76	9.95	9.79	8.20	9.97	9.80	9.44	9.45	9.53	9.59	10.16	9.63	9.85	8.18	9.89
F	6.38	5.49	5.04	4.73	3.92	4.68	4.96	4.44	5.27	4.45	5.46	4.67	7.38	5.35	4.86	6.08
Cl	0.09	0.00	0.56	0.12	0.00	0.00	0.18	0.00	0.00	0.32	0.65	0.00	0.00	0.00	0.03	0.00
Li_2O*	4.33	3.94	3.74	3.55	2.76	4.30	3.94	3.80	2.92	2.99	3.40	4.05	4.50	4.22	2.89	4.84
H_2O*	1.17	1.53	1.62	1.96	1.90	2.13	1.91	2.11	1.63	2.02	1.30	2.03	0.80	1.58	1.52	1.44
Subtotal	99.09	97.32	97.80	102.28	87.10	102.60	103.32	100.32	100.59	103.26	97.67	100.94	102.13	95.37	91.36	101.96
O=F,Cl	2.71	2.31	2.25	2.02	1.65	1.97	2.13	1.87	2.22	1.95	2.45	1.97	3.11	2.25	2.05	2.56
Total	96.38	95.01	95.56	100.26	85.45	100.62	101.19	98.45	98.37	101.32	95.22	98.98	99.03	93.12	89.31	99.40
Cell formulae (to 22 oxygen)																
Si	6.88	6.82	6.69	6.46	6.85	6.65	6.55	6.62	6.31	6.22	6.67	6.70	6.83	7.00	6.78	6.96
Al ^{iv}	1.12	1.18	1.31	1.54	1.15	1.35	1.45	1.38	1.69	1.78	1.33	1.30	1.17	1.00	1.22	1.04
Al ^{vi}	2.16	2.24	2.30	2.03	2.49	2.18	2.05	2.08	2.08	2.00	2.12	2.04	2.12	2.29	2.19	2.00
Ti	0.01	0.01	0.03	0.01	0.01	0.00	0.00	0.01	0.03	0.03	0.02	0.01	0.01	0.00	0.01	0.01
Fe	0.98	1.12	1.03	1.68	0.98	1.25	1.59	1.49	1.80	2.00	1.42	1.43	1.21	0.82	1.50	1.21
Mn	0.02	0.02	0.02	0.03	0.02	0.03	0.02	0.02	0.02	0.00	0.02	0.01	0.01	0.01	0.02	0.01
Mg	0.15	0.00	0.06	0.06	0.08	0.03	0.03	0.07	0.08	0.08	0.06	0.04	0.02	0.05	0.04	0.04
Li*	2.48	2.30	2.17	2.02	1.77	2.38	2.21	2.18	1.71	1.71	2.02	2.30	2.53	2.48	1.82	2.70
Na	0.04	0.04	0.04	0.06	0.03	0.07	0.05	0.06	0.07	0.07	0.05	0.03	0.04	0.04	0.05	0.04
K	1.79	1.81	1.83	1.77	1.67	1.75	1.74	1.71	1.75	1.73	1.81	1.83	1.71	1.83	1.63	1.75
OH*	1.11	1.48	1.56	1.85	2.02	1.96	1.77	2.00	1.58	1.92	1.28	1.91	0.74	1.53	1.59	1.33
F	2.87	2.52	2.30	2.12	1.98	2.04	2.19	2.00	2.42	2.00	2.55	2.09	3.26	2.47	2.40	2.67
Cl	0.02	0.00	0.14	0.03	0.00	0.00	0.04	0.00	0.00	0.08	0.16	0.00	0.00	0.00	0.01	0.00
TOTAL	19.63	19.54	19.50	19.66	19.06	19.69	19.69	19.61	19.53	19.62	19.52	19.70	19.66	19.53	19.26	19.76
Y total	5.79	5.69	5.62	5.84	5.35	5.87	5.91	5.85	5.72	5.82	5.67	5.84	5.90	5.65	5.57	5.97
X total	1.84	1.85	1.88	1.83	1.70	1.82	1.79	1.77	1.82	1.80	1.86	1.86	1.75	1.88	1.68	1.79
Al total	3.28	3.41	3.60	3.57	3.65	3.53	3.50	3.46	3.77	3.78	3.46	3.34	3.29	3.29	3.41	3.04
Fe/Fe+Mg	0.87	1.00	0.94	0.97	0.93	0.98	0.98	0.95	0.96	0.96	0.96	0.97	0.98	0.94	0.98	0.96

Table 3 (continued)

Zinnwaldite

Ident. No.	77	78	79	80	81	82	85	86	87	88	89	90	91	92	93	94	95	96	Average
SiO_2	50.17	48.05	43.19	47.92	46.90	45.97	46.91	44.61	46.68	48.62	43.91	46.15	45.68	48.90	47.73	47.90	49.55	50.47	***46.81 (2.12)***
TiO_2	0.11	0.04	0.07	0.04	0.16	0.16	0.18	0.13	0.03	0.02	0.05	0.25	0.21	0.24	0.28	0.20	0.20	0.18	***0.13 (0.09)***
Al_2O_3	18.90	20.67	22.61	20.69	20.30	21.22	20.32	20.58	22.19	20.85	21.89	21.29	20.76	20.71	20.80	20.60	19.74	20.42	***20.60 (1.05)***
FeO	10.25	12.46	9.34	14.12	12.61	13.51	13.06	13.56	11.46	11.45	10.93	12.00	14.00	10.60	14.57	13.16	13.21	11.53	***11.78 (2.25)***
MnO	0.11	0.00	0.07	0.09	0.10	0.20	0.16	0.14	0.29	0.06	0.32	0.23	0.26	0.17	0.13	0.20	0.10	0.12	***0.15 (0.07)***
MgO	0.21	0.18	0.28	0.18	0.39	0.34	0.45	0.41	0.21	0.19	0.22	0.21	0.17	0.24	0.23	0.22	0.29	0.30	***0.26 0.12)***
CaO	0.00	0.00	0.00	0.00	0.00	0.00	0.00	0.00	0.00	0.00	0.02	0.00	0.00	0.00	0.00	0.00	0.00	0.00	***0.00 (0.01)***
Na_2O	0.13	0.22	0.13	0.17	0.21	0.12	0.28	0.14	0.23	0.23	0.09	0.31	0.33	0.27	0.22	0.23	0.09	0.07	***0.19 (0.07)***
K_2O	9.81	10.03	9.14	10.15	9.75	9.99	9.62	9.72	10.05	9.97	8.54	9.52	9.44	9.75	9.66	9.67	9.70	9.58	***9.62 (0.47)***
F	5.39	4.99	2.65	5.13	5.16	4.64	4.65	4.20	4.00	5.10	3.30	4.54	4.49	5.50	4.74	5.29	3.26	2.20	***4.78 (0.99)***
Cl	0.39	0.00	0.00	0.00	0.00	0.15	0.71	0.18	0.03	0.92	0.80	0.00	0.00	0.00	0.47	0.15	0.00	0.15	***0.17 (0.27)***
Li_2O*	4.85	4.24	2.84	4.20	3.91	3.64	3.91	3.25	3.85	4.40	3.05	3.69	3.56	4.48	4.15	4.19	4.67	4.93	***3.88 (0.61)***
H_2O*	1.68	1.96	2.73	1.92	1.79	2.00	1.87	2.07	2.38	1.70	2.27	2.06	2.07	1.74	1.99	1.79	2.86	3.38	***1.91 (0.47)***
Subtotal	101.99	102.84	93.05	104.60	101.27	101.94	102.13	98.98	101.39	103.51	95.38	100.26	100.96	102.59	104.97	103.60	103.66	103.33	***100.28***
O=F,Cl	2.36	2.10	1.12	2.16	2.17	1.99	2.12	1.81	1.69	2.35	1.57	1.91	1.89	2.32	2.10	2.26	1.37	0.96	***2.05***
Total	99.64	100.74	91.93	102.44	99.09	99.95	100.01	97.18	99.70	101.16	93.81	98.35	99.07	100.28	102.87	101.34	102.29	102.37	***98.23***
Cell formulae (to 22 oxygen)																			
Si	6.94	6.67	6.49	6.60	6.64	6.50	6.61	6.51	6.54	6.71	6.53	6.56	6.52	6.74	6.56	6.63	6.75	6.79	***6.66***
Al ^{iv}	1.06	1.33	1.51	1.40	1.36	1.50	1.39	1.49	1.46	1.29	1.47	1.44	1.48	1.26	1.44	1.37	1.25	1.21	***1.34***
Al ^{vi}	2.02	2.05	2.49	1.96	2.03	2.04	1.99	2.05	2.20	2.10	2.36	2.13	2.02	2.10	1.93	2.00	1.92	2.02	***2.11***
Ti	0.01	0.00	0.01	0.00	0.02	0.02	0.02	0.01	0.00	0.00	0.01	0.03	0.02	0.02	0.03	0.02	0.02	0.02	***0.01***
Fe	1.19	1.45	1.17	1.63	1.49	1.60	1.54	1.65	1.34	1.32	1.36	1.43	1.67	1.22	1.68	1.52	1.50	1.30	***1.40***
Mn	0.01	0.00	0.01	0.01	0.01	0.02	0.02	0.02	0.03	0.01	0.04	0.03	0.03	0.02	0.02	0.02	0.01	0.01	***0.02***
Mg	0.04	0.04	0.0	0.04	0.08	0.07	0.09	0.0	0.04	0.04	0.0	0.04	0.04	0.05	0.05	0.05	0.06	0.06	***0.06***

			6					9			5								
Li*	2.70	2.37	1.72	2.33	2.22	2.07	2.22	1.91	2.17	2.44	1.82	2.11	2.04	2.48	2.29	2.34	2.56	2.67	***2.21***
Na	0.03	0.06	0.04	0.05	0.06	0.03	0.08	0.04	0.06	0.06	0.03	0.09	0.09	0.07	0.06	0.06	0.02	0.02	***0.05***
K	1.73	1.78	1.75	1.78	1.76	1.80	1.73	1.81	1.79	1.75	1.62	1.73	1.72	1.71	1.69	1.71	1.69	1.64	***1.74***
OH*	1.55	1.81	2.74	1.77	1.69	1.89	1.76	2.02	2.22	1.56	2.25	1.96	1.97	1.60	1.83	1.65	2.60	3.03	***1.81***
F	2.36	2.19	1.26	2.23	2.31	2.08	2.07	1.94	1.77	2.22	1.55	2.04	2.03	2.40	2.06	2.32	1.40	0.94	***2.15***
Cl	0.09	0.00	0.00	0.00	0.00	0.04	0.17	0.04	0.01	0.21	0.20	0.00	0.00	0.00	0.11	0.03	0.00	0.03	***0.04***
TOTAL	19.74	19.74	19.25	19.79	19.67	19.66	19.69	19.58	19.64	19.73	19.28	19.59	19.63	19.69	19.74	19.72	19.78	19.74	***19.61***
Y total	5.97	5.90	5.46	5.96	5.85	5.83	5.88	5.73	5.79	5.91	5.64	5.77	5.82	5.90	5.99	5.95	6.07	6.08	***5.81***
X total	1.76	1.83	1.79	1.83	1.82	1.84	1.81	1.85	1.86	1.82	1.65	1.81	1.81	1.79	1.75	1.77	1.71	1.66	***1.80***
Al total	3.08	3.38	4.00	3.36	3.39	3.54	3.38	3.54	3.66	3.39	3.83	3.57	3.49	3.36	3.37	3.36	3.17	3.24	***3.46***
Fe/Fe+Mg	0.96	0.97	0.95	0.98	0.95	0.96	0.94	0.95	0.97	0.97	0.97	0.97	0.98	0.96	0.97	0.97	0.96	0.96	***0.96***

Table 3 (continued)

muscovites							
Ident. No.	**45**	**64**	**67**	**68**	**83**	**84**	**Average**
SiO_2	46.33	47.48	47.15	47.14	46.72	49.25	***47.35 (1.01)***
TiO_2	0.10	0.05	0.05	0.08	0.14	0.00	***0.07 (0.05)***
Al_2O_3	32.82	31.18	30.74	32.43	28.78	30.01	***30.99 (1.51)***
FeO	2.77	3.29	4.37	3.76	5.18	2.11	***3.58 (1.11)***
MnO	0.09	0.04	0.10	0.09	0.02	0.03	***0.06 (0.04)***
MgO	0.24	0.11	0.11	0.14	0.30	1.28	***0.36 (0.46)***
CaO	0.00	0.00	0.00	0.00	0.01	0.03	***0.01 (0.01)***
Na_2O	0.23	0.14	0.14	0.14	0.14	0.06	***0.14 (0.05)***
K_2O	10.34	10.44	10.44	10.42	10.12	9.32	***10.18 (0.44)***
F	1.40	1.50	0.93	0.81	2.18	0.95	***1.30 (0.51)***
Cl	0.03	0.00	0.00	0.00	0.00	0.00	***0.01 (0.01)***
Li_2O*	0.36	0.39	0.21	0.18	0.60	0.22	***0.33 (0.16)***
H_2O*	3.72	3.67	3.91	4.04	3.25	3.96	***3.76 (0.29)***
Subtotal	98.44	98.28	98.15	99.22	97.43	97.22	***98.12***
O=F,Cl	0.60	0.63	0.39	0.34	0.92	0.40	***0.55***
Total	97.84	97.65	97.76	98.88	96.52	96.82	***97.58***
Cell formulae (to 22 oxygen)							
Si	6.326	6.500	6.489	6.389	6.541	6.699	***6.46***
Al ^{iv}	1.674	1.500	1.511	1.611	1.459	1.301	***1.51***
Al ^{vi}	3.608	3.532	3.475	3.571	3.291	3.511	***3.50***
Ti	0.010	0.005	0.006	0.008	0.014	0.000	***0.01***
Fe	0.317	0.377	0.502	0.426	0.607	0.240	***0.41***
Mn	0.010	0.005	0.012	0.010	0.002	0.003	***0.01***
Mg	0.049	0.022	0.023	0.029	0.062	0.260	***0.07***
Li*	0.198	0.216	0.119	0.096	0.339	0.120	***0.18***
Ca	0.000	0.000	0.000	0.000	0.002	0.004	***0.00***
Na	0.060	0.038	0.038	0.036	0.037	0.015	***0.04***
K	1.801	1.823	1.832	1.802	1.807	1.617	***1.78***
OH*	3.388	3.350	3.594	3.653	3.035	3.591	***3.44***
F	0.605	0.650	0.406	0.347	0.965	0.409	***0.56***
Cl	0.007	0.000	0.000	0.000	0.000	0.000	***0.00***
TOTAL	18.053	18.017	18.007	17.979	18.162	17.771	***18.00***
Y total	4.192	4.157	4.137	4.140	4.315	4.135	***4.18***
X total	1.861	1.860	1.870	1.839	1.846	1.636	***1.82***
Al total	5.282	5.032	4.986	5.181	4.750	4.812	***5.01***
Fe/Fe+Mg	0.865	0.944	0.956	0.936	0.907	0.480	***0.85***

Table 4: Microprobe data of magnetic mica

Other minerals														
Ident. No.	**52**	**48**	**56**	**57**	**74**	**75**	**Average**	**50**	**51**	**65**	**66**	**73**	Average	**47**
SiO_2	88.01	99.11	98.10	98.34	98.91	98.74	***96.87 (4.35)***	65.12	59.99	63.98	62.83	63.70	***63.12 (1.94)***	0.00
TiO_2	0.01	0.00	0.00	0.01	0.01	0.00	***0.00 (0.01)***	0.00	0.00	0.00	0.00	0.01	***0.00 (0.01)***	0.00
Al_2O_3	5.32	0.00	0.00	0.00	0.02	0.07	***0.90 (2.16)***	18.47	17.34	18.14	18.12	18.18	***18.05 (0.42)***	0.00
FeO	0.52	0.05	0.05	0.00	0.52	0.52	***0.28 (0.27)***	0.00	0.16	0.21	0.00	0.10	***0.09 (0.09)***	1.07
MnO	0.01	0.00	0.00	0.06	0.00	0.10	***0.03 (0.04)***	0.00	0.00	0.08	0.00	0.01	***0.02 (0.03)***	4.35
MgO	0.02	0.00	0.00	0.02	0.00	0.00	***0.01 (0.010***	0.01	0.00	0.00	0.01	0.00	***0.00 (0.01)***	0.02
CaO	0.06	0.01	0.01	0.02	0.01	0.01	***0.02 (0.02)***	0.02	1.13	0.00	0.00	0.00	***0.23 (0.50)***	47.85
Na_2O	0.06	0.02	0.01	0.00	0.01	0.00	***0.01 (0.02)***	0.25	0.30	0.25	0.33	0.15	***0.26 (0.07)***	0.00
K_2O	0.13	0.02	0.00	0.02	0.02	0.02	***0.03 (0.05)***	15.67	15.39	15.59	15.56	14.54	***15.35 (0.46)***	0.02
F	0.53	0.08	0.00	0.02	0.11	0.02	***0.13 (0.20)***	0.14	0.04	0.00	0.00	0.00	***0.03 (0.06)***	3.82
Cl	0.00	0.00	0.31	0.69	0.00	0.25	***0.21 (0.27)***	0.24	0.39	0.00	0.27	0.18	***0.21 (0.14)***	0.00
Total	94.43	99.25	98.42	99.01	99.54	99.66	***98.38***	99.80	94.63	98.59	97.06	96.84	***97.38***	55.53

Note: In Table 4, the microprobe analysis of identification numbers 48, 52, 56, 57, 74 and 75 appears to grains of quartz; 50, 51, 65, 66 and 73 are K-feldspar. The analysis of number 47 appears to be that of apatite.

Appendix G: Cleaner flotation test results balance sheets.

Table 1: Run 1

Flotation Time (sec)	Fraction	Weight (g)	Weight (%)	Content (%) SiO_2	Al_2O_3	Fe_2O_3	TiO_2	MgO	CaO	K_2O	Na_2O	P_2O_5	F	LOI
480	Conc. 1	1111.60	93.91	48.260	30.480	4.643	0.181	0.342	0.034	8.203	0.131	0.038	2.400	5.630
	Tail	72.10	6.09	73.290	16.730	0.652	0.822	0.219	0.053	5.570	0.490	0.128	0.970	1.960
	Head Cal.	1183.70	100.00	**49.785**	**29.642**	**4.400**	**0.220**	**0.335**	**0.035**	**8.043**	**0.153**	**0.043**	**2.313**	**5.406**
Time		**Weight**	**Weight**	**Recovery %**										
(sec)	Fraction	(g)	(%)	SiO_2	Al_2O_3	Fe_2O_3	TiO_2	MgO	CaO	K_2O	Na_2O	P_2O_5	F	LOI
480	Conc. 1	1111.60	93.91	91.03	96.56	99.10	77.25	96.01	90.82	95.78	80.48	82.07	97.45	5.630
	Tail	72.10	6.09	8.97	3.44	0.90	22.75	3.99	9.18	4.22	19.52	17.93	2.55	1.960
				100.00	100.00	100.00	100.00	100.00	100.00	100.00	100.00	100.00	100.00	5.406

Table 2: Run 2

Flotation Time (sec)	Fraction	Weight (g)	Weight (%)	Content (%) SiO_2	Al_2O_3	Fe_2O_3	TiO_2	MgO	CaO	K_2O	Na_2O	P_2O_5	F	LOI
480	Conc. 1	1099.00	93.10	48.330	30.450	4.814	0.186	0.345	0.042	8.367	0.130	0.041	2.030	5.360
	Tail	81.40	6.90	72.880	17.120	0.675	0.104	0.224	0.067	5.635	0.485	0.154	1.000	1.840
	Head Cal.	1180.40	100.00	**50.023**	**29.531**	**4.529**	**0.180**	**0.337**	**0.044**	**8.179**	**0.154**	**0.049**	**1.959**	**5.117**
Time		**Weight**	**Weight**	**Recovery %**										
(sec)	Fraction	(g)	(%)	SiO_2	Al_2O_3	Fe_2O_3	TiO_2	MgO	CaO	K_2O	Na_2O	P_2O_5	F	LOI
480	Conc. 1	1099.00	93.10	89.95	96.00	98.97	96.02	95.41	89.47	95.25	78.35	78.23	96.48	5.360
	Tail	81.40	6.90	10.05	4.00	1.03	3.98	4.59	10.53	4.75	21.65	21.77	3.52	1.840
				100.0	100.0	100.0	100.0	100.0	100.0	100.0	100.0	100.0	100.0	5.11

Table 3: Run 3

Flotation Time (sec)	Fraction	Weight (g)	Weight (%)	Content (%) SiO_2	Al_2O_3	Fe_2O_3	TiO_2	MgO	CaO	K_2O	Na_2O	P_2O_5	F	LOI
480	Conc. 1	1114.10	94.59	48.400	30.630	4.766	0.186	0.336	0.039	8.213	0.129	0.036	2.220	5.270
	Tail	63.70	5.41	75.290	15.340	0.572	0.070	0.194	0.045	5.493	0.527	0.129	0.930	1.570
	Head Cal.	1177.80	100.00	**49.854**	**29.803**	**4.539**	**0.180**	**0.328**	**0.039**	**8.066**	**0.151**	**0.041**	**2.150**	**5.070**
Time		**Weight**	**Weight**	**Recovery %**										
(sec)	Fraction	(g)	(%)	SiO_2	Al_2O_3	Fe_2O_3	TiO_2	MgO	CaO	K_2O	Na_2O	P_2O_5	F	LOI
480	Conc. 1	1114.10	94.59	91.83	97.22	99.32	97.88	96.80	93.86	96.32	81.06	83.00	97.66	5.270
	Tail	63.70	5.41	8.17	2.78	0.68	2.12	3.20	6.14	3.68	18.94	17.00	2.34	1.570
				100.0	100.0	100.0	100.0	100.0	100.0	100.0	100.0	100.0	100.0	5.07

Appendix H1: The Gypsum Method.

Table 1: Effect of temperature on lithium, rubidium and iron extraction efficiencies- Gypsum method (Leaching at 85°C; L:S = 10; leaching time = 60 minutes; natural pH of 7; sinter ratio = 2:1).

Sintering Temperature (°C)	Sinter grade (%)			Weight of sinter leached (g)	Concentration of elements in solution (µg/ml) (250 ml)			Extraction efficiency (%)		
	Li	Rb	Fe		Li	Rb	Fe	Li	Rb	Fe
900	0.78	0.50	2.76	10.36	96.92	5.25	12.27	30.10	2.52	1.07
925	0.77	0.50	1.65	10.37	178.7	9.45	13.72	55.97	4.55	2.00
950	0.78	0.51	3.94	10.37	194.8	15.22	8.49	60.32	7.25	0.52
975	0.78	0.50	4.55	10.37	213.5	19.13	11.85	65.90	9.15	0.63

Table 2: Effect of temperature on lithium, rubidium and iron extraction efficiencies- Gypsum method (Leaching at 85°C; L:S = 10; leaching time = 60 minutes; natural pH of 6-8; sinter ratio = 2:1).

Test Number	Sinter Temp (°C)	Sinter grade (%)			Weight of sinter leached (g)	Concentration of elements in solution (µg/ml) (250 ml)			Extraction Efficiency (%)		
		Li	Rb	Fe		Li	Rb	Fe	Li	Rb	Fe
1a	250	0.76	0.52	3.12	10.21	0.72	0.20	0.12	0.23	0.09	0.01
1b	250	0.76	0.52	3.12	10.55	0.43	0.20	0.06	0.13	0.09	0.00
2a	500	0.76	0.52	3.12	9.92	2.15	0.15	0.09	0.71	0.07	0.01
2b	500	0.76	0.52	3.12	10.04	2.65	0.17	0.07	0.86	0.08	0.01
3a	750	0.76	0.52	3.12	10.19	7.01	0.35	0.07	2.25	0.16	0.01
3b	750	0.76	0.52	3.12	10.27	7.19	0.31	0.01	2.29	0.15	0.00
4a	800	0.76	0.52	3.12	10.11	4.75	0.34	0.08	1.54	0.16	0.01
4b	800	0.76	0.52	3.12	9.34	4.31	0.30	0.08	1.51	0.15	0.01
5a	850	0.76	0.52	3.12	10.48	2.52	0.26	0.08	0.79	0.12	0.01
5b	850	0.76	0.52	3.12	10.41	2.63	0.28	0.02	0.83	0.13	0.00
6a	900	0.76	0.52	3.12	10.44	84.85	2.12	0.01	26.60	0.98	0.00
6b	900	0.76	0.52	3.12	10.05	63.9	1.95	0	20.81	0.93	0.00
7a	950	0.76	0.52	3.12	10.13	165	4.45	0.06	53.30	2.11	0.00
7b	950	0.76	0.52	3.12	10.48	161.3	4.56	0.07	50.37	2.10	0.01
8a	1050	0.76	0.52	3.12	10.78	277	30.52	0.04	84.07	13.62	0.00
8b	1050	0.76	0.52	3.12	10.61	272	30.31	0	83.87	13.74	0.00
9a	1100	0.76	0.52	3.12	10.87	280.3	32.56	0	84.37	14.41	0.00
9b	1100	0.76	0.52	3.12	10.84	280.7	32.43	0	84.72	14.39	0.00

Table 3: Effect of leaching bath temperature on lithium, rubidium and iron extraction efficiency - Gypsum method (L:S = 10; leaching time = 35 minutes; natural pH of 7; sinter ratio = 2:1; sinter temperature = 1050°C).

Leaching temperature (°C)	Sinter Grade (%)			Weight of sinter leached (g)	Concentration of elements in solution (µg/ml) (250 ml)			Extraction efficiency (%)		
	Li	Rb	Fe		Li	Rb	Fe	Li	Rb	Fe
20	0.68	0.33	2.55	10.00	163.7	16.30	0.0	60.17	12.48	0.00
30	0.68	0.33	2.55	10.00	169.32	16.21	0.08	62.22	12.41	0.01
45	0.68	0.33	2.55	10.00	188.5	16.53	0.0	69.29	12.66	0.00
65	0.68	0.33	2.55	10.00	209	17.57	0.03	76.82	13.45	0.00
75	0.68	0.33	2.55	10.00	212	17.59	0.0	77.91	13.47	0.00
85	0.68	0.33	2.55	10.00	233.9	18.97	0.05	85.95	14.52	0.01

Table 4: Dissolution kinetics on lithium, rubidium and iron - Gypsum method (Leaching at 85°C; L:S = 10; leaching time = 60 minutes; natural pH of 7; sinter ratio = 2:1; sinter temperature = 1050°C).

Leaching time (min)	Sinter grade (%)			Weight of sinter leached (g)	Concentration of elements in solution (µg/ml) (250 ml)			Extraction efficiency (%)		
	Li	Rb	Fe		Li	Rb	Fe	Li	Rb	Fe
2	0.68	0.33	2.55	10.01	155.0	15.58	0	56.95	11.92	0.00
6	0.68	0.33	2.55	10.01	212.0	16.79	0	77.89	12.85	0.00
10	0.68	0.33	2.55	10.00	220.8	17.27	0	81.16	13.23	0.00
20	0.68	0.33	2.55	10.00	218.0	17.00	0	80.12	13.02	0.00
30	0.68	0.33	2.55	10.00	221.3	16.42	0	81.33	12.57	0.00
60	0.68	0.33	2.55	10.00	228.8	17.19	0	84.09	13.16	0.00

Table 5: Effect of sinter ratio on lithium, rubidium and iron extraction efficiency - Gypsum method (Leaching at 85°C; L:S = 10; leaching time = 35 minutes; natural pH of 7; sinter temperature = 1050°C).

Sinter ratio	Sinter Grade (%)			Weight of sinter leached (g)	Concentration of elements in Solution (µg/ml) (250 ml)			Extraction efficiency (%)		
	Li	Rb	Fe		Li	Rb	Fe	Li	Rb	Fe
3:1	0.82	0.58	4.45	10.00	218.6	19.16	0	66.42	8.22	0.00
3:1	0.82	0.58	4.45	10.00	221	19.11	0	67.14	8.20	0.00
4:1	0.86	0.53	4.22	10.00	179.6	10.62	0	52.16	5.04	0.00
4:1	0.86	0.53	4.22	10.00	204.6	11.84	0	59.41	5.62	0.00
5:1	0.87	0.50	4.46	10.00	184.4	9.93	0	53.04	4.98	0.00
5:1	0.87	0.50	4.46	10.00	180.9	9.89	0	52.03	4.96	0.00
6:1	0.85	0.55	4.63	10.00	151.2	8.26	0	44.61	3.76	0.00
6:1	0.85	0.55	4.63	8.45	137.9	7.42	0	48.16	4.00	0.00
7:1	0.90	0.56	4.50	10.00	149.4	7.62	0	41.51	3.42	0.00
7:1	0.90	0.56	4.50	10.00	148.4	7.53	0	41.23	3.38	0.00
8:1	0.92	0.67	5.21	10.00	135.9	5.82	0	37.09	2.17	0.00
8:1	0.92	0.67	5.21	10.00	137.5	5.81	0	37.53	2.16	0.00
9:1	0.92	0.66	4.95	10.00	127.2	6.54	0	34.69	2.48	0.00
9:1	0.92	0.66	4.95	10.00	103.3	5.58	0	28.17	2.12	0.00
10:1	0.93	0.64	5.03	10.00	87.42	5.86	0	23.38	2.30	0.00
10:1	0.93	0.64	5.03	10.00	86.35	5.68	0	23.10	2.23	0.00

Table 6: Extraction efficiency of mica cleaner concentrate – gypsum method (Leaching at 85°C; L:S = 10; leaching time = 60 minutes; natural pH of 7; sinter ratio = 2:1; sinter temperature = 1050°C).

Test	Sinter Grade (%)			Weight of sinter Leached (g)	Concentration of elements in Solution (µg/ml) (250 ml)			Extraction efficiency (%)		
	Li	Rb	Fe		Li	Rb	Fe	Li	Rb	Fe
run 1	0.39	0.26	2.35	10.00	67.01	7.36	0	42.89	7.16	0.00
run 2	0.39	0.26	2.35	10.00	71.3	10.19	0	45.63	9.91	0.00

Table 7: Effect of sintering un-pulverised mica on lithium extraction efficiency- gypsum method (Leaching at 85°C; L:S = 10; leaching time = 60 minutes; natural pH of 7; sinter ratio = 2:1; sinter temperature = 1050°C).

Test	Sinter Grade (%)			Weight of sinter Leached (g)	Concentration of elements in Solution (µg/ml) (250 ml)			Extraction efficiency (%)		
	Li	Rb	Fe		Li	Rb	Fe	Li	Rb	Fe
run 1	0.76	0.45	3.98	10.00	167.4	21.89	0.0	55.02	12.28	0.0
run 2	0.76	0.45	3.98	10.00	100.1	16.64	0.0	32.91	9.33	0.0

Table 8: Extraction efficiency based on the grade of leach residue and leach solution of mica-gypsum-$Ca(OH)_2$ (sinter ratio 3:2:1; L:S =10:1; Leaching at 85°C; Leaching time = 30 min).

Sinter Temp (°C)	wt of residue (g)	Grade of Residue (%)			Concentration of Elements in Solution (µg/ml) (250 ml)			Extraction Efficiency (%)		
		Li	Rb	Fe	Li	Rb	Fe	Li	Rb	Fe
900	7.62	0.25	0.38	3.08	187.7	35.9	0.03	71.38	23.76	0.0
900	8.22	0.25	0.38	3.08	189.3	35.7	0.03	69.98	22.31	0.0
925	8.42	0.12	0.34	3.24	236.6	63.8	0.03	85.33	35.75	0.0
925	8.30	0.12	0.34	3.24	235.6	63.5	0.04	85.46	35.97	0.0
950	8.19	0.10	0.30	3.25	250.4	76.7	0.03	88.32	43.75	0.0
950	8.26	0.10	0.30	3.25	243.9	79.6	0.03	87.95	44.45	0.0
975	8.25	0.09	0.30	3.00	240.9	78.3	0.06	88.93	44.58	0.0
975	8.46	0.09	0.30	3.00	244.9	89.0	0.05	88.85	47.13	0.0

Table 9: Extraction efficiency based on the grade of leach residue and leach solution of mica cleaner conc.-gypsum (sinter ratio = 2:1; L:S =10:1; Leaching at 85°C; Leaching time = 30 min).

Sinter Temp (°C)	wt of residue (g)	Grade of Residue (%)			Concentration of Elements in Solution (µg/ml) (250 ml)			Extraction Efficiency (%)		
		Li	Rb	Fe	Li	Rb	Fe	Li	Rb	Fe
850	9.39	0.49	0.45	2.32	3.11	0.23	0.00	1.66	0.14	0.00
850	9.44	0.49	0.45	2.32	3.02	0.23	0.00	1.60	0.13	0.00
950	9.65	0.46	0.47	2.59	35.41	3.34	0.00	16.57	1.82	0.00
950	9.71	0.46	0.47	2.59	35.97	3.54	0.00	16.71	1.91	0.00
1050	8.97	0.26	0.43	2.79	157.1	32.87	0.00	62.42	17.65	0.00
1050	8.89	0.26	0.43	2.79	157.8	32.83	0.00	62.72	17.76	0.00

Table 10: Extraction efficiency based on the grade of leach residue and leach solution of Non-magnetic mica-gypsum (sinter ratio = 2:1; L:S =10:1; Leaching at 85°C; Leaching time = 30 min).

Sinter Temp (°C)	wt of residue (g)	Grade of Residue (%)			Concentration of Elements in Solution (µg/ml) (250 ml)			Extraction Efficiency (%)		
		Li	Rb	Fe	Li	Rb	Fe	Li	Rb	Fe
850	9.52	0.16	0.22	0.93	2.03	0.28	0.00	3.28	0.34	0.00
850	9.53	0.16	0.22	0.93	1.88	0.32	0.00	3.04	0.38	0.00
950	9.51	0.15	0.22	0.94	1.56	0.11	0.00	2.60	0.12	0.00
950	9.59	0.15	0.22	0.94	1.57	0.12	0.00	2.59	0.13	0.00
1050	9.78	0.14	0.23	1.00	10.22	1.96	0.00	15.59	2.12	0.00
1050	9.78	0.14	0.23	1.00	9.76	1.70	0.12	14.98	1.84	0.03

Appendix H2: The Limestone Method.

Table 1: Effect of temperature on lithium, rubidium and iron extraction efficiencies- Limestone method (Leaching at 85°C; L:S = 10; leaching time = 60 minutes; natural pH of 10).

Sinter ratio	Sintering Temp (°C)	Sinter grade (%)			Weight of sinter leached (g)	Concentration of elements in solution (µg/ml) (250 ml)			Extraction efficiency (%)		
		Li	Rb	Fe		Li	Rb	Fe	Li	Rb	Fe
5:1	800	0.92	0.63	6.08	10.24	1.47	0.81	8.01	0.39	0.31	0.32
3:1	800	0.87	0.59	5.54	10.26	2.53	1.75	5.62	0.71	0.72	0.25
5:1	825	0.92	0.62	5.38	10.25	23.13	4.85	6.32	6.14	1.91	0.29
3:1	825	0.87	0.59	5.03	10.26	1.97	0.90	6.68	0.55	0.37	0.32
5:1	850	0.92	0.63	5.90	10.26	2.46	0.12	9.98	0.65	0.04	0.41
3:1	850	0.88	0.59	5.38	10.26	1.95	0.48	14.43	0.54	0.20	0.65
5:1	900	0.94	0.61	7.92	40.00	16.45	1.96	12.72	2.19	0.40	0.20

Table 2: Effect of sintering temperature on lithium, rubidium and iron extraction efficiencies- Limestone method (Leaching at 85°C; L:S = 10; leaching time = 60 minutes; natural pH of 8-12; sinter ratio = 5:2).

Test number	Sinter Temp (°C)	Sinter Grade (%)			Weight of sinter leached (g)	Concentration of elements in Solution (µg/ml) (250 ml)			Extraction efficiency (%)		
		Li	Rb	Fe		Li	Rb	Fe	Li	Rb	Fe
1a	250	0.78	0.50	2.98	10.19	1.06	0.21	0	0.33	0.11	0.00
1b	250	0.78	0.50	2.98	10.46	0.65	0.19	0	0.20	0.09	0.00
2a	500	0.78	0.50	2.98	9.96	0.9	0.10	0	0.29	0.05	0.00
2b	500	0.78	0.50	2.98	10.01	0.86	0.09	0	0.27	0.05	0.00
3a	750	0.78	0.50	2.98	10.21	0.9	0.32	0	0.28	0.16	0.00
3b	750	0.78	0.50	2.98	10.74	0.87	0.33	0	0.26	0.15	0.00
4a	800	0.78	0.50	2.98	10.52	1.03	0.43	0	0.31	0.21	0.00
4b	800	0.78	0.50	2.98	10.58	4.62	0.52	0	1.39	0.25	0.00
5a	850	0.78	0.50	2.98	10.72	4.14	0.43	0	1.23	0.20	0.00
5b	850	0.78	0.50	2.98	10.69	6.34	0.51	0	1.89	0.24	0.00
6a	900	0.78	0.50	2.98	10.81	1.74	0.10	0	0.51	0.05	0.00
6b	900	0.78	0.50	2.98	10.80	0.12	0.10	0	0.04	0.05	0.00
7a	950	0.78	0.50	2.98	10.53	15.12	0.74	0	4.59	0.35	0.00
7b	950	0.78	0.50	2.98	10.64	16.52	0.75	0	4.96	0.35	0.00
8a	1000	0.78	0.50	2.98	10.88	30.42	0.78	0	8.93	0.36	0.00
8b	1000	0.78	0.50	2.98	10.85	29.85	0.73	0	8.79	0.34	0.00
9a	1050	0.78	0.50	2.98	10.87	8.04	0.60	0	2.36	0.28	0.00
9b	1050	0.78	0.50	2.98	10.89	10.18	0.65	0	2.99	0.30	0.00

Appendix H3: The Sodium Sulphate Method.

Table 1: Effect of sintering temperature on lithium, rubidium and iron extraction efficiencies- sodium sulphate method (Leaching at 85°C; L:S = 10; leaching time = 30 minutes; natural pH of 6 ; sinter ratio = 2:1).

Test number	Sinter temp (°C)	Sinter Grade (%)			Weight of sinter leached (g)	Concentration of elements in solution (µg/ml) (250 ml)			Extraction efficiency (%)		
		Li	Rb	Fe		Li	Rb	Fe	Li	Rb	Fe
1a	350	0.68	0.39	2.81	10.01	1.63	0.85	0.06	0.60	0.54	0.01
1b	350	0.68	0.39	2.81	10.08	1.28	0.78	0.07	0.47	0.49	0.01
2a	550	0.68	0.39	2.81	10.08	8.32	0.78	0.05	3.04	0.49	0.00
2b	550	0.68	0.39	2.81	10.01	7.92	0.72	0.08	2.92	0.46	0.01
3a	750	0.68	0.39	2.81	10.00	21.62	2.43	0.06	7.97	1.55	0.01
3b	750	0.68	0.39	2.81	10.00	21.34	2.44	0.03	7.86	1.56	0.00
4a	850	0.68	0.39	2.81	10.01	255.6	25.15	0.05	94.13	15.99	0.00
4b	850	0.68	0.39	2.81	10.01	271.3	27.59	0.06	99.91	17.54	0.00
5a	900	0.68	0.39	2.81	10.00	242.3	26.55	0.21	89.27	16.89	0.02
5b	900	0.68	0.39	2.81	10.01	220.7	24.90	0.06	81.26	15.82	0.01
6a	950	0.68	0.39	2.81	10.01	269.9	36.75	0.08	99.42	23.37	0.01
6b	950	0.68	0.39	2.81	10.01	237.6	33.50	0.07	87.53	21.31	0.01
7a	1000	0.68	0.39	2.81	10.01	243.6	66.88	0.12	89.71	42.52	0.01
7b	1000	0.68	0.39	2.81	10.00	237.7	32.83	0.21	87.58	20.88	0.02

Table 2: Effect of leaching time on lithium, rubidium and iron extraction efficiencies- sodium sulphate method (Leaching at 85°C; L:S = 10; natural pH of 6; sinter ratio = 2:1).

Leaching time (min)	Sinter Grade (%)			Weight of sinter Leached (g)	Concentration of elements in Solution (µg/ml) (250 ml)			Extraction efficiency (%)		
	Li	Rb	Fe		Li	Rb	Fe	Li	Rb	Fe
4	0.76	0.42	2.22	10.02	187.2	18.79	2.32	61.74	11.08	0.26
10	0.76	0.42	2.22	10.00	261.6	19.43	0.62	86.41	11.48	0.07
20	0.76	0.42	2.22	10.00	242.5	18.64	0.3	80.08	11.01	0.03
30	0.76	0.42	2.22	10.01	264.5	19.32	0.23	87.31	11.40	0.03
60	0.76	0.42	2.22	10.01	270.2	19.21	0.28	89.20	11.34	0.03

Table 3: Effect of leaching bath temperature on lithium, rubidium and iron extraction efficiencies- sodium sulphate method (Leaching time = 30 min; L:S = 10; natural pH of 6; sinter ratio = 2:1).

Leaching Temp (°C)	Sinter Grade (%)			Weight of sinter leached (g)	Concentration of elements in solution (µg/ml) (250 ml)			Extraction efficiency (%)		
	Li	Rb	Fe		Li	Rb	Fe	Li	Rb	Fe
20	0.76	0.42	2.22	9.95	262	18.96	0.75	86.98	11.25	0.08
45	0.76	0.42	2.22	9.98	270.1	19.10	0.91	89.42	11.31	0.10
60	0.76	0.42	2.22	10.00	279.2	19.35	0.5	92.24	11.43	0.06
85	0.76	0.42	2.22	10.00	281.1	19.4	0.5	92.83	11.46	0.06

Table 4: Effect of sinter ratio on lithium, rubidium and iron extraction efficiencies- sodium sulphate method (Leaching at 85°C; L:S = 10; leaching time = 30 minutes; natural pH of 6 - 7).

Test number	Sinter ratio	Sinter grade (%)			Weight of sinter leached (g)	Concentration of elements in solution (µg/ml) (250 ml)			Extraction efficiency (%)		
		Li	Rb	Fe		Li	Rb	Fe	Li	Rb	Fe
1a	2:1	0.68	0.39	2.81	10.01	255.6	25.15	0.05	94.13	15.99	0.00
1b		0.68	0.39	2.81	10.01	271.3	27.59	0.06	99.91	17.54	0.00
2a	3:1	0.82	0.37	2.06	10.00	319.5	17.92	0.26	97.00	11.98	0.03
2b		0.82	0.37	2.06	10.00	301.0	17.92	0.39	91.39	11.98	0.05
3a	5:1	0.87	0.49	3.17	10.00	299.2	14.87	0.47	86.27	7.57	0.04
3b		0.87	0.49	3.17	10.00	306.5	14.73	0.45	88.39	7.49	0.04
4a	7:1	0.88	0.50	3.35	10.00	159.8	13.21	0.40	45.26	6.63	0.03
4b		0.88	0.50	3.35	10.00	113.5	13.10	0.57	32.15	6.57	0.04

Table 5:Extraction efficiency based on the grade of leach residue and leach solution of mica-Na_2SO_4-$Ca(OH)_2$ sinter (sinter ratio 6:2:1; L:S =10:1; Leaching at 85°C; Leaching time = 30 min).

Sinter Temp (°C)	wt of residue	Grade of residue (%)			Concentration of Elements in Solution (µg/ml) (250 ml)			Extraction Efficiency (%)		
		Li	Rb	Fe	Li	Rb	Fe	Li	Rb	Fe
800	7.37	0.64	0.51	4.52	148.2	57.88	0.04	43.87	27.75	0.00
800	7.34	0.64	0.51	4.52	127.4	54.62	0.03	40.30	26.69	0.00
850	7.98	0.26	0.51	4.21	328.1	24.60	0.02	80.04	13.12	0.00
850	7.99	0.26	0.51	4.21	325.5	25.29	0.05	79.90	13.43	0.00
900	8.12	0.23	0.56	4.50	335.7	14.13	0.05	81.54	7.25	0.00
900	8.01	0.23	0.56	4.50	328.8	14.02	0.06	81.44	7.29	0.00
975	8.18	0.31	0.54	3.68	301.0	11.95	0.01	74.89	6.36	0.00
975	8.12	0.31	0.54	3.68	274.9	12.19	0.03	73.29	6.52	0.00

Table 6:Extraction efficiency based on the grade of leach residue and leach solution of mica cleaner conc-Na_2SO_4 sinter (sinter ratio = 2:1; L:S =10:1; Leaching at 85°C; Leaching time = 30 min).

Sinter Temp (°C)	wt of residue	Grade of residue (%)			Concentration of Elements in Solution (µg/ml) (250 ml)			Extraction Efficiency (%)		
		Li	Rb	Fe	Li	Rb	Fe	Li	Rb	Fe
850	6.52	0.17	0.63	3.13	185.5	7.26	0.13	80.27	4.24	0.02
850	6.36	0.17	0.63	3.13	171.2	7.28	0.00	79.39	4.36	0.00

Table 7:Extraction efficiency based on the grade of leach residue and leach solution of Non-magnetic mica-Na_2SO_4 sinter (sinter ratio = 2:1; L:S =10:1; Leaching at 85°C; Leaching time = 30 min).

Sinter Temp (°C)	wt of residue	Grade of residue (%)			Concentration of Elements in Solution (µg/ml) (250 ml)			Extraction Efficiency (%)		
		Li	Rb	Fe	Li	Rb	Fe	Li	Rb	Fe
850	6.31	0.06	0.33	1.25	44.73	4.37	5.83	73.18	4.98	1.81
850	6.32	0.06	0.33	1.25	46.65	4.18	5.66	73.96	4.77	1.76

Appendix H4: Leaching Reagents Specifications.

Table 1: Limits of impurities in calcium sulphate dihydrate reagent.

Element	Content
Assay	100.35%
Total chloride (Cl)	< 0.005%
Copper (Cu)	0.077 ppm
Iron (Fe)	6.760 ppm
Potassium (K)	1.820 ppm
Magnesium (Mg)	6.830 ppm
Sodium (Na)	4.180 ppm
Total nitrogen (N)	4.000 ppm
Total phosphorus (P)	73.130 ppm
Lead (Pb)	0.880 ppm
Total silicon (Si)	6.910 ppm
Zinc (Zn)	0.088 ppm

Table 2: Limits of impurities in sodium sulphate anhydrous powder(AnalaR).

Element	Content
Assay	99.5%
Insoluble matter	0.005%
chloride (Cl)	0.001%
Iron (Fe)	0.0005%
Potassium (K)	0.01%
Arsenic (AS)	0.00004%
Calcium group and Magnesium (Ca)	0.013%
Ammonium (NH_4)	0.0005%
Nitrate (NO_3)	0.001%
Phosphate (PO_4)	0.002%
Lead (Pb)	0.001%
Oxidising substances	No reaction
Reducing substances (O)	0.002%
Loss at 300^oC	0.5%

Table 3: Limits of impurities in calcium carbonate (AnalaR).

Element	Content
Assay	minimum 99.0%
Hydrochloric acid insoluble matter	0.005%
Chloride (Cl)	0.005%
Copper (Cu)	0.0005%
Iron (Fe)	0.001%
Sulphate (SO_4)	0.01%
Potassium (K)	0.01%
Magnesium (Mg)	0.05%
Sodium (Na)	0.2%
Nitrogen compounds (N)	0.001%
Aluminium (Al)	0.005%
Lead (Pb)	0.0005%
Barium (Ba)	0.005%
Strontium (Sr)	0.1%
Particle size	approx. 14 µm

Appendix I: Processing Equipment Selection and Costing.

The following assumptions were used to arrive at the expected unit treatment capacity in tonnages:

- A total annual production of 55,000 tonnes of china clay by Goonvean Ltd.
- A ratio of mica to china clay production of 1:1.
- Specific gravity of flotation solids of 2700 kg/m^3.
- Calcined ore density of 2640 kg/m^3
- 365 working days of 24 hours.
- 60% mica recovery by weight at flotation stage.
- 50% magnetic mica recovery by weight at WHIMS stage.

1. Flotation Section

Selection of the size and number of cells for a single roughing bank of mica flotation circuit operation is made by a three step calculation based on the information obtained in the Handbook, Selection Guide for Process Equipment (SVEDALA):

- Determination of total flotation cell volume
- Cell size selection
- Determination of number of cells

Flotation is carried out at 30% solids by weight.

55000 t/yr = 150.68 t/day = 6.28 t/h (dry solids)

For calculation purposes 7 t/h was used as mass flowrate of dry solids whose density is 2691 kg/m^3.

Volumetric flowrate of solids in slurry stream $= \frac{mass\ \ flowrate}{Density} = \frac{7\ x\ 1000\frac{kg}{h}}{2700\frac{kg}{m^3}} = 2.59\ m^3/h$

Mass flowrate of water in slurry stream = mass flowrate of solids x dilution ratio

$$= 7\ x\ \frac{70}{30} = 16\ t/h$$

Therefore, volumetric flowrate of water = 16.33 m^3/h.

Thus volumetric flowrate of slurry = 16.33 + 2.59 = 18.92 m^3/h.

Total flotation cell volume required can be calculated from formula:

$$V_{(tot)} = \frac{Q * T_r * S}{60 * a}$$

where, Q = pulp flow, m^3/h; T_r = retention time, 8 min in this case; S = scale up factor, for lab. batch tests, S = 1.7; a = aeration factor, normally 0.85.

a. Required flotation volume

$$Vol_{(tot)} = \frac{18.92\ x\ 8\ x 1.7}{60\ x\ 0.85} = 5.05\ m^3\ flotation\ (bank)\ volume.$$

b. Cell size selection

Minimum cell size to handle 18.92 m^3/h is DR 15

DR 15 requires 5.05/0.34 = 14.9 cells

However, the selection gives more cells per bank than common practice

For mica this would be 4-8 cells/bank (average 6 cells/bank)

Preliminary cell size would be 5.05/6 i.e. 0.84 m^3/cell

Hence the nearest cell size from the available machine data is DR 18 sp – 0.71 m^3/cell

c. Number of cells

Number of cells determined by simple calculation based on required bank volume and the best cell size.

DR 18 sp would require: 5.05/0.71 = 7.1 cells

Select: 8 cell bank

d. Cost

From the handbook of capital cost, Price = aX^b in US dollars, where X is the cell volume in cubic feet, a = 3223, b = 0.3999 at a cost index of 1400.

Price = $3223(25)^{0.3999}$ = $11,676

$$\frac{Price_{(now)}}{Price_{(then)}} = \frac{Index_{(now)}}{Index_{(then)}}$$

$$Price_{(now)} = \frac{1573}{1400}\ x\ 11676 = \$\ 13,119 \text{ / cell} = £8{,}233\text{/ cell}$$

Now for 8 cell bank, the cost = 8 x 8233 = **£65, 864**

2. **Magnetic Separator**

Magnetic separator capacity = 4.2 t/h = 4.6 short tonnes /h.

From the Handbook of capital cost, the nearest separator which can handle 5 short tonnes had the horsepower of 9HP. The cost of a 9HP separator was $ 100,000 at a cost index of 1400 and therefore, the cost now at an index of 1573 in British pounds = **£70, 514**.

3. **Pressure Filter VPA - Sizing**

We are sizing the filter required to handle the mica flotation concentrate by using the cycle method as explained in the Handbook (Basic selection Guide for Process Equipment).

(a) Cake bulk weights

Specific dry weight of the filter cake inside each chamber is called the cake bulk weight (kg/litre). The mica concentrate cake bulk weight (ρ_{cake}) = 2.82 kg/l.

(b) Plant capacity

By dividing the required plant throughput S (t/h) with cake bulk weight the required cake volume per hour is obtained. $V = S/\rho_{cake}$

(c) Cycle time

Is calculated as the sum of

- Filtration
- Compression
- Washing
- Throughblow (drying)
- Service time (discharge, washing and closing)

Total cycle time t (min/cycle)

Number of cycles per hour n = 60/t

The required volume per cycle equals required filter volume.

Filter volume = V/n = (S x 1000 x t) / (ρ_{cake} x 60) litre

<u>Sample calculation</u>

Capacity 4.2 t/h (dry solids); Cake bulk weight = 2.82kg/l;

Plant capacity V = 4.2/2.88 = 1.46 m^3/h; Cycle time t = 8 min (estimate);

Cycles per hour n = 60/8 = 7.5;

Filter volume V / n = (1.46 x 1000) / 7.5 = 195 l

From the Handbook, Basic selection Guide for Process Equipment, select VPA 1030 – 10 (200 litres).

Pressure Filter VPA – Chamber data

Chamber area (working area)

VPA 10 with chamber dimensions (outer) 10 x 10 (max 40 chambers)

VPA 10 = 0.65 m^2/chamber (7 ft^2/chamber)

Filtration area = 2 x chamber area (each chamber has double cloths and filtering takes place on both sides). = 2 x 7 x 10 = 140 ft^2 (13m^2)

Chamber volume

VPA 1030 (32 mm chamber depth) = 20.0 litre (5 USG)

Pressure Filter VPA – Nomenclature

Type VPA = **V**ertical **P**ressure Filter **A**ir through-blow

VPA 1030-10 = Pressure filter type VPA with chamber dimensions 10 x 10 dm, chamber depth 30 mm and number of chambers 10.

Cost

From the above calculation a nearest vertical plate and frame pressure filter of area 133 ft^2 was chosen from the Handbook of Capital Cost (1998).

The price in US dollars for an automated one is given by the equation, Price = aX^b, where X is the filter area in square feet, a = 4085, b = 0.5409 at the cost index of 1400. The cost in British pounds at the cost index of 1573 was **£40,575**.

4. Rotary Gas Dryer

It was difficult to select suitable dryer because of lack of information on the drying capacity in the Handbook for Capital Cost. The information available was size in terms of diameter, length and horsepower. Thus the price given below is based on the rotary dryer of diameter 4 ft, length 40 ft and 10 horsepower.

Price = aX^b, US Dollars at a cost index of 1400.

Where X, in cubic feet, is diameter squared times length, a = 8309 and b = 0.4409.

Therefore, the cost of the suggested dryer at the cost index of 1573 in British pounds = **£101,174**.

5. Rotary Dry Blenders

Capacity = 2.1 t/h; ore density = 2.88 t/m^3

Volumetric flowrate of solids = 2.1/ 2.88 =0.73 m^3/h = 0.012 m^3/min.

Residence time = 10 min

Effective tank volume = 0.012 x 10 = 0.12 m^3

To cater for the amount of sodium sulphate and calcium hydroxide to be added plus the uncertainty of the residence time, the effective volume is multiplied by 10.

Thus the effective tank volume = 1.2 m^3 = 42 ft^3

A rotary dry blender of diameter 3 ft and length 5ft was suggested, Volume = 45ft^3.

Price aX^b, US Dollars and a cost index of 1400, where X is the operating volume in cubic feet, a = 5071 and b = 0.415. The cost in British pounds at a cost index of 1573 = **£17,356**.

6. Direct-fired rotary kiln

Due to scarce information on the prices of rotary kilns, the price quoted by Klaas Peter van der Wielen (2008) in his master thesis was used as the basis to estimate the price. According to Van der Wielen, the price of a 66t/h directly fired rotary kiln reported in the Mine and Mill Cost Handbook (Western Engineering, 2005) was £416,667. The cost index in 2005 was 1245.

For a kiln to treat 2.1 t/h of material, the following equation was used to estimate the price now at cost index of 1573:

$$Cost\ of\ equip.a = cost\ of\ equip.b\ \left(\frac{capac.equip.a}{capac.equip.b}\right)^{0.7}$$

$Cost_{2.1t}$ = 416667(2.1/0.66)$^{0.7}$ = £936,832

$Cost_{now}$ = (1573/1245) x 936832 = **£1, 184, 119**

7. Pulveriser

In order to calculate the power drawn by the pulveriser, one needs to know the bond work index of the sinter material. Since no such data was available a 15 horsepower pulveriser is suggested for price determination only based from the Handbook for Estimating Mining and Mineral Processing Equipment Cost and Capital Expenditure (1998).

Price = aX^b, US dollars

where X is the required horsepower.

Heavy Duty Range in X, hp: 10 to 62.3, a = 13800 and b = 0.3698 at a cost index of 1400.

Therefore, Price now at a cost index of 1573 = **£26,490** for a 15 hp pulveriser.

8. Leaching Tank Selection

Feed rate = 3 t/h; Calcined ore density = 2.64t/m^3 ; Leaching time = 30 min; Liquid:Solid ratio = 10 (9% solids by weight).

Volumetric flowrate of solids $= \frac{3\ t/h}{2.64\ t/m^3} = 1.14\ m^3/h$

Mass flowrate of water in slurry $= 3\ x\ \frac{91}{9} = 30.3\ t/h$

Therefore, volumetric flowrate of water = 30.3 m^3/h, and thus

Volumetric flowrate of slurry = 30.3 + 1.14 = 31.44 m^3/h = 0.52 m^3/min

Effective tank volume $= pulp\ rate\ x\ leaching\ time = 0.52\ x\ 30 = \mathbf{15.6\ m^3}$

The nearest agitator tank specification obtained from the Hand book (Basic Selection Guide for Process Equipment) is:

Tank dimensions		**Volume (effective including freeboard)**	
Dia. x height [(m]	**Dia. x height [ft]**	**[m^3]**	**[ft^3]**
3 x 3	10 x 10	19.1	705

Price = aX^b, US Dollars

where X = tank capacity in US gallons. Round, open top tanks with slope bottoms:

316 Stainless; Range in X, US gallons: 168 to 1540 a = 16.78 b = 0.791

The required tank volume is beyond the range and therefore we upgrade using capacity equation.

$$Cost\ of\ equip.a = cost\ of\ equip.b\ \left(\frac{capac.equip.a}{capac.equip.b}\right)^{0.7}$$

19.1 m^3 = 5053 US gallons.

The cost of a 550 gallons tank = $16.78(550)^{0.791}$ = $2468.41

$Cost_{(now)} = \frac{1573}{1400}\ 2468.41 = \$\ 2773.44 = £\ 1{,}741$

Therefore, the cost of a 5053 gallons tank $= 1741\ x\ \left(\frac{5053}{550}\right)^{0.7} = \mathbf{£8{,}223}$